THE UNIVERSITY OF ASTON IN BIRMINGHAM
(U.K.)

"MEASUREMENTS AND CALCULATIONS OF SPATIAL DISTRIBUTION OF FAST NEUTRON SPECTRA IN IRON AND IRON-URANIUM ASSEMBLIES FROM A 14-MEV SOURCE"

A thesis submitted for the Degree of

DOCTOR OF PHILOSOPHY

by

SYED M. KABIR, B.Sc.(Hons.), M.Sc.

March, 1971

Department of Physics

THE UNIVERSITY OF ASTON IN BIRMINGHAM
(U.K.)

"MEASUREMENTS AND CALCULATIONS OF SPATIAL DISTRIBUTION OF FAST NEUTRON SPECTRA IN IRON AND IRON-URANIUM ASSEMBLIES FROM A 14-MEV SOURCE"

A thesis submitted for the Degree of

DOCTOR OF PHILOSOPHY

by

SYED M. KABIR, B.Sc.(Hons.), M.Sc.

March, 1971

Department of Physics

ABSTRACT

The spatial distribution of fast neutron spectra in two assemblies of iron and the combination of iron and natural unranium of about equal ratio by volume have been measured with five threshold reactions:- $^{63}Cu(n, 2n)$, $^{27}Al(n, \alpha)$, $^{56}Fe(n, p)$, $^{27}Al(n, p)$ and $^{31}P(n, p)$. 14 Mev source neutrons were produced with a 150 KV SAMES accelerator.

The assemblies were of cylindrical annular geometry - the inner radius about 10 cm, and the outer radius slightly larger than 30 cm. The source was centrally located. The absolute source strength of the neutrons was determined by the associated alpha-particle counting technique. The induced activities in the foils were measured by counting gamma-rays with a NaI(Tl) scintillator coupled to a multichannel analyser and the beta particles with a plastic scintillator. The counting systems were calibrated for each type of foil and the absolute activity was determined from that.

Measurements were also made with the $^{115}In(n, \gamma)$ reaction for both bare and cadmium covered foils to assess the intensities of the lower energy neutrons.

Multigroup diffusion and removal diffusion calculations were made by solving the equations numerically. The diffusion coefficients in the calculations were obtained with higher order transport corrections than commonly used. The group parameters were obtained from the more recent 20 group Yiftah-Sieger cross-section set which considers the presence of a 14 Mev source and divides the Mev energy region into seven groups. Calculations were also made with a "hybrid" set mainly based on the Russian ABBN set, but the top two groups contained data supplimented from the Yiftah-Sieger set.

Results are compared for experimentally obtained normalised absolute activities with those predicted by the calculations. Satisfactory agreement is obtained between them and results show some interesting features.

ACKNOWLEDGEMENTS

I would like to thank Dr. P. N. Cooper for his help and guidance throughout the whole of the project.

I should also like to thank Professor S. E. Hunt for his interest in the project.

Thanks are also due to the laboratory technical staff for help in maintenance of the accelerator during the project work.

Help and encouragement was also obtained from various other people and organizations, some of whom at least should be acknowledged. Most of the iron used in the project was obtained on loan from the Shielding Group of the UKAEA, Harwell; some of the threshold foils were also obtained from them. Information and suggestions obtained from the Radiation Shielding Information Centre, Oak Ridge National Laboratory, U.S. and the ENEA Computing Centre at Ispra, Italy, helped in assessing the status of the up-to-date computational techniques and the cross section data. The Library of the University made a conscientious effort throughout the period to make available many of the cross section data used and some of the literature and references consulted for the work from various sources both in this country and outside. The staff of the University Computer Centre should also be acknowledged for their help in running the programmes and data preparation.

My thanks are also due to the Colombo Plan Authority for the award of the financial assistance, and to the Pakistan Atomic Energy Commission for granting me leave of absence for the period of this work. The British Council and in particular its local centre, must be thanked for looking after the various arrangements which made my stay comfortable.

Birmingham
March, 1971

Syed M. Kabir

TABLE OF CONTENTS

Page No.

Page No.

Page No.

CHAPTER 6. FLUX MEASURING TECHNIQUE WITH FOILS

Page No.

Page No.

LIST OF FIGURES

(Figures are in general placed below the page where they are first mentioned and discussed)

CHAPTER 1

INTRODUCTION

The present work was undertaken with a view to improving understanding of fast neutron behaviour in materials of interest to nuclear technology - both present and future. It was not aimed at a particular problem with a direct application, rather it was felt that the study should be useful in branches of the technology, where the transport and slowing down of the fast neutrons, mainly by inelastic scattering with or without some fission, are important. In spite of the prominant role that inelastic scattering plays in several important fields, many uncertainties about its characteristics and behaviour still remain. The gap in the knowledge can only be filled by studying systems where inelastic scattering is important and to correlate experimental results with theoretical predictions based on the present computing techniques and whatever knowledge has been acquired about the fundamental cross-section data.

Relevant fields are the core and blanket study of the fast breeder reactors, the radiation damage study of the structural materials of the reactors, the optimization of the shields of the power reactors, and the use of the fusion reactors when they become feasible. In view of the energy of the source neutrons and the geometry, dimensions and compositions of the assemblies studied, the present work is more directly relevant to the fusion reactors. The materials that will be present around them will have iron in the container vessels and the magnets for the plasma, and uranium—either natural or depleted—in bulk for production of power and breeding of plutonium. Though no attempt has been made to simulate the exact configurations, in view of the large mean free paths of the 14 Mev neutrons a practical configuration to a large extent will behave as homogeneous mixture of these two elements. For design, the behaviour of the source neutrons and the degraded neutrons will have to be known. The extent to which this can be predicted is

of prime interest.

For shields and blankets of the fission reactors, 14 Mev neutrons are at the extreme top end of the neutron spectra and are not so significant. Nevertheless 14 Mev neutrons have played a significant rôle in the development of neutron physics. Several attractive features of these accelerator produced neutrons cause them to be widely used. Monoenergetic source neutrons free the analysis from the complexities that dealing with spectra introduce and enable the studies to be concentrated on other factors of interest.

The deep penetration problems for reactor shields have some similarities to the monodirectional fast neutrons produced from accelerators. After crossing sufficient distances into the shield only the foward peaking high energy end of the spectrum survives and in most shields they behave as monodirectional neutrons of about 8 Mev. The scattering properties of the 14 Mev neutrons are not much different from those of the 8 Mev neutrons. Attenuation and transport of the latter can be understood from those of the 14 Mev neutrons which can be studied on a small laboratory scale, while the practical shields cannot be simulated easily.

The radiation damage done to the pressure vessels and constructional materials by the high energy component of the neutron spectrum in reactors is still an underdeveloped science. The life-period of a power reactor is mainly decided by the radiation damage in the pressure vessel and structural framework. The economics of nuclear power is in turn strongly dependent upon the life-time. In a typical thermal power reactor it is estimated, about 60% of the damage to its pressure vessel is due to neutrons above 0.5 Mev [180]. Very little however is known

about the deterioration of the structural materials in the long run, in steel,due to accumulation of hydrogen and helium which will result from the (n,p) and (n,α) reactions with iron. Both cross-sections and spectral profile of the fast neutrons will dictate this.

The detailed shape of the high energy end of the spectra in shields is also of interest to know the origin of the secondary activities, particularly the gamma-rays induced by the (n,p) and (n,α) reactions. For further improvement and reliability of the shielding calculations, these predictions will have to be known with better accuracy.

Because of the behaviour of the general cross-sections, particularly the rapid fall of the cross-section of hydrogen with energy, when biological shields are followed by considerable amount of medium and heavy elements, what happens to the fast neutrons in the latter strongly defines the final shielding performance. Thus Shure [181] has shown that a 10% change in the inelastic scattering in an iron shield has a marked effect on the relaxation length of the neutrons emerging into a subsequent water shield, amounting to a 50% change after 40 cms. of water.

Both ^{238}U and iron are by far the most abundant materials in fast breeder reactors. In large breeder reactors, typically 60% of the fertile material in the blanket and 10% or more in the core can be ^{238}U; 25% of the core may contain steel. In the studies of the fast systems, it is often found that calculations - both multigroup diffusion and Sn - tend to predict harder spectra than is experimentally encountered. This is most possibly due to the underestimation of the leakage of the fast neutrons by the calculations. The predictability of the parameters of the fast reactors is yet to be as accurate as that of the the thermal

reactors. As the fast reactor technology gathers momentum and larger breeder reactors are about to be constructed the need for improved predictions becomes more important. Test of the existing knowledge of the cross-sections and any multigroup parameters obtained by averaging them is necessary for as many different systems as possible. In spite of the more sophisticated computational techniques the multigroup diffusion method of calculations still remains the most widely used and relied upon technique for practical calculations of the reactors. The cross-section sets in vogue so far, combines the whole spectrum above about 2.2 to 3 Mev into one group. The Yiftah-Sieger cross-section set is the only one that tries to resolve the higher energy flux into several groups. Comparison with experiments has not yet been reported, for this multigroup cross-section set.

In the present work this set has been put to use for multilgroup calculations. Also used was the up-to-date data for 5 threshold reaction cross-sections - another region of major uncertainty in the nuclear technology.

CHAPTER 2.

INTERACTION OF FAST NEUTRONS WITH MATTER

I. REACTIONS EXCEPT FISSION

2.1) The Neutron.

The neutron has a mass of 1.00866 atomic mass units ($^{12}C = 12$), and is a fundamental nuclear particle. The unique properties of the neutron which make it of such decisive importance in nuclear physics and engineering are due to the fact that it is electrically neutral so that its electrostatic interaction with electrons and nuclei is negligible. Consequently, it can diffuse through matter unhindered until it encounters a nucleus, with which it can react by virtue of the existence of short range forces that are specifically nuclear in character. Owing to the relatively small size of the nucleus ($\sim 10^{-12}$ cm.) in comparison with interatomic dimensions ($\sim 10^{-8}$ cm.), the mean free path of such encounters may be several centimeters. Like other elementary particles, the neutrons show dual nature of both wave and particle properties. The wave length is given by $\lambda = 2.86 \times 10^{-9}/\sqrt{E}$ cms, where E is in ev.

2.2) The Nucleus.

2.2.1) Constituents.

Nuclei are made up of neutrons and protrons. The general term nucleon is used for these constituents. The number of nucleons in a nucleus is A, the mass number and the number of protons is Z, the atomic number; the number of neutrons is A-Z.

2.2.2) Size.

Nuclei are very nearly spherical with a radius R given by the approximate formula

$$R = 1.5\, A^{\frac{1}{3}} \times 10^{-13} \text{ cm.} \qquad 2.1$$

This implies that the volume of the nucleus is proportional

2.2) contd.

2.2.2) contd.

to the number of nucleons A which it contains. Some of the heavy nuclei depart from spherical form and are ellipsoidal; however the ratio of the semi-major axis to the semi-minor axis is never greater than 1.2.

Experiments with high energy electrons show that there is a diffusivity in charge distribution at the outer fringe of the sphere, over which the charge drops to zero. Inside this diffuse boundary the density of nuclear matter is constant up to the centre.

2.2.3) Binding Energies.

Inside the nucleus the constituent nucleons may be thought of as being in constant agitation, but prevented from leaving the nucleus by strong, short range attractive forces, which are operative only inside the distance R. Outside this, only repulsive Coulomb forces on the protons are effective.

The exact mass M_o of a nucleus differs from an integral number of proton and neutron masses. The difference, a small fraction of the total mass, gives the binding energy B of the nucleons inside the nucleus. This is given by the Einstein euqation

$$B = \Delta M.C^2 \qquad 2.2$$

with $$\Delta M = Z.M_p + (A-Z)M_n - M_o \qquad 2.3$$

where M_p is mass of a free proton and M_n that of a neutron. ΔM is known as the mass defect. The average binding energy per nucleon of a nuclide is

2.2) contd.

2.2.3) contd.

$$f = \frac{B}{A} \qquad 2.4$$

By knowing the mass defect from experimental measurements the binding energy can be known. When the mass defect is known in amu (atomic mass units), B can be calculated in Mev by noting that 1 amu = 931.1 Mev. The binding energy per nucleon is in the region of 8 Mev for all nuclides except those with $A < 8$. For the heavier nuclei f increases up to about $A = 60$, when it is slightly below 9 Mev and thereafter slowly decreasing with increasing A; for ^{238}U it is about 7.6 Mev.

The general features of this have been calculated from the theoretical considerations supported by experimental evidence; by considering the various forces on a nucleon inside a nucleus, an expression known as the semi empirical binding energy formula can be obtained, from which f as a function of A and Z can be computed. However it cannot explain the peculiar stability of nuclides with "magic numbers" of neutrons and protons.

2.2.4) Stability of the Nuclei.

Among the lighter elements ($Z < 20$), the stable nuclei have mostly equal numbers of protons and neutrons. The number of neutrons is, however, always in excess of the number of protons for $Z > 20$, and this tendency to an excess of neutrons increases steadily with Z. It is a significant fact that over half of the stable nuclides occurring in nature have an even number Z of protons and

2.2) contd.

2.2.4) contd.

an even number N = A-Z of neutrons and that practically none has both Z and N odd. The remainder are about equally distributed between odd Z - even N and even Z - odd N. This indicates that even Z-even N nuclides, in which nucleons of the same kind can occur in pairs, are particularly stable and that odd Z-odd N nuclides in which there can be an unpaired proton and an unpaired neutron, are unstable. There is evidence of particular stability of nuclides with certain numbers of neutrons or protons; these numbers called magic numbers are 2,8,14,20,28,50,82,126. Experimental evidence suggests that nuclei form closed shells with these numbers.

2.3) Interactions between Neutron and Nuclei.

2.3.1) Types of Reactions.

The interaction between neutron and matter is very different from that of protron or gamma rays. Over the wide range of energies that neutrons can have they are capable of reacting in a variety of ways. The nature of reaction depends both upon the matter through which they pass and the energy of the neutrons. Like gamma-rays they can penetrate deep into matter; but unlike gamma-rays they react primarily with the nuclei of the atoms of the medium.

If the nucleus is unchanged in either isot opic composition or internal energy after interacting with a neutron, the process is called elastic scattering. If the nucleus is still unchanged in composition but is left

2.3) contd.

2.3.1) contd.

in an excited state, the process is called inelastic scattering. The symbols (n,n) and (n,n') are used to denote these processes. In these interactions one to one correspondence of the neutron before and after the interaction is maintained. For most cases elastic scattering is generally considered an external event though in some of the elastic scatterings the neutron might have penetrated into the nucleus; inelastic scattering however takes place if the neutron enters the nucleus. The emerging neutron may not be the same neutron that struck the nucleus. The inelastically scattered neutron will have energy less than the original one; the balance at first absorbed by the nucleus comes out as gamma rays.

The neutron may disappear as a result of being absorbed by the nucleus followed by an emission of gamma rays only. This process is called radiative capture, denoted by (n,γ). Neutrons also disappear in charged particle reactions such as the (n,p) or (n,α) reactions. When the energy of the neutron is high enough two or more neutrons can be emitted; these are (n,2n) or (n,3n) reactions. A closely related process is the (n,pn) reaction which also occur with high energy neutrons. In all these reactions the product nucleus is usually radioactive. Finally, when a neutron collides with certain heavy nuclei, the nucleus splits into two fragments with release of considerable energy; this is the fission process.

2.3) contd.

2.3.1) contd.

Characteristics of these reactions vary with neutron energy and also the target isotope. More than one reaction can occur with neutrons of the same energy incident on a given isotope, but with different probabilities.

2.3.2) Cross-section and Flux.

The probability of any neutron-induced event which is independent of the other events can be described in terms of a cross-section. Cross-sections can be assigned for scattering, capture, fission etc. The usual unit of cross-section is the barn (10^{-24} cm^2). Cross-section which is an average property of many nuclei is numerically equal to a geometrical cross-sectional area which individual nuclei would need to possess in order to give the observed reaction rate when bombarded by neutrons of the given energy. Because of the wave nature of the neutron this is in general different from the geometric area of the nucleus.

The study of interaction of neutrons is in fact the study of the cross-sections. The probability that a neutron in a medium will interact with a nucleus, regardless of what type of interaction, is called the total cross section, σ_T. It can be subdivided into partial cross-sections each proportional to the probability of the particular events. Thus

$$\sigma_T = \sigma(\text{el.scattering}) + \sigma(\text{inel.}) + \sigma(\text{capture}) + \ldots$$

The product of nuclear (microscopic) cross-

2.3) contd.

2.3.2) contd.

section and the number of atoms per unit volume is described as the macroscopic cross-section; it is usually denoted by Σ, with the appropriate subscript, and is measured in units such as cm^2 per cm^3 or more concisely in cm^{-1}. It is the macroscopic cross-section which is in general observed, and from it the nuclear cross-section can be deduced.

The macroscopic interaction rate is studied in terms of the neutron concentration in the medium. However, it is more convenient to deal with flux, which is given by concentration times velocity of the neutrons. Let a beam of neutrons of density n per c.c. having velocity v cm/sec be normally incident on a thin slab of material containing N nuclei. If σ is the cross-section per nucleus for a particular reaction then

interactions per second = σ nv N

The scalar quantity nv is known as the flux of neutrons of velocity v. In general, n incident neutrons can have any angular distribution and the reaction rate does not depend upon it. The general definition of flux is the number of neutrons passing through a sphere of 1 cm^2 cross sectional area around the position of consideration, with any angular direction. Its unit is cm^2 sec^{-1}. For some cases, such as when the flux is not isotropic, it becomes convenient to express an angular flux and from there the scalar flux; the flux that is commonly referred to is scalar flux -- flux density. The neutron flux is a measure of the combined

2.3) contd.

2.3.2) contd.

effect of the motions of neutrons, as evidenced by the interaction rate to which they give rise. This is analogous to chemical concentration or voltage. As voltage difference gives rise to flow of electric current between two points in an electrical circuit, so also flux difference gives rise to neutron current. Physically this is due to difference in reaction rates between the points.

2.3.3) Q-value of Reactions.

In all nuclear reactions except elastic scattering the internal energy of the nucleus is changed and the kinetic energy of the outgoing particle is different from that of the incident particle. The principle which governs the energy relationship is the law of conservation of energy - in the relativistic sense, with the equivalence of mass and energy. The Q-value of a reaction is the energy-equivalent of the difference in binding energies of the reaction system before and after the reaction. Thus for a reaction

$$a + X \rightarrow Y + b + Q$$

denoted by X(a,b)Y, the Q-value is

$$Q = (M_x + M_a - M_y - M_b)c^2 \qquad 2.5$$

The reaction is called exoergic or endoergic according as Q is positive or negative respectively. For an endoergic reaction energy must be supplied in order that it can take place. For neutron induced reactions this can be supplied through the kinetic energy of the

2.3) contd.

2.3.3) contd.

neutron. If Q is positive, energy is released and for most cases, except some fission reactions, the reaction can take place with zero energy neutrons. The released energy is mostly shared by the nucleus Y and the outgoing particle b, as their kinetic energies. The sharing is governed by the law of conservation of momentum before and after the reactions, and accordingly most of the energy is carried by the lighter particle b.

2.4) Classification of Neutron Interactions.

The complexity and diversity of the behaviour of neutron interactions with matter can be somewhat simplified by classifications depending upon similarities or dissimilarities, and schematics emerge out of these classifications. Several attempts have been made for such classifications [1,2,3]; most useful ones are according to target mass, neutron energy and reaction products. Divisions are however somewhat arbitrary.

According to Mass-number A:

Light nuclei, A = 1 to 25

Intermediate nuclei, A = 26 to 80

Heavy nuclei, A above 80.

According to Neutron Energy E_n:

Thermal neutrons. Those neutrons in thermal equilibrium with the matter of the medium in which these neutrons diffuse. They have a Maxwellian distribution in energy in a weakly absorbing medium the peak corresponding to 0.025 ev at 20°C.

Epithermal neutrons. The neutrons in the energy region above 0.2 ev.

2.4) contd.

Resonance neutrons	From about 1 ev to 1 kev
Intermediate neutrons	From 1 kev to 0.5 Mev.
Fast neutrons	Neutrons of energy above 0.5 Mev.
Fission neutrons.	Neutrons produced by fission which have a continuous spectrum from a few kev to about 20 Mev. The most probable energy is 0.8 Mev and average energy is 2 Mev.

According to Reaction Products.

This is a more clearly defined classification and follows according to reaction types mentioned in section 2.3.1 of this chapter - (n,γ), (n,n') etc.

Some of these reactions are sometimes grouped together e.g. the non-elastic cross-section, which is the total cross-section minus elastic scattering.

2.5) Mechanisms of Nuclear Reaction.

It is at present agreed that the various neutron interactions may occur by one or more of those fundamentally different mechanisms; these are

i) compound nucleus formation,

ii) direct interaction and

iii) potential or shape scattering,

Most of the elastic scatterings occur by shape scattering and some through compound nucleus formation while all other reactions take place is either or both of the first two processes. The importance of the different mechanisms varies over the energy range for different mass numbers of the nuclei. The potential scattering and compound nucleus formation is present at all energies but with variable cross-sections; the direct interaction becomes important only at higher energies.

2.5) contd..

2.5.1) The Compound Nucleus Formation.

The main feature of the mechanism of a reaction that proceeds by way of the compound nucleus is that the incident neutron is absorbed and a compound system is formed as an intermediate state. The compound nucleus then decays in various ways corresponding to the observed reactions.

The incident neutron brings in with it the binding energy B. In addition it will have some kinetic energy EK. The energy (B+EK) is available to the compound nucleus which raises it to an excited state.

2.5.2) Energy Levels in the Nuclei.

The nucleus like other quantum mechanical systems, possesses a set of characteristic energies or excited state. Of these the most stable or ground state is that in which nuclei are normally found. The general features of the excited states is that the first few levels above the ground state are widely spaced but the higher states get closer to each other; at very high energies they completely overlap. This pattern is found for both heavy and light nuclei but the scale changes very considerably in going from the lightest to the heaviest elements. For the lightest the first excited levels are a few Mev above the ground states; in the heaviest the corresponding figures are only several kev's. Over this general trend is superimposed the effect of odd-even combinations of protons and neutrons, due to which there are ups and downs in the energy state of the first levels

2.5) contd.

2.5.2 contd.

and interlevel spacings in the neighbouring isotopes of the same element. The energy states are thus peculiar to an individual nucleus and their close spacing is characteristic of a many body system. This fact - that a number of nucleons are simultaneously excited at a given energy state - greatly affects the characteristics of the nuclear reactions. For this reason excited states in nuclei can exist above the binding energy of a single nucleon.

The energy above which the contiuum excitation states can be assumed to exist (it does not have a definite boundary), is important for the nuclear theories of the reactions. For the medium weight nuclei, such as iron, they are assumed to exist for excitation energies above about 5 Mev and for the heaviest nuclei above 2 Mev. At an excitation energy of 7 or 8 Mev (corresponding to the neutron binding energy) the compound nucleus is in the contiuum but the residual nucleus is not; a generalized characterstic of the decay products emerge when both the compound and the residual nuclei can be at continuum region. The energy limits for continuum region therefore refer to the kinetic energy of the neutrons. At 14 Mev the excitation energy of the compound nucleus is considerable - for all but the lightest nuclei ($A<8$) it is above 21 Mev.

2.5.3) Decay of the Compound Nucleus.

The compound nucleus in the excited state, being unstable is able to decay. The decay can occur

2.5) contd.

2.5.3) contd.

in several ways. Limitations are in general imposed by energy availability.

The binding energy of the least bound nucleon in nucleus is called the virtual energy; excited states above the virtual energy are called virtual states or levels and below that bound levels. For nucleon emission to take place, it must be provided with at least the binding energy to make up for the mass defect. Thus nucleon emission can take place only from the virtual states. The virtual energy need not be the same as the binding energy of the absorbed neutron. In a few cases the virtual energy may be smaller and nucleon emission can take place with neutrons of zero energies e.g. $^{14}N(n,p)$ reaction. From the bound states, which are normally attained following particle emissions from the higher states, the nucleus can decay to the ground state only by gamma emission. The next important energy state is the first excited state of the residual nucleus. Below that a neutron may be emitted but it will come out with the total excitation energy (less the nucleus recoil energy), and gives the compound elastic scattering of the neutrons. The only other mode of decay available is of course by gamma emissions. When the incident neutron energy is at least equal to the first excited state of the residual nucleus, the nucleus may be left in that state following neutron emission. The nucleus then decays by a gamma emission. This explains the threshold for the (n,n') process. With the onset of inelastic scattering the

2.5) contd.

2.5.3) contd.

compound elastic scattering and gamma emission probabilities compete with it and gradually decline . At higher energies more than one level in the residual nucleus can participate. The mechanism of compound elastic and inelastic scattering from the individual levels is illustrated in Figure 2.1.

The decay of the compound nucleus proceeds as a statistical process. Following the formation of compound nucleus the nucleons are involved in continuous interchange of energy among them. Sufficient time is elapsed between formation and decay, which (of the order of 10^{-15} sec.) is large on nuclear scale. Through statistical fluctuations sufficient energy is concentrated on one of the particles so that it can come out of the nucleus. Like the radioactive decay law, a decay constant λ can be associated to the decay of a particular level. For practical purposes the decay is spontaneous as the decay is over in less than 10^{-14} sec. A given state will have a mean life time $\tau = 1/\lambda$. In accordance with the uncertainty principle a level width giving the uncertainty and hence spread of a quasi-stationary state, is defined by

$$\Gamma = \frac{\hbar}{\tau} \qquad 2.6$$

where $\hbar$ is the rationalised Planck's constant; Γ has units of energy. It can be seen the width is inversely proportional to the life time of the level.

The probability per unit time of each mode of decay of an excited state is described in terms of a

FIGURE 2.1-- Mechanism of Inelastic and Compound Elastic Scattering from an Individual Level of the Compound Nucleus: (after Lamarsh, ref.31.)

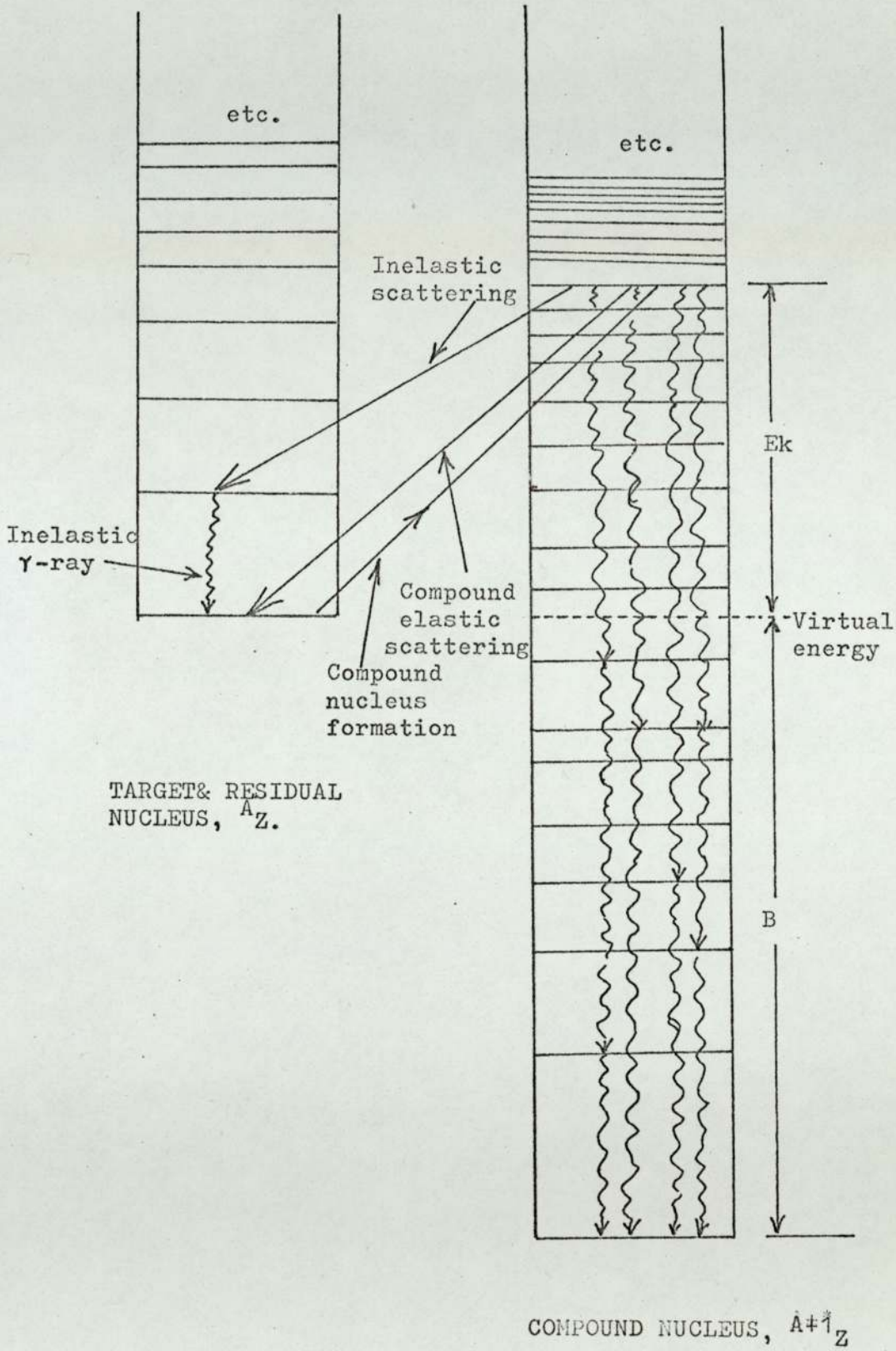

2.5) contd.

2.5.3) contd.

partial width, characteristic of each process. For instance Γ_γ, the radiation width is the probability (expressed in energy units) per unit time that the excited nucleus decays by γ-ray emission. Since the total decay probability is the sum of the probabilities for all possible processes at energies where only radioactive capture, compound elastic and inelastic scattering is possible, the total width is

$$\Gamma = \Gamma_\gamma + \Gamma_n + \Gamma_{n'} \qquad 2.7$$

and the relative probability for gamma emission is Γ_γ/Γ. From the definition of cross-section it is evident that this should be equal to $\sigma_\gamma/\sigma_{CN}$ where σ_{CN} is the cross-section for the formation of a compound nucleus. Hence at a neutron energy E the radiative capture cross-section is given by

$$\sigma_\gamma(E) = \sigma_{CN}(E) \ \frac{\Gamma_\gamma}{\Gamma} \qquad 2.8$$

These considerations enable one to see the various partial cross-sections as competitive to each other. At higher energies, as the cross-section for compound nucleus formation is smoothly varying with energy, at the onset of the threshold of a reaction which becomes energetically possible the other cross-sections usually begin to fall.

2.5.4) Cross-section for Compound Nucleus Formation.

If there is an excited state in the compound nucleus in the vicinity of the energy (B+EK), the excitation energy, the probability of the formation of

2.5) contd.

2.5.4) contd.

the compound nucleus is very lage; the cross-sections for the reactions that are energetically possible are also high. The distinct peaks in the cross-sections that corresponds to nuclear excited states are called resonances. In the neighbourhood of a resonance, and when only one level is close enough in energy to be important the cross-section for the formation of a compound nucleus by neutron absorption is given by Breit-Wigner one level formula

$$\sigma_{CN}(E) = g\pi\lambda^2 \quad \frac{\Gamma\Gamma_n}{(E-E_o)^2 + \Gamma^2/4} \qquad 2.9$$

Here Γ is the total width for the excited level, Γ_n is the partial width for neutron emission (compound elastic scattering), E is the excitation energy provided by the incident neutron and E_o is that for the peak of resonance. The factor 'g' is the statistical weight factor. If ℓ is the angular momentum of the incident neutron, $g = 2\ell+1$. For low energy neutrons (below a few hundred kev), only neutrons of zero angular momentum are involved and g=1. λ is the rationalised wavelength of the incident neutrons

The Breit-Wigner single level formula is one of the few happy instances when the theoretical relation agrees well with experiments over a wide range. The parameters are however empirically obtained. At the low energies the resonances are mostly composed of radiative capture and compound elastic scattering, the relative proportion of which vary from resonance to resonance.

~~For high energy neutrons when the levels begin~~

2.5.4) cont'd.

For high energy neutrons when the levels begin to interfere with each other the single-level formula does not apply. In the continuum region in general the σ_{CN} vary smoothly in contrast to its behaviour in the resonance region. Weisskopf and co-workers have developed the theory for continuum region, which can be used for incident energies greater than about 3 Mev for elements with A > 50, averaged over many resonances to give

$$\sigma_{CN} \simeq (R + \lambda\!\!\!^{-})^2 . T\ell \qquad 2.10$$

where R is the nuclear radius and $T\ell$ is called transmission coefficient, the fraction of the particles that will penetrate the nuclear surface. $T\ell$ can be calculated in terms of wave number of the neutron inside and outside the nucleus. However, at the high enough energy when the wave length of the neutron is very small compared to the nuclear dimension $T\ell$ approaches unity and σ_{CN} approaches

$$\sigma_{CN} \simeq (R + \lambda\!\!\!^{-})^2 \simeq \pi R^2 \qquad 2.11$$

Equation 11 is a well verified formula. For example, at 14 Mev the experimental non-elastic cross-section which is equal to the compound nucleus formation cross-section at high energies, for all the elements of mass number from above 20 is found to agree with those given by equation 2.10 [4].

The cross-section for potential scattering also tends to a value of πR^2 at high energies, so that the total cross-section tends to a value of $2\pi R^2$. This is only approximate and does not include broad resonances.

2.5) contd.

2.5.5) Direct Interaction.

Neutrons above a few Mev are known to interact with nuclei also by direct interaction. A direct process is essentially a one step process in which particles can be emitted. At higher energies thus (n,n'), (n,p),(n,α) etc. have got two components - one due to compound nucleus formation and the other by direct process. With increasing neutron energy the direct process contributes more.

The direct process is a nuclear surface phenomena. Some of the direct interactions are studied in other branches of physics; these are stripping and pickup reactions. In the process involving particle emission the first event is a collision between the incident particle and a nucleon near the surface of the target nucleus and the momentum is transferred to it. If a mean free path of the latter is assumed of the order of nuclear dimensions the struck nucleon may emerge from the nucleus without the formation of a compound nucleus and the direct process is complete. The conservation of angular momentum restricts the emissions to the surface of a certain cylinder and nuclear absorption confines it to large radii [5,6]. Thus the effective scattering elements are the two spherical caps at the ends of the cylinder.

The energies of the emitted particles are higher for direct interactions than the average energy of evaporation spectrum of compound nuclear products. Another feature of the direct interaction is that the emitted particles are forward peaked compared to a symmetry around 90° in the angular distribution of the latter.

2.5) contd.

2.5.5) contd.

This property is often used to seek out the direct interaction components in the observed spectra. Above the bombarding neutron energy of 10 Mev, the direct mechanism can contribute 15 to 30 per cent of non-elastic scattering events.

2.5.6) Potential Scattering.

While the compound elastic scattering is only significant at lower energies, particularly at the resonances, potential scattering can be prominent at all energies. At the higher energies most of the elastic scattering is through potential scattering mechanism. The process is analogous to diffractions in optics, in which the nucleus appears as a black circular disc(in the mathematical scheme of the optical model the nucleus represents a potential) in the path of a nuetron wave and diffraction patterns are produced as a result of interference between the incident wave and the scattered wave. The resultant pattern has a pronounced maximum in the forward direction into a cone of semi-angle λ/R, followed at moderate angles by successive minima and maxima. There can be small peaks at back angles. The intensity of the forward peak increases with increasing energy. Since the potential scattering is dependent upon the size and shape of the nucleus this process is also called shape elastic scattering.

2.6) Nuclear Models.

That both the static and dynamic properties of the nuclei are dealt with by models rather than exact theories is due to the fact that we are unable to solve the nuclear many body problem exactly. The purpose of a model is to provide a means of explaining the nuclear properties and if possible predict the cross-sections. In the models our knowledge of the fundamental laws of nuclear force is incorporated in a general phenomenological and simplified way. However, as nuclear reactions proceed via several mechanisms in a complex way it is hardly possible for one model to cope with all the nuclear properties. In the absence of any catholic concept several models survive side by side, each successful in its own way but failing in some other tests.

The models have been developed almost in two extreme lines. The liquid drop model type which explains the reactions through compound nucleus formation has little connection with structural models of the individual particle type which can describe the direct interaction mechanism. Inherently this diversity is due to the wave and particle duality shown by the neutron, like other fundamental particles. The optical model attempts to fuse together these two types of approach. In particular, the optical model combines together the compound nucleus model and the statistical model. Also the shape elastic scattering which cannot be described well by the other models finds an adequate description in the optical model. The essential features of the optical model and statistical model calculations has been worked out by several authors within a few years of the early fifties, when the experimental evidence of the properties of the reactions with the high energy neutrons accumulated and

2.6) contd.

the general patterns emerged. Several versions of them exist but the formulation that is extensively used for the statistical theory calculations is that of Hauser and Feshbach [7]. Modifications and extensions to this have been made later by others.

2.6.1) The Compound Nucleus Hypothesis.

The general features of nuclear reactions with the slow and intermediate energy neutrons are easily explained by the Bohr-Breit-Wigner compound nucleus theory. There are several evidences that compound nucleus is formed for these reactions. For example, the delay between the incidence of the neutron and the emission of the gamma rays following it is too large to be explained otherwise. The delay which can be inferred from the measured radiation widths, is about 10^{-15} second while the time needed for straight forward crossing of the nucleus by the neutron is only about 10^{-21} second. The other assumption in the original Bohr's model, that the particle or particles emitted from the compound nucleus would bear no genetic relation to the way the compound nucleus was formed, is found to be inadequate. However, where the simple compound nucleus picture of Bohr is found to fail and the optical model to suceed is at the high energies, when the cross-sections show definite broad resonances (called giant resonances), that cannot be explained by the Bohr model. Apart from the direct interaction component, the rest of the reactions is still assumed to result ultimately through the

2.6) contd.

2.6.1) contd.

formation of compound nucleus. But the formation mechanism in the new model is basically altered, according to which the compound state proceeds through several steps, which are elaborated in the optical model.

2.6.2) Statistical Model.

The statistical model practically, though not conceptually, can be considered as an extension or complement to the compound nucleus theory at higher energies. In this model, assumptions are made of the internal state of the nucleus at high excitation energies and the behaviour of the reactions are worked out from it.

The statistical model deals with the cross-sections in the continuum region of the excited states. In the theoretical development it is assumed that the phases of the resonances have random sign and similar magnitude so that they add up to zero. To a great extent the treatment of average cross-section employs an evaporation model with only a partial basis in nuclear reaction. The nucleons in the nucleus behaves as the heat motion of the molecules of a liquid involving continuous interchange of energy between nucleons by means of collisions. Through statistical fluctuation enough energy is concentrated on one particle to eject it from the nucleus - a process analogous to evaporation from a liquid. The usual thermodynamic quantities, including

2.6) contd.

2.6.2) contd.

entropy and temperature are introduced in this way and the velocity distribution of the emitted particle is Maxwellian with a characteristic "temperature". Developments of nuclear reaction theory along statistical lines are due to Wolfstein [8] and to Hauser and Feshbach [7]. Later modifications have been made by Moldauer [9].

The statistical model gives qualitative agreement with many features of nuclear reactions including the yield energy curves of proton and α-particles induced reaction, the relative yields of single and double neutron emission and their energy distribution following nuetron bombardment. However the quantitative predictions of the statistical model are less satisfactory.

2.6.3) The Shell Model.

The shell model is a structural model and explains many of the finer characteristics of the nuclei. In its simplest form the shell model assumes independent particle motion, i.e. the nucleons are virtually free to move about in an average uniform field and are subject only to the requirements of the exclusion principle. Most of the nucleons are paired and this way odd-even variation in the excitation energy level and the binding energies are explained. The nuclear configuration is such that the nucleons are arranged to close in succeeding shells. The periodicities in nuclear cross sections and the level densities can be adequately explained in terms of this.

2.6) contd.

2.6.4) The Optical Model.

The optical model treats the nuclear reactions in analogy with the propagation of light through a partially absorbing medium. According to this model the target nucleus consists of nucleons in independent particle states given by an average potential. The incoming neutron wave encounters firstly this potential which leads one part of the wave to be reflected and the other part entering inside the potential. The latter at first encounters one nucleon in the target nucleus and then with others until a state of compound system is formed. At energies above the threshold for particle emission the formation of the early two particle state will include the possibility of direct ejection of a nucleon from a shell model state and this process will compete with the more complicated reactions which proceed via chaotic conditions in the compound system. At low energies the compound state simply leads to an absorption. At higher energies, for which the model is more suited, the compound system decays as in the statistical theory.

The incident particle sees the target nucleus as a region of complex potential given by

$$V(r) = - [V_o(r) + i\, W_o(r)] \qquad 2.12$$

The real part V_o is the potential required by the shell model and accounts for reflection while the imaginary part for absorption. The Schrödinger equation when solved for the optical potential gives the shape elastic scattering and the reaction cross-section.

2.6) contd.

2.6.4) contd.

The model predicts the total cross-section directly. The absorption cross-section calculated from the model is identified as the mean cross-section for formation of the compound nucleus which includes both the reaction cross-section and the compound elastic cross-section. However at higher energies, when several decay modes are possible the compound elastic tends to zero. The model does not predict compound elastic scattering. If the parameters of the models are known the angular distribution of potential scattering can be predicted to a satisfactory degree. The giant resonances of width about 2 Mev, and regular variation of their positions with size of the target nucleus can also be accounted for by the optical model. These two successes mainly underlines the validity of the model within the approximations used as its basis.

Provided the parameters of the model are known other cross-sections at the high energies can also be obtained using the Hauser-Feshbach version of the statistical theory of compound nucleus. The parameters can be obtained from the experimentally obtained shape elastic angular distribution. Several forms have been suggested for the potential. The potential that has been most successful is the one proposed by Björklund and Feshbach [10].

Predictions for the (n,p) and (n,α) cross-sections by the optical model is not satisfactory; the

2.6) contd.

2.6.4) contd.

calculated values may disagree with the experimental ones by a factor of 2 or more [29]. That is why these are the least known of all cross-sections. However, satisfactory agreement for inelastic neutron scattering can be obtained on a semi empirical treatment [20]. The region of validity of the model begins at energies where the energy levels of the residual nucleus begins to merge into a continuum. For lower energies, reference must be made to the more complete resonance theory of nuclear reaction.

Relevance of the optical model to the cross-section technology is that, experimental values are not available at all the energy points for an isotope nor for all nuclides at a given energy. The optical model as it stands at present can be reliably used to extrapolate and interpolate the data with respect to energy or mass number, from the known values. The use of the optical model to fill the experimental data of the ^{238}U up to 15 Mev has been listed in detail by Parker [20] in his compilation work on uranium.

2.7) General Features of the Cross Sections.

The general features of cross sections, correspond to the energy levels of the nuclei. In the light nuclei the resonances persist up to 6 to 8 Mev; they are few in number and are broader. The resonances in the heavy nuclei on the other hand are narrow and high and more numerous. The first resonance of ^{238}U is at 6.7 ev; they can hardly be resolved

2.7) contd.

after 4 kev.

The thermal region is free from resonances. There are two general types of total cross-sections at this region. If the nucleus is weakly absorbing most of the interaction is elastic scattering, which gives a flat curve. But if the absorption is significant, the absorption cross-section increases monotomically with the decreasing energy from the valley of the first resonance well into the thermal region, and this is superimposed on the constant cross-section for scattering.

At the high energies, in general, the total as well as the partial cross-sections are smooth function of energy, and their values are moderate. The total cross-section for all elements at 1 Mev is only a few barns. The cross-sections of iron and uranium - 238 in the region from about 1 Mev to 15 Mev are shown in figures 2.2 and 2.3 respectively.

2.8) Elastic Scattering.

Elastic scattering is one of the more difficult neutron interactions to measure; it is often obtained by subtracting the cross-sections for all other processes from the total cross-section, which can be more easily measured in the transmission type experiments. However, elastic scattering is of great interest for reactor calculations and to nuclear theory.

Elastic scattering consists of the shape
elastic scattering and compound
elastic scattering and experimentally
one cannot be separated from the other. However, at lower energies and away from the resonances the elastic scattering

Figure 2.2-- Cross-sections of Iron from 1Mev to 15Mev. (After Howerton [180]).

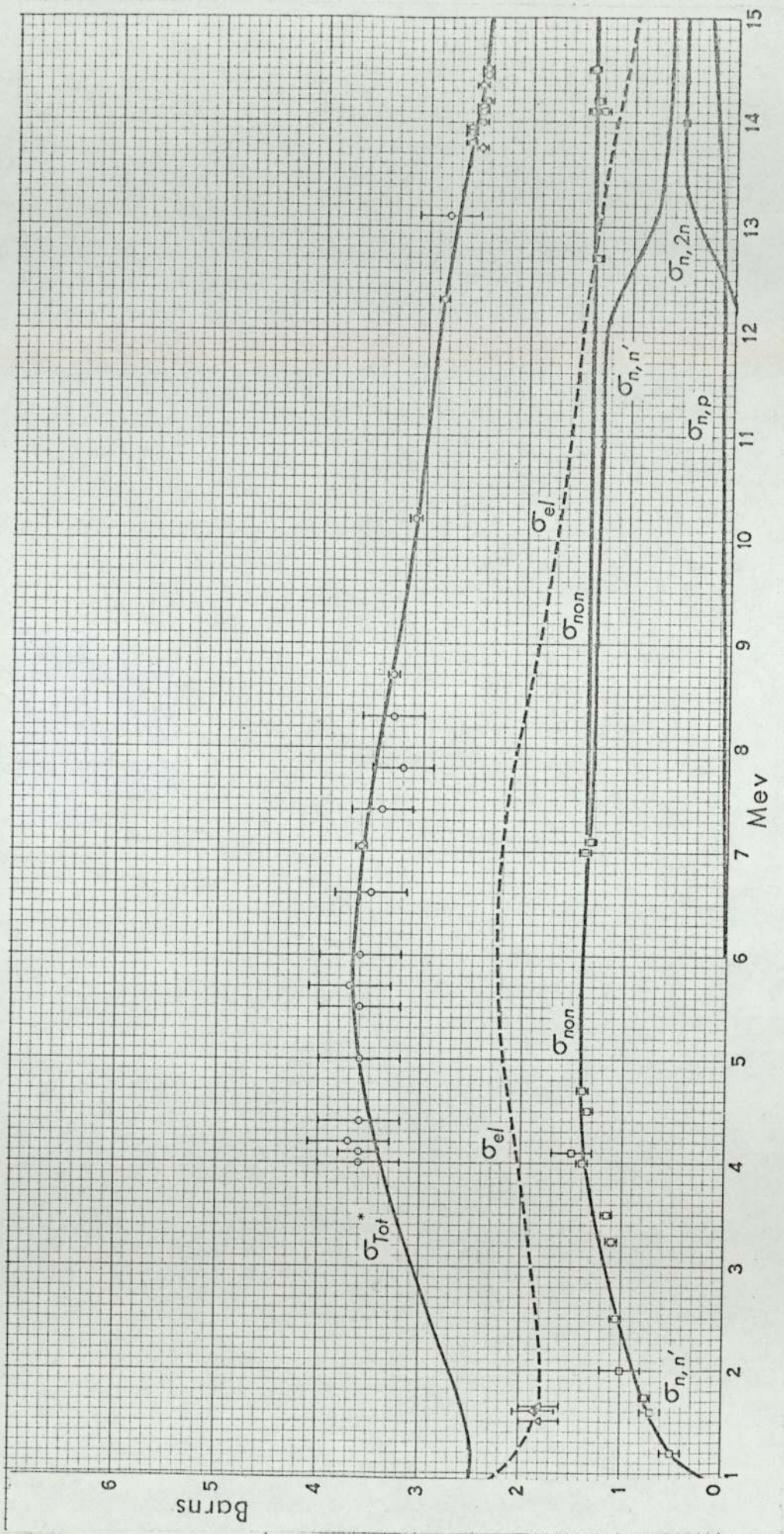

Figure 2.3-- Cross-sections of Uranium-238 from 1Mev to 15Mev. (After Howerton [180]).

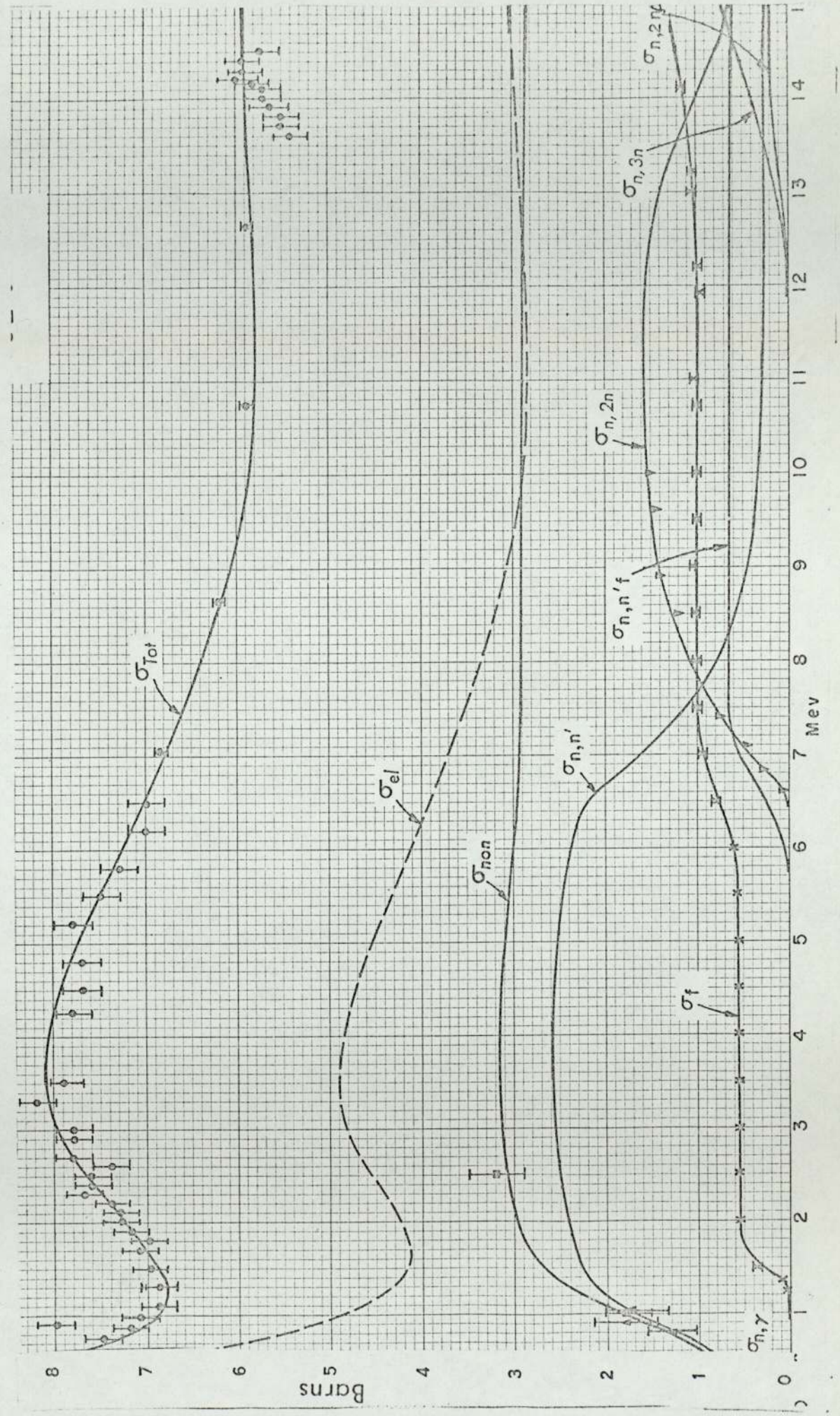

2.8) contd.

is constant and is adequately given by

$$\sigma_{s.p} = 4\pi R^2 \qquad 2.13$$

where R is the geometrical radius of nucleus as given by eqn.2.1. This expression gives a value of about 10.5 barns for the fissionable nuclei.

Near and at resonances the contribution from compound nucleus will be added; this is represented by the single level Breit-Wigner formula. However the component terms cannot be algebraically added due to the interference of the potential scattering with the resonance scattering, their amplitude being added coherently. The interference effect results in pronounced asymmetry with a dip in the lower side of the resonance, where the resultant is smaller than the cross-section due to potential scattering alone. This feature can be used to distinguish the resonances where scattering is predominant from those where capture is the main phenomenon. Iron has a deep minima at 29 kev, which is of particular interest in shield designs, as it sets up a "window" for neutron streaming. Above the resonance region the potential scattering decreases from its low-energy value of $4\pi R^2$ and begins to approach the asymptotic high energy value:

$$\sigma_{s.p} \simeq \pi(R+\lambda\!\!\!^{-})^2 \simeq \pi R^2 \qquad 2.14$$

However a few broad resonances are still exhibited, which occur at the same energies as the giant resonances in the total cross-section.

The compound elastic scattering becomes negligible with increasing energies away from the resonances. This is particularly so as soon as other modes of decay becomes

2.8) contd.

available. Thus at high energies approximately half of the total cross-section is of elastic scattering which is mostly potential scattering.

2.8.1) Angular Distribution of Elastic Scattering.

The angular distribution from resonances is complex as it depends upon the angular momentum of the level, but in general is assumed isotropic. Potential scattering of s-wave neutrons ($\ell=0$) is isotropic in the centre-of-mass system; s-wave scattering is the only mode of potential scattering possible when $KR \ll 1$ where $K(= {}^{1}/\lambda)$ is the wave number of the neutrons. Isotropic s-wave scattering is observed in the light nuclei up to a much higher energy than in heavy nuclei. However when $KR \approx 1$ (at few hundred kev for the medium and heavy elements) the s-wave begins to interact with the nucleus and scattering ceases to be isotropic. The angular distribution in this case tends to become forward peaked. As the value of KR is increased with increasing energy, more partial waves interact and the scattering becomes increasingly forward peaked, when a large fraction of the scattering is confined in the forward peak - a cone of semi-angle $\sim \lambda/R$. Secondary maxima and minima appear at larger angles; with increasing neutron energy they move to smaller angles. With increasing mass number the effect is similar (but not identical) to that due to increasing energy. However isotopes of different elements but same mass number have similar differential elastic scattering cross-sections.

2.8) contd.

2.8.1) contd.

Angular distribution of elastic scattering of fast neutrons of several energies with iron and uranium are shown in Fig.2.4.

2.8.2) Average Cosine of Scattering-angle: $\bar{\mu}$

In general scattering is anisotropic in the laboratory system. For the light elements the scattering is assumed isotropic in the c.m (centre of mass) system up to several Mev; this means scattering is anisotropic in the laboratory system even at low energies. On the other hand for heavy elements the laboratory system is practically the same as the c.m. system. For them scattering can be assumed spherically symmetric up to about 100 kev or so. For reactor physics calculations the average effect of anisotropy is considered by the average cosine of the scattering angle per collision measured in the laboratory system. This is given by

$$\bar{\mu} = \frac{2\pi}{\sigma_s} \int_{-1}^{+1} \sigma_s(\mu)\mu \, d\mu \qquad 2.15$$

where $\mu = \cos\theta$ and θ is measured in laboratory system. In the simple cases where scattering is isotropic in the centre of mass system, for an element of atomic weight A, the average cosine is given by, $(A >> 1)$:

$$\bar{\mu} = \frac{2}{3A} \qquad 2.16$$

For anisotropic scattering in the centre of mass system $\bar{\mu}$ is numerically calculated from experimentally known distribution, according as equation 2.15.

The forward scattering lessens the effectiveness

FIGURE 2.4a-- Differential Elastic Scattering Cross sections of Iron at Several Incident Neutrons Energies as a Function of the Scattering Angle.(From BNL-400 , 181).

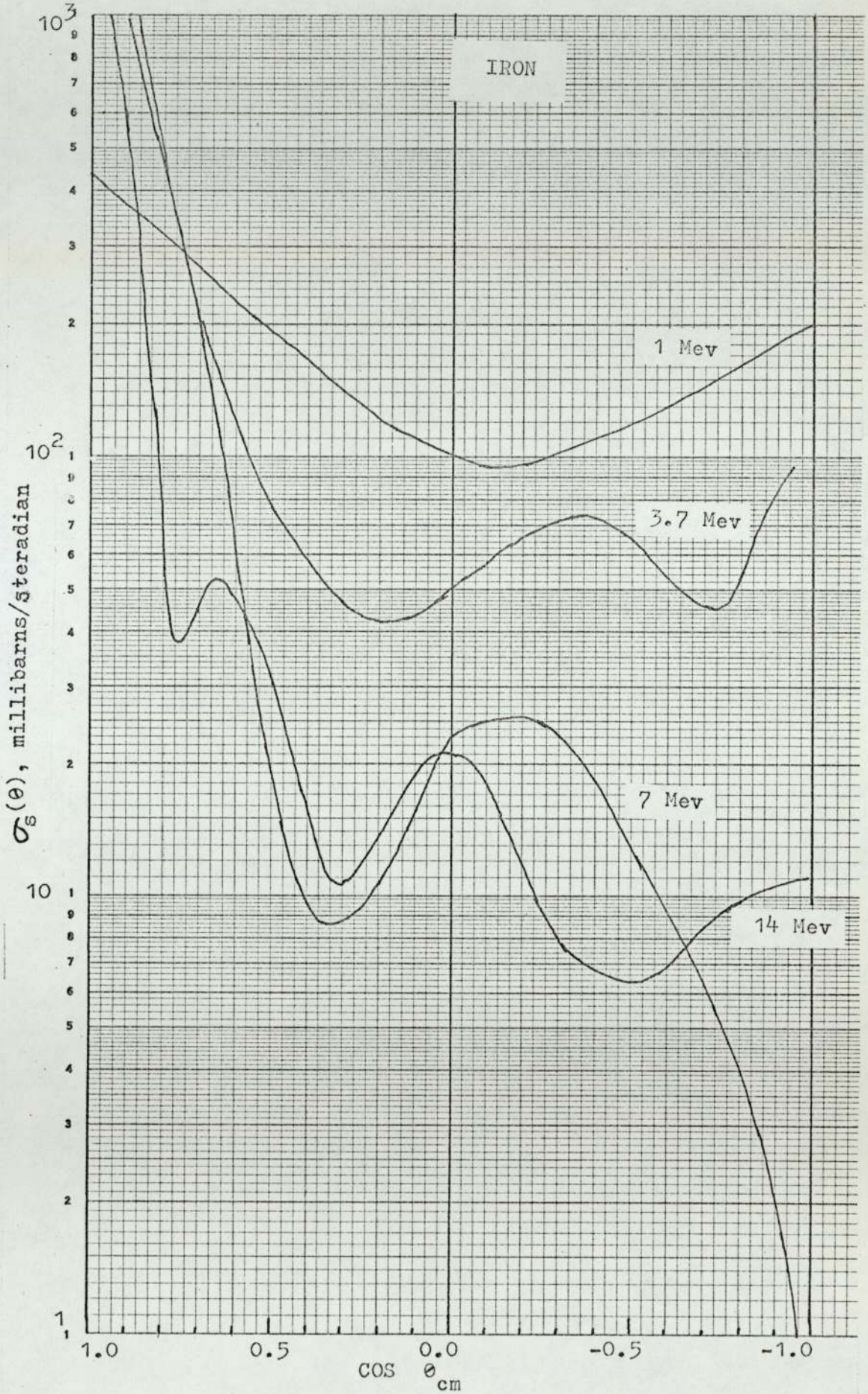

FIGURE 2.4b-- Differential Elastic Scattering Cross Sections of Uranium at Several Incident Neutron Energies as a Function of the Scattering Angle. (From BNL-400,181).

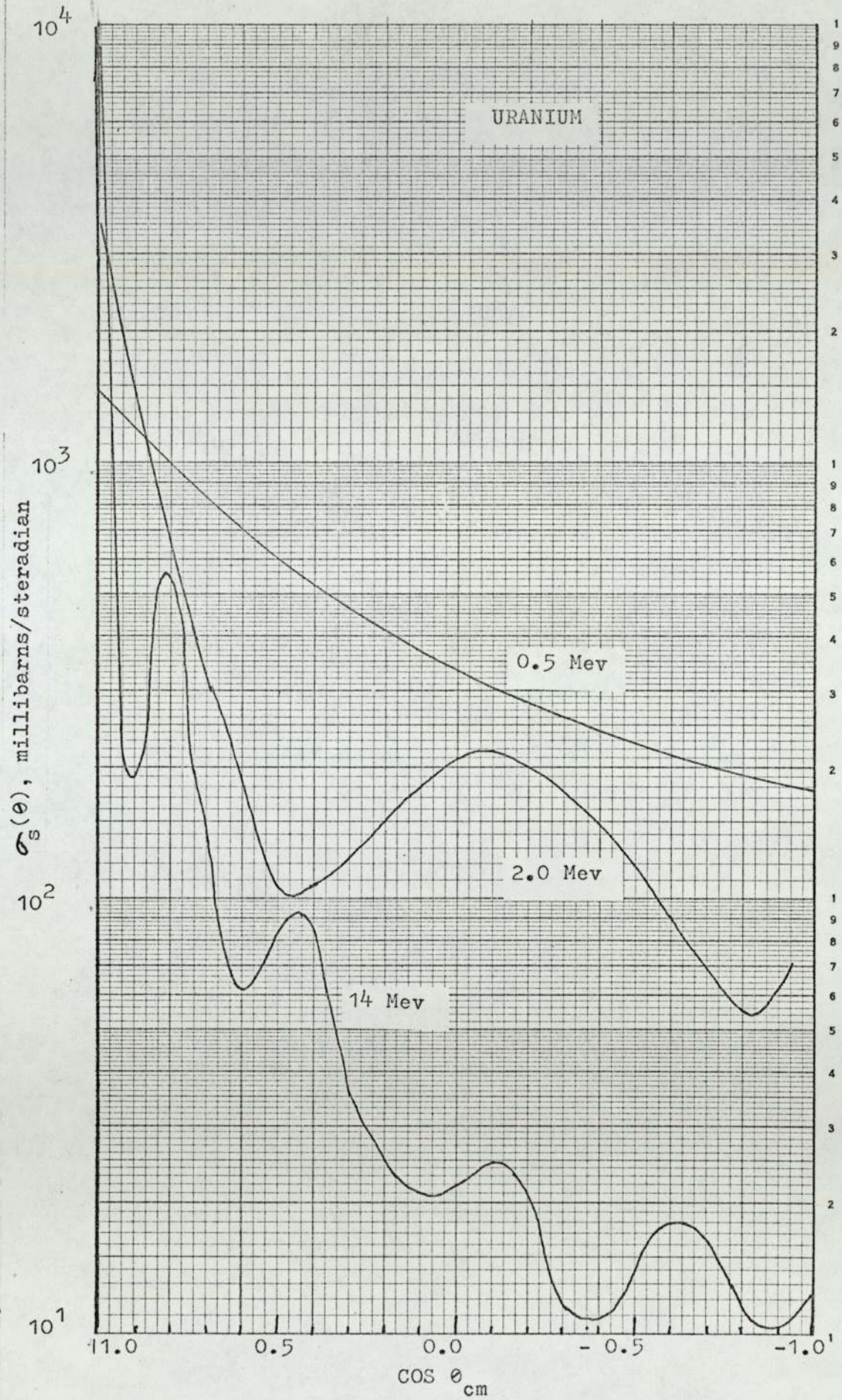

2.8) contd.

2.8.2) contd.

of moderators in slowing down because the energy loss is smaller at smaller scattering angle and the average distances which neutrons migrate before being slowed down increases. For this reason also the leakage of the neutrons is increased. Variation of μ with energy for three elements (uranium, iron and aluminium) are shown in Fig.2.5. At 14 Mev for the medium weight and heavy nuclei $\bar{\mu}$ is greater than 0.8. The nuclei have the same value for average cosines down to about 5 Mev. A few broad resonances are exhibited below 1 to 2 Mev.

2.8.3) Slowing Down of Neutrons by Elastic Collisions.

The energy of the neutrons is reduced as they suffer elastic scattering with nuclei of the medium. The angular distribution is interpreted in terms of neutron waves; for reduction of energy hard billiard ball like collision is valid. Below 15 Mev the neutrons are non-relativistic (change in mass is less than 2%) and Newtonian mechanics can be used. The energy loss as function of angle through which the neutron is scattered and the mass of the nucleus, can be obtained from the principle of conservation of kinetic energy and momentum. The calculations turn out to be simpler in the centre of mass system, in which the frame of reference has its origin fixed at the centre of mass of the neutron and the nucleus. The results can then be converted into the laboratory system (view point is that of an

Figure 2.5-- Average Cosine of the Elastic Scattering Angles for Uranium, Iron and Aluminium as Function of Energy.

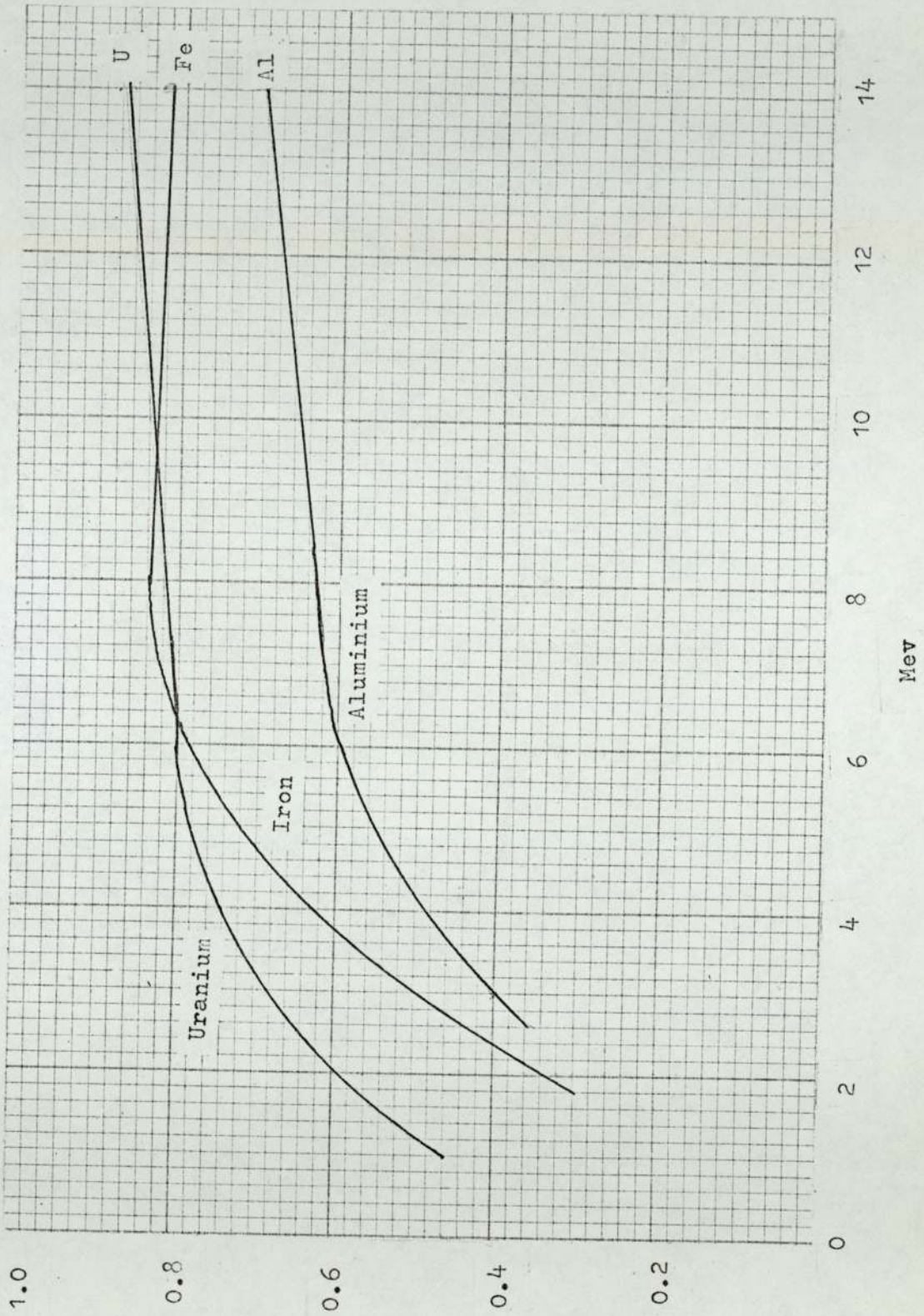

2.8) contd.

2.8.3) contd.

external observer). The calculations are given in the standard text books on reactor physics. Some of the important results are as follows.

If ψ is the scattering in the c.m. system, and A is the atomic weight of the target nucleus, the ratio of the neutron energy after collision to that before, E_2/E_1 is given by

$$\frac{E_2}{E_1} = \frac{A^2+2A\cos\psi+1}{(A+1)^2} \qquad 2.17$$

If θ is the angle of scattering in the laboratory system

$$\cos\theta = \frac{A\cos\psi + 1}{(A^2 + 2A\cos\psi + 1)^{\frac{1}{2}}} \qquad 2.18$$

Equation 2.17 shows that the maximum possible energy loss in a collision with a nucleus of given mass occurs when $\psi = 180°$:

$$\left(\frac{E_2}{E_1}\right)_{min} = \left(\frac{A-1}{A+1}\right)^2 \qquad 2.19$$

When $\psi = 180°$, $\theta = 180°$; they have the same values also at 0°. But at all other angles θ is always less than ψ. When A is large E_2/E_1 is very close to 1 for all ψ. For carbon, the maximum loss is 28%, for iron it is 7% and for uranium only 1.7%. For cases when scattering is isotropic in the c.m. system the average loss is half of the corresponding maximum loss. For forward bias in scattering the average loss is obviously less than that.

2.9) Inelastic Scattering.

2.9.1) (n,n') Reaction Neutrons.

When the energy E_o of the incident neutron exceeds the excitation energy of the first level above the ground state of target nucleus, inelastic scattering becomes energetically possible, since the product nucleus may then be left in an excited state following the neutron emission. For (n,n') reaction the target and product nucleus differ only in that the product nucleus is in an excited state. If E_1 is the energy of the first excited level the kinetic energy of the emitted neutron is $E = E_o - E_1$. Thus for incident monoenergetic neutrons above the first level but below the second, the emitted neutrons will also be monoenergetic. If energy is high enough to involve several of the excited states of the product nucleus, the compound nucleus can decay via any one of these levels and the emitted neutrons will have discrete energy spectrum, the spacing of the lines being equal to the energies of the excited levels. Such a spectrum from iron with 4 Mev neutrons is shown in Fig.2.6; this was obtained by Hopkins and Silbert[11] by the time of flight technique at a laboratory angle of 50°. The corresponding levels of ^{56}Fe are also shown in the figure. Energy of the first level of some of the reactor materials are shown in table below. The first level practically gives the inelastic threshold energy for the isotope.

FIGURE 2.6-- Spectrum of the Inelastically Scattered Neutrons from Iron with 4 Mev Incident Neutrons. (From Hopkins and Silbert, 11).

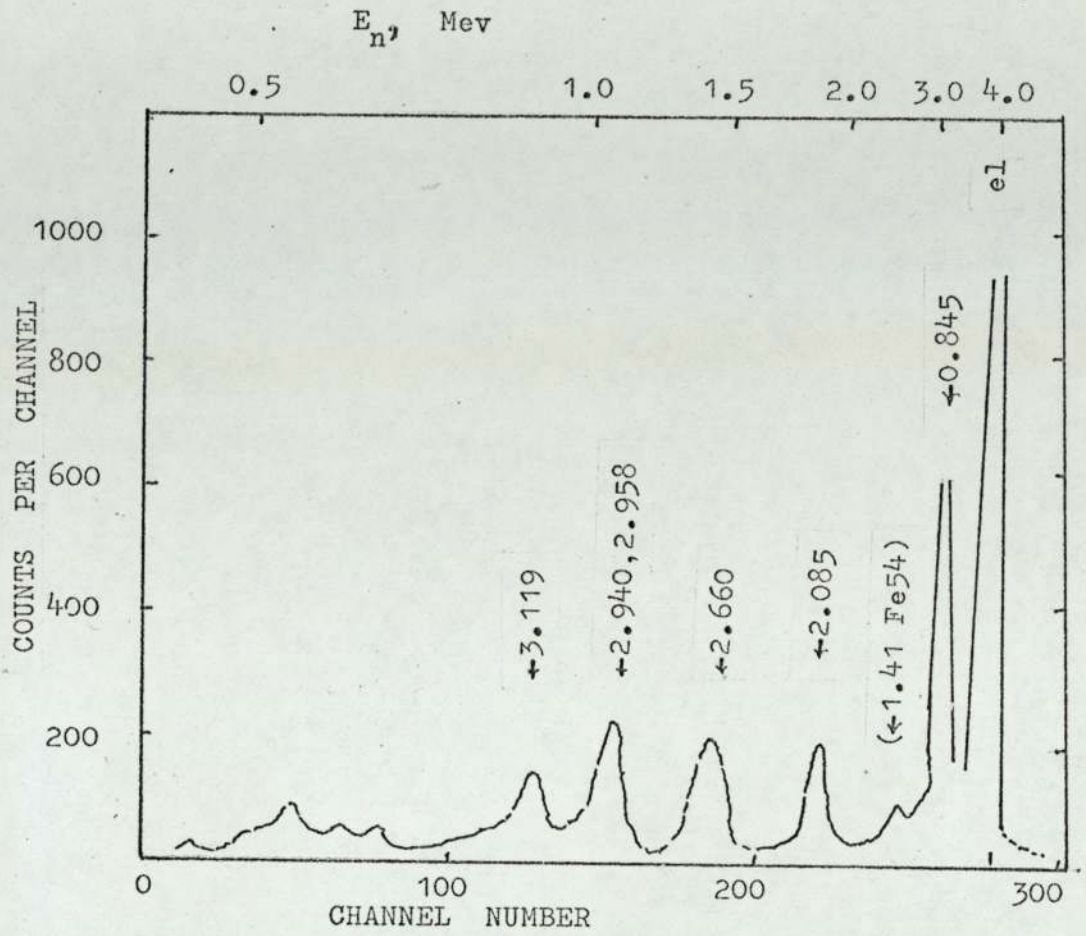

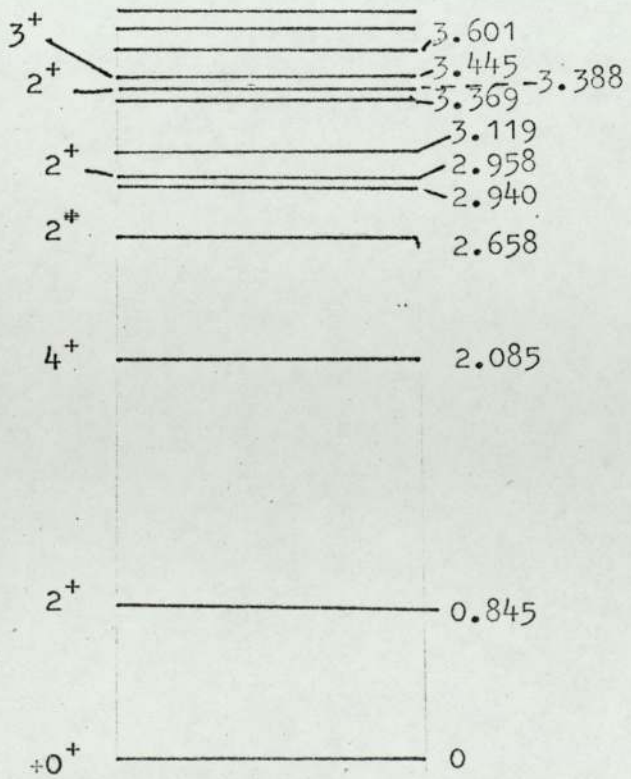

Energy level diagram of ^{56}Fe (in Mev).

2.9) contd.

2.9.1) contd.

TABLE 2.1

Inelastic Scattering Threshold Energies in Some of the Reactor Materials (After Ref. 12)

Nucleus	Threshold Energy
^{23}Na	0.45 Mev
$^{27}A\ell$	0.84 "
^{54}Fe	1.41 "
^{56}Fe	0.84 "
^{57}Fe	0.014 "
^{58}Fe	0.80 "
^{232}Th	50 kev
^{235}U	13 "
^{238}U	45 "
^{239}Pu	7.8
^{240}Pu	43 kev

It will be noticed that the threshold energy is considerably higher for the even-even (Z and A), nuclei than those of the even-odd or odd-odd nuclei. It is also known that the level spacings for the first few excited states are wider for the even-even nuclei. Hence on the whole even-even nuclei give less inelastic scattering than the odd nuclei. This speaks in favour of even elements for structural material and heat transfer agents in the fast reactors. In practice other considerations decide the selection. However it can be noticed that both ^{238}U and ^{56}Fe, the major isotope of iron, are even-even. But ^{23}Na and $^{27}A\ell$, that may be present in the core and

2.9) contd.

2.9.1) contd.

the blanket are odd; despite this the threshold is still high due to the low mass number. In any case, the major fuels ^{235}U and ^{239}Pu are both odd and have the lowest of the thresholds for inelastic scattering.

There is a distinct cross-section for the excitation (called excitation function) of every level below E_o, as a function of E_o. These are in fact branching ratios for the compound nucleus decay. The observed inelastic scattering cross-section is the sum of these individual levels. The cross-section for the first 3 levels of uranium-238 is shown in Fig.2.7, as a function of incident neutron energy. When the levels at higher energies are available with increasing incident energy the cross-section for the lower levels begins to fall, though the total inelastic corss-section may be increasing. At higher energies when the continuum region of the product nucleus becomes energetically available the contribution from the lowest levels gets negligible and the spectrum for the emitted neutrons tends to be continuous. In the intermediate states a few small peaks may be resolvable at the upper region of the spectrum while the lower end is continuous as predicted by the statistical theory. At the upper end, small peaks may still be observed with high energy neutrons; these are mostly from direct interactions, and are superimposed on the continuous spectra given off by the compound nucleus (Fig.2.8). At energies when the effect of the individual levels are predominant, the experimental

FIGURE 2.7 -- The Cross Section for Exitation of the First Three Levels and the Total Inelastic Cross Section of ^{238}U. (The cross section for the levels higher than 300 kev are not shown.) From Yiftah et al, ref.183.)

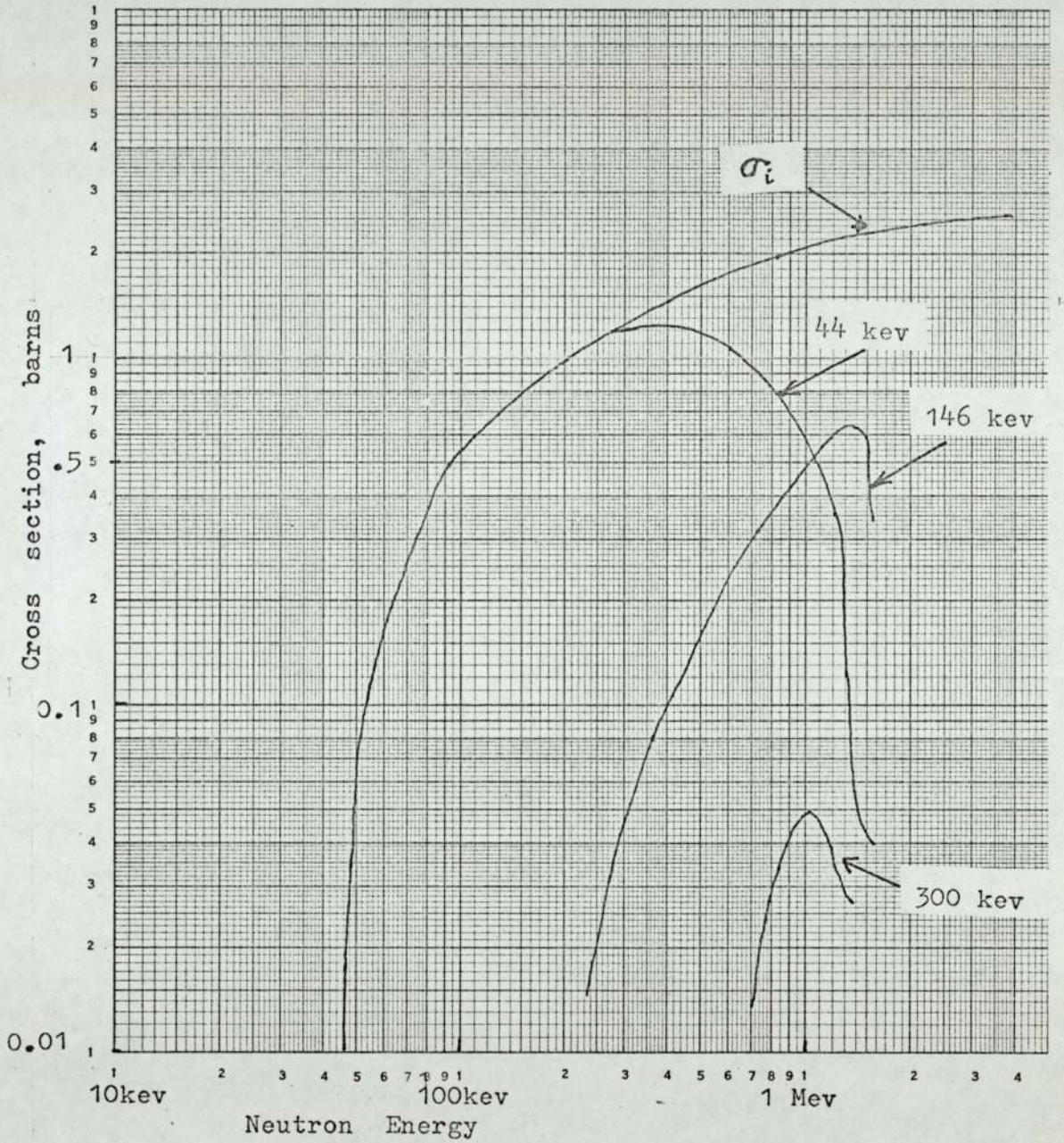

FIGURE 2.8-- Typical Spectrum of the Inelastically Scattered Neutrons with High Energy Incident Neutrons.

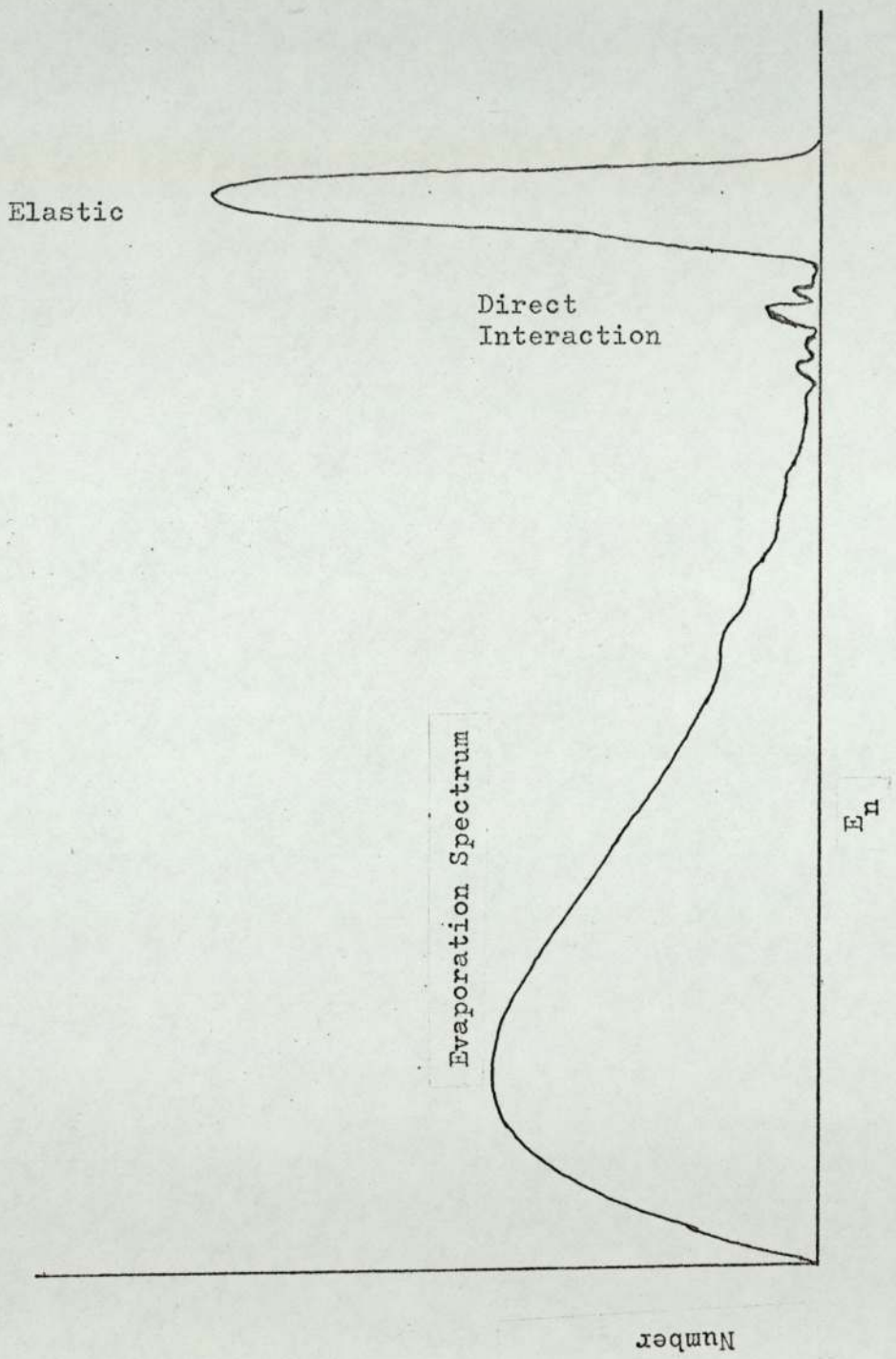

2.9) contd.

2.9.1) contd.

results [13,14] can be interpreted in terms of the detailed level theory [15] , while the continuous spectra with the high energy neutrons are adequately interpreted by the evaporation model of the statistical theory. For ^{56}Fe this begins at about 5 Mev and for ^{238}U about 2 Mev. The evaporation spectra is characterised by the nuclear temperature, T. If E_o is the incident neutron energy and $\sigma_{nn'}(E_o)$ is the cross-section for (n,n') reaction then the energy spectrum of the emitted neutrons is given by

$$\sigma_n(E_oE') = \sigma_{nn'}(E_o) \frac{E'}{T^2} e^{-E'/T} \qquad 2.20$$

According to the theory T should vary according to the square root of the ratio of incident energy to the product nucleus mass number. The constant of proportionality is obtained from experimentally obtained values. T is found to be given by the approximate relationship

$$T = 3.2 \sqrt{\frac{\overline{E}_o}{A}} \qquad 2.21$$

where T and E_o are expressed in Mev. This at 14 Mev for ^{56}Fe gives T = 1.61 Mev and for ^{238}U, T = 0.78 Mev.

The peak of the continuous spectrum is located at T. The average energy of the spectrum can be obtained by integrating equation 2.20; this gives

$$\overline{E}' = 2T \qquad 2.22$$

According to this result the bulk of the neutrons from the (n,n') reactions of the high energy neutrons around

2.9) contd.

2.9.1) contd.

14 Mev, with ^{56}Fe have energies in the range 1 to 3 Mev. The average energy for them is about 3.2 Mev. This means that a 14 Mev neutron loses on the average about 11 Mev on inelastic interaction. The slowing down capacity of inelastic scattering is demonstrated by this. The average energy loss by this process is not so strongly dependent upon the mass number of the target atoms, though it is more for the heavier nuclei, in contrast to the energy loss by elastic scattering. However the energy spread of the evaporation spectrum is so large that the neutrons cannot be described by the average energy, while elastic nutrons can often be. The fractional energy loss is more,higher the incident energy. The inelastic energy loss is obviously not applicable once the neutrons are below the threshold. This puts 850 kev for iron and 45 kev for uranium as the limit below which no degradation is done by inelastic scattering.

Most of the characteristics of inelastic neutrons with 14 Mev were known from measurements by Groves and Rosen and others [16,17,18] with nuclear emulsions in the early fifties. The evaporation type spectra is essentially observed. However for some elements including iron the data does not fit with a single Maxwellian. This is because of the contribution from the (n,2n) reactions with iron at 14 Mev. The (n,2n) threshold energies for these elements are below 14 Mev and for iron has got a substantial value at 14 Mev. For the heaviest elements the (n,3n) threshold energy is below 14 Mev

2.9) contd.

2.9.1) contd.

and this introduces further complexity in the emitted spectrum.

2.9.2) (n,2n) and (n,3n) Reactions.

Usually the inelastic scattering refers solely to (n,n') reactions, in reactor studies. Neutrons from multiple emission reactions are generally neglected because very few neutrons are available above the (n,2n) threshold. This omission is also caused by the fact that the (n,2n) reactions have not been studied in detail. They cannot be readily separated in the observations from the (n,n') neutrons. When they are assumed to be present, they are also termed inelastically scattering neutrons.

The same emission mechanism as of the (n,n') neutrons can be used to describe the multiple emissions; the process is just repeated. Accordingly, the first neutron of the (n,2n) and the (n,n') neutrons are emitted from the same state of the compound nucleus and given by one temperature, T_1 for the first nucleus. The energy distribution of these neutrons will be

$$\sigma(E_o,E') = \left[\sigma_{nn'}(E_o) + \sigma_{n,2n}(E_o)\right] \frac{E'}{T_1^2} e^{-E'/T_1} \qquad 2.23$$

Following this the residual nucleus is left with an excitation energy $E_1^* = E_o - E'$. If E_1^* is below the threshold B for the (n,2n) reaction the nucleus will decay to its ground state by gamma emission. But if E_1^* is above B, a second neutron can be emitted with a high

2.9) contd.

2.9.2) contd.

probability. The second neutron will be characterised by another temperature T_2 corresponding to an excitation energy $E_2^* = E_1^* - B = E_0 - E' - B$. An average value of T_2 can be assigned to it. The threshold of the (n,2n) reaction for iron is 10.8 Mev. Thus for 14 Mev incident energy the second neutron can be emitted corresponding to the first neutron energy below 3.2 Mev. Since a good fraction of the first neutron has this energy the (n,2n) reaction attains a substantial value soon after the threshold energy. At 14 Mev the iron (n,2n) cross-section is 500 mb. Further, as is evident from these considerations the (n,2n) reaction takes place at the expense of the (n,n') reaction, as a good fraction of the first neutrons are now included as part of the (n,2n) reaction. On the onset of the (n,2n) reaction the (n,n') cross-section begins to fall. From a value of 1.40 barns below the (n,2n) threshold the (n,n') cross-section falls to about half this value at 14 Mev. The second neutron gets its binding energy from the excitation energy left and the remainder may appear as kinetic energy. But for decay by inelastic scattering the residual nucleus (^{55}Fe) is left at least at its first excited state, so that the emitted neutron energy is less than the balance. These considerations show that the neutrons associated with the (n,2n) reaction are at lower energies while the high energy neutrons are from the (n,n') reaction.

The cumulative distribution of the first and the second neutron is given by

2.9) contd.

2.9.2) contd.

$$\sigma(E_o,E') = \left[\sigma_{nn'}(E_o)+\sigma_{n2n}(E_o)\right] \frac{E'}{T_1^2} e^{-E_1'/T_1} + \sigma_{n2n}(E_o) \frac{E'}{T_1^2} e^{-E_1'/T_2} \quad 2.24$$

Troubetzkoy [19] found agreement of this equation with experimental data from iron with high energy nuetrons; the values for the temperatures for iron he assigned

$$T_1 = \left(\frac{E_o}{4.3}\right)^{\frac{1}{2}} \text{ and } T_2 = \left(\frac{E_o-10.8}{2.8}\right)^{\frac{1}{2}}$$

where E_o is the incident neutron energy. This gives for 14 Mev T_1 = 1.80 Mev and T_2 = 1.07 Mev.

The relationship between the first and the second neutrons can be extended to that between the second and a third when the incident energy exceeds the threshold for (n,3n) reaction. For ^{238}U the threshold for the (n,2n) reaction is 6 Mev and for the (n,3n) 11.5 Mev. However in the fissionable nuclei the multiple neutron emission competes with fission i.e. instead of emitting the second and the third neutrons following the first, some of the nuclei undergo fission, increasing the fission cross-section. Nevertheless, ^{238}U has substantial (n,2n) cross-section of 1 barn at 14 Mev. As can be seen in Figure 2.3 both the (n,n') and (n,2n) cross-sections are falling, while the (n,3n) cross-section rising at 14 Mev. Parker [20] gives the energy distribution of these neutrons from ^{238}U.

2.9) contd.

2.9.2) contd.

Since the charged particle emission cross-section is small for the medium weight nuclei and insignificant for the heavy nuclei the compound nucleus formation cross-section is mostly composed of the neutron emission cross-sections for the medium weight nuclei and the neutron emission plus fission cross-sections for the heaviest isotopes.

2.9.3) Angular Distribution of Inelastic Neutrons.

The angular distribution of particles emitted from the decay of compound nucleus is expected to be symmetric about 90°, with more or less a flat profile. From the experimental evidence available for angular distribution from excitation of the individual levels of iron and other nuclei [11,21,22], it can be concluded, this is valid.

With higher incident neutron energy when the continuum region is reached part of the neutrons coming out with high energies are found to be forward peaked. The fraction with the forward bias increases with increasing incident energy as well as with the mass number of the target nucleus. With the 14 Mev nuetrons experimental work on iron and other materials [23-26] show that the part of the evaporation spectra below 4 to 5 Mev are emitted isotropically, while above that energy a considerable fraction is preferentially found in the forward hemisphere. At the backward direction from 90° to 180°, neutrons at all energies are found to

2.9) contd.

2.9.3) contd.

have a flat distribution. Bonazzola et al. [26] have measured the angular distribution in groups of 1 Mev energy spread above 5 Mev, from iron for an incident energy of 14 Mev; a rough calculation of μ, the average of the cosines of the scattering angle, gives a value of 0.26 for the group 9 to 10 Mev and 0.11 for the group 6 to 7 Mev. However the average cosine for the entire spectrum will be much less than these figures, because relatively fewer neutrons are emitted with high energies. The forward bias is due to the direct interaction component in the (n,n') reaction.

For uranium as well, below 5 Mev the secondary neutrons are found to be isotropic, while those with higher energies are found to have stronger anisotropy than for iron. The angular distribution of the energy band 5-12 Mev from ^{238}U, with incident energy 14 Mev are shown in Figure 2.9.

2.10) Radiative Capture (n,γ) Reaction.

The (n,γ) reaction is one of the most important reactions for reactor physics. The neutron balance and economy mostly depends upon it. The conversion and breeding of the fertile isotopes into fissile take place through this reaction. The reason why breeding is possible in fast reactors and not the thermals is based upon the fact that the proportion of the (n,γ) reaction at fast reactor energy is smaller in the medium weight structural materials than that in the heavy fertile

FIGURE 2.9--- Angular Distribution of Inelastically Scattered Neutrons of Energies from 5 to 12 Mev, from Uranium-238 with Incident Neutron Energy of 14 Mev. (After Parker[20]).

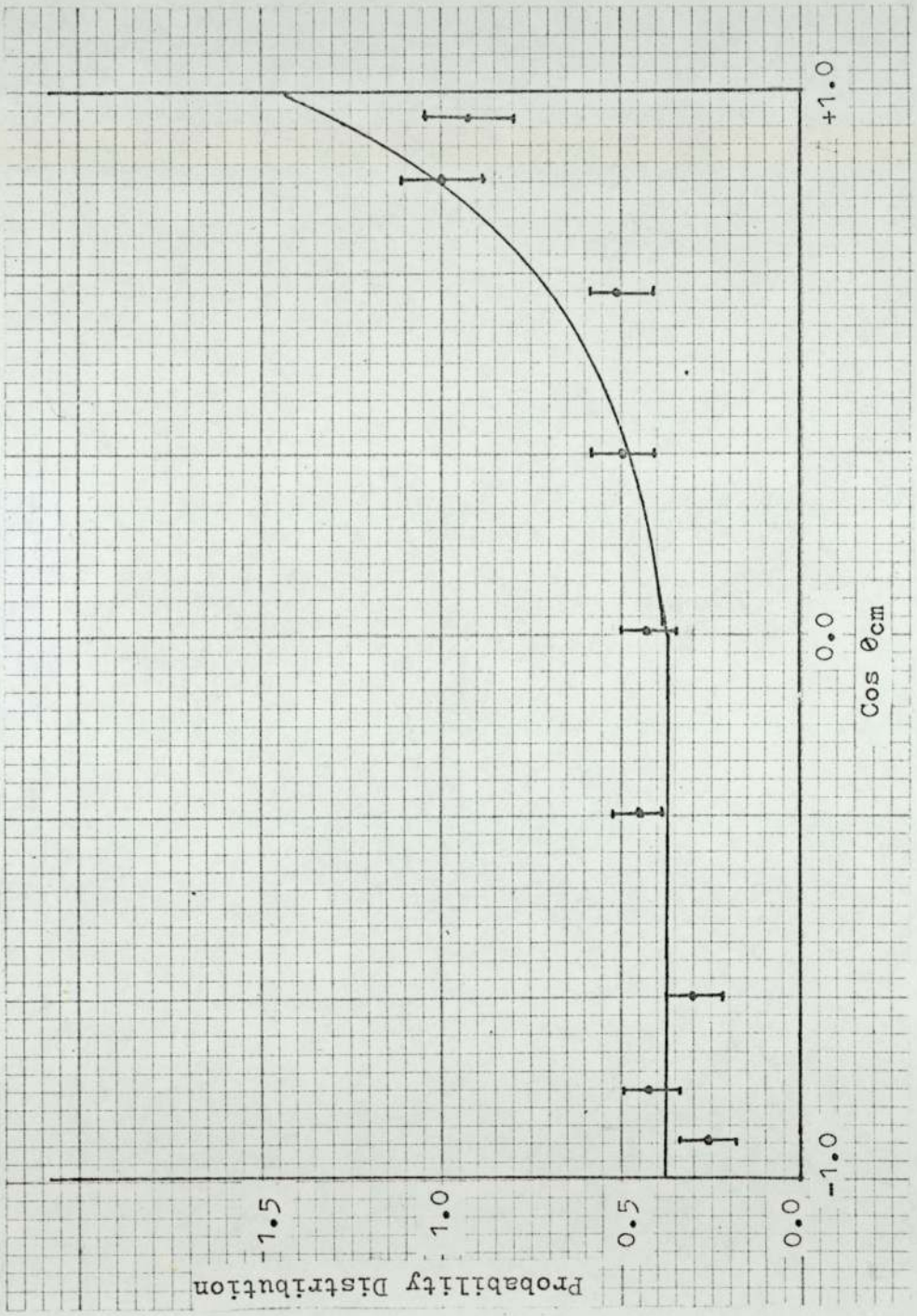

2.10) contd.

materials so that a good neutron economy is possible while at thermal energy the bulk of the excess neutrons are absorbed in the structural materials and the moderators, as the (n,γ) cross-section is high at thermal energies.

Most nuclei have some absorption for the thermal neutrons; however the cross-section for this varies from element to element and isotope to isotope, from a few millibarns to thousands and sometimes millions of barns. The cross-section for the light nuclei in general is small and capture is an important process (exceptions are ^{10}B, ^{6}Li etc.); for these nuclei the resonances are few and occur at high energies and even then they are mostly scattering resonances. For nuclei of relatively heavier masses, the resonances become more numerous, some of which are almost exclusively for capture with relatively small fractions for scattering. The capture cross-section variation of the wings of a resonance is given by Breit-Wigner formula:

$$\sigma(n,\gamma) = \pi\lambda^2 g. \frac{\Gamma_\gamma \Gamma_n}{(E-E_o)^2 + \Gamma^2/4} \qquad 2.25$$

where the terms have the same meaning as equations 2.8 and 2.9; equation 2.25 can be written from these latter equations. The Breit-Wigner formula asserts that the caputre wings on either side of the peak are symmetrical. Away from the resonance the $\sigma(n,\gamma)$ is still determined by the character of the nearest resonance or, if there are several near enough to be effective, by their resultant effects, which unlike the scattering are algebraically additive. Far from the resonance i.e. away from the foot of the resonance $\sigma(n,\gamma)$ varies as $1/v$, where v is the velocity of the neutron. This relationship

2.10) contd.

dominates the capture at and near thermal energies; the value of the $^1/_v$ - relationship is determined by the first peak above the thermal energy.

The absorption behaviour in the absence of any other competitive reaction is determined by the ratio Γ_γ/Γ_n. The general pattern is that while the average neutron width increases with the neutron energy ($\overline{\Gamma}_n$ varies as about $\sqrt{\overline{E}_n}$), radiation width for the medium and heavy nuclides is of the order of 0.1 ev and is more or less independent of energy. At some energy, of the order of a few kilovolts the gamma and neutron widths become equal. At higher energy the total width Γ is approximately equal to Γ_n, and the $\sigma(n,\gamma)$ averaged over many resonances varies as $^1/E_n$, in contrast to the $^1/\sqrt{\overline{E}_n}$ law which prevails at low energies. However the $^1/E_n$ relationship of higher energies is only approximate compared to the more rigorous $^1/v$ relationship of lower energies. When more reactions become available the captive cross-section falls faster than as $^1/E_n$.

The variation with the mass number also shows some regularity at high energies. At a given energy, $\sigma(n,\gamma)$ at first increases rapidly with increasing atomic weight up to about 100, after which the cross-section levels out around a steady value, which at 1 Mev is 100 mb. There are some scattered exceptions to this. The nuclei with magic numbers in particular have very small capture cross-sections compared to the neighbouring isotopes.

The capture cross-section of iron and uranium-238 above 1 kev are shown in figures 2.10 and 2.11 respectively. The uranium-238 cross-sections at high energies are better

Figure 2.10-Capture Cross-section of Iron from 30ev to 1 Mev.

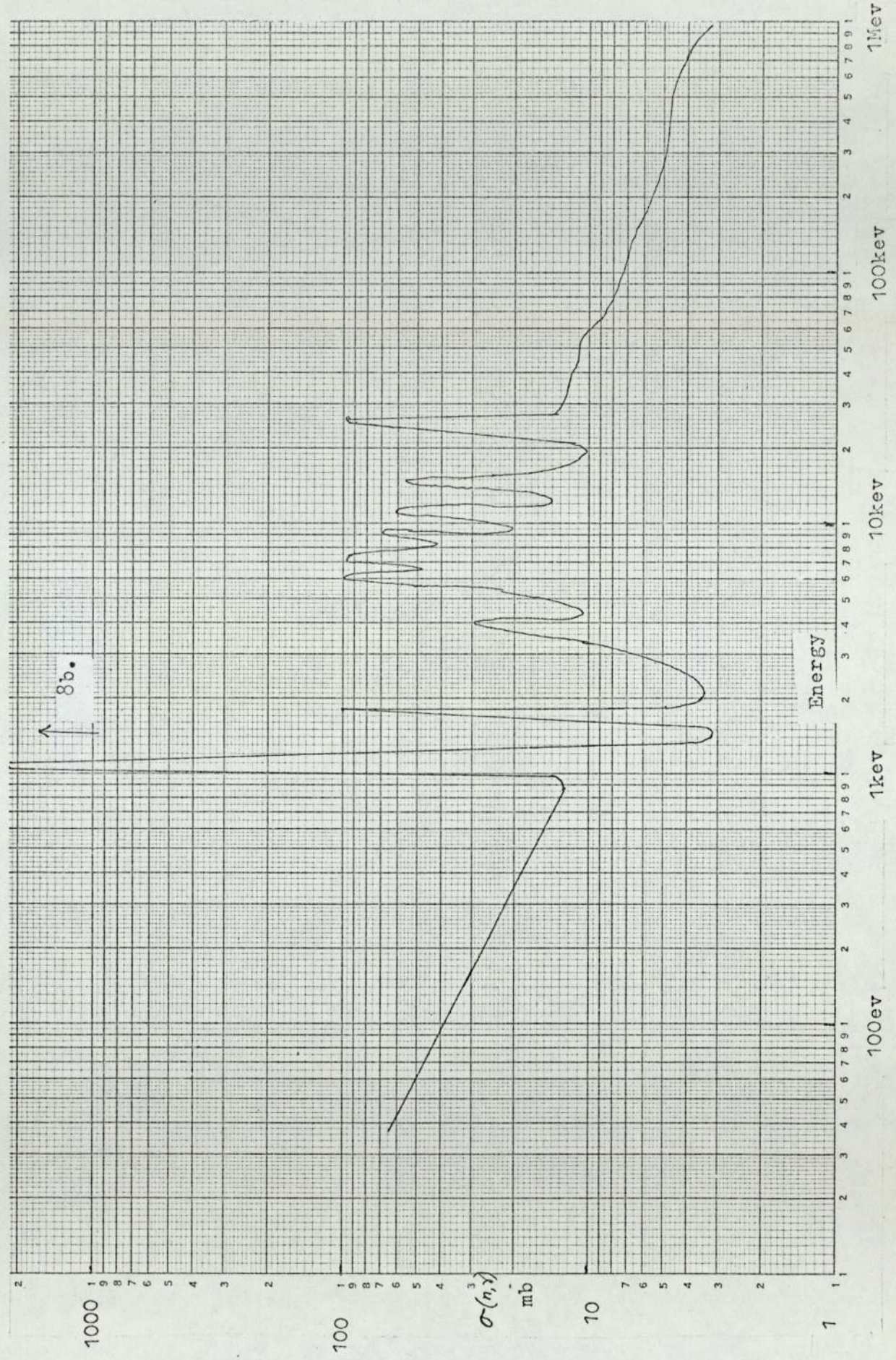

Figure 2.11– Capture cross-section of Uranium-238 from 2 kev to 15 Mev. (After Davey [28]).

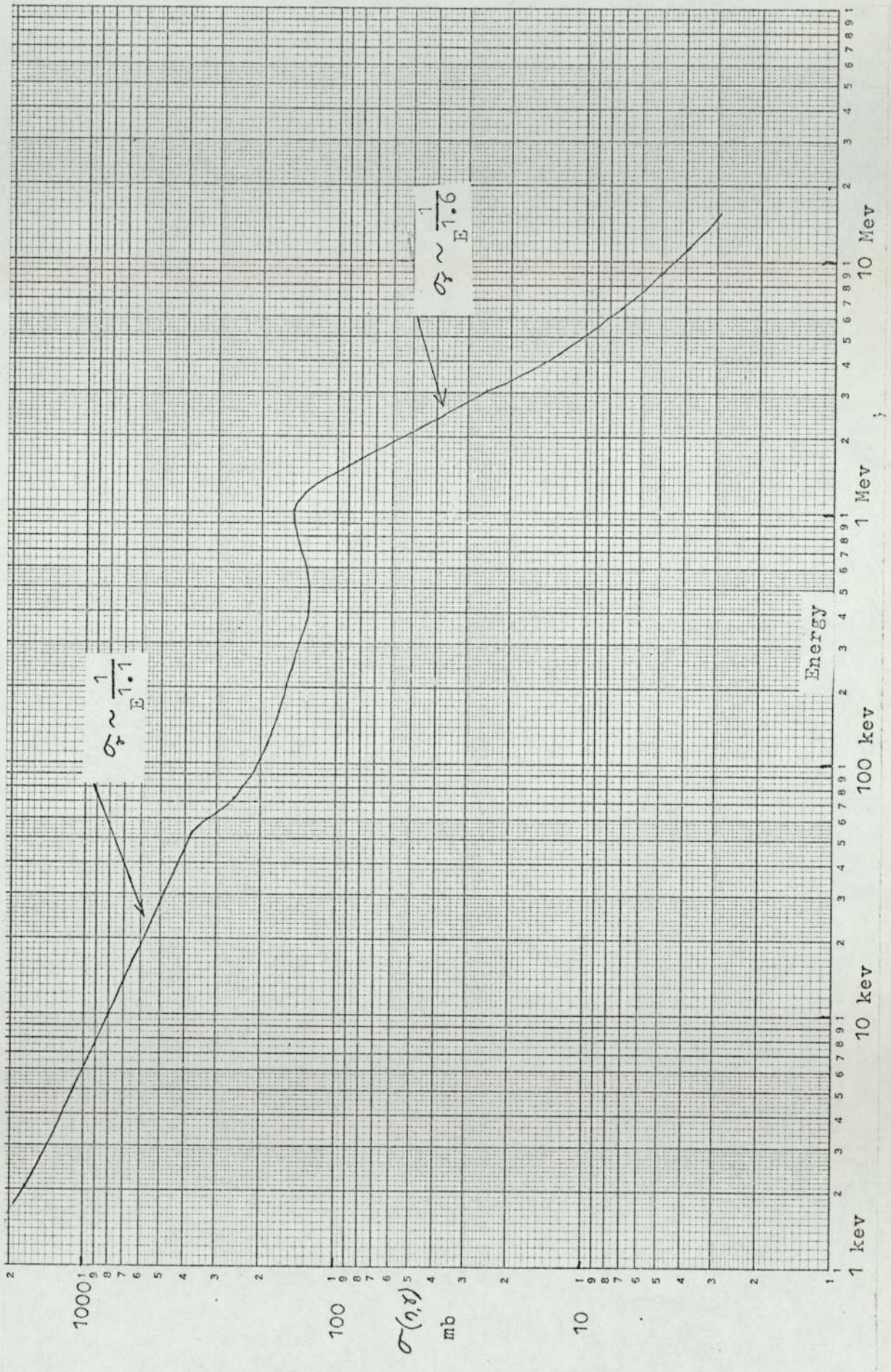

2.10) contd.

known. Davey [27] has recently made an extensive study of it from 1 kev to 15 Mev; figure 2.11 is due to him. The thermal (2200 m/s) cross section for ^{238}U is 2.70 barns. The same value is also for ^{56}Fe; for natural iron the cross-section is 2.53 barns. The capture cross-section for iron at high energies is poorly known. It is not shown in BNL-325. The figure is after the measurements of Moxon and Rae, as reported by Barre et al. [28]. The $1/v$ fall from thermal region persists up to about 1 kev. Between 1 kev and 20 kev there is some resonance structure. Above 20 kev there is a considerable spread in values of different authors [28]. However the cross-section is considerably small after the resonance region; it is only about 7 mb or so at 100 kev and about 2 mb only at 1 Mev, compared to 200 mb and 150 mb respectively for uranium. However the latter also drops rapidly after 1 Mev, as the fission reaction begins; it is only about 25 mb at 3 Mev.

2.11) Charged Particle Emission Reactions.

The principal reactions of this type are the (n,p) and (n,α) reactions. These reactions are usually endothermic (negative Q-value) and do not occur below a threshold energy, given by

$$E_{th} = \frac{A+1}{A} |Q|$$

The maximum kinetic energy available to the charged particle, x is $E_x = E_n - Q$, where E_n is the incident neutron energy. The cross-section for the reaction as a function of energy is governed mainly by the Gamow factor for tunnelling as long as E_x is not greater than the Coulomb barrier height. At a

2.11) contd.

given energy available for emission, the proton emission will be more probable than alpha particle emission because of the lower height of the barrier for the proton. The cross-section for charged particle emission is usually small, compared to the neutron emission reactions and decreases with increasing Z. With the 14 Mev neutrons it does not exceed 150 mb for mass number above about 70, and decreases very rapidly to, of the order of 1 mb for the heavy nuclei. With increasing energy the cross-section increases from the threshold and in general approaches a constant value.

Both the compound nucleus formation and direct interaction mechanisms are effective for charged particle emission. The direct effect is more prevalent in the heavier nuclei and for (n,p) rather than (n,α). The emitted protons have an evaporation Maxwellian spectrum - with the lower part of the spectrum suppressed due to the coulomb barrier. As in neutron emission, the higher energy protons are anisotropic while lower energy ones are symmetric about 90°.

Some endothermic charged particle reactions are important in reactors even though their thresholds are high. In water reactors, for example, the $^{16}O(n,p)\ ^{16}N$ is the principal source of the radioactivity of water, despite the fact that its threshold is about 9 Mev. Similarly (n,α) and (n,p) reactions in the materials such as aluminium and iron that are present around reactors can induce activities by high energy neutrons.

CHAPTER 2 (contd)

INTERACTION OF FAST NEUTRONS WITH MATTER

II. FISSION

2.12) Introduction.

Nuclear fission is a process in which a heavy nucleus splits into two fragments, with release of considerable amount of energy and emission of neutrons and gamma-rays. Since its discovery in 1939 it has found immense applications both in war and peace.

With sufficiently high energy of bombarding particles such as neutrons, proton, alpha particles or gamma rays, fission can be induced in most of the heavy elements. However it is only with elements from thorium upwards in the periodic table that fission occurs with low and moderately high energy neutrons (up to several Mevs); they also undergo spontaneous fission. These elements that are of interest from the practical uses of fission, are known as fissionable elements. Of these there are two types - those that fission at all energies from thermal and above and those that can fission only for neutron energies above a threshold value. They are usually termed fissile and fertile respectively. For self-sustained nuclear reactions fissile isotopes are essential. Fertile isotopes however can be converted to fissile by neutron capture.

2.13) Mechanism of Fission.

2.13.1) Critical and Threshold Energy for Fission.

Study of the binding energy curve shows that the binding energy per nucleon is maximum for nuclei of mass number about 50 to 60 and it decreases from there on with increasing mass number. Thus it is possible that when a nucleus of A exceeding 120 is subdivided into two fragments the mass of the fragments will be less

2.13) contd.

2.13.1) contd.

than that of the original nucleus, the balance being converted into energy. As the fragments would be more stable, the nuclei of mass numbers greater than 120, in principle, would split on their own. This cannot happen, because a nucleus must acquire some energy before it can disturb the balance of various energies that are holding it together. The energies in balance are the coulomb repulsive force and the short range nuclear attractive force. The coulomb force is proportional to $Z(Z-1)/A^{\frac{1}{3}}$ ($\simeq Z^2/A^{\frac{1}{3}}$), while the attractive force is proportional to the surface area i.e. $A^{\frac{2}{3}}$; the ratio is proportional to Z^2/A. Since the quantity Z^2 increases faster than A with increasing Z, fission becomes easier with the heaviest nuclides. Some additional energy is still needed because absolute value of the attractive force is still less than that of the coulomb force. For some of the heavy nuclei, just the energy brought in as the binding energy of an absorbed neutron is enough to upset the balance while for others, still more energy is needed which can be supplied by the kinetic energy of the neutron. The minimum energy needed for fission to occur is called the critical energy.

The critical energy can be explained in terms of the liquid drop model of fission, which is believed to describe the basic process by which a nucleus undergo fission. According to this picture the short range nuclear force contributes a surface tension to the nucleus similar to that of a liquid drop. With the added energy,

2.13) contd.

2.13.1) contd.

due to the binding energy and kinetic energy of the incident neutron, oscillations are set up within the drop and these tend to distort its original spherical shape and make it ellipsoidal. More energy is needed for further elongation, since surface to volume ratio is increased in such a process. The stages leading to fission are shown in Figure 2.12. With sufficient availability of energy the deformed nucleus develops a saddle point somewhere near its middle and if it can reach the position C, then coulomb repulsive force takes over and the two blobs of nuclear mass are pushed away from each other until they are completely separated from each other; the fission fragments are now fully accelerated.

The critical energy E_c is the minimum energy required to pass from original nucleus to a critical deformation. This is equal to the difference between the coulomb energy E_q and Q-value of the reaction (Fig.2.12):

$$E_c = E_q - Q \qquad 2.26$$

with $$Q = [(M_o + m_n) - (M_1 + M_2)]c^2 \qquad 2.27$$

where M_o is the mass of the original nucleus, m_n that of the neutron absorbed and M_1 and M_2 are the (rest) masses of the fission fragments before the emission of the neutrons. The Q-value can also be written from detailed energy balance of the fission products.

The term "fission threshold", on the other hand indicates the lowest kinetic energy at which fission is observed and is equal to the difference between E_c and

FIGURE 2.12-- Potential Energy of a Fissioning Nucleus at the Successive Stages; (shown as exess of the rest-mass energy of the fragments)

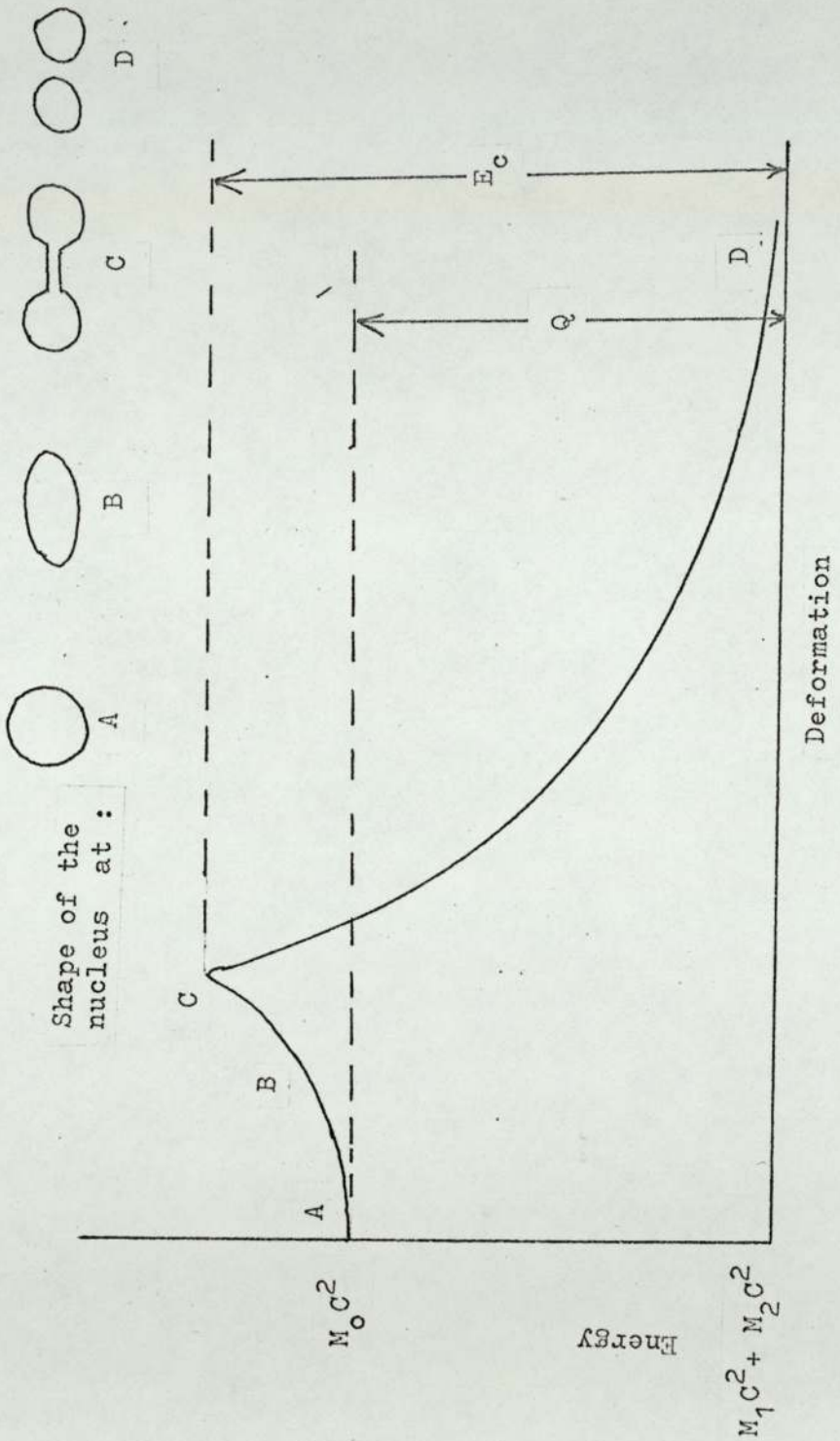

2.13) contd.

2.13.1) contd.

the binding energy of the absorbed neutron, when E_c is larger than the latter. If E_c is smaller, neutrons of zero energy can induce fission.

The Q-value for fission is the average of Q-values over all possible values, as the masses of the fission fragments are not fixed, as the nucleus can split in several ways. However the Q-value of fission reaction is positive. Unlike other exoergic nuclear reactions which do not have threshold energies some of the fission reactions have.

The critical energy E_c can be given to a fissioning nucleus in several ways e.g. it can be given by energetic gamma-rays. In photo fission studies the excitation energy E_c can be directly measured. Its value is around 5 Mev; for some of the common fissionable isotopes this is listed in Table 2.2.

TABLE 2.2

Critical and Threshold Energies for Fission of Several Nuclei (After Ref.31)

Target Nucleus	Compound Nucleus	Critical Energy E_c, Mev.	Binding Energy of the last neutron, E_n	Threshold Energy $\simeq E_c - E_n$
^{232}Th	^{233}Th	6.5 Mev	5.1 Mev	1.4 Mev
^{235}U	^{236}U	5.3	6.4	-1.1
-	^{238}U	5.85	*	-
^{238}U	^{239}U	5.15	4.9	0.6
-	^{239}Pu	5.5	*	-
^{239}Pu	^{240}Pu	4.0	6.4	-2.4
-	^{235}U	5.75	*	

*Binding energy for these nuclei is not relevant, since they cannot be formed by neutron capture.

2.13) contd.

2.13.1) contd.

Form Table 2.2 it is observed that isotopes with even-A (target nuclei) can undergo fission only if the neutron has sufficient kinetic energy, while isotopes with odd-A have negative threshold values, for which fission is possible by excitation of the bound-states; experimentally fission at "negative" neutron energies can be studied with deuteron stripping reactions [32]. This odd-even characteristics is the general rule for the fissile-fertile materials - fissile isotopes have even atomic number and odd mass number while fertile isotopes have even atomic number but even mass number. This is because, the binding energy of the incident neutron to an even-A nucleus is always less than that to an odd-A nucleus.

2.13.2) Theories.

The liquid drop model, since its introduction by Bohr and Wheeler [33] , has served as the basic conceptual framework for the fission problem. In spite of its sweeping simplicity the model, based on hydrodynamical analogy has accounted for many properties of fission. This model is still being actively exploited to study many of the features of the fissioning nucleus [34] .

From the assumptions of the liquid drop model a saddle configuration can be found from the potential energy considerations. However the theory loses track from saddle point to its descent to scission. From the study of fission resonances it is generally agreedthat

2.13) contd.

2.13.2) contd.

the number of channels for the fission reaction i.e. the modes of arrangements of the fissioning nucleus over the fission barrier are a few - two or three [35,36]. This defines the possible saddle points. However since there are 40 or so ways in which the nucleus finally breaks up, it is supposed that the transition from saddle point to scission point allows time for considerable rearrangement of the nuclear material. In spite of the large energy available for excitation that only few channels are observed, has been explained by Aage Bohr [37] as due to the fact that the amount of potential energy of deformation leading to saddle point is so large that very little is left for excitation of the compound nucleus at that stage.

The liquid drop model predicts a monotonic behaviour of the critical energy as a function of Z and A, and does not take into account the odd-even characteristics of the heavy isotope that dictate fission cross-section. The fission fragment distribution indicates some role of the shell structure of the nuclei and attempts have been made to apply the shell model. However application of the other models into fission theory has been to complement the liquid drop picture rather than replacing it.

2.13.3) Products of Fission.

Immediately following fission there are two fission fragments as two deformed blobs of nuclear mass, moving in opposite directions. About 205 Mev is available

2.13) contd.

2.13.3) contd.

between them, which is the Q-value of the reaction. Bulk of it, about 170 Mev on the average is in the form of kinetic energy and the rest initially appears as the excitation energy of the fragments. Most of the fragments fall in two groups with peaks at mass-numbers 140 and 95.

The neutron to proton ratio of stable isotopes of intermediate weight is much less than that of heavy ones. The compound nucleus ^{239}U has 147 neutrons and 92 protons and the ratio is 1.60. The corresponding ratios for the stable isotopes of some of the fission products - krypton, iodine, xenon and caesium- vary from 1.17 to 1.52. The immediate fission fragments therefore have excess neutrons and the emission of neutrons from these nuclei therefore becomes most probable. The proton deficiency of the fragments decreases the binding energy of the neutrons; its value in the lighter fragments is about 5.5 Mev and in the heavier fragments about 5 Mev. The corresponding values in the stable nuclei of same masses are about 7.7 and 7.2 Mev. Neutron emission will be the most likely process as long as the excitation energy of the fragment exceeds the neutron binding energy by a few kev. There can be occasional emission of protons and alpha-particles. If the excitation energy drops below neutron binding energy, γ-emission will become most likely. Because of the higher excitation energy of the lighter fragments, more neutrons are emitted by them. Furthermore because of the large spread in the excitation energy, the

2.13) contd.

2.13.3) contd.

total number of neutrons per fission also shows considerable fluctuation over the average number. As many as five or even more neutrons may be emitted for which the total excitation energy needed is well over 30 Mev.

The fragments lose energy in the surrounding matter by ionization and excitation of the atoms of the material around and are soon brought to rest. The maximum range of the fragments is about 6.7×10^{-4} cm. in uranium and 1.4×10^{-3} cm. in aluminium. The nascent fission products are still proton deficient; they begin to adjust the charge through a series of β-disintegrations. The first few β-rays are emitted in the course of seconds; the lifetimes of some of the later products range up to years. The beta emission is naturally accompanied by anti-neutrinos, which carry away on the average 11.9 Mev per fission of ^{238}U and somewhat less for ^{235}U or ^{239}Pu [38].

Not all beta decays lead to the stable ground state of the daughter. Some of them are in excited states which decay promptly after their formation by γ-radiation. Some of these excited states are also responsible for the delayed neutrons which is though a small fraction (about 1%), plays a prominant part in the kinetices of reactors.

Thus average fission has produced:

1) 2 nuclei with mass numbers near around 95 and 140;

2) about 2 or 3 neutrons with about 2 Mev kinetic energy each;

2.13) contd.

2.13.3) contd.

3) about 5 prompt gamma rays, with a total energy of about 6 Mev in all;

4) about 5×10^6 ion pairs and a similar number of excited states in the medium traversed by fission products and

5) about 7 beta-rays and antineutronos and an equal number of gamma-rays during the decay of fission products and

6) an occasional neutron (delayed) of average energy 0.3 Mev.

2.14) Fission by Fast Neutrons.

2.14.1) Cross Section.

For the even-even isotopes the fission threshold lies between 0.4 and 1.2 Mev and the cross-section systematics with energy is simple. The fissile isotopes, on the other hand have high cross-section at thermal energies and richly populated resonances near that. In fact the high cross-section of the three major fissile isotopes, ^{239}Pu, ^{235}U and ^{233}U at thermal energies can only be explained by assuming one or two resonances at 'negative' energies i.e. bound states. The resonances can be resolved experimentally up to 1 kev and unresolved resonances are believed to be effective up to 10 kev. The asymmetry of the fission resonances and other interesting features of them have been extensively studied from both theoretical and practical considerations [39-42]. Above the resonance region the fission cross-section becomes smoothly falling off with energy to approach the value of $\pi R^2 \sim 2$ barns. At 10 kev the fission cross-section of ^{235}U is 3.8 barns; by 100 kev that of both

2.14) contd.

2.14.1) contd.

^{239}Pu and ^{235}U is already below 2 barns.

In the neighbourhood of 1 Mev neutron energy, fluctuations are observed in the fission excitation curves of almost all of the fissionable isotopes. For example in σ_f of ^{239}Pu there is a rise at 1.2 Mev. The cross-section of ^{238}U rises through 3 short plateaus at 610, 950 and 1180 kev. Except for the low and long tail beginning at 0.6 Mev, the ^{238}U threshold from practical purposes is taken to be 1.2 Mev, from where it rises to a plateau of about 0.6 barn at 2 Mev. In the Mev region the fission cross-section is determined as a result of competition between inelastic scattering and fission process, since de-excitation of the compound nucleus by gamma-emission can be neglected. For all the isotopes, including those thermally fissile, the first plateau continues up to about 6 Mev (Fig.2.13); the heights of the plateaus are below 2 barns.

In the 5 to 6 Mev range one encounters the gamma-fission, (γ,f) threshold for each of the isotopes; at this energy an increase occurs which brings the fission cross-section to a second plateau. This increase is explained in terms of the inelastic scattering of the neutrons by the fissionable nucleus. Following the inelastic scattering, the nucleus may now be left in a sufficiently excited state; and the state of the nucleus can be the same as that following the absorption of an energetic gamma-ray - when the excitation can cause a fission. For the de-excitation, however, there is a competition between emission of a second neutron and the fissioning of the

FIGURE 2.13 -- Fission Cross Section of Some of the Fissionable Nuclei for Fast Neutrons, Showing the First Plateau. (After Henkel, ref. 43.)

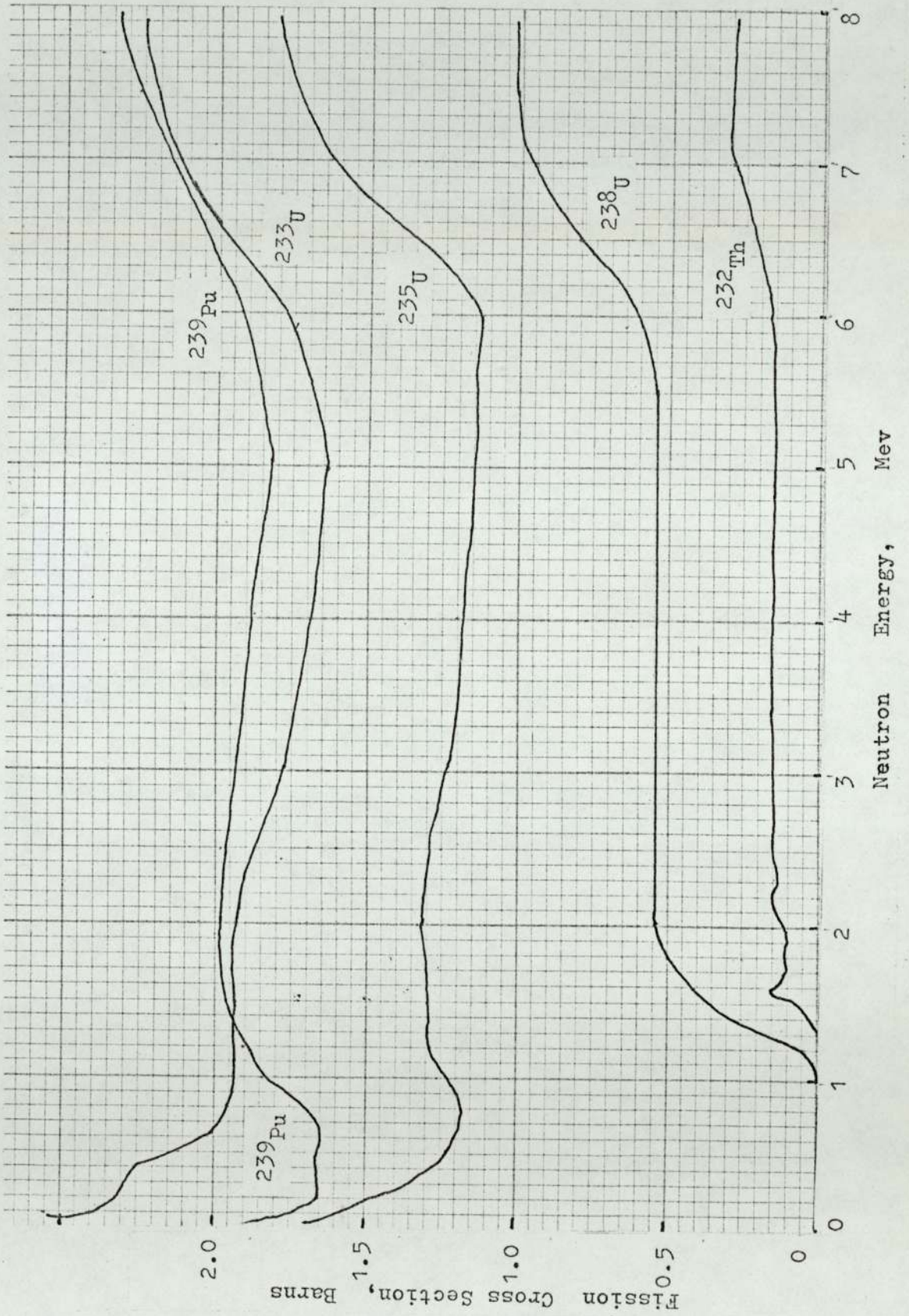

2.14) contd.

2.14.1) contd.

nucleus. The former is the (n,2n) reaction and the latter is term (n,n'f) reaction which is added to fission by directly following the absorption of a neutron. A second rise and a subsequent third plateau will occur at the sum of the (n,2n) and (γ,f) threshold energies. The nucleus which is fissioning at the third plateau is the (A-1)* nucleus. At higher energies, thus fission is made up of component parts and the observed fission cross-section is equal to

$$\sigma_F = \sigma(n,f) + \sigma(n,n'f) + \sigma(n,2nf) + \ldots \qquad 2.28$$

Early work on fission by fast neutrons has been discussed by Henkel, Hemmendinger and Kalanin [43-46]. Later measurements have been made by Pankratov, White and Warner [47-49]. The measured cross-section of ^{238}U from 3 to 37 Mev by Pankratov is shown in Figure 2.14. The first four plateaus and beginning of perhaps a fifth can be seen.

2.14.2) Fast Fission and Chain Reaction.

A self-sustained chain reaction is not possible with the isotopes having a positive threshold alone. This is because nuclei like ^{238}U have larger cross-section for inelastic scattering than fission with the fission-energy neutrons and the inelastic threshold is much lower than fission threshold. Consequently most of the neutrons produced in fission are rapidly slowed down below fission threshold.

Figure 2.14-- Fission Cross-section of Uranium-238 from 3Mev to 37 Mev. (From Pankratov [49]).

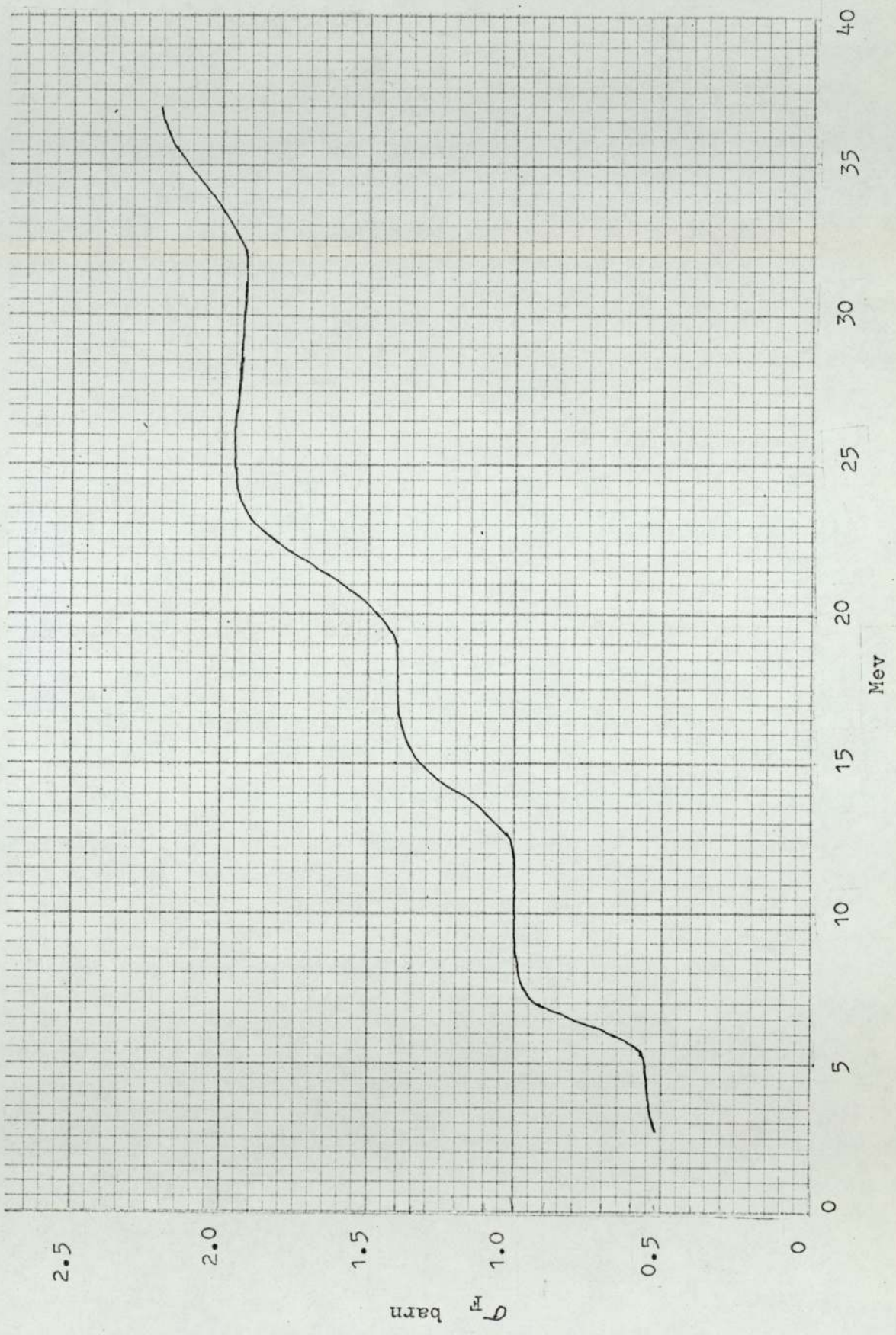

2.14) contd.

2.14.2) contd.

However, energetically 60% of the prompt neutrons are above ^{238}U fission threshold and if the system contains large amount of ^{238}U it can make substantial contribution to total fission. With increased concentration of ^{239}Pu or ^{235}U in ^{238}U, chain reactions can be self-sustained; thus with about 6% enrichment of ^{235}U in ^{238}U an infinite system will be self-sustaining. In practical fast reactors the enrichment is anything above 10 to 15%; the remainder is ^{238}U, which can easily be assembled in such a way that between 15% and 30% of all fissions occur in it [50]. Many of them, though, occur in the reflector region and proportionately makes less contribution towards criticality. The main aim with the ^{238}U isotope is to let (n,γ) reaction happen so that ^{239}Pu is produced.

2.15) Neutrons from Fission.

2.15.1) Energy Spectrum.

The prompt neutrons, it is now certain are emitted from the fission-fragments within a short time after fission, as the deformed nuclei of the fragments rearrange their nuclear configuration, and find themselves in excited states with excess neutrons. The mechanism therefore is similar to emission of inelastic neutrons through evaporation, the spectrum of which is a Maxwellian. However the numerical values for such an expression can only be empirically obtained and consequently these values are not unique. In fact several sets of values

2.15) contd.

2.15.1) contd.

from the data-fit has been put forward. For the neutrons from ^{235}U by thermal neutron induced fission the following formulae describe the spectrum:-

$$\psi(E) = 0.453 \exp(-1.036E)\mathrm{Sinh}(2.29E)^{\frac{1}{2}}$$
[Cranberg] ... 2.29(a)

$$\psi(E) = 0.484 \exp(-E)\mathrm{Sinh}\,(2E)^{\frac{1}{2}}$$
[Watt] ... 2.29(b)

$$\psi(E) = 0.7696\, E^{\frac{1}{2}} \exp(-0.775E)$$
[Maxwellian] ... 2.29(c)

where E is in Mev and $\psi(E)$ is so defined that $\psi(E)dE$ is the number of neutrons emitted with laboratory energy between E and E+dE per fission neutron, that is $\psi(E)$ is normalised

$$\int_0^\infty \psi(E)dE = 1 \qquad 2.30$$

The first two are named after the authors who obtained the constants. Of these Watt-spectrum is the one generally used. Watt [51] also considered finer expressions considering neutrons from different groups of fission fragments, each group giving their own sets of values but he concluded that, a finer expression did not substantially vary from the averaging expression in 2.29(b). Bonner et al. [53] reports that the Watt equation fits experimental data down to 75 kev.

Cranberg et al. [52] also gave a simpler expression which they found describes data below 9 Mev adequately

2.15) contd.

2.15.1) contd.

$$\psi(E) = 0.77 \sqrt{\bar{E}} \exp(-0.776E) \quad \ldots 2.29(d)$$

This is also known as Cranberg-spectrum.

The above expressions all fitted to thermal neutron induced fission of ^{235}U, also fairly well describes neutrons from other nuclei with low energy induced neutrons. The spectrum changes slowly with higher energies of neutrons; this is considered later. The energy of the neutrons described by equations 2.29 yields a value for average energy $\bar{E}$ = 1.98 Mev. The most probable energy, corresponding to the peaks is only about 0.85 Mev.

The distribution $\psi(E)$ and the number of neutrons above energy E is given in Table 2.3 below. This is according to the Watt-spectrum.

2.15) contd.

2.15.1) contd.

TABLE 2.3

Fission neutrons spectrum and fraction of neutrons above a given energy, for the Watt-Spectrum; (after ref.54).

Energy E,Mev	$\psi(E)$ per Mev	Fraction emitted above E, per cent
0.1 Mev	0.2023	98.60 %
0.2	0.2676	96.23
0.5	0.3450	86.79
0.8	0.3542	76.15
1.0	0.3446	69.18
1.4	0.3073	56.17
2.0	0.2371	39.72
3.0	0.1384	21.24
4.0	0.07472	10.86
5.0	0.03847	5.37
6.0	0.01916	2.61
8.0	-	0.57
10.0	-	0.12
12.0	-	0.0247
14	-	0.0049
15	-	0.0022

2.15.2) Variation of $\bar{\nu}$ with E_n:

$\bar{\nu}$, the average number of prompt neutrons emitted per fission, is important both for reactor and breeding calculations. It is a function of the energy of the neutrons inducing fission, as well as of the nucleus undergoing fission.

Assuming that the fragment kinetic energy does not vary with the incident neutron energy, Leachman [55]

2.15) contd.

2.15.2) contd.

and Usachev and Trubitsyn [56] have demonstrated that $\bar{\nu}$ is expected to increase linearly with the neutron energy E_n in the form

$$\nu(E_n) = \nu_o + a\, E_n \qquad 2.31$$

where ν_o and 'a' are constants for a given nucleus; however 'a' is found to vary slightly with E_n.

By a neutron emission the excited fission fragment loses its internal energy equal to the binding energy and kinetic energy of the neutron. The average energy of emitted neutrons according to Weisskopf model [1] is 2T where T is the nuclear temperature. The increased energy of the incident neutron, increases the excitation energy of the fragments and as a result both the number of emitted neutrons as well as their average energy increases. From these considerations Bondarenko et al. [57] derives the rate of variation of ν as

$$\frac{d\bar{\nu}}{dE} = \frac{0.9}{E_b + 2T} \qquad 2.32$$

The variation in the slope can be explained from the above relation by considering that E_b, the average binding energy increases with increasing number of neutrons emitted by the fragments. Also due to variation of E_b, the slope should vary with different nuclei. Equation 2.32 gives values in agreement with the experimental ones for several nuclei [57].

The ^{238}U data are found to be given by one

2.15) contd.

2.15.2) contd.

value of the slope for the energy range up to 14 Mev. From their recent measurements Soleilhac et al. [58] finds that ^{238}U and ^{239}Pu data for least square fit can be represented by the following equations for incident energy from 1.3 to 15 Mev:

$$^{238}U: \quad \bar{\nu}(E) = 2.28 + 0.154E \qquad 2.33$$

$$^{239}Pu: \quad \bar{\nu}(E) = 2.87 + 0.150E \qquad 2.34$$

The ^{235}U data are however more complex and there are disagreements between the quoted values. While Soleilhac et al. finds the necessity of three separate lines in the above range, Fraser and Mitton [59] finds a fit to a polynomial of second order between thermal energy and 8 Mev.

2.15.3) Variation of $\bar{E}$ with E_n:

The variation of the average energy $\bar{E}$ of the emitted neutrons with the incident neutron energy has been investigated by Terrell [60], Leachman [61] and recently by Doyas and Howerton [62].

Assuming that the Weisskopf model is correct for emission mechanism of the neutron from the fission fragments, Terrell shows that their average energy $\bar{E}$ is given by

$$\bar{E} = \bar{E}_f + 2\bar{T} \qquad 2.35$$

where $\bar{E}_f$ is the average kinetic energy per nucleon of the fragments and $\bar{T}$ is the average nuclear temperature of the fragments. From the known kinetic energy

2.15) contd.

2.15.3) contd.

distribution of fission fragments, which does not vary significantly with incident neutron energy, Terrell estimated $\bar{E}_f = 0.75$ Mev. The temperature T could be related to $\bar{\nu}$ from the fact that $\bar{\nu}$ increases linearly with the excitation energy E_x, while T is given by

$$T = \sqrt{E_x/a}$$

where a is a constant. This gives

$$T = b\sqrt{\nu+1} \qquad 2.36$$

where b is another constant. The unity in $(\nu+1)$ accounts for the gamma ray energy. b is obtained empirically and is found to be 0.65 [62] . Thus from equations 2.35 and 2.36 above

$$\bar{E} = 0.75 + 0.65\ (\bar{\nu} + 1)^{\frac{1}{2}} \text{ Mev.} \qquad 2.37$$

Thermal neutron fission data for several isotopes have been found to agree with equation 2.37 [52]. At higher energies up to 14 Mev there are (n,2n) and (n,3n) in addition to fission. If ν_T is the number of neutrons observed per fission event for all processes then the neutrons due to fission alone is given by

$$\bar{\nu}_f = \frac{\nu_T\ \sigma_F - \sigma(n,n'f) - 2\sigma(n,2nf)}{\sigma_F} \qquad 2.38$$

where σ_F is the total fission cross-section as has been defined by equation 2.28. Doyas and Howerton [62] , studying the available data conclude that Terrell's equation (eqn.2.37) gives a good description of $\bar{E}$ for incident energies between thermal and 14 Mev and also for spontaneous fission and is applicable to all isotopes.

According to equation 2.37, substituting the

2.15) contd.

2.15.3) contd.

published values of the average number of neutrons per fission, we get that average energy for fission neutrons for ^{238}U increases from 1.96 Mev with incident neutron energy of 1.4 Mev to 2.25 Mev with 14 Mev neutrons - an increase of 300 kev.

2.16) Breeding Properties and Parameters.

2.16.1) Breeding Possibility.

The only fissile material that is naturally occurring is ^{235}U which is present as only 0.7% of the natural element. For the future of nuclear power, therefore there is a strong incentive to change the fertile isotopes into fissile through neutron capture in reactors. The reaction and decay scheme with ^{238}U are

$$^{238}U + n \rightarrow {}^{239}U$$

$$^{239}U \xrightarrow[23.5m]{\beta^-} {}^{239}Np \xrightarrow[2.36d]{\beta^-} {}^{239}Pu$$

The process is called Conversion. Similarly ^{232}Th another fertile material can be converted to ^{233}U. For the present, the production of ^{239}Pu from ^{238}U is of more importance, since ^{238}U is almost always present in reactors of both thermal and fast type; ^{239}Pu is produced in them as by-product. With special care in design it is possible to produce more plutonium than the number of ^{235}U consumed by fission and absorption, and the reactor is said to breed.

Breeding is possible because per fission more than 2.5 neutrons are emitted in a reactor. Of these

2.16) contd.

2.16.1) contd.

only 1 goes back to sustain the chain reaction while the remaining 1.5 or more neutrons are to be got rid of through leakage and capture. It is now almost certain that in practical thermal reactors, breeding is not possible in the ^{238}U-^{239}Pu cycle. This is determined by the relative cross-sections of the materials. However breeding with a narrow margin is only possible in thermal thorium reactors with heavy water, carbon or berylliam as the moderator [63].

The breeding possibility becomes more promising in the fast reactors. In the thermal energy region though the fission cross-section is hundreds of barns compared to a few barns in the kev regions, the capture in the fuel and the structural and moderator materials is also high. While in the energy range above 100 kev absorption in reactor materials other than fuel becomes almost negligible. From the performance of the present generation of the fast reactors, it been found that breeding ratio - the ratio of the number of ^{239}Pu produced to that of ^{235}U destroyed - can be about 1.77 with the uranium-plutonium cycling.

Attractive breeding possibilities are also there with the fusion reactors when they will come into existence.

2.16.2) <u>α and η</u>.

The breeding possibility with a nuclide can be judged from a study of these two parameters. The ratio of capture to fission cross-section is called alpha,

$$\alpha = \frac{\sigma_\gamma}{\sigma_f} \qquad 2.39$$

2.16) contd.

2.16.2) contd.

Eta is defined as the average number of neutrons emitted per neutron absorbed by a fissionable isotope. Below the (n,2n) threshold

$$\eta = \nu \frac{\sigma_f}{\sigma_a} \qquad 2.40a$$

where $\sigma_a = \sigma_f + \sigma_\gamma$, so that

$$\eta = \frac{\nu}{1+\alpha} \qquad 2.40b$$

Since ν and α are functions of neutron energy η is also energy dependent; however ν is only slowly varying with energy, compared to α which shows ups and downs in the resonance region but falls steadily at higher energies. A high η is desirable for breeding gain and so low α. On the average α for ^{233}U or ^{239}Pu is smaller than that for ^{235}U. In the energy range of 3 ev to 100 ev, α for ^{235}U is greater than 1 (i.e. $\sigma_\gamma > \sigma_f$), while for ^{233}U and ^{239}Pu it is considerably below 1. The situation is better for all three above 10 kev. The η for these three major fissible isotopes at several energies is shown in Table 2.4 below.

TABLE 2.4

'Eta' for the Three Major Fissile Isotopes at different energies.

Energy	^{233}U	^{235}U	^{239}Pu
0.025 ev	2.29	2.08	2.12
100 kev	2.37	2.16	2.44
1 Mev	2.45	2.30	2.70

The quantity η can also be defined for a mixture of isotopes. Thus for natural uranium,

2.16) contd.

2.16.2) contd.

below ^{238}U fission threshold η is given by

$$\eta = \frac{\nu(235)\ \Sigma_f\ (235)}{\Sigma_a(235)+\Sigma_a(238)} \qquad 2.41$$

At thermal energy (0.025 ev) this gives $\eta = 1.31$ for natural uranium.

2.16.3) Breeding with 14 Mev Neutrons.

In a fusion reactor, using the D-T reaction, most of the energy released will be carried away by the 14 Mev nuetrons. For the gainful extraction of energy the neutrons will have to be slowed down in a material surrounding the reactor. If it is surrounded by a shell of natural uranium, in addition to giving up their energies the neutrons will liberate further energy by causing fission in ^{238}U, which will give about 200 Mev per fission - much higher than the energy of the neutrons. With the 14 Mev neutrons incident, the number of neutrons will be multiplied as the (n,2n) and (n,3n) reactions can take place in addition to fission. The η will be given by

$$\eta = \frac{\bar{\nu}\ \sigma_F + \sigma_{nn'} + 2\sigma(n,2n) + 3\sigma(n,3n)}{\sigma_{non}} \qquad 2.42$$

where σ_F is the observed fission cross-section as has been defined by equation 2.28 and includes (n,n'f) and (n,2nf) contributions; σ_F for ^{238}U at 14 Mev is 1.13 barns. $\bar{\nu}$ is the average number of neutrons emitted from fission alone (eqn. 2.38). Rearranging equation 2.42 we get

2.16) contd.

2.16.3) contd.

$$\eta = 1 + \left[\frac{(\bar{\nu} - 1)\sigma_F + \sigma_{n,2n} + 2\sigma_{n,3n}}{\sigma_{non}}\right] \qquad 2.43$$

$(\eta-1)$ is the number of neutrons gained by interaction of the 14 Mev neutrons in uranium. If the partial cross-sections are known, η can be readily calculated from equation 2.43.

Several authors have directly measured η in natural uranium with 14 Mev neutrons [64, 65]. The value is about 3.30 $\pm$ 0.15. This is a considerably high value which gives possibility of high breeding from a blanket around a fusion reactor, as these neutrons after being slowed down by inelastic scattering can be absorbed in ^{238}U to give ^{239}Pu. The amount of ^{239}Pu produced could be controlled by the thickness of the uranium shell; the power produced in it will also depend upon the thickness and of course the strength of the fusion reactor. The design and cost of such a fission-fusion system will be simplified by the fact that the fission part will be subcritical and power extraction from the fusion core need not be of high efficiency. More power will be extracted from the fission part than from the fusion reactor itself. Weale et al. [66] infers that a thin shell of uranium can be sufficient. Thus they estimate with a 30 cm. thick shell of natural uranium the system would generate about 220 Mev of energy and product more than 2.5 atoms of ^{239}Pu for each 14 Mev neutrons produced (i.e. fusion event taking place). In addition it can produce at least the same amount of tritium, from an outer blanket of lithium, that is burnt in the fusion reactor.

CHAPTER 3.

SURVEY OF POSSIBLE FLUX MEASURING TECHNIQUES.

3.1) Introduction.

A great variety of techniques for measurement of neutron spectra are available. They range from such ingenious ideas as measuring flux by weighing [67] to detection of protons given off as the neutron decays [68]. However, neutron detection techniques are in general more crude than the sophisticated computational techniques available for spectral studies. Because of their complicated nature neutron spectrometers cannot be expected to be as versatile as charged particle spectrometers; also there exists nothing like the standardization of their detection system as the "Heath-table" [81] for gamma ray spectrum analysis. The wide range of neutron energies of interest makes it virtually impossible to use any one detector. The selection of the detection method or methods depends eventually on the experimental environment and the aim of the experiment. Conversely the experimental arrangements may often be adjusted to suit the detection systems.

3.2) Selection Criteria of Detection Systems for Fast Neutrons.

Generally, a detection system is required to give information about the energy and intensity of the neutron spectra in a medium. The following factors need be studied to select a detector:

(i) Energy range,

(ii) Magnitude of the flux,

(iii) Sensitivity,

(iv) Physical size and flux perturbation and

(v) Sensitivity to gamma radiation

In addition, the experimental facilities available and the cost of a detector are also practical limiting factors. In the above

3.2) contd.

list the first two parameters are defined by the experiment itself. Detectors have their energy range of applicability, beyond which the information becomes unreliable because of poor response or interference from other competing effects. The sensitivity defines the efficiency of a detector, in the useful range of energy. Also it should be known as a function of energy. The known sensitivity gives the absolute intensity of the spectrum. In practice the detector is often calibrated with monoenergetic neutrons of known intensity and from the knowledge of relative cross-section it may be possible to compute efficiency throughout the energy range; otherwise the detector has to be calibrated with neutrons of several energies of known source strength.

Physical size can be a limiting factor in many cases, as a detector of large size will perturb the flux it is measuring. For these cases a re-entrant hole is made in the medium and flux is measured outside. Again this hole can distort the flux but under certain circumstances the emergent flux spectral profile can be representative of the true flux, but this has to be experimentally confirmed. Flux perturbation can also take place for small detectors e.g. resonance foils; but well developed theory and experimental parameters are available to take account of this.

Neutrons are usually accompanied by gamma rays, and interference from the gammas must be negligible. In case the detector is sensitive to gamma-rays means and techniques must be available to eliminate their effects e.g. by applying bias or by pulse shape discrimination.

Two parameters that are basic to detectors are energy

3.2) contd.

resolution and efficiency and these are usually inter-related. Thus a detector with low efficiency will give few counts and resolution is limited by statistics. In many spectrometers the resolution and efficiency compete. For example, in time-of-flight spectromers increasing the flight path to improve resolution results in reduced efficiency.

3.3) Basic Detection Reactions:

In principle any mode of interaction of neutrons with matter can be the basis for neutron detection but up to the present time the main fast neutron detection systems depend upon one of three reactions:

(i) n-p scattering - nuclear emulsion, cloud chambers, proportional counters, hydrogeneous phosphors, radiator surface barrier spectromers etc.,

(ii) Exo-ergic Reactions - ^{6}Li I phosphors ^{6}Li I loaded emulsion, ^{6}Li - surface barrier, ^{3}He proportional counter etc.,

(iii) Threshold Reactions - fission counters, fission foils, threshold foils etc.,

Proportional counters with elastic scattering of helium have also been used. In the above list (n,γ) reactions have not been included, as these reactions are mostly used for thermal and resonance energy regions.

3.3.1) n-p Scattering.

In the fast neutron region, the centre-of-mass angular distribution of the protons recoiling from neutron collisions in a hydrogeneous medium, is spherically

3.3) contd.

3.3.1) contd.

symmetric, resulting in an energy distribution of the recoil protons in the laboratory reference system with equal probability of any energy between zero and E_o, the energy of the incident neutron - giving a rectangular profile for energy distribution of the protons. The energy of the recoiling proton is given by

$$E_p(\theta) = E_o \cos^2\theta \qquad 3.1$$

where θ is the angle, the proton makes with the incident neutron direction in laboratory system. In a continuous energy spectrum each group of neutrons will give rise to its own distribution and the total recoil spectrum will be the super-position of various rectangular distributions. The relation between proton recoil distribution and the neutron spectrum is given by

$$N_n(E)dE = - \frac{dN_p(E)}{dE} \cdot \frac{E}{4\pi n \sigma_{np}(E)} \, dE \qquad 3.2$$

where $N_n(E)$ is the neutron spectrum

$N_p(E)$ is the proton spectrum

n is the number of hydrogen nuclei in the specimen

$\sigma_{np}(E)$ is the scattering cross-section of hydrogen

This equation shows that the neutron spectrum can be obtained by differentiating the proton spectrum.

In practice the rectangular distribution is somewhat distorted by the range energy relation for the protons and other instrumental conditions. The neutron

3.3) contd.

3.3.1) contd.

spectrum from this non-rectangular proton shape can be obtained by matrix inversion process.

The hydrogen cross-section is known to great accuracy. Its value however falls rapidly with increasing energy after 200 kev. The isotropic scattering assumption in the c.m.system is well valid up to 10 Mev, and can be assumed to be so up to 15 Mev with little error.

3.3.2) Exo-ergic Reactions.

Reactions with fast neutrons of energy E_n give kinetic energy to the reaction products equal to $(Q+E_n)$. By measuring this energy, the neutron energy E_n can be obtained. Two exo-ergic reactions that are the basis of several of the fast neutron spectrometers are $^6Li(n,\alpha)T$ and $^3He(n,p)T$ with respective Q-values of +4.8 Mev and +765 kev.

The cross-section of both these reactions falls as $^1/v$ in the lower energy range with the $^3He(n,p)$ cross-section about 6 times larger than the $^6Li(n,\alpha)$ cross-section. The latter has a broad resonance peak of 2.75 barns at 265 kev but drops thereafter; it is only 50 mb at 8 Mev. The ^3He cross-section drops as $^1/v$ up to about 50 kev and thereafter slightly faster, with 0.75 barns at 1 Mev and about 0.5 barns at 14 Mev.

^3He spectrometers can show good resolution below 1 Mev. On the other hand, the ^6Li reaction, due to its high Q-value cannot resolve low-energy pulses;

3.3) contd.

3.3.2) contd.

if these pulses can be eliminated, it is ideal for neutrons above 1 Mev. However above 10 Mev recoil pulses begin to interfere. Lithium has no useable gaseous compound but can be used as $^{6}Li\ I(E_n)$ scintillator or loaded in glass or emulsion plates and with solid state detectors.

3.3.3) Threshold Reactions:

These may be caused only by neutrons whose energy is above a certain value. The reaction may be exoergic or endoergic. Possible uses include the following:

(i) Fission. Fission is an exo-ergic reaction and there is a variety of fissile materials in which the cross-section for fission rises reasonably sharply to a fairly constant value. A major difficulty, particularly with uranium isotopes is that of admixture of thermally fissile isotopes. Pulsed type fission counters in which fission materials are usually coated on chamber electrodes are commercially available. Alternately, sample of fissile materials may be examined for radio-activity after irradiation by fast neutrons.

(ii) (n,x) reactions. The emitted particles are protons, alpha-particles or two neutrons. In general, cross-sections vary more with energy than those of fission reactions.

(iii) Inelastic neutron scattering. The detection of low lying isomeric states of heavy nuclei with long half-lives is the basis of these detectors.

(iv) Shielded detectors. Basically they are not

3.3) contd.

3.3.3) contd.

(iv) contd.

threshold detectors; but they can give 'effective' thresholds by covering them with moderators or absorbers. In the first type hydrogeneous layers are added to thermal neutron detectors e.g. ^{6}Li I(Tℓ) scintillators and BF_3 counters, to extend their useful response beyond 14 Mev. A particular case is BF_3 counters covered with 6 to 7 cms paraffin in thickness when the efficiency of detection becomes practically constant over a large energy range of incident neutrons; this is the so called 'long-counter', a crude but much used detector. In the second type by varying the thickness of absorbers such as boron around ^{239}Pu - fission chambers, effective threshold can be varied from 10 kev to 1 Mev. The major disadvantage of such a detector system is the large amount of material around the detector.

The threshold detectors, in contrast to those using exoergic reactions of ^{6}Li and ^{3}He give only integral spectral index. Nevertheless they are widely used in several types of measurements for which they prove to be superior to the other spectrometers.

3.4) Various Detection Systems.

Based on the above principles several detectors have come to use. For many of them, a broad division can be made, in the types of information obtained and also in design, whether the

3.4) contd.

detector is located inside the medium with 4π-reception or whether it is outside the medium and a beam is extracted which is measured. General characteristics of various detection systems for fast neutron flux measurements are discussed below.

3.4.1) 4π Recoil Proportional Counters:

Hydrogen gas filled under pressure can constitute a gaseous recoil counter. The stopping power is improved by introducing some heavy noble gas such as argon or krypton. Heavy hydrogeneous compounds such as ethane or methane are also used.

The energy range of proportional counters is limited. Below 1 kev the energy expended per ion pair formed increases rapidly and reasonable energy resolution becomes impossible. The useful upper limit is set by wall and end-effects; practical limit of small size counters of 2 to 5 cm diameter is 1 Mev. Interference can be produced in the sub-Mev region by pulses due to higher energy neutrons, particularly if the Mev region is rich in pulses. Within certain limits corrections can be made to observed pulses by Monte Carlo calculations. For the unfolding of spectra, computer codes such as Fortran SPEC4 [69] can be used.

Upon the same principle as proton recoil, ^{4}He gas spectromers have been used.

3.4.2) ^{3}He-Counters:

Proportional counters filled with ^{3}He gas can give information with good resolution in the energy range 100 kev to 1 Mev. By applying proper corrections to the

3.4) contd.

3.4.2) contd.

observed pulses, the upper limit can be extended to 2 to 3 Mev. ^{3}He elastic recoil would mask the lower energy neutron pulses; the situation can be improved by electronically eliminating recoil distortion [70].

The efficiency is several orders of magnitude below that for organic scintillators and nuclear emulsions. Its main virtue is the reliability of data and direct production of the differential spectra between 100 kev to 1 Mev, a range difficult for many spectrometers.

3.4.3) Organic Scintillators:

Proton recoil process is again the basis for fast neutron detection with organic scintillators. Scintillators such as NE-213 and stilbene are commercially available and can be liquid or solid. Analysis of the recoil energy spectra will be essentially identical with that of the proton recoil gas counters. The effects of finite size of the scintillator are analogous to wall effects in the counter. But because of their much higher densities organic scintillators have got higher efficiencies than gaseous counters by a factor of about 10^3 on a volume basis. Thickness of an organic scintillator is limited by considerations to reduce multiple scattering of an incident neutron. The energy range, most favourable for organic scintillators is 1 to 10 Mev, with perhaps several sizes for different energy regions. Below 1 Mev gamma-rays begin to interfere; this is a particular problem with them as the output pulse is higher from electrons than from protons of the same energy. However, Furuta et al. [72] has recently

3.4) contd.

3.4.3) contd.

reported of using NE-213 scintillators down to 52 kev with specially designed electronics for discrimination of gamma-rays.

The output is non-linear for organic scintillators with heavy particles. This effect of non-linearity in constructing the neutron differential spectra can be reduced by the use of an unscrambling code which uses accurately measured pulse height distribution for mono-energetic neutrons. Much work in this direction has been done by Verbinski and co-workers to standardize 2" × 2" and 5" × 5" NE-213 and 2" × 2" stilbene scintillators [73,74].

3.4.4) Inorganic Scintillators:

Lithium iodide crystals activated with thallium or europium using (n,α) reaction can be used for the neutron energy range of 0.8 Mev to 5 Mev. However the low energy neutrons which will not be resolved due to high Q-value may be piled up if abundant. On the other hand due to the high Q-value the gamma pulses may be discriminated better.

Z_nS activated with silver has been used in a variety of forms. It has high efficiency for light conversion; but its chief limitation is its opacity. A small amount in the powdered form suspended in transparent organic material like lucrite or perspex has been used; this gives better gamma-discrimination capacity than pure organic scintillators. Thin scintillators of Z_nS-B_2O_3 glass mixture in which alpha particles form $^{10}B(n,\alpha)^7Li$

3.4) contd.

3.4.4) contd.

reaction cause scintillation, are used for low energy and thermal neutrons only.

3.4.5) Semi-conductor Detectors.

Basically, semi-conductor detectors detect charged particles such as protons, alphas or fission products from a variety of characteristic reactions. Usually a small amount of the reaction material, either in the form of a thin film or gas is placed in front of one or in between two detectors facing each other. In spite of their very low efficiency (of the order of 10^{-6}) they present some attractive features. The extremely low efficiency is somewhat offset by the high resolution. They have small size and can operate with low voltage and simple electronics.

For recoil protons a thin layer of paraffin or mylar film is used. With the exo-ergic reactions both the particles are detected by two surface barrier detectors facing each other; the signals are summed up to give their total energy and the pulses are counted in coincidence to reduce background etc., ^{3}He gas at a pressure, put in a chamber can be used. Above 4.5 Mev peaks due to (n,p) and (n,α) reaction in silicon are observed even with co-incidence. The lower limit of energy range depends on the magnitude of thermal neutron flux and the gamma-field. A thin film of ^{6}Li or ^{6}LiF can be used and reaction products counted in the same way as the ^{3}He counters. Solid state fissionable counters can give a variety of information when several isotopes are used one after the other; they also

3.4) contd.

3.4.5) contd.

show better gamma-ray discrimination. An outstanding feature of the fission counters is their self-calibrating capability as they are alpha emitters. Storminger [75] describes in detail successful counters using several isotopes. However the information obtainable from fission counters is integral in nature as the energy of the fission fragments hardly change with incident neutron energy.

3.4.6) Nuclear Emulsion:

Spectrum measurements are made by measuring the recoil proton spectrum in emulsion plates. For 4π-detection the differential spectrum of neutrons can be obtained by differentiating the observed proton spectrum, according to eqn.3.2. The proton energies can be obtained by measuring their track lengths and from a knowledge of energy-range relationship. The lower range limit is imposed by proton range straggling which increases rapidly below 2 Mev and below 0.5 Mev becomes prohibitively large. The lower limit can be pushed further with special emulsions if fogging of the plates due to gamma-rays is not high. The upper limit is imposed by the emulsion thickness; for 15 Mev protons the range is about a thousand microns.

In the 1950's emulsions were the much used technique and much useful information for fast neutrons was obtained with them [76,77]. In the 1960's the relative importance of emulsions reduced because of development of other methods. However, even now emulsion is perhaps the technique

3.4) contd.

3.4.6) contd.

that can cover the widest range of energy in a single measurement. The short-comings of emulsions have been described by Barschall et al. [78] . The most serious difficulty concerns the accurate delineation of the solid angle, in which the proton tracks are counted. The best estimates have an error of ± 15% for neutrons of 1 Mev and ± 10% for neutrons of energy greater than 3 Mev. The solid angle problem is improved if a separate hydrogeneous radiator is used: this has to be outside the medium. Another uncertainty arises in the determination of the number of hydrogen atoms in the emulsion; this is usually subject to an error of about ± 12%.

In addition a large number of tracks have to be measured to build up any significant statistics. Also for successful measurements previous experience is needed. The otherwise apparent simplicity of the method is thus very deceptive.

3.4.7) Time-of-Flight Technique.

Neutron spectrometry by time of flight technique involves the production of a short burst of neutrons together with the measurement of their time of arrival at a detector some 5 m to 60 m distant. For all time of flight measurements, the neutron energy E in electron volts, and flight time t in microseconds for a flight path D, measured in metres is given by

3.4) contd.

3.4.7) contd.

$$t = 72.3 \frac{D}{\sqrt{E}} \qquad 3.3$$

For fast neutrons in the range 0.1 to 15 Mev and path length of several metres, the flight times are in the range of 10^{-9} to 10^{-7} seconds. An uncertainty in timing is introduced due to several factors including the characteristics of the electronics, detector size and its rise time and the moderation time of the neutrons in the medium. Corresponding to this an uncertainty in energy is introduced which is given by

$$\Delta E \quad \alpha \quad E^{3/2} D \qquad 3.4$$

The resolution consideration limits the usual energy range of detection in the ev and kev region.

3.4.8) Threshold Detectors:

In general, characteristic activities induced are measured for the threshold detectors. The information is of integral nature and for the threshold foils the information is obtainable only after the irradiation is over i.e. it is not instantaneous. In spite of their limitations the threshold detectors still continue to find important uses. For example, in weapon environment where high temperature, physical shock and intense gamma radiation make many of the other detectors useless, threshold detectors can give reliable information. Their small physical size makes them readily applicable where space limitation is critical. They are characteristically

3.4) contd.

3.4.8) contd.

suited for shielding and radiation damage type of investigations [79], where the high-energy component of the neutron spectrum is of particular interest. The advantages of foil detectors can be summarised as below:-

(1) The foils can be very small in both size and mass;

(2) The foils require no electronic devices and connections during irradiation;

(3) Discrimination against gammas and betas are excellent (this may not be true for fission foils used near the Linacs);

(4) Foils can integrate the neutron flux overy very short or very long times;

(5) Foils are insensitive to shock, electromagnetic disturbances and temperature effects;

(6) Most foils are inexpensive and a wide variety is available for choice.

Limitations of threshold foils are:

(1) Fine structure of a spectrum is not revealed and energy resolution is not sharp;

(2) It is difficult to find suitable threshold foils for the sub-Mev region;

(3) There is uncertainty about many threshold cross-sections; some are unknown;

(4) They cannot be used if flux is low e.g. they cannot be used with neutrons from D(d,n) ^{3}He reaction with the low-energy accelerators.

It is difficult to define sensitivity of threshold foils. Cross [182] has tried to define it as counts per minute per gm of detector, with an assumed average cross-sectiin over the energy region of response. Foils are more limited than other types of detectors, if the flux level is low. While with counters or emulsion plates sufficient statistics can be built up with longer irradiation time, with foil detectors the saturation-effect limits the

3.4) contd.

3.4.8) contd.

activity induced as proportional to flux level. However, within limits this can be compensated for by counting the foils for longer time.

When the neutron flux varies during the period of irradiation the induced activity gives the 'effective' flux averaged over the period. However this effective flux depends upon the half-life of the activity being induced, so that for different foils of different half-lives it will be different even though they were irradiated together. For inter-comparison it is necessary to have a record of the time-variation of the flux level. If the absolute counting efficiencies of the foils are known, it is not necessary to know the absolute flux level; variation of a quantity, such as rate meter flow chart readings from a pulsed counter, which is directly proportional to the absolute flux is adequate. This is again a special requirement for threshold foils due to simultaneous build up and decay of the activity during irradiation.

3.5) Intercomparison of the Properties of Detection Systems.

It can be seen that there is no single detector that covers the entire fast neutron energy range below 14 Mev. At present the ideal choice of a single spectrometer which produces a direct readout and a few per cent resolution of the energy distribution of neutrons approaching the detector from a 4π direction is beyond the scope of the technology. Organic scintillators - probably in several different sizes - with pulse discrimination can cover the Mev range. Below 1 Mev ^{3}He-spectrometer is the best choice. Present day measurements, with fast critical assemblies

3.5) contd.

tends to use three detection systems to cover the range of importance which is about 5 Mev to 100 ev. The Mev region is measured with emulsion plates, ^{7}Li detectors, threshold foils and organic scintillators, the high kev region is covered with proton recoil counters and ^{3}He proportional counters and the lower energy region usually measured by the time-of-flight technique. The time-of-flight technique is frequently used because it is possible from these measurements to correlate the decay rate of the pulsed neutrons to the reactivity of the assembly which is of special interest to the critical or near-critical system, and measurements with a representative flux drawn usually from the centre is adequate for that. Fast neutron studies by pulsing the assemblies with 14-Mev neutrons have been reported [82,83]. For the SUAK fast assembly at Karlsruhe the spectrum is taken from the centre and as the target is also at the centre there is no flux gradient for the degraded neutrons there; at any other position gradient exists so that the extracted spectrum is not representative of the true spectrum at the point. Spectra can also be studied without distortion if they are taken from the surface. It is not necessary to confine measurements to the time-of-flight technique. Using detectors such as an organic scintillator and shielding it, the energy and angular distribution of emergent spectra can be studied for the steady state case. However theoretical interpretation becomes very complicated and in addition there is no practical application for the angular energy distribution of leakage neutrons.

To measure the flux inside an assembly almost all the detectors except the emulsion plates and the threshold foils must have an entrance channel for thier physical passage and for the connecting cables. Once the detector is fixed the

3.5) contd.

rest of the space can be filled with the material of the medium and for spatial distribution of neutron flux the detector position could be changed along this channel and irradiations repeated. However such a channel would unavoidably leave some empty space even for the smallest detection systems. Distortion of the spectra would be caused by the empty space and due to mismatching of the materials of the detector and container and this, in a small assembly could be considerable. Only in Monte Carlo type of calculations can such arbitrary discontinuity be adequately represented. Semi-conductor detectors have a very low efficiency. A possible detector namely, the organice scintillator would have hydrogeneous materials in the scintillator and the light guide which would produce serious perturbations for a fast system.

In the present assemblies the neutron field almost anywhere except near the outer boundaries is dominated by the abundance of the 14 Mev neutrons. Several of the detectors including proton recoil and ^{3}He counters have their spectra distorted by high energy neutrons. The reason they can measure reactor-type spectra is because of low proportion of the fast neutrons in them above 5 Mev. For the recovery of the portion of the spectrum due to low energy neutrons extensive Monte Carlo calculations become necessary.

The perturbations produced both in the flux itself and in the induced responses in the detectors are least with the threshold foils and the emulsions. For the distribution of the spectra at different positions simultaneous irradiation is possible. However the difficulties in obtaining the data from the emulsion plates, as has been discussed, are considerable. On the contrary the data from the threshold foils can be obtained by direct measurements with electronic counters. So far as the high energy

3.5) contd.

region is concerned, the high mass number of the foil materials makes them compatible with those of the media. No characteristic fine-structure of interest is expected in the Mev regions inside iron and uranium assemblies. Thus the integral nature of the response is not a serious drawback. The D(t,n) ^{4}He reaction can produce neutrons of sufficient intensity so that meaningful activities can be obtained throughout the thickness of the assemblies. In the absence of slowing down by elastic collisions, the sub-Mev region can be measured with ^{115}In (n,γ) reaction, to supplement information obtained with the threshold foils.

Another advantage with the threshold detectors is that absolute efficiency as a function of energy is known by measuring it at one energy - 14 Mev, if the cross-section curve is known with sufficient accuracy. With most other detectors the efficiency is a complex function of several factors and for certainty should be calibrated with mono-energetic sources of several energies. The efficiencies of the common detection systems are shown in Figure 3.1; this is after Wallace [80]. As can be seen in the figure the efficiency in general decreases with increasing energy and has a small value at 14-Mev. For the threshold foils the reaction cross-sections generally increase with increasing neutron energy and have high values around 14 Mev, so that reliable accuracy for the calibration with the 14 Mev neutrons can be expected.

A 3" × 3" NaI(Tℓ) gamma scintillation detector coupled to a 400 channel RIDL analyser was available in the laboratory. With this versatile equipment counting could be done with desirable precision and reliability.

FIGURE 3.1-- Typical Efficiencies of Various Fast Neutron Counters as a Function of Energy. (From Wallace, ref. 80).

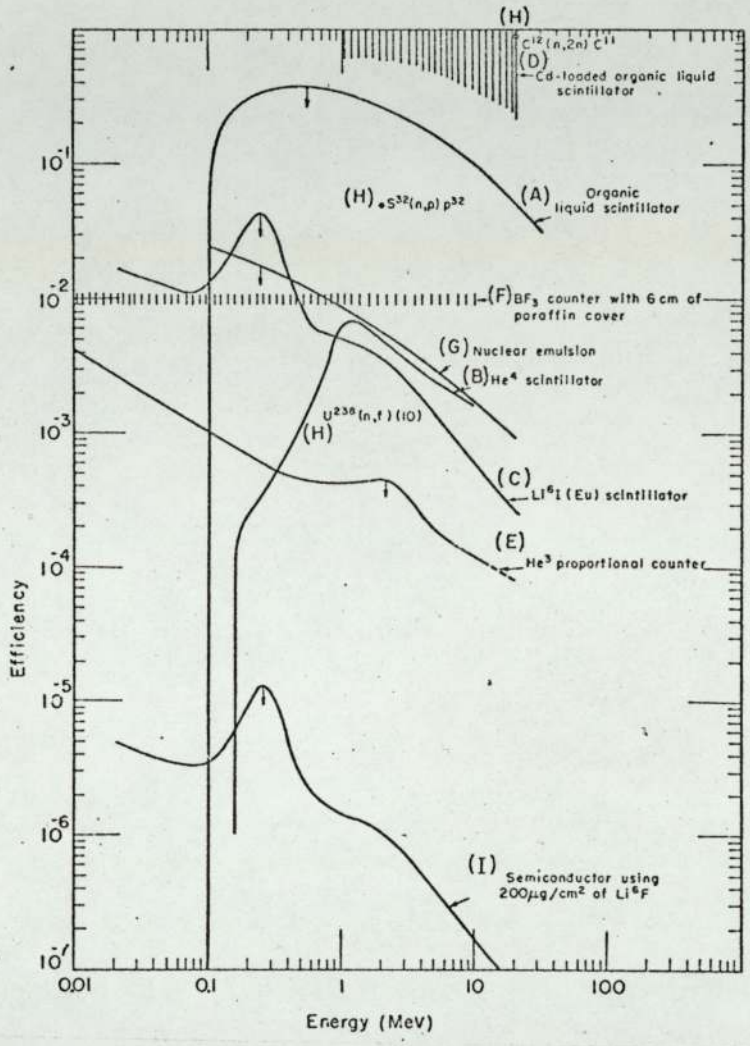

The relative vertical positions of the curves may move up or down by several factors depending upon conditions. Downwards arrows indicate observed efficiency is usually smaller than shown here; (80).

CHAPTER 4.

EXPERIMENTAL ARRANGEMENTS.

4.1) Introduction.

Two different experimental assemblies were studied for flux measurements - one of iron only and the other of iron and uranium. Both were of cylindrical geometry with generally similar dimensions. The bulk of the iron used for the construction of the assemblies was obtained on loan from the Shielding Division of the UKAEA, Harwell Centre. The uranium used was shared with the subcritical assembly in this laboratory.

A cell made of concrete bricks housed the assemblies and also shielded the fast neutrons. A water filled tank above the cell shielded the floor overhead.

Neutrons were produced by a SAMES accelerator which provided a beam of deuterons on to a tritium target located in the centre of the assembly.

4.2) Geometry of the Assemblies.

The ideal geometry for comparing experiment and theory would have been spherical, since the neutron source was effectively a point source. However the iron obtained from Harwell was in the form of plates and were of the following dimensions

122 cm × 40 cm × 1.27 cm (48" × 16" × $\frac{1}{2}$").

To shape the plates into parts for a true sphere was formidable. Also the uranium rods were of comparable length. It was decided that the plates would be used as they were and a geometry approximating the spherical would be constructed for both the iron and iron-uranium assemblies. This led to the cylindrical configuration to be built around the target, which gave circular symmetry. Iron plates of smaller widths were used to round the edges of the cylinders.

The cylinders were made hollow and placed horizontally with the deuteron beam along the axis so that the beam tube could be positioned easily into the assemblies. The outer radius was

4.2) contd.

decided by the level of induced activities there and to a lesser extent by the availability of the materials. The inner radius was made larger than the beam tube; this extended the overall size and increased the proportion of the secondary neutrons to the primary 14 Mev neutrons.

4.3) Construction of the Fast Spectrum Cell.

4.3.1) Concrete Chamber.

The line of the ion beam emerging from the accelerator and therefore the position of the neutron source was 147 cm above the floor level. The experimental assemblies had to be raised to have their centres at the target. All the support of the iron and uranium was on the concrete bricks. The rectangular cell was built of concrete bricks 15 cm × 23 cm × 46 cm (6 in × 9 in × 18 in). The inner dimensions of the cell were such that the assemblies were securely supported at the edges and the walls sufficiently far away to reduce the back scattered neutrons. The inner sides of the cell were about 90 cm × 90 cm which gave a supporting edge of about 15 cm at either end of the iron plates. The thickness of the walls of the cell had to be sufficient to adequately shield the fast neutrons. Thickness of concrete on the accelerator side was 94 cm, on the left side 70 cm and behind 84 cm (Figure 4.1). The right hand side was shielded by the sub-critical assembly and so no extra shielding was needed.

4.3.2) Shielding Considerations.

The shielding requirements are dictated by the maximum permissible level (mpℓ) of the radiation field

FIG. 4.1. Schematic Diagram of the Concrete Chamber Housing the Assemblies and Shielding Radiations.

: Not to the Scale.

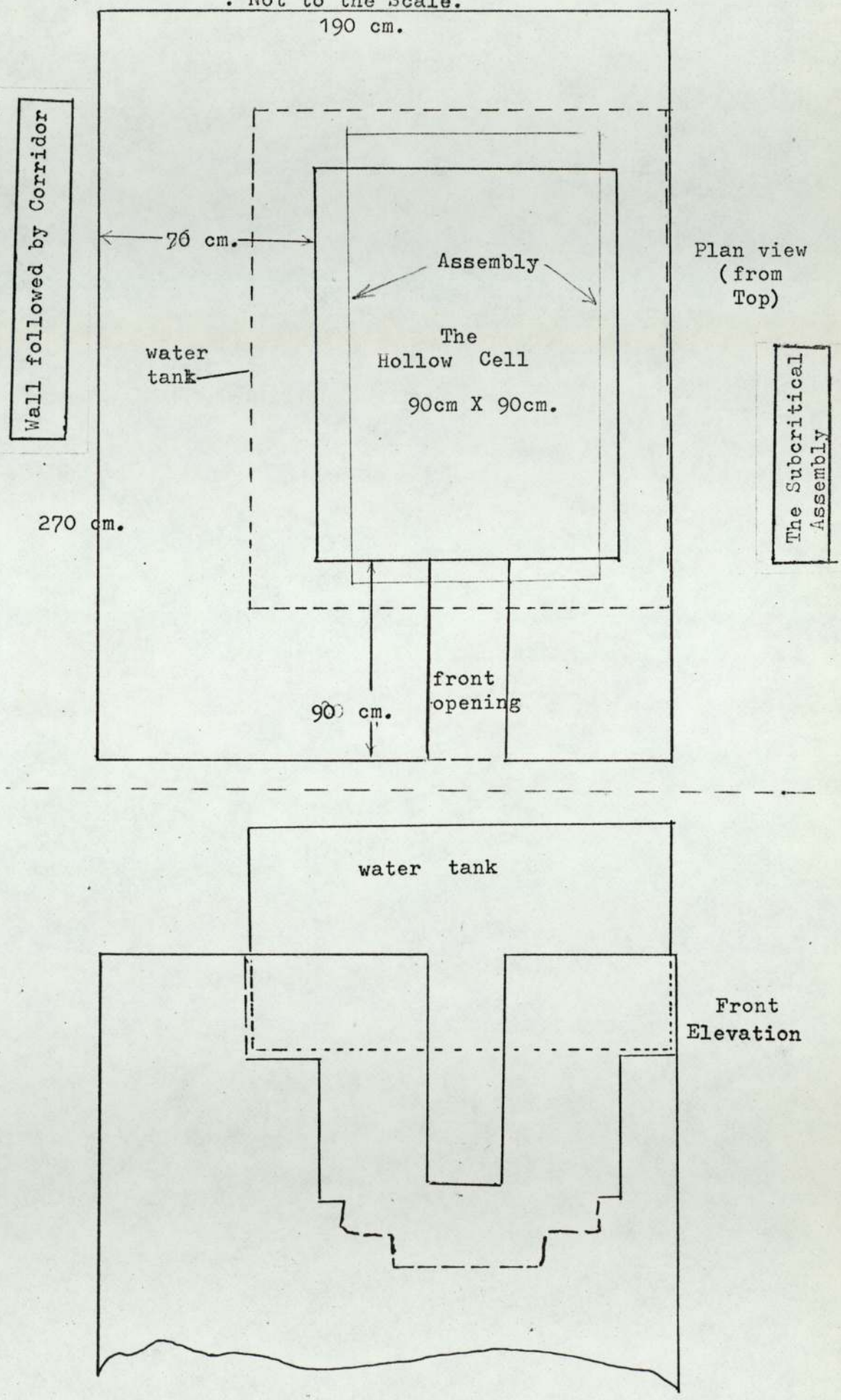

4.3) contd.

4.3.2) contd.

in which personnel of laboratory work. The amount of energy deposited by radiation in body, mostly to ionize the atoms in the tissue is called dose. The unit of absorbed dose is called the Rad; 1 rad is equal to a deposited energy of 100 ergs per gm of the tissue. However different types of radiations produce different amounts of damage to the tissue (breaking the molecular bonds) for the same amount of dose, depending upon the mechanism by which they interact. Damage by fast neutrons is mostly caused through elastic collisions with the protons in the body. The knock on protons are intensely ionizing and produce about ten times the damage of similar energy electrons. There are about 10% by weight but 63% by atoms of hydrogen in the human body [84]. The relative biological potency for damage is called Quality Factor (QF). The QF for 14 Mev neutrons is 6; for the lower energy fast neutrons this factor varies between 6 and 10. The product of absorbed dose in rads and the QF, is called the dose in Rem, which gives a measure of radiobiological effects of any type of radiation in man. The maximum yearly dose must be less than 5 rems in order to avoid harmful biological effects. This gives an average value of 2.5 milli-rem hr^{-1} for a 40 hour week and is referred to as one mpℓ.

Several values for shielding of 14 Mev nuetrons by concrete are available. The following calculation is after the recent work of Hacke [85], who made a compilation and evaluation of the different theoretical

4.3) contd.

4.3.2) contd.

and experimental studies reported on shielding of 14 Mev source neutrons by concrete.

If Q is the source strength per second, then flux of 14 Mev nuetrons at a distance R cm is

$$\phi_o = \frac{Q}{4\pi R^2} \qquad 4.1$$

The corresponding dose is $D(o) = \phi_o \times F$ 4.2

where F is the factor to convert flux density into equivalent dose rate. For 14 Mev neutrons [85]:

$$F = 0.2 \text{ mrem. } h^{-1}/cm^{-2} \text{ sec}^{-1}$$

If concrete of thickness d is now interposed between source and position R, then it is found that the reduced dose can be given by

$$D(d) = D(o)\ Ze^{-\mu d} \qquad 4.3$$

where μ = attenuation coefficient for the dose rate

Z = a build-up factor taking into account scattering phenomena

D(o) is the dose rate at the same point without shielding - defined by eqn.4.2. The ratio of the doses with and without shielding is called the attenuation factor,

$$\frac{D(d)}{D(o)} = K = Ze^{-\mu d} \qquad 4.4$$

If D(d) is given, say 1 mpℓ then the minimum shield thickness, d corresponding to D(d) can be found if K is known as a function of thickness. The dose attenuation factor is expected to be different from attenuation factor for the 14 Mev neutrons alone. Some of the neutrons removed from the primary beam will reappear with lower energy and contribute

4.3) contd.

4.3.2) contd.

to the dose. Also the build up factor Z depends in a complex way on the geometry of the shield and the energy of the neutrons and resort has to be made on experiments. Hacke has compiled various experimental values of K published by several authors with different geometries; results are shown by him graphically. Also a Monte Carlo calculated value is given for comparison. The calculated values over-predict attenuations by factors up to 2. However, a confidence limit can be obtained from the experimental curves. The average value for K for 50 cm concrete is about 6×10^{-2} and for 1 metre is 5×10^{-3}. The fall is faster with further increase in thickness; thus with 1.5 m of concrete K is less than 5×10^{-5}.

It is evident from equations 4.1 to 4.4 above that dose from a source can be reduced both by increasing the distance R and by increasing concrete thickness. The combined effect gives dose

$$D(d) = 0.016Q \frac{K}{R^2} \text{ mrem } h^{-1} \qquad 4.5$$

where Q is source strength per second and R is in cms. With K obtained from Hacke's curves for a source strength of 2×10^9 neutrons per second (obtainable from SAMES with fresh targets), computed dose at the interlocking door behind the accelerator is about 2 mrem/hr; at the corridor on the left this is about 12 mrem/hr and behind the concrete cell 10 mrem/hr for the normally incident neutrons. However during experiments the dose was drastically attenuated further by the iron and uranium surrounding the source;

4.3) contd.

4.3.2) contd.

also the usual source strength was about 10^9 neutrons per sec. or less for most of the time and the observed dose rate was within limit.

4.3.3) Further Shielding.

There was an opening in the front wall of 30 cm. width; this opening was left for positioning and removal of the foils before and after irradiations. This gap was plugged with paraffin wax contained in rectangular wooden boxes. There were two boxes, one containing the beam tube and a larger one to be placed above it. The larger one had a hook attached to it and could be raised easily and quickly with the overhead crane. This allowed enough space to pull out the foil-carriers at the end of the irradiation. The block containing the beam tube only needed to be taken out for purposes such as changing target or alpha-particle detector.

To shield the radiations from people working in the floor above a large steel tank (150 cm. × 140 cm. × 70 cm. high) was placed on top of the raised concrete walls. These raised walls on the sides were of the same thickness as that of the chamber, while at the front and backside they were raised just outside the assemblies. The base of the tank could be adjusted between 5 and 25 cms above the assemblies. The tank when filled with water sufficiently shielded the floor above.

In all cases radiation levels were monitored

4.3) contd.

4.3.3) contd.

with fast neutron, thermal neutron and gamma ray dosimeters; in the places where people would work or move the level was below 1 mpℓ.

4.4) The Iron Assembly.

4.4.1) Cylindrical Configuration.

The cross-sectional view of the iron cylinder can be seen in Figure 4.2. It was all made up of plates of different widths piled up on one another. The thickness and length of all the pieces were the same - 12.7 mm and 122 cm. respectively. The upper and lower parts of the cylinder were mostly made of the larger plates; while the sides were made of 5 cm, 10 cm, 13 cm and 15 cm pieces arranged to give a roughly circular profile of 20.4 cm diameter. 5 more plates of 40 cm width placed vertically on either sides, extended the dimensions. In the upper part gaps of 3.2 mm were left in between the plates for placing the foils vertically above the target. The first gap was above the first plate from the inner boundary and the remaining gaps after every two plates. Thus in all there were seven gaps inside the medium for insertion of the foils. A position at the outer boundary gave eight positions in all. The gaps were maintained with iron strips of the same thickness; their width was about 2.5 cm and length the same as that of the plates.

No gaps were left in the lower part or at the sides of the cylinder. For calculations the whole cylinder was taken to be represented by the upper part. The beam spot was about 8 mm below the centre of the cylinder, so

FIG. 4.2 -- A Cross-sectional View of the Iron Cylinder.

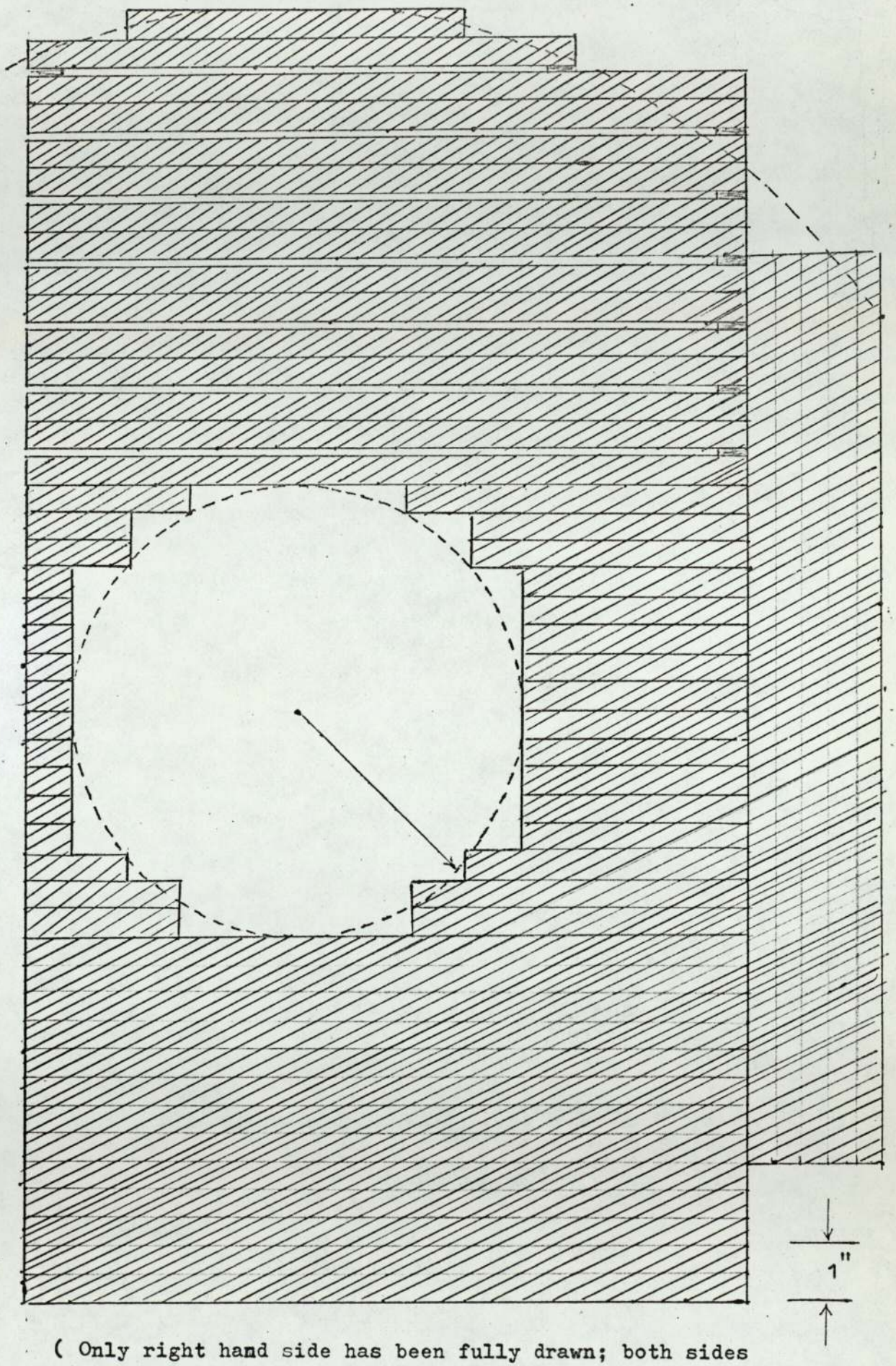

(Only right hand side has been fully drawn; both sides were symmetrical .)

FIG. 4.3

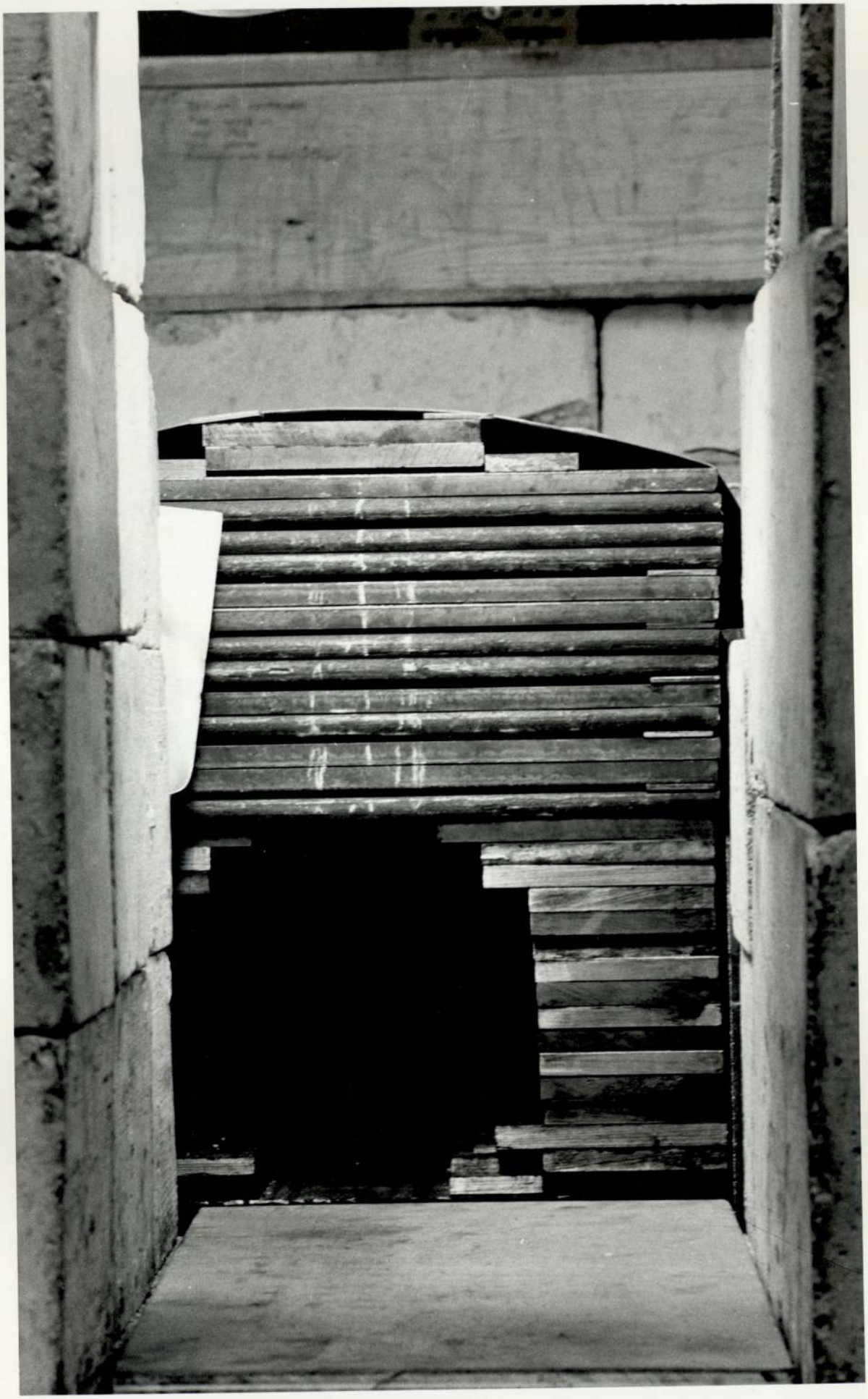

4.4) contd.

4.4.1) contd.

that the distance from target to base of the first upper plate was 11 cm. This was taken to be the inner radius of the cylinder. The outer radius was taken to be the physical boundary vertically above the target.

Handling of the iron plates was facilitated with the help of an electromagnet made for the purpose. Front view of the cylinder is shown in Figure 4.3.

4.4.2) Constants of the Iron Cylinder.

Inner Radius	=	11.0 cm.
Outer Radius	=	32.0 cm.
Length	=	122.0 cm.
Thickness	=	21.0 cm.

Number density of iron in this thickness (upper) = 7.54×10^{22} per c.c.

Hence the ratio of the outer to inner radius $\simeq 3$ and that of thickness to inner radius $\simeq 2$. Thickness in terms of the mean free paths of the 14 Mev neutrons in the medium (with dilution) was as below:

Total cross section : Thickness	=	$4.17\ \lambda_T$
Scattering	=	$1.92\ \lambda_s$
Non-elastic	=	$2.24\ \lambda_{ne}$
Transport	=	$2.56\ \lambda_{tr}$

4.4.3) Cadmium Covers.

There was the possibility of thermal neutrons being scattered back into the assembly from the water tank and the concrete surround. A sheet of cadmium 1 mm thick was laid at the bottom of the tank. In addition

4.4) contd.

4.4.3) contd.

the cylinder was wrapped with cadmium sheets (of same thickness). The wrapped cylinder viewed from top can be seen in Figure 4.4.

4.5) The Iron-Uranium Assembly.

4.5.1) Uranium Rods.

About 100 cylindrical rods of natural uranium with plain aluminium cans were available in the laboratory. Their dimensions were fixed for the lattice configuration of the subcritical assembly. The exact dimensions for uranium was 81 cm. in length and 2.9 cm. in diameter. The cans were made of B.A 99.5% aluminium of inner diameter 2.946 cm. and thickness 0.9 mm. Their length was somewhat larger than that of uranium bars inside - about 88 cm; the extra length contained an internally sealed aluminium cap and some empty space. While placing in the assembly the middle point of the uranium rod was at the middle of the assembly. Weight of each bar was about 10 kgm.

4.5.2) Cylindrical Configuration.

The layout and construction of the iron-uranium assembly was similar to those of the iron cylinder. The cross-sectional view of the assembly can be seen in Figure 4.5. The basic pattern was 2 iron plates followed by a row of uranium bars next to each other and lying on the iron plate below; this was repeated. In order to avoid weight on the uranium bar the iron plate above was resting on two rectangular iron bars of slightly thicker than the

FIG. 4.4

FIG. 4.5 -- A cross-sectional View of the Iron-Uranium Cylinder.
(Only right hand side has been fully shown.)

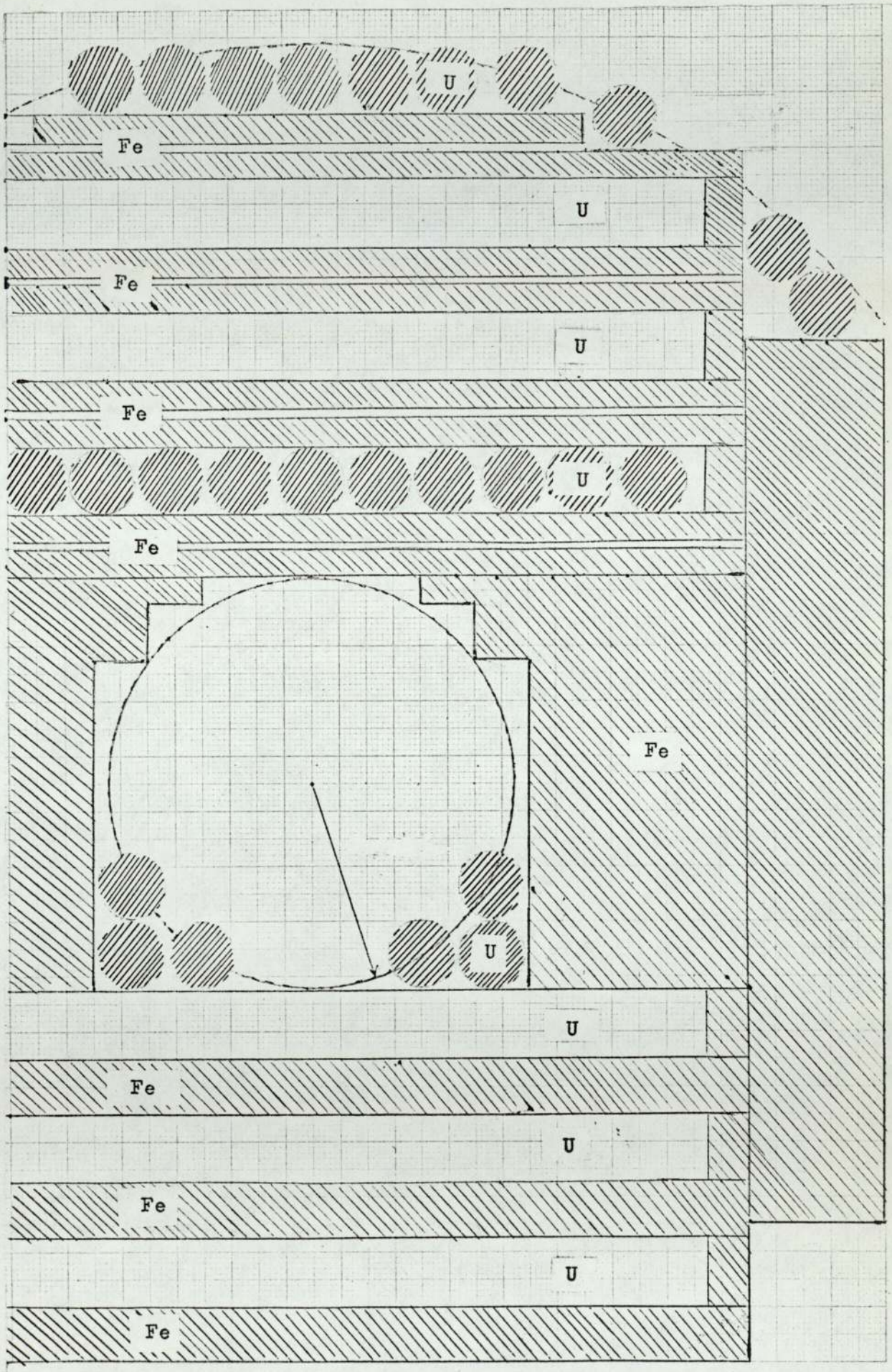

FIG. 4.6

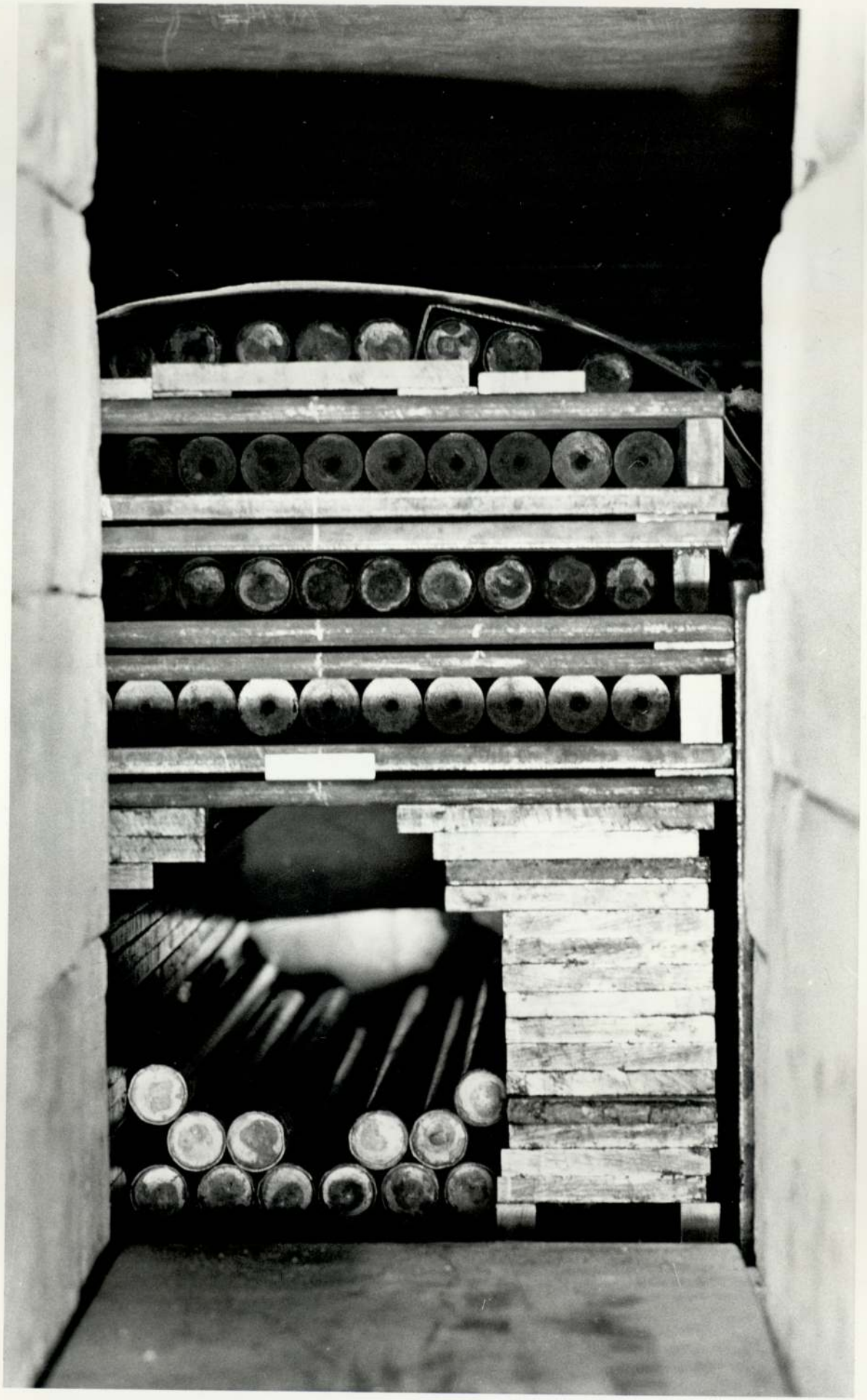

4.5) contd.

4.5.2) contd.

clad uranium - about 3.2 cm. Gaps were maintained in the upper section of the cylinder in between the iron plates in the same way as those in the iron assembly; (gap thickness 3.2 mm).

The lower part was very similar to the upper part, except for the gaps. However the upper part had 3 full layers of iron-uranium and a truncated layer at the outer boundary, the lower part had 3 full layers. There was no uranium in the mid-section of the sides made of iron plates of smaller width as before. The six extra bars of uranium at the lower corners of the inner boundary should somewhat compensate for that. As before, the whole cylinder was assumed to be represented by the upper part of the assembly.

This assembly was also covered with cadmium, as the iron assembly.

4.5.3) Constants for the Fe-U Assembly.

Inner Radius = 10.0 cm

Outer Radius = 34.0 cm

The volume ratios can be obtained by considering a rectangular element of width equal to the diameter of the clad uranium bar, and of height, one layer of the basic pattern of iron and uranium, and finding the ratios of the cross-sectional areas of different constituents in it.

4.5) contd.

4.5.3) contd.

In the diagram below this "unit cell" is shown. The volume ratios were

Iron = 0.424

Uranium = 0.360

Aluminium = 0.046

Air = 0.170

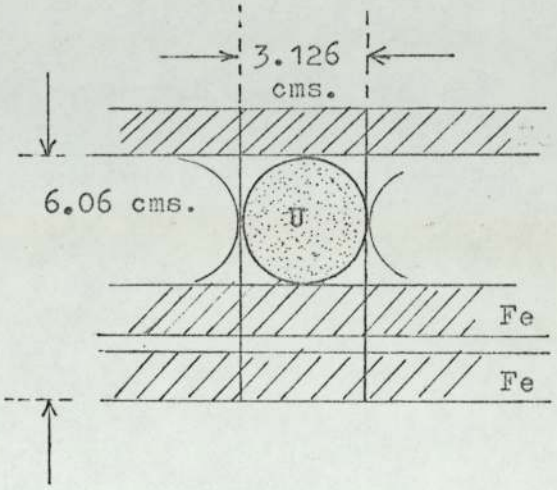

This gives the number densities as

Iron 3.598×10^{22} atoms per c.c.

Uranium 1.7399×10^{22} " " "

It has been assumed that uranium and iron components have the same length. In the calculations aluminium was neglected.

It is of interest to find the equivalent thickness of uranium. The physical thickness can be obtained by considering the uranium smeared into a rectangle of width equal to the diameter of the uranium bar and then equating the cross sectional areas of the rectangle to that of the circle. This gave, if r is the radius

$$\text{thickness} = \frac{\pi r^2}{2r} = \frac{\pi r}{2} = 2.29 \text{ cm.}$$

However the effective thickness of the uranium to the neutrons can be obtained from the experimentally observed removal cross section for the combination; this gave an effective thickness of about 2 cm for the uranium.

CHAPTER 5

PRODUCTION OF NEUTRONS

5.1) Introduction.

Neutrons were produced from the $T(d,n)^4He$ reaction by the bombardment of a tritium - titanium target with a deuteron beam produced by a low energy S.A.M.E.S, type-J accelerator. The neutron energy was about 14 Mev with a small spread. Absolute measurement of the neutron yield was performed by counting the associated alpha particles at 178° to the beam direction, with a silicon surface barrier detector. The anisotropy factor has been taken into account to compute the neutron source strength from the alpha counts.

5.2) Accelerator and Beam tube.

5.2.1) The S.A.M.E.S - accelerator:

The accelerator (Figure 5.1) in the nuclear physics laboratory of this university is a J-type SAMES accelerator, with an electrostatic high voltage generator of maximum output + 150 kV. The machine, in new condition, is capable of giving up to 0.6 mA of ion current of which more than 80% is mono-atomic [86]. The high vacuum is maintained with an oil diffusion pump, which is separated from the accelerator tube by a liquid nitrogen cold trap. An adjustable voltage from 0 to -45 kV is applied for focussing, to the intermediate electrode of the accelerator tube; this voltage comes from a Cockroft-Walton type power pack situated inside the aluminium top terminal which also contains the ion source, extraction voltage unit etc.

The machine is remotely operated from the control panel which is adequately shielded behind a concrete wall.

FIG. 5.1

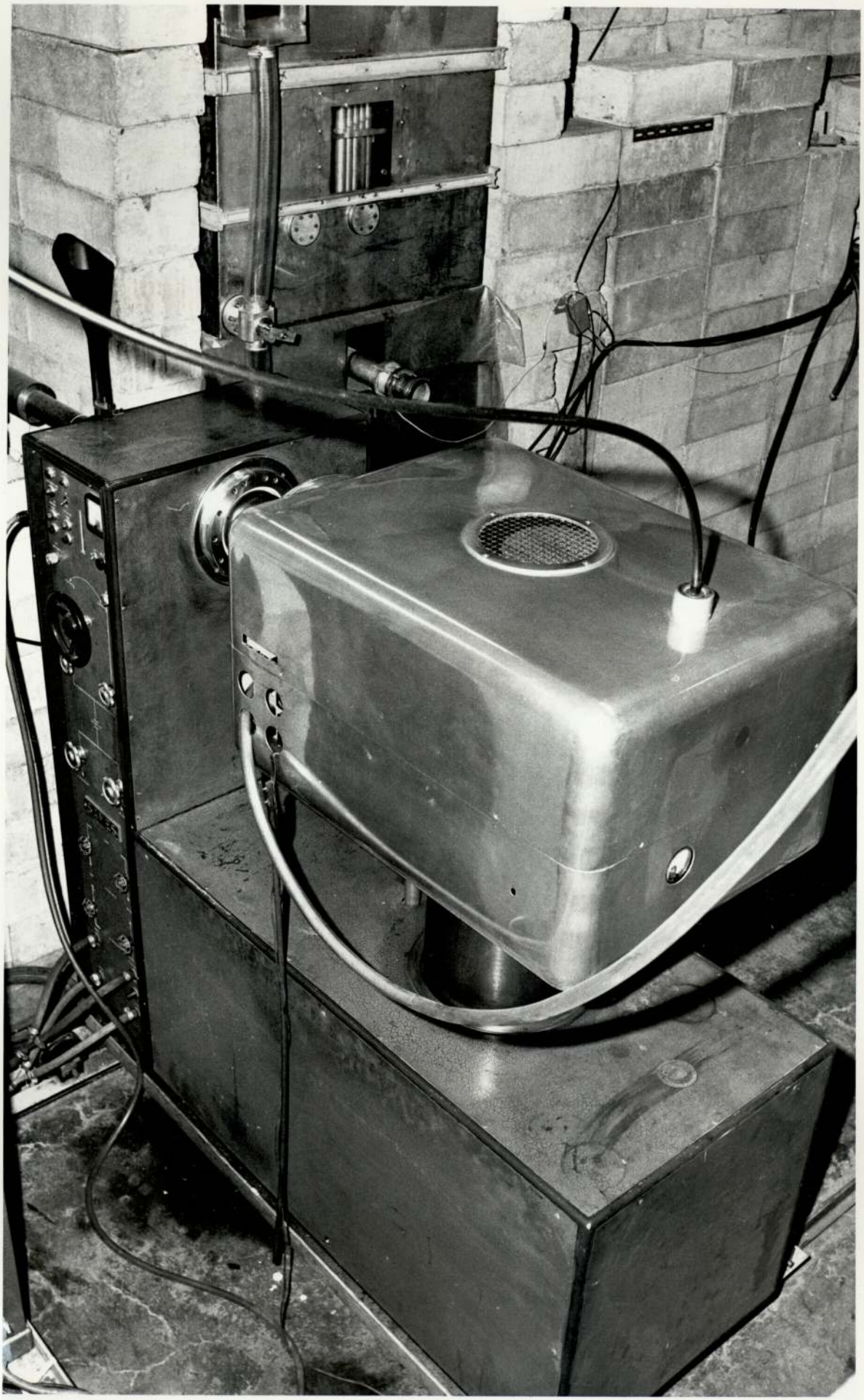

5.2) contd.

5.2.2) Beam tube.

The target, which is situated in the centre of the experimental assembly, is at the end of a 1.75 m long beam tube connected on to the accelerator. This is normally pumped from the accelerator but can be isolated by means of a gate valve for target changing etc. It is shown in Figures 5.2 and 5.3.

The beam tube also houses the SSB (silicon surface barrier) detector. The housing divides the main tube into two parts; apart from this section the tube is made of brass of inner diameter 6.5 cm. and wall thickness 1.5 mm. All the separate joints have rubber O-rings.

The target is water cooled to avoid release of tritium due to temperature rise from deuteron bombardment. The holder for the target is made of thicker brass to include this cooling facility. It is insulated from the rest of the beam tube so that the deuteron ion current falling on the target can be measured. The secondary electrons emitted by the impinging ions from the target are suppressed by applying a voltage (- 150 volts) between the target and an insulated ring in front of it; this is necessary to obtain the correct beam current from meter reading. The aperture in the suppression ring is of the same diameter as the sensitive area of the target (2.5 cm), so that it acts as a collimator to the deuteron beam. Insulators are made of Araldite casting resin. Four metal strips to act as beam sensing probes are supported on leads through ceramic insulators which are soldered into the beam tube. These are at right angles to each other and an

FIG. 5.2. The Beam-Tube

Sames end to Target 162.5 cms.

Beam tube
inner dia= 6.5 cms.
outer dia= 7.0 cms.

Narrow tube
inner dia= 2.5 cms.
length= 2.9 cms.

Flange joining SSB
to Target = 66.5 cms.
to SSB tip = 6.5 cms.

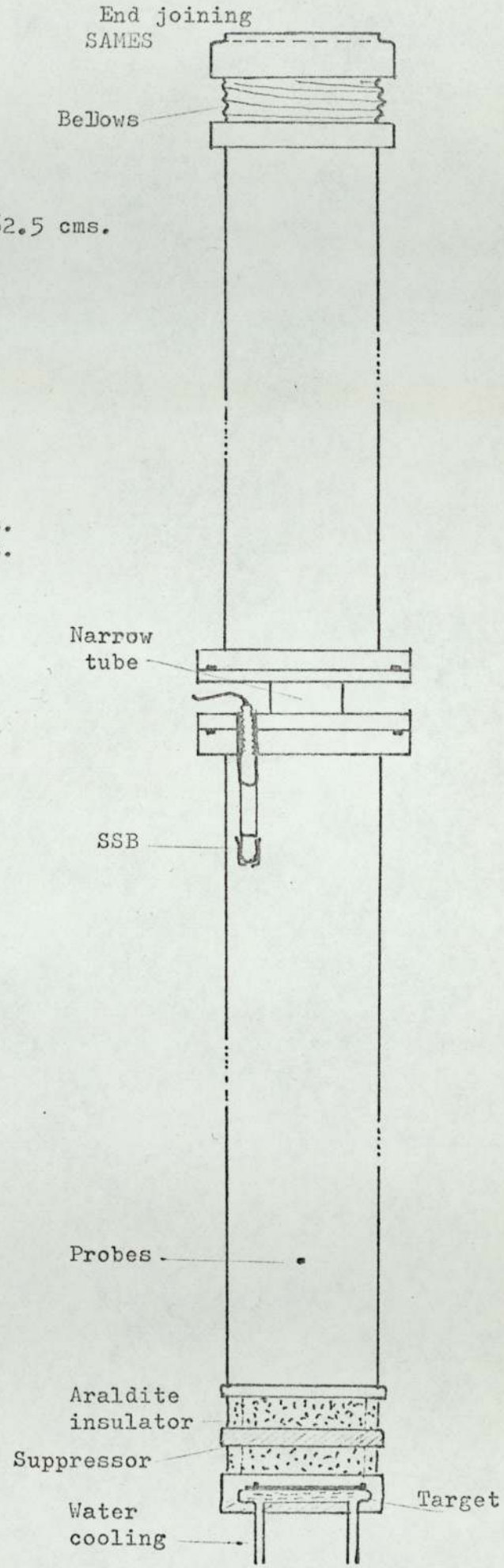

FIG. 5.3

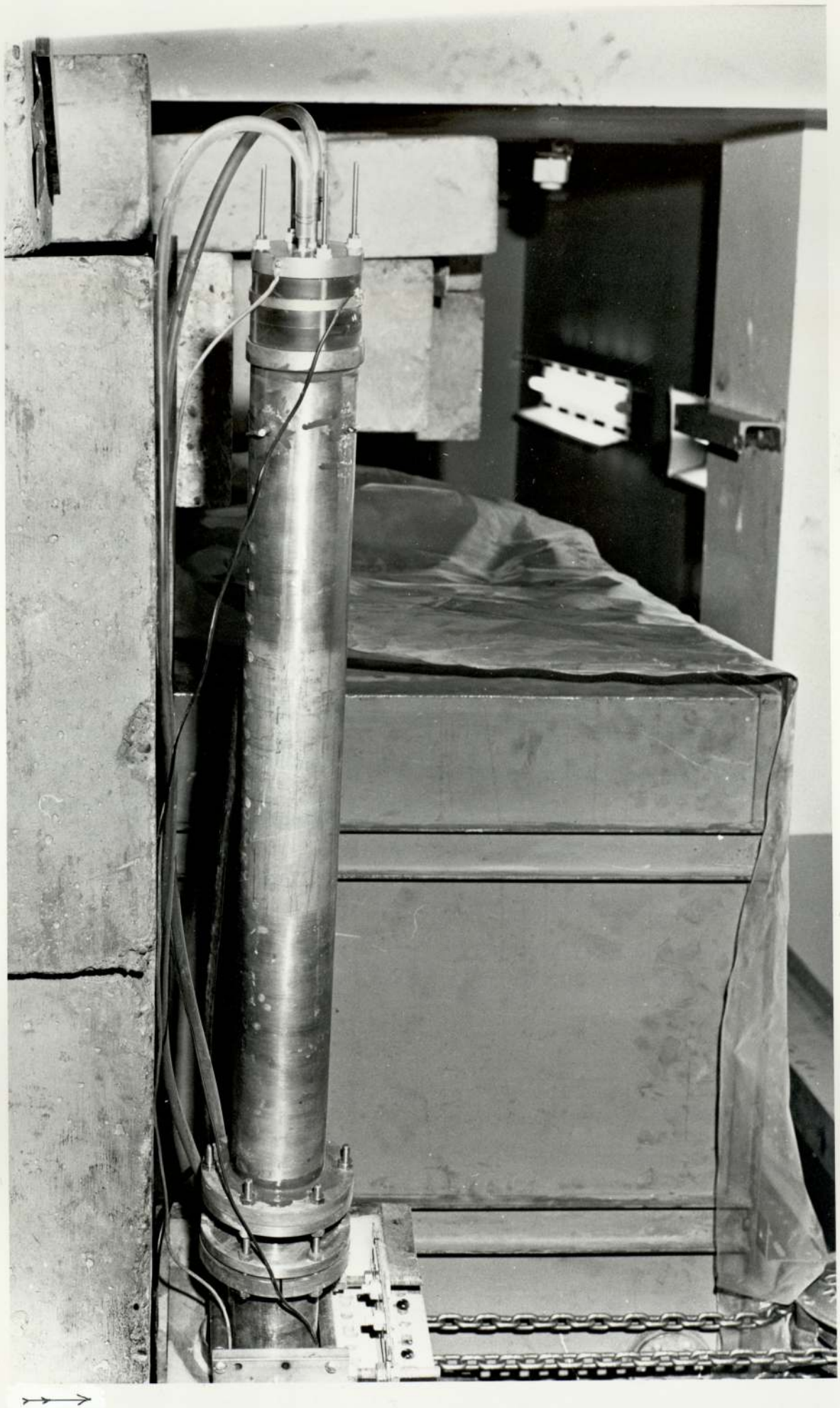

5.2) contd.

5.2.2) contd.

aligned beam would just graze them. Connected into separate meters they are helpful in aligning the target to the beam. A rigid metal frame fixed to the wooden cover of the paraffin shield holds the front half of the beam tube and with the adjustable screws in the frame the target could be moved with respect to the beam.

The SSB is supported by a vacuum-tight lead through insulator in the flange facing the target. A narrow piece of tube connects the two flanges which mate with flanges in the main tube. The flanges also protect the SSB from direct deuteron current.

5.3) Neutrons from T(d,n) ^{4}He Reaction.

5.3.1) Q-value and Neutron Energy:

The reaction

$$ {}_1{}^3H + {}_1{}^2H \rightarrow {}_2{}^4He + n + Q \qquad 5.1 $$

is exo-ergic. The mass difference between the particles in either side is 0.01888 amu, which gives a Q-value of +17.578 Mev. Because of the high Q-value the variation of neutron energy with deuteron energy is relatively small. The energy is shared by the neutron and the alpha particle as inverse ratio of their masses, which gives the neutron about 14 Mev and the alpha particle about 3.5 Mev.

The deuteron needs some initial energy to penetrate the Coulomb barrier; the cross-section for the reaction below 20 kev is very small but it rises to a peak of 5.1 barns at 110 kev (Figure 5.4). As the cross-section falls slowly at higher energies, the neutron output can be

FIGURE 5.4 -- Cross Section Of the $t(d,n)^4He$-Reaction as a Function of Energy.

(Upto 120 kev from Arnold etal and Conner etal; after 120 kev from Marrian& Fowler; refs.91,92 and 88 respectively.)

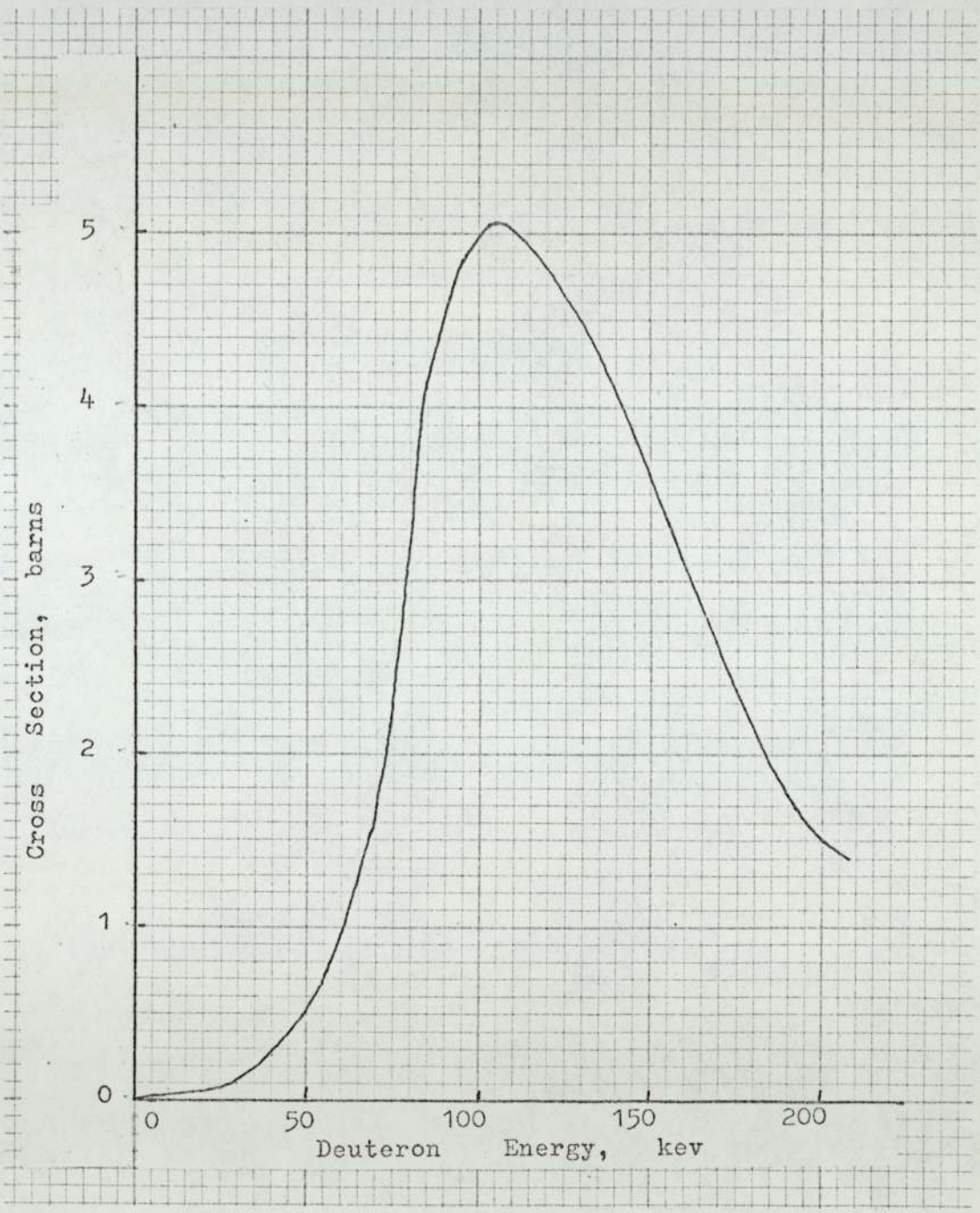

5.3) contd.

5.3.1) contd.

increased by raising the beam energy and using a thick target, although this increases the spread in neutron energy. Deuteron energies of several Mev have been used in order to obtain neutrons with a wide range of energies by kinematic collimation; neutrons of 10 to 30 Mev have been obtained from this reaction [87, 88].

5.3.2) Angular Variation of Neutron Energy.

If a particle of mass m_1 is incident on another particle of mass m_2 which is at rest in the laboratory system, and m_3 and m_4 are the masses of emergent particles after the reaction, then the energy of the particle m_3

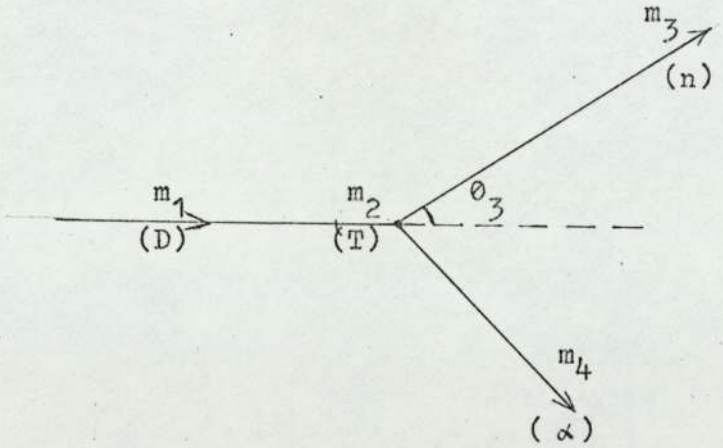

as a function of θ_3, the angle in the laboratory system that m_3 makes with the velocity direction of m_1 before the reaction is given by [89], the general expression

5.3) contd.

5.3.2) contd.

$$E_3(E_o,\theta_3) = \left(\frac{m_1}{m_1+m_2}\right)^2 \frac{m_3}{m_1} E_o \cos 2\theta_3 + \frac{m_4}{m_3+m_4}\left(\frac{m_2}{m_1+m_2} E_o + Q\right)$$

$$+ \frac{2\cos\theta_n}{m_1+m_2}\left[m_1 m_3 \frac{m_4}{m_3+m_4} E_o\left(\frac{m_2}{m_1+m_2} E_o + Q\right)\right.$$

$$\left.\left\{1 - \frac{m_1 m_3}{(m_1+m_2)} \frac{E_o \sin^2\theta_3}{m_4\left(\frac{m_2}{m_1+m_2} E_o + Q\right)}\right\}\right]^{\frac{1}{2}} \quad \ldots 5.2a$$

where E_o is the energy of the incident particle. For the case T(d,n) ^{4}He reaction, the particle of mass m_1 be deuteron and let its velocity be now denoted by E_d. The particle of mass m_3 is then the neutron, for which energy and angle be denoted by E_n and θ_n respectively. The following value of nuclear masses obtained from the Segre'chart [90] are substituted in equation 5.2a

deuteron, m_1 = 2.0141874 amu

tritium, m_2 = 3.0164493 amu

meutron, m_3 = 1.0089830 amu

alpha, m_4 = 4.0027753 amu

This gives for neutron energies in kev

$$E_n(E_d,\theta_n) = 0.080307\, E_d \cos 2\theta_n + 0.798676\,(0.599615\, E_d + 17578.5) + 0.795126 \cos\theta_n\left[0.405783\, E_d\,(0.599615\, E_d + 17578.5)(1-0.100925\, E_d \sin^2\theta_n)/(0.599615\, E_d + 17578.5)\right]^{\frac{1}{2}} \quad \ldots 5.2b$$

The computed neutron energies for several values of deuteron energy up to 200 kev are shown in Figure 5.5. This agrees fairly well with similar values given by Fowler and Brolley [87]; the disagreement is due to atomic masses having been used by them

FIGURE 5.5 -- Angular Energy Variation of the Neutrons at Different Deuteron Energies from the D-T Reaction.

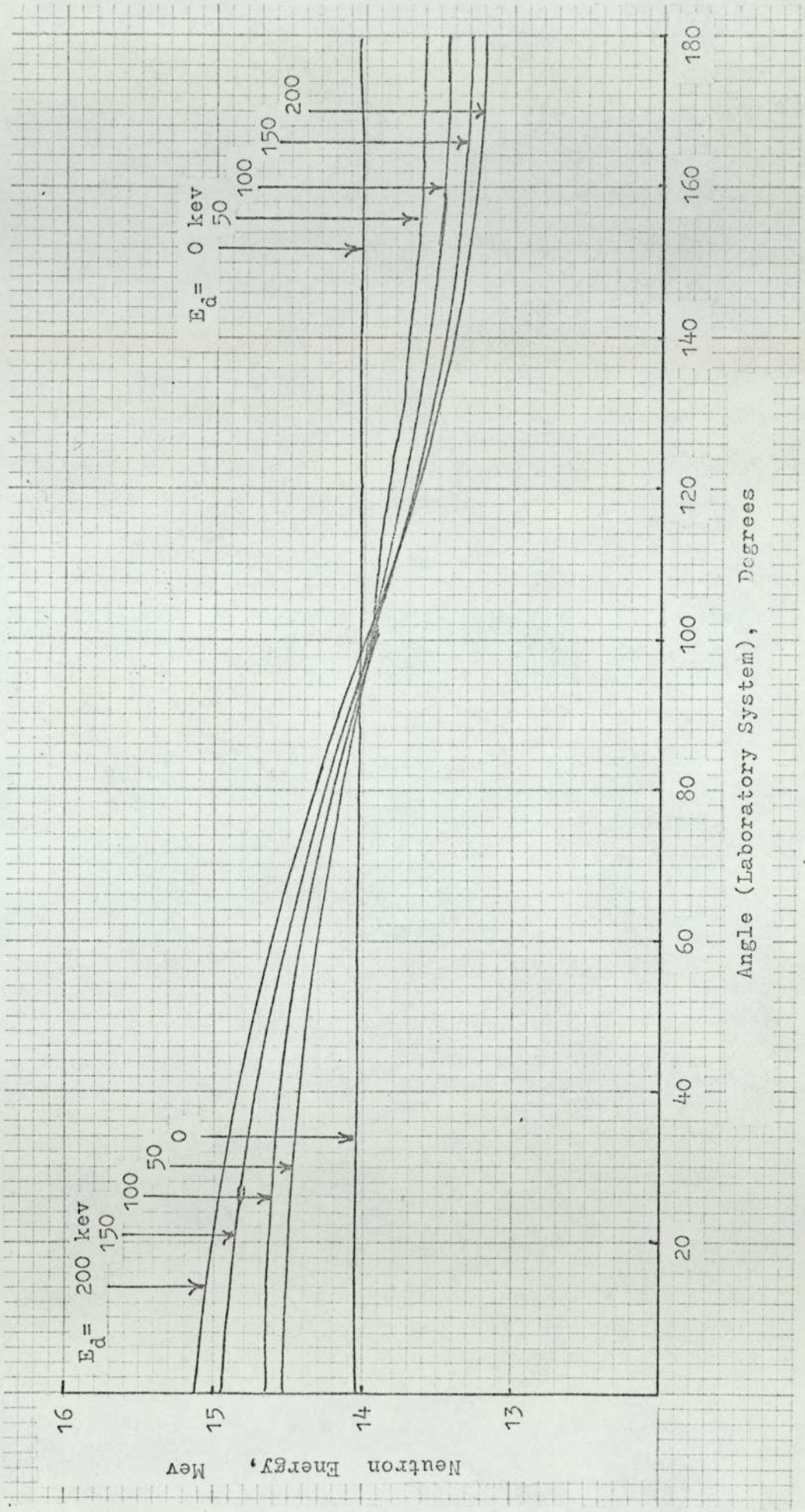

5.3) contd.

5.3.2) contd.

while nuclear masses have been substituted in equation 5.2b above.

A study of Figure 5.5 shows that the neutrons are almost mono-energetic at about 100-degree to the deuteron beam direction, and energy spread increases in either direction away from this angle, being maximum in the forward direction (0-degree). Also, the spread increases with increasing deuteron energy.

5.3.3) Targets.

The targets used were supplied by the Amersham Radio-Chemical Centre of the UKAEA. The targets have a copper disc, of 2.85 cm. diameter and 0.025 cm. thickness, as the base on which a thin layer of titanium of 2.5 cm. diameter is deposited by vacuum evaporation and tritium is absorbed on this. Titanium absorbs tritium by exothermic occlusion involving the formation of a solid solution and interstitial compounds. The composition of the 'compound' varies from tritium: titanium as from 1:1 to 2:1 in these targets. They can withstand up to 200°C in vacuo [93], beyond which tritium begins to come out. The target types vary according to the thickness of the titanium layer, and can be called thick or thin according to the range of the incident ions in them.

There is some uncertainty about the tritium distribution in these targets and perhaps it depends upon the manufacturing process and conditions, and the exact distribution may vary with individual targets. However, it is generally accepted that the tritium content peaks near the

5.3) contd.

5.3.3) contd.

middle of the titanium layer, with very little near the surface and the backing material [94,95]. This is explained by the effects of atmospheric oxidation on the surface and the absorption of gases left in the chamber of the vacuum coating, giving oxides or nitrides near the backing, so that titanium in these sections is not available for tritium absorption. Gunnerson and James [95] determined the distribution in a thin target (15,000 A°) by examining the variation of neutron yield with incident angle and energy of the bombarding deuteron beam and found that the concentration peak is within 3000 A° below the surface and that there is very little tritium contained in an upper surface layer of about 500 A° and the lower 6000 A° of the titanium tritide material.

In the present work two types of targets have been used. Most of the earlier results were obtained with thick targets (type TRT 7, equivalent to present type TRT 51), but the later results have been obtained with a medium thick type (TRT 31). The titanium amounts in them were 2.0 mg/cm^2 and 0.85 mg/cm^2. Titanium lattice undergoes 15% expansion during tritation [95], which gives a physical thickness of titanium in TRT 31 about 21,000 A° and in TRT 7 about 45,000 A°. Range of the 150 kev deuterons in tritium-titanium of typical ratio has been calculated to be 20,000 A° (discussed later); however the range to be slowed down to 20 kev (after which the D-T reaction cross section is negligible) is only 10,000 A°. With a Gunnerson-James type of distribution most of the tritium should be within 12,000 A° from the surface in the TRT 31 type, while for the thick type bulk of the

5.3) contd.

5.3.3) contd.

tritium is below the deuterium range, if the variable profile is correct. This seems to be the case, as was indicated by the fact that the neutron yield for the same deuteron current was 2 to 3 times larger from the fresh TRT 31 type than from TRT 7 in its fresh condition; the output was also falling at a slower rate from the TRT 31 than from the TRT 7.

Possible distributions of tritium in the TRT 31 target is shown in Figure 5.6. A distribution has been constructed from the distribution obtained by Gunnerson and James [95] and the area under the curve has been normalised to that under the rectangle representing uniform distribution. Idealised triangular distributions with peaks at different depths from the surface were also considered; the height of the triangle is equal to twice that of the rectangle so that the total amount of tritium is the same.

For the thick target, the result assuming a uniform rectangular distribution has been compared to that with an idealised triangular distribution peaking at the centre, and the height of the peak twice the rectangle height. As the range of the 150 kev deuterons is small compared to the titanium layer thickness in it, results are not very sensitive to the position of the peak. No definite experimental distribution was available for a thick target.

5.3.4) Line-shape, Average Energy and Yield.

The probability of reaction for a deuteron passing a distance dx through a target containing n_t tritium atoms per c.c. is given by $n_t \sigma dx$, where σ is the cross-section for

FIGURE 5.6 -- Distribution of Tritium in a Titanium Target (TRT-31).

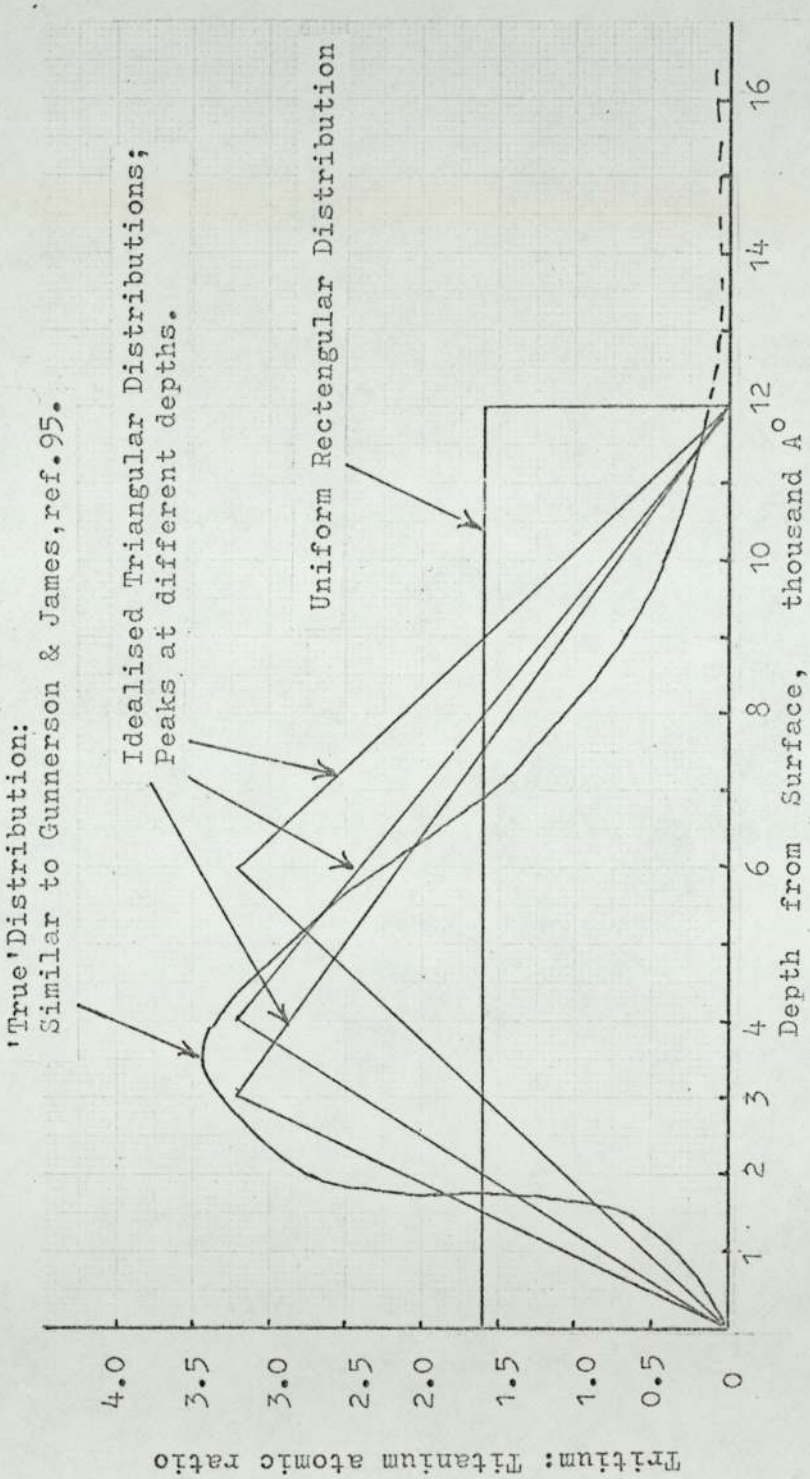

5.3) contd.

5.3.4) contd.

the reaction. Since σ is a function of energy we have

$$\sigma\, dx = \sigma\, dE \Big/ \frac{dE}{dx} \qquad 5.3$$

The number of neutrons at any given angle is given by

$$N(E)dE = \frac{1}{4\pi} \left(\frac{d\sigma}{d\omega}\right)_{E,\phi} n_t(E)\, \frac{dx}{dE}\, dE \qquad 5.4$$

The angular intensity of the neutrons can be computed from this equation if the differential cross-section $d\sigma/d\omega$ is known as a function of energy and angle. However, a simplification and generalization occurs if the neutrons are isotropic in the centre of mass system. The reaction is found to be isotropic to a first approximation for deuteron energies below 1 Mev [88]; it is strictly isotropic below 200 kev [96]. For these cases the anisotropy in the laboratory system is then given by

$$A_n = \frac{\text{neutron flux in the lab system}}{\text{neutron flux in the c.m.system}}$$

$$= \frac{\text{element of solid angle in c.m.}}{\text{element of solid angle in lab}}$$

$$= \frac{d\omega'}{d\omega}$$

$$A_n = \frac{\sin \theta_n\, d\theta}{\sin \phi_n\, d\phi} \qquad 5.5$$

where $d\omega'$ and $d\omega$ are elements of solid angles in c.m. and lab systems respectively and θ_n is the neutron emission angle in the c.m. system and ϕ_n that in the lab system. Further expansion of the right side of equation 5.5 is given by Benveniste and Zenger [89]; the following is after them.

5.3) contd.

5.3.4) contd.

$$\frac{d\omega'}{d\omega} = \frac{\cos\phi_n + \sqrt{\frac{1}{\gamma_n^2} - \sin^2\phi_n}}{\frac{1}{\gamma_n}\sqrt{\left(\frac{1}{\gamma_n^2} - \sin^2\phi_n\right)}} \qquad 5.6$$

where $\frac{1}{\gamma_n^2} = \frac{\text{velocity of the neutron in the c.m.system}}{\text{velocity of the centre of mass in lab system}}$

$$= \frac{m_4(m_1+m_2)}{m_3 m_1}\left[\frac{m_2}{m_1+m_2} + \frac{Q}{E_d}\right] \qquad 5.7a$$

where m_1 and m_2 are the masses of the deuteron and tritium respectively and m_3 and m_4 those of the neutron and the alpha particle. Substituting their values in equation 5.7a we get

$$\frac{1}{\gamma_n^2} = 9.9468\left(0.5996 + \frac{17578}{E_d}\right) \qquad 5.7b$$

where E_d is in kev. Substituting 5.7b in equation 5.6, neutron anisotropy can be calculated. The relative intensity of the neutrons as a function of deuteron energy, from the incident to the lower energies can be computed from

$$N(E_d)dE = \sigma(E_d)\, n_t(E_d)\left(A_n\right)_{\phi_n}\left(\frac{dx}{dE}\right)_{E_d} dE \qquad 5.8$$

The corresponding neutron energy in kev is given by

$$E_n(E_d,\phi_n) = 0.08\, E_d \cos 2\phi_n + 0.8(0.6\, E_d + 17578) + 0.8\cos\phi_n\left[0.4\, E_d(0.6\, E_d + 17578)\left(1 - \frac{E_d \sin^2\phi_n}{10(0.6E_d+17578)}\right)\right]^{\frac{1}{2}} \qquad 5.9$$

Equation 5.9 is the same as equation 5.2b, with the relaxation in accuracy when the numerical values are rounded. Equations 5.8 and 5.9 are the basis for obtaining the properties of the

5.3) contd.

5.3.4) contd.

emitted neutrons. They directly give the line shape of the neutrons. The total number of neutrons per incident deuteron is obtained by integrating equation 5.8:

$$\int N \, dN$$

The average energy of the neutrons is given by

$$\frac{\int E_n . N . dN}{\int N . \, dN} \qquad 5.10$$

The program DTANGENYLD was written to compute the line-shape, average energy and relative yield at several neutron angles with an incident deuteron energy of 150 kev. Some of the results are shown in Figures 5.7, 5.8 and 5.9. The slowing down rate of the deuterons $^{dE}/_{dx}$ in equation 5.8 was obtained as follows, which is also the procedure followed by other authors [89, 95, 97].

There is no available experimental results on the rate of energy loss of deuterons in either titanium tritide or titanium alone. However Warshaw [98] has made some good measurements of the rate of energy loss of proton in Aℓ, Cu, Ag and Au in the energy range 50 to 350 kev and Reynolds et al. [99] have made some energy loss measurements of deuterons in tritium in the range 60 to 700 kev; these agree well with similar measurements by Phillips [182] from 20 to 160 kev, in the overlapping regions. To obtain the required slowing down rate, first the rate of energy loss of protons per mg of Ti is obtained

FIGURE 5.7 -- Line-shape of the Neutrons at Different Angles of Emission.

TRT-7 Target;

Deuteron Energy 150 kev.

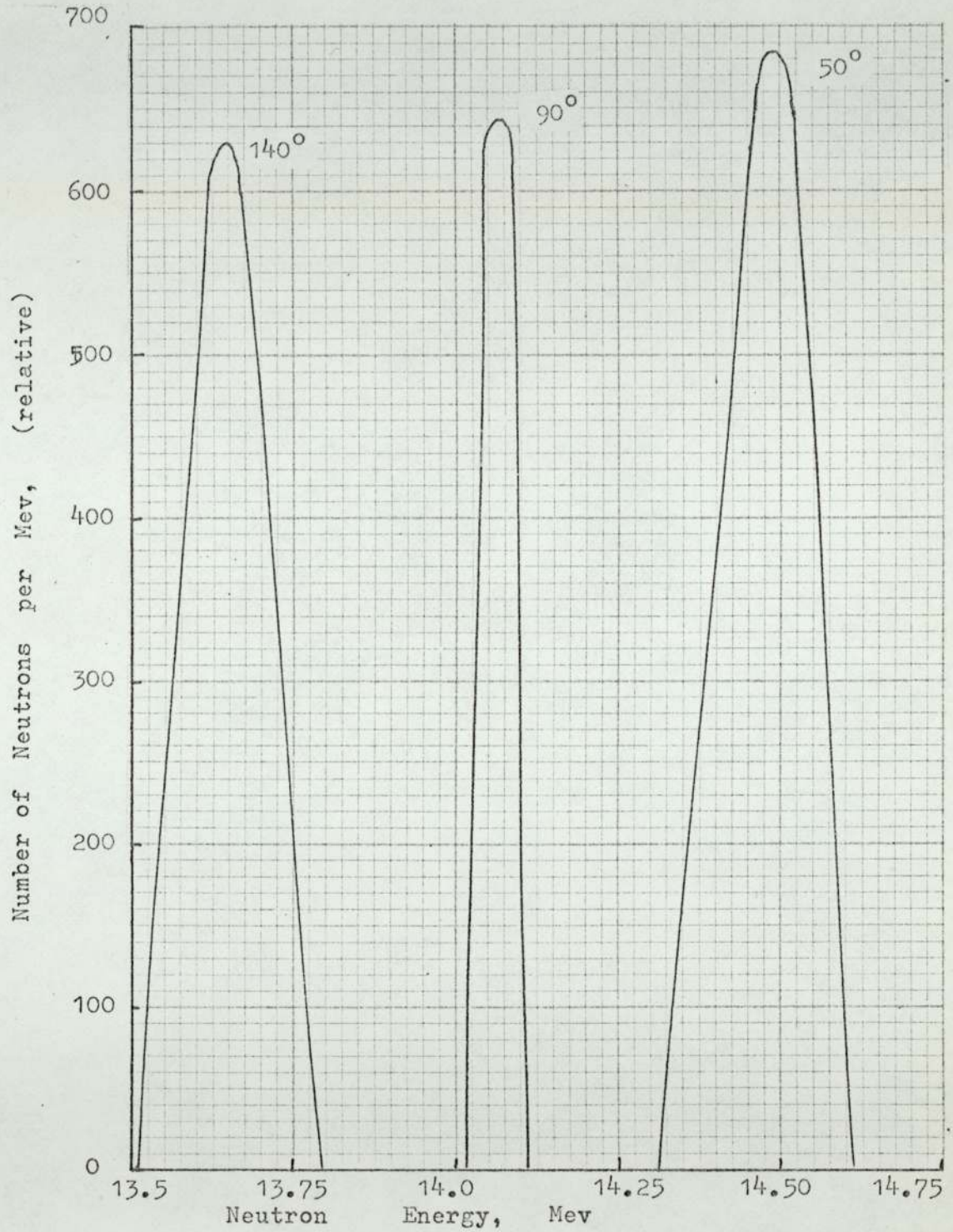

FIGURE 5.8 -- Average Energy and Energy Spread of the Emitted Neutrons as a Function of Emission Angle.

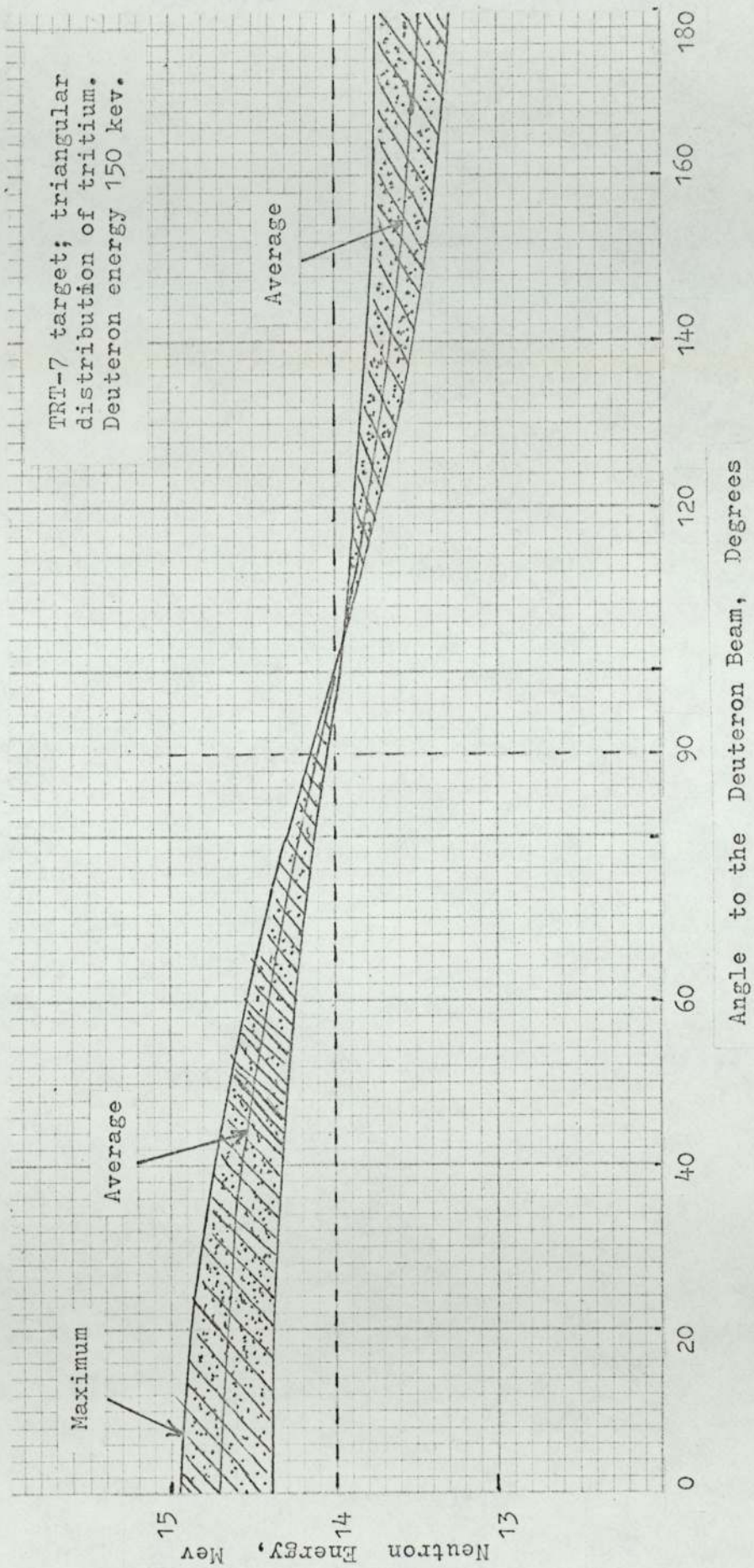

FIGURE 5.9 -- Angular Distribution of the Neutrons Produced from the D-T Reaction.

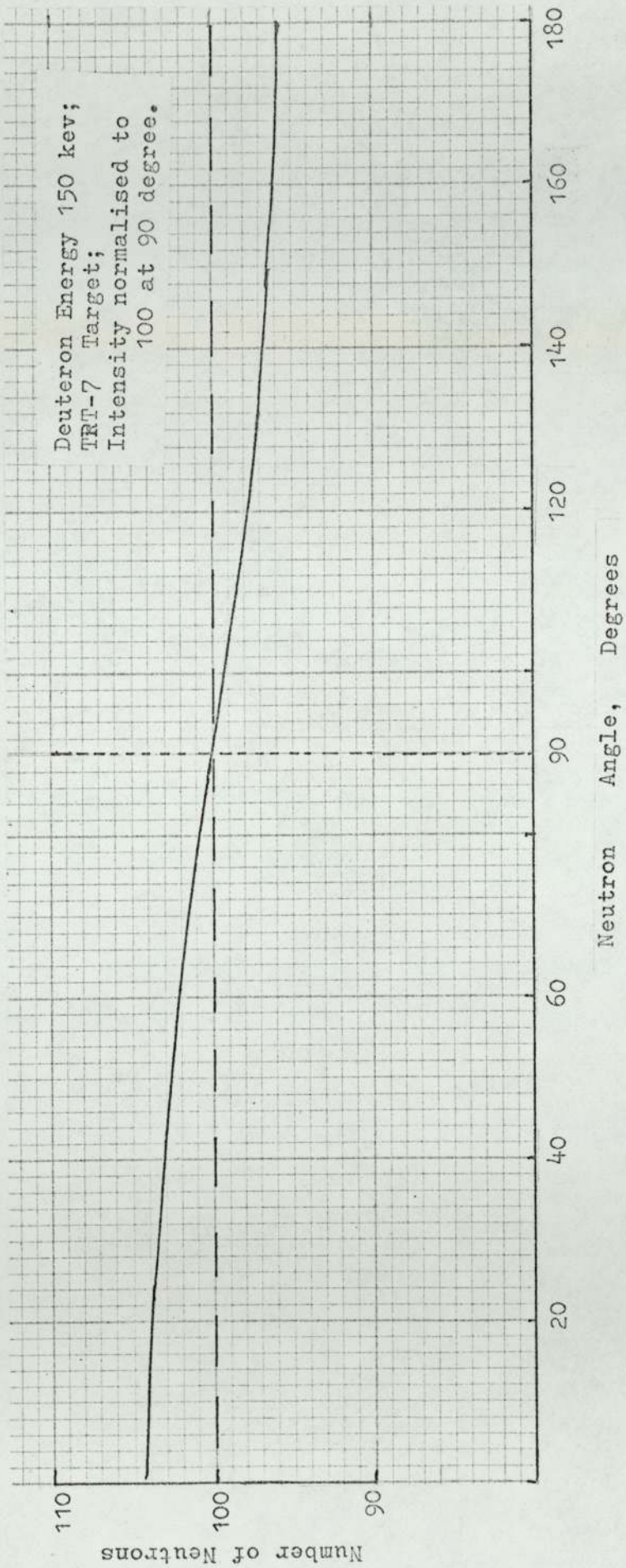

5.3) contd.

5.3.4) contd.

by interpolating between Al and Cu. Next, the slowing down rate for deuterons is obtained by assuming that the rate of energy loss is proportional to the velocity of the particle, so that, the rate for protons at energy E is equal to that for deuterons at energy 2E. The rate for titanium tritide is obtained by combining the individual rates assuming that Bragg's law holds - that the energy loss in a compound is the sum of the energy losses in its separate constituents. Thus if N is the atomic ratio of titanium (and as atomic number of titanium is 48 and that of tritium 3), we have

$$\left(\frac{dE}{dx}\right)_{target} = \frac{3N}{48+3N}\left(\frac{dE}{dx}\right)_{tri} + \frac{48}{48+3N}\left(\frac{dE}{dx}\right)_{Ti} \qquad 5.11$$

Gunnerson and James [95] have made a direct measurement of energy loss of deuterons in titanium-hydride foils in the energy range 40 to 120 kev and found good agreement with the values by the interpolation method.

The computed values of slowing down rate of deuterons in titanium-tritide according to equation 5.11 for a uniform tritium to titanium ratio of 1.27 is shown in Figure 5.10. It was noted that contribution to slowing down rate due to the tritium content is small, even though the slowing down per mg of tritium is more than that of titanium; this is because of small weight of the gas in targets. These considerations also showed that not much difference results, for slowing down with a true profile of tritium concentration and with a uniform distribution of tritium. For these reasons the same calculations can

FIGURE 5.10-- Slowing Down Rate in a Tritium-Titanium Target; (tritium to titanium atomic ratio= 1.27).

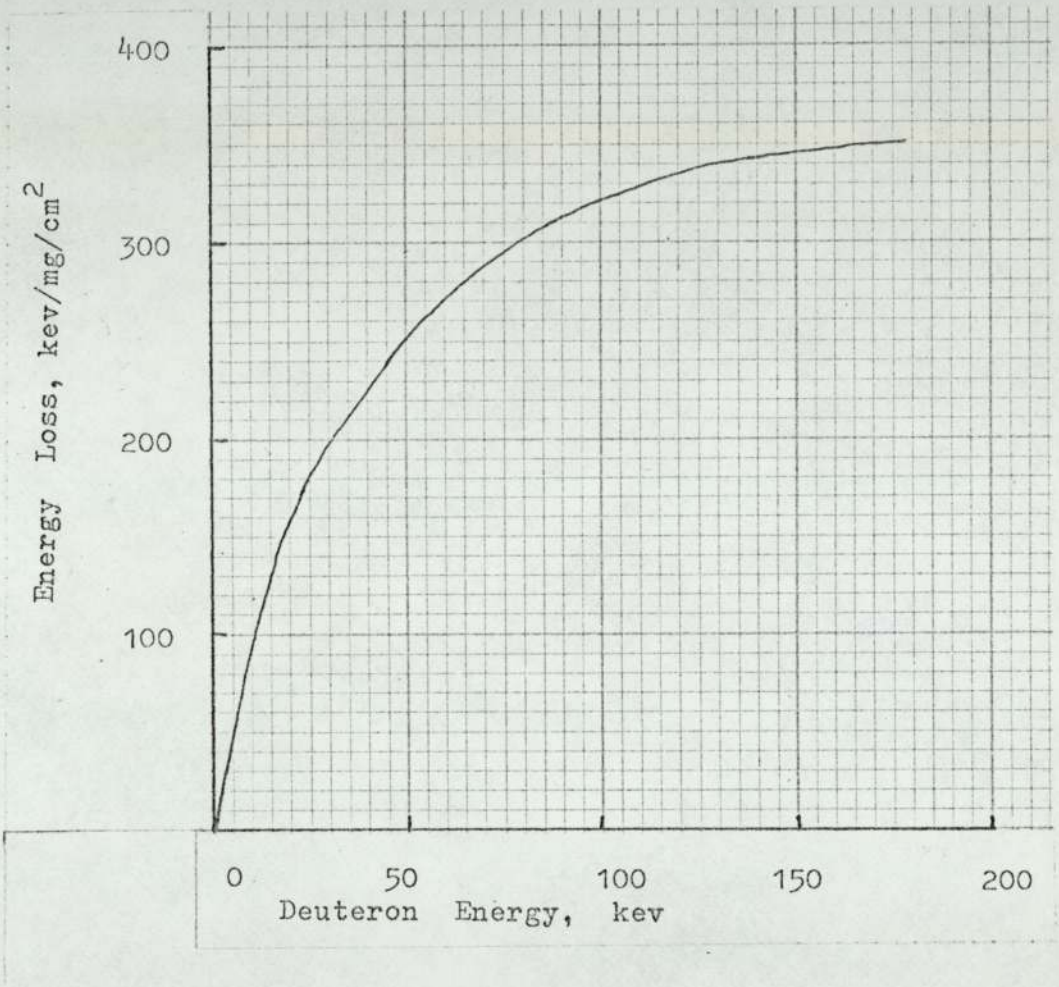

5.3) contd.

5.3.4) contd.

be used with little error as the tritium is depleted with irradiation. Benveniste et al. [96] also consider variations in slowing down rate due to different loadings of tritium and conclude that the error in the results in using one set of slowing down values is small.

The effect of variation of tritium-profile inside the target is that, for an assumed uniform distribution more neutrons are emitted corresponding to higher deuteron energies, which makes the line-shapes of the emitted neutrons asymmetrical about the peak, while for triangular distributions more symmetrical shapes are obtained (Fig.5.7). However the energy spread of the neutrons (the maximum and minimum values at a given angle) is a function of the deuteron energy only. The average value of the neutron energy would be somewhat different; but this is small. At 90° the average neutron energy is only 7 kev less with a triangular distribution than that with a uniform distribution (in TRT 7). The maximum difference is at 0° when it is 70 kev less; but in the backward directions, 180°, it is 50 kev more. However appreciable differences occur in the computed values of the average anisotropy factor; this is due to the variation in tritium concentration itself rather than the variation in slowing down rate. This is discussed more later.

The range of the deuterons can also be calculated from the slowing down rate values shown in Figure 5.10. It can be seen that the rate falls sharply below a deuteron energy of 20 kev, so that the deuterons travel a considerable

5.3) contd.

5.3.4) contd.

distance after reaching 20 kev before they are finally stopped. However as noted earlier the cross-section for the DT reaction becomes negligible at low energies; at 20 kev it is only 50 mb.

5.4) Absolute Yield Measurements by Associated Particle Detection.

5.4.1) Detection Principle and System.

There is one-to-one correspondence in the alpha particle and the neutrons produced from the DT reaction. The average energy of the alpha particles is about 3.6 Mev, which is high enough for accurate counting by a suitable detector placed facing the target. The knowledge of the angular distribution of the alpha particles is necessary in order to translate the alpha counts to the total yield. From the knowledge of the neutron angular distribution the number of neutrons emerging at a given direction can also be obtained. Below 200 kev deuteron energy the angular distributions of both are isotropic in the centre of mass system, so that the angular distribution in the laboratory system - the anisotropy - can be accurately computed. The alpha-anisotropy considerations can be by-passed if they are detected at an angle of 90° to the incident deuteron beam, since at 90° the angular distribution in the lab system is the same as in the c.m. system. However practical experimental set-ups do not always allow a long arm to be attached at 90°.

In the present work, the alpha particles were detected in the backward direction - near the deuteron beam -

5.4) contd.

5.4.1) contd.

at an angle of 178° to it. The detector was a silicon surface barrier detector placed inside the beam tube at a distance of 60 cm. from the target. The mounted detector can be seen in Figure 5.11. A metallic cap with a small aperture of accurately measured diameter defined the solid angle of reception of the alpha-particles by the detector. Detectors used were the 20th Century 05K and Neutronics ND7, both of similar physical and electronic characteristics. A pre-amplifier (design suggested by 20th Century Electronics) was fabricated for initial pulse amplification from the detectors. These pulses were further amplified and counted by the RIDL 400-channel pulseheightanalyser, used on the Time Sequence Scaling mode of the analyser. The block diagram of the arrangement is shown in Figure 5.12.

Early work on counting of the alphas from the DT reaction used to be done with low pressure proportional counters with thin mica windows [91]. Since their development, solid state detectors are now used for the purpose. Their small size (about 1 cm. dia × 1.5 cm.) and tolerable mechanical toughness together with the ability to operate in high vacuum make them more suitable for such work. The low voltage requirement and simple electronics that need not be in direct contact with the detector are also advantageous. This can be more appreciated if they are compared with plastic scintillators that can also be used for alpha detection but need bulky photomultiplier tubes and electronic components in contact with the scintillator. The main disadvantages of surface

FIG. 5.11

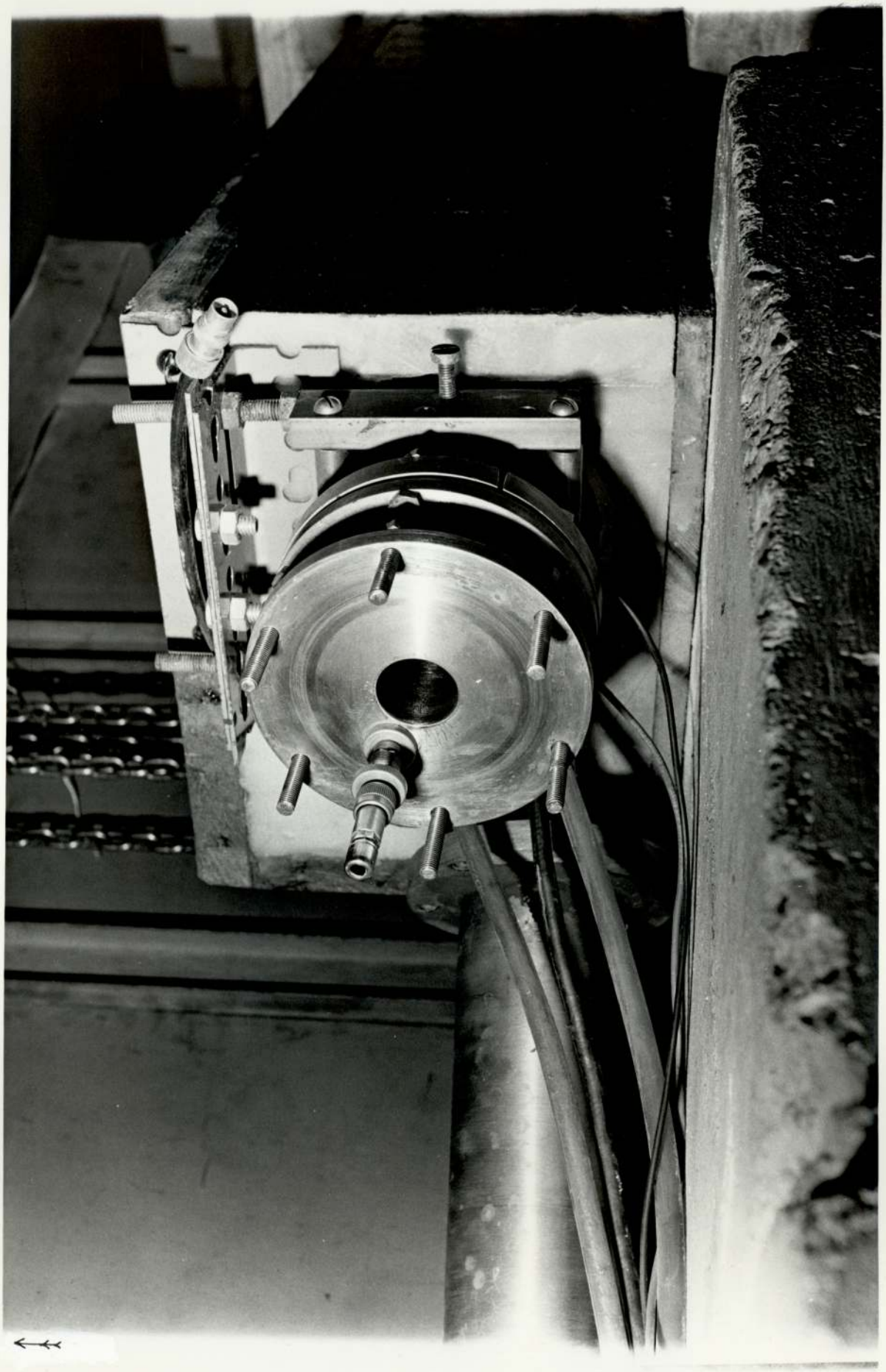

FIG. 5.12 -- Block Diagram of the Electronics for Detecting and Counting the Alpha-particles.
(RIDL Analyser set on TSS mode.)

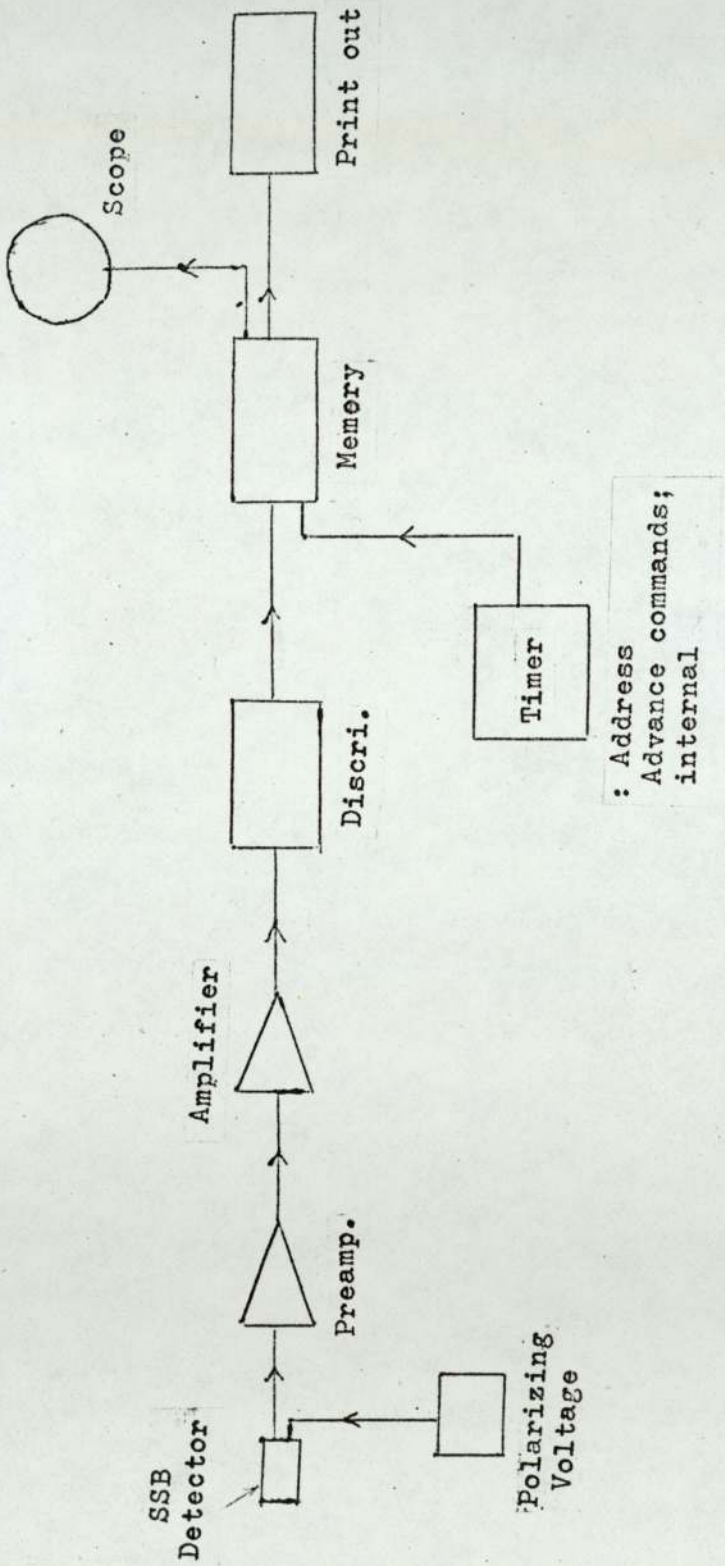

5.4) contd.

5.4.1) contd.

barrier detectors are their radiation damage in a high energy neutron field and surface degradation that might occur due to oil vapour or other organic vapours which can be present in a high vacuum system and get deposited unless excessive care is taken throughout the operation.

5.4.2) SSB Detector Characteristics.

Silicon Surface Barrier detector is a semiconductor junction diode. The p-type layer which is very thin is near the surface and is coated with a thin gold film. The detector is operated only with reverse bias i.e. the n region is given a positive voltage with respect to the gold-layer electrode, which is earthed. The depth of the depletion layer which is the sensitive region is proportional to $\sqrt{\rho V}$ where ρ is the resistivity of the base material (silicon) and V is the applied voltage. The maximum voltage the detector can tolerate without damage is specified by the manufacturer; for the 05K detector it was 25 Volts.

5.4.3) The Electronics.

The circuit diagram of the pre-amplifier is shown in Figure 5.13. The input cable joining the SSB was kept short in order to obtain good signal to noise ratio. The polarizing voltage for the detector was connected through a variable resistor so that voltage to the SSB could be applied or disconnected gradually to avoid voltage shocks to it.

Care had to be taken to avoid earth loops

FIG.5.13.-- Circuit of the Pre-amplifier

(type: DSA/2).

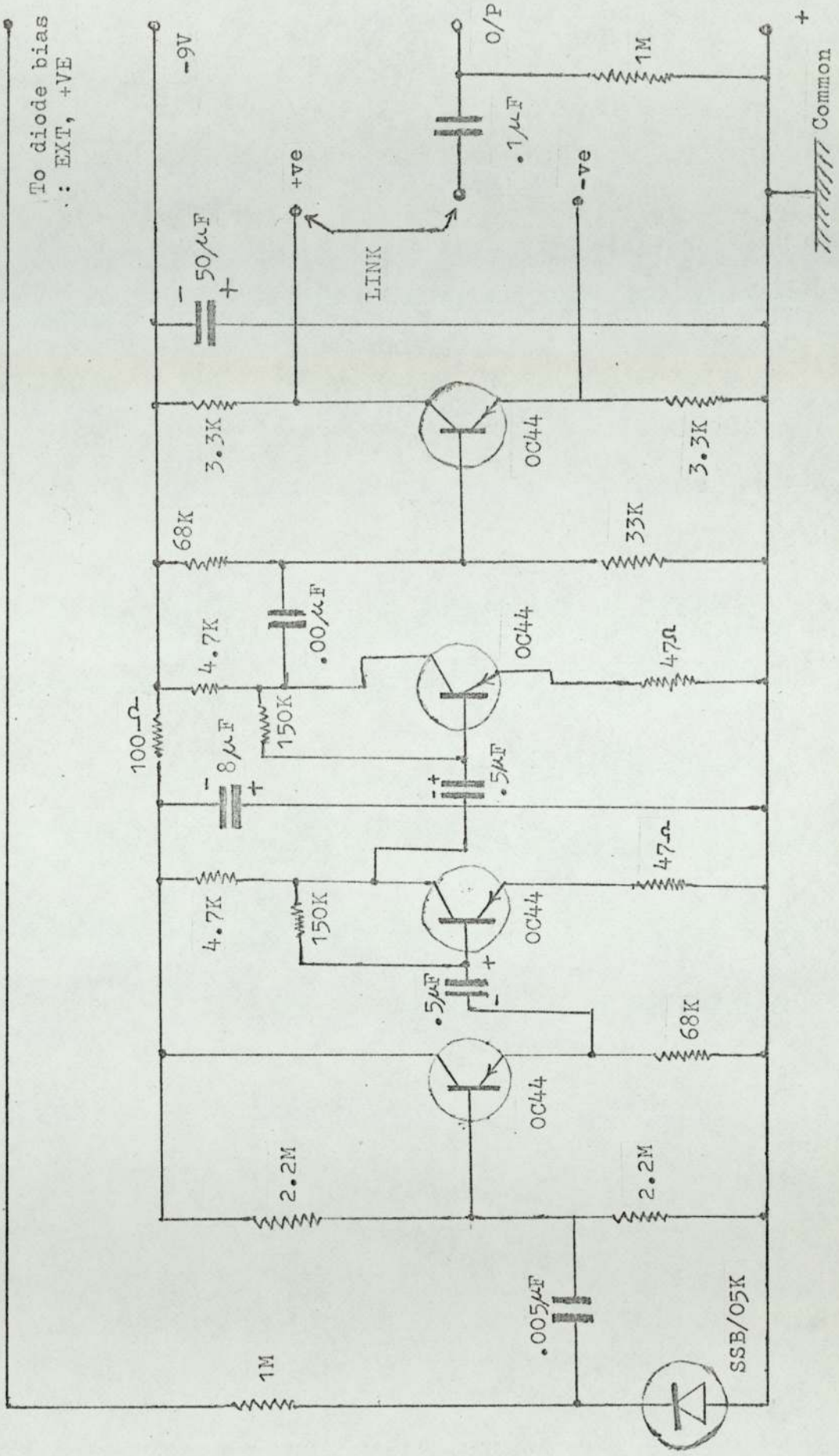

5.4) contd.

5.4.3) contd.

which produced spurious signals in the detector.

The spectrum of the alpha-particles received at 178° is shown in Figure 5.14. This gives a resolution of about 10%. From statistical consideration of monenergetic alpha particles of energy 3.6 Mev this is poor. But the alpha-particles received were not monenergetic. They had an energy spread of about 0.5 Mev at that angle. The poor resolution however is not a problem for absolute counting, so long as the spectrum is well separated from the noise spectrum. This can be a problem when the detector has too much of radiation damage from the fast neutrons, when the peak height decreases and the width broadens and towards the end spurious counts are recorded due to increased reverse current in the detector.

A typical instantaneous variation of alpha-particle output (and hence of neutrons) is shown in Figure 5.15 which is a recording of the rate meter flow-chart. The depression in the middle was caused by a sudden shutdown of the high tension generator due to flashover. EHT was restored manually as soon as possible. The width of the depression indicates the time for which the neutron production stopped. In stabilized condition such stoppage would occur a few times in an hour of irradiation and was the major cause of discontinuity in irradiation.

5.4.4) Geometry Factor.

If S_o is the source strength of an isotropic α-source (lab), the alpha-particle counts by the detector

Fig. 5.14. -- Spectrum of the Alpha Particles.

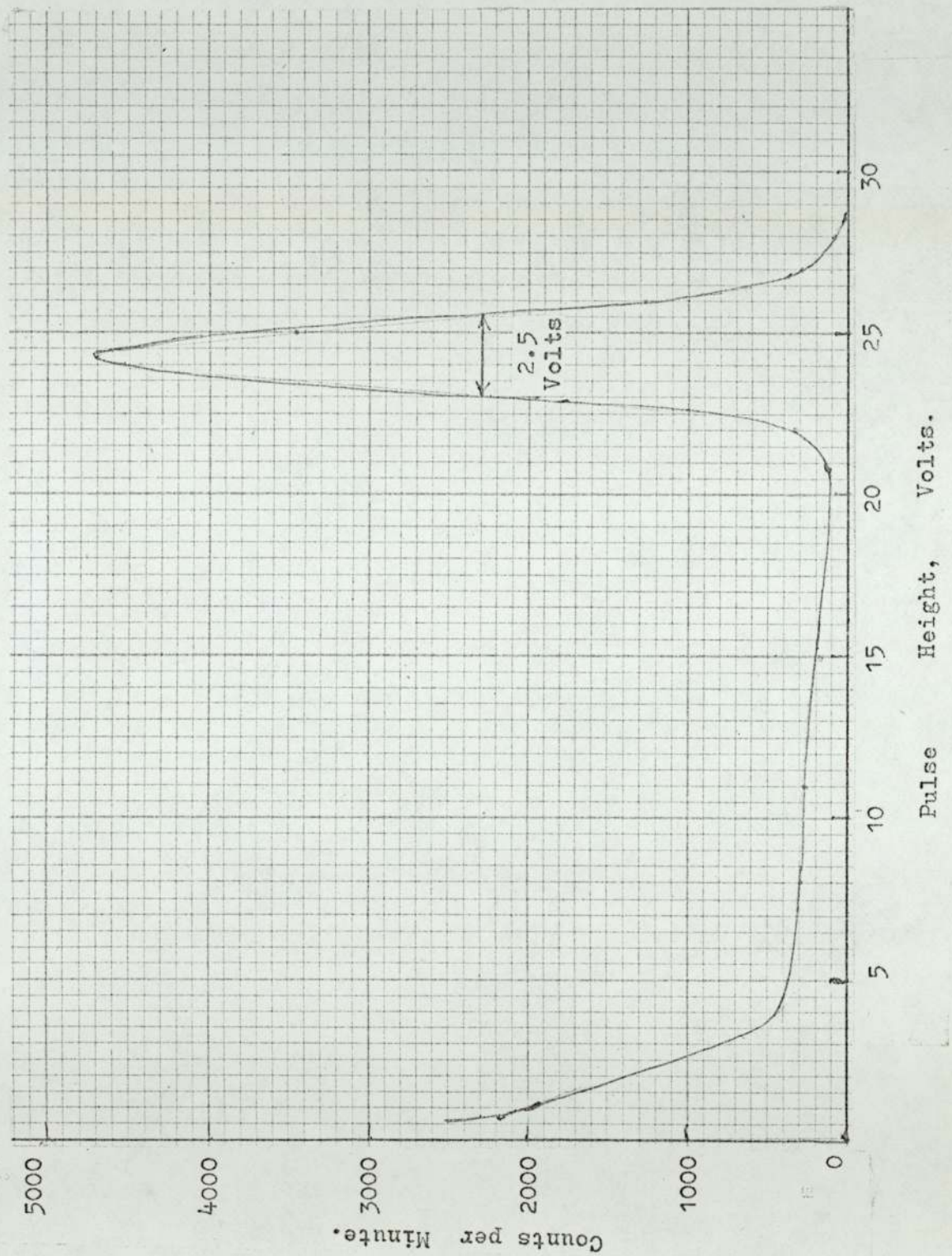

FIG. 5.15. -- Recording of Rate-meter Flow-chart Showing Variation of Alpha Particle Output.

(Trace level corresponds to about 3×10^8 neutrons/ sec.)

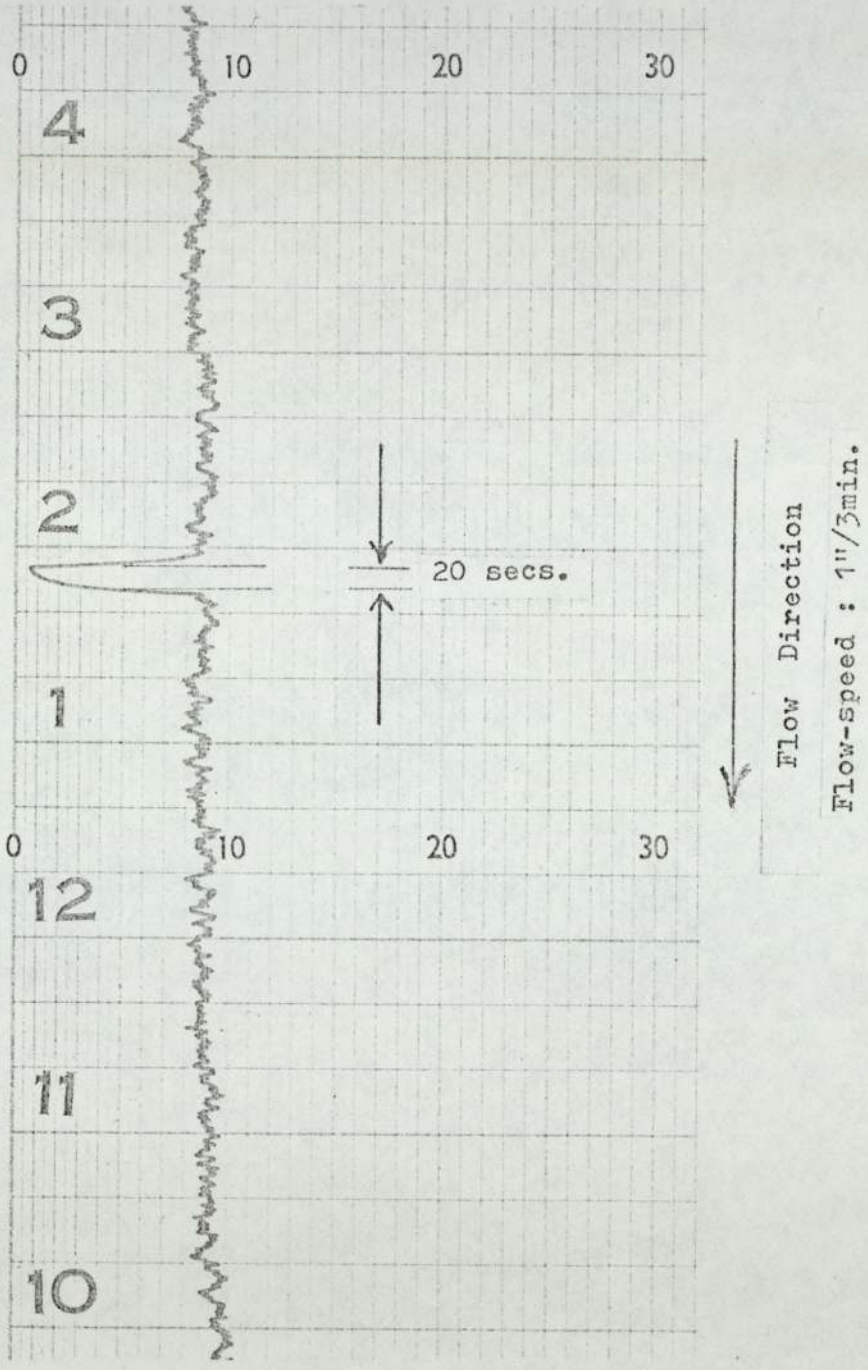

5.4) contd.

5.4.4) contd.

at R cms. away from the source and having a circular apertue of diameter D, held normally to the line joining it with the source is given by

$$C_\alpha = S_o \ \Delta\Omega$$

$$= S_o \ \frac{\pi D^2/4}{4\pi R^2}$$

$$= S_o \ \frac{1}{16} \left(\frac{D}{R}\right)^2 \qquad 5.12$$

where $\Delta\Omega$ is the solid angle having the value as in eqn.5.12. It is assumed that R is large and the target area is small enough so that it is effectively a point source as viewed by the detector. From here we have

$$S_o = C_\alpha \ 16 \frac{R^2}{D^2}$$

$$= G. \ C_\alpha \qquad 5.13$$

where G is termed the geometry-factor which is inverse of the solid angle asdefined by eqn.5.13. It is evident that both D and R has to be accurately obtained as both are squared; but since D is very small and it is obtained for an aperture, special care was needed when measuring it. A clean well defined hole was drilled in the centre of the aluminium cap. It was then measured with a 'Genevoise' Universal Measuring Machine (in Production Engineering Department), which would magnify the aperture and measurements could be made accurate to one-thousandth of a cm. Several measurements were taken and the mean gave a diameter of 0.1908 cm, giving an area 0.02859 cm^2 ($\pm$ 0.6%). The distance from the target was measured as 60.0 $\pm$ 0.3 cm. This gave

5.4) contd.

5.4.4) contd.

$$G = 1.5821 \times 10^{6} \ (\pm 1.2\%).$$

5.4.5) Anisotropic Factor.

The alpha anisotropy A_α can be defined [89] in the same way as the neutron anisotropy, A_n has been defined by equations 5.5 - 5.7, by replacing the corresponding quantities with values for alpha in these equations. The total anisotropy is

$$A = A_n / A_\alpha \qquad 5.14$$

for any two fixed angles of alpha and neutron and for a given deuteron energy. The average for the whole range of deuteron energy from the bombarding to zero energy is given by

$$\overline{A} = \frac{\int A\sigma(E_d) n_t(E_d) \frac{dx}{dE_d} \cdot dE_d}{\int \sigma(E_d) n_t(E_d) \frac{dx}{dE_d} \cdot dE_d} \qquad 5.15$$

With the effect of anisotropy, the neutron source strength (angular) is given by

$$S_o = \overline{A}.G.C_\alpha \qquad 5.16$$

The source strength defined by equation 5.16 is that which would give the same intensity of the neutrons at a given angle for an isotropic distribution. However, if the neutron observation angle is 90°, it then also gives the total yield for the non-isotropic source.

The program DTNTAVANIS was written for the evaluation of $\overline{A}$ from equation 5.15. The numerical integration is performed by Simpson's rule. The program

5.4) contd.

5.4.5) contd.

calculates $\bar{A}$ for any given tritium profile and also for a uniform distribution of tritium. For the thick target with α-counting at 178° and neutron emission at 90°, $\bar{A}$ is 1.2149 with an idealized traingular distribution peaking in the middle; $\bar{A}$ is 1.1944 for a uniform distribution of tritium, which is 1.7% smaller.

Error in Anisotropy Factor.

Previous calculations of $\bar{A}$ by other authors [89, 95, 97] were all made by assuming a uniform distribution. Benveniste et al. [96] reports a discrepancy of 2% in the calculated and observed anisotropy for an alpha-particle counting angle of 135° with thick targets and 500 kev bombarding energy, the true source strength being obtained from simultaneous counts at 90°.

From the computations described above it seems the magnitude of error in assuming a uniform distribution of tritium depends upon target thickness. For the medium thick target of type TRT 31, calculations were for the 5 profiles - uniform, true and 3 triangles - as shown in Figure 5.6, and all normalised to the same tritium loading. For 90° reception of the neutrons and 178° alpha-counting, the error in all cases is less than $\pm$ 1% with respect to the true profile, the maximum being - 0.98% for the triangle peaking at half-thickness of the sensitive target layer. The error for the traingular distribution peaking at $\frac{1}{4}$-thickness is minimum. The small amount of error for the medium-thick target is because the deuteron range is of the same order as the thickness of the sensitive layer.

5.4) contd.

5.4.6) Accuracy of Absolute Counting.

Apart from the errors noted above, the other possible errors in alpha-particle counting are considered below.

There is a possible error due to alpha-particle counts from the $^{3}He(d,p)\ ^{4}He$ reaction, with the helium-3 which is produced as the tritium decays with the half-life of about 12 years. The reaction has a high Q-value (about 18 Mev) and the alpha-particle energy would have almost the same energy as that from the DT reaction. If all the ^{3}He remained in the target then in six months this would be about 2.8% of the tritium content. However the cross-section for the D-P reaction is very small, being about 25 mb at 120 kev [91]. With the above concentration, alpha-particles from this reaction cannot be more than 0.0% of those from the main reaction. Similar conclusions are reached by Fieldhouse et al. [101].

Another possible reaction that might contribute to charged particle counting is the DD reaction, the deuteron being deposited in the target from the bombarding beam. This reaction, if significant can also introduce low energy neutrons into the system. Again, several considerations exclude the possibility of any appreciable contribution. The Q-value is +3.27 Mev; the average neutron energy is 2.45 Mev and ^{3}He energy 0.8 Mev. With an SSB detector the ^{3}He peak should be easily separable from the ^{4}He peak of 3.5 Mev. It was not observed. Secondly, in the energy range involved the DD cross section is about 300 times smaller than the DT cross section [91].

5.4) contd.

5.4.6) contd.

The deuteron targets (similar to the tritium targets in titanium thickness) used with the SAMES, give about 100 times less yield of neutrons than the tritium targets. Thus in the extremely hypothetical case of deuterium being in the same ratio as tritium in the target, only 1% of neutrons can be expected from DD. Most of the deuterons are however carried up to the distance where they come to rest. If they accumulate around that region then further incoming deuterons will not react, as the reaction is zero at zero energy.

It was not possible to collimate the detector against the alpha-particles that might reach it being scattered from the walls of the beam tube. However the aperture of the defining slit is so small that this could not be significant. Such scattered alpha-particles will have less energy and could be seen from the spectrum. Removal of the alpha particles by the strip-probes is negligible for the following reasons. The strips are at right angles to each other and their position is such that none are in the same line joining the target centre to the detector. The probes make a narrow but well defined shadows on the target due to the beam; these shadows could be seen when the target was taken out. It can be inferred no reaction takes place in the shadows. The only alpha-particles that could be stopped by the probes from reaching the detector are those that could originate in the shadows, as the detector is near the line of the deuteron beam.

Standard error of the source strength expressed

5.4) contd.

5.4.6) contd.

as percentage, composed of

area of aperture	0.65%
distance of the target from detector	1.0%
anisotropy factor	0.5%

giving a combined error of 1.3%. A further systematic error of ± 0.58% was associated with the counting of the alpha-particles, giving a total of ± 1.4%.

5.4.7) Attenuation of Neutrons by the Target Holder:

From the composition and geometry of the target holder and the observed counting efficiencies it was indicated that the target holder attenuated the source neutrons by about 8% at and around 90° to the beam. This effect cancels out in the final flux measurements, as the foils were calibrated using the same target assembly and at the same direction as the measurement positions in the experimental set up.

CHAPTER 6.

FLUX MEASURING TECHNIQUE WITH THRESHOLD AND RESONANCE FOILS.

6.1) Threshold Foils.

6.1.1) Thresholds.

In endoergic reactions (Q-value negative), energy has to be supplied for the total balance of the reaction system. Threshold energy of a reaction with neutrons can be defined as the minimum energy of the neutrons for which the reaction can take place. However, due to the need of the conservation of momentum the threshold energy is slightly larger than the Q-value and is given by

$$E_{th} = Q \frac{M+m}{M} \simeq Q \frac{A+1}{A} \qquad 6.1$$

where M is the mass of the target nucleus at rest and m is that of the neutron.

For fission the Q-value is positive and the above equation for neutron threshold energy is not valid. The threshold for fission can be simply taken to be the minimum energy of the incident neutron with which fission is observed.

6.1.2) Measurements with Threshold Foils.

In reactions such as (n,p), (n,α) and (n,2n) the proton-neutron equilibrium ratio is disturbed and the product nucleus is found to decay by beta or positron emission, often followed by gamma-rays. From the absolute measurement of the activity and irradiation history the magnitude of the flux of the neutrons above the threshold energy can be found.

In some of the (n,n') reactions the product nucleus is left in a metastable excited state, from which

6.1) contd.

6.1.2) contd.

it decays to the ground state by gamma-emission. Such (n,n') reactions can also be used as threshold detectors. By analysis of the fission products the isotopes with even-mass number can be used as threshold detectors.

The (n,γ) reactions which take place with neutrons of all energies from zero upwards are mainly used to measure the thermal and epithermal flux. In some cases they however can be used in the high kev region.

6.1.3) "Effective" Threshold Energy and Cross-Section:

The reaction cross section beginning from zero at the threshold energy increases in magnitude with increasing neutron energy, and reaches a maximum. The cross-section may then remain constant over a considerable energy range or it may begin to fall off with still further increase in energy. The reaction sensitivity thus varies with energy and in particular just above the threshold the sensitivity is low over a considerable range. It is often convenient to idealise the cross-section curves as a step function at an energy E_{eff}, somewhat higher than the true threshold E_{th}, such that the reaction rate is given on the simple assumption that no neutrons below E_{eff} contribute to the reaction but all above it contribute with equal probability. This can be seen from Figure 6.1. The reaction rate as a function of energy is given by $\phi(E)\ \sigma(E)$, the product of flux and cross-section. The total reaction is proportional to the area B and D. The vertical line through E_{eff} is drawn

FIGURE 6.1 -- Definition of 'Effective' Threshold Energy

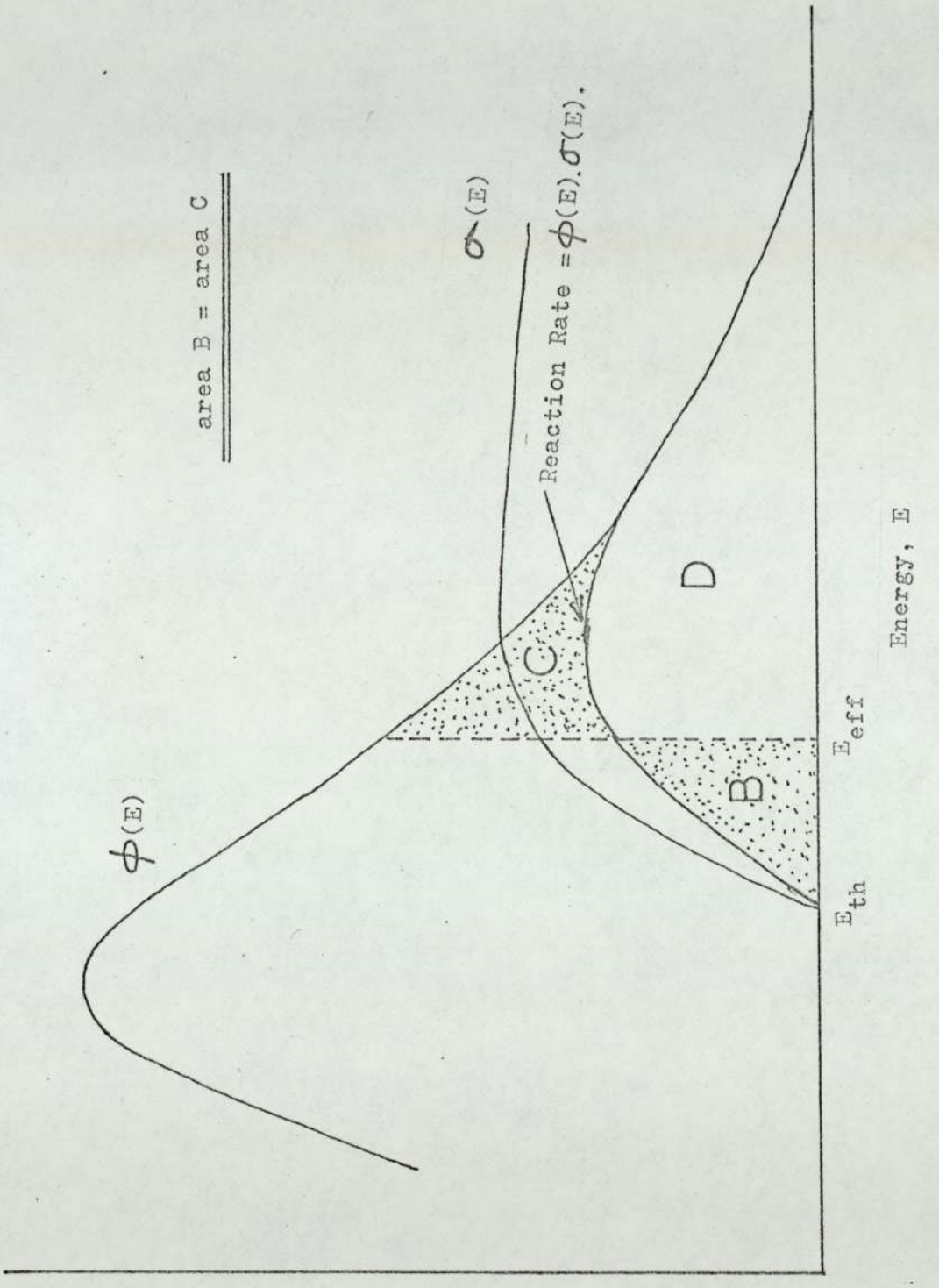

6.1) contd.

6.1.3) contd.

such that area B is equal to area C so that the total reaction is the same but now it can be assumed that reaction rate follows the same profile as of the flux above E_{eff}. The constant reaction rate in the latter case is the average value also called effective cross-section σ_{eff}. Thus the threshold reaction is such that it has a step function at E_{eff} - rising to a value σ_{eff} and remaining at that value in the rest of the energy region of interest.

Obviously, E_{eff} and σ_{eff} are functions of the flux profile and vary in different systems. However as a means of convenience and also due to the fact that the threshold detector techniques have been developed around reactors, the effective threshold is often defined for fission neutron spectrum. For the cross-section the average value $\bar{\sigma}_f$ through the entire region 0 to ∞ (practically, about 18 Mev) of the fission spectrum is used, rather than σ_{eff}. Analytically,

$$\int_0^\infty \sigma(E)\ \phi_f(E)dE = \bar{\sigma}_f \int_0^\infty \sigma_f(E)\ dE$$

$$= \sigma_{eff} \int_{E_{eff}}^\infty \phi_f(E)\ dE = \sigma_{eff}\ \phi_f(E_{eff}) \qquad 6.2$$

where ϕ_f is the fission spectrum and $\phi_f\ (E_{eff})$ is the fission spectrum above E_{eff} only. With the integral of fission spectrum normalised to unity

$$\bar{\sigma}_f = \sigma_{eff}\ \phi_f\ (E_{eff}) \qquad 6.3$$

6.1) contd.

6.1.3) contd.

The average cross-section $\bar{\sigma}_f$ for various materials has been directly measured by several authors with ^{235}U converter plates in the thermal column of reactors. Its use and determination has been prompted by the fact that the cross-section for threshold reactions is not accurate enough throughout the energy range and in some cases is not known. Because a large proportion of the fission neutrons is below the threshold of most of the reactions, the average value is much smaller than the maximum values.

For an unknown flux having a comparable profile to fission neutrons, a quantity, equivalent fission flux density is used. This is given by, if $\phi_x(E)$ is the unknown spectrum measured,

$$\phi_{eq} = \frac{\int_0^\infty \phi_x(E)\ \sigma(E)dE}{\int_0^\infty \phi_f\ (E)\ \sigma(E)dE}$$

$$= \frac{\int_0^\infty \phi_x(E)\ \sigma(E)\ dE}{\bar{\sigma}_f} \qquad 6.4$$

Because of the dissimilarity from the fission spectrum the results in the present work have not been analysed in terms of equivalent fission spectrum. In fact, this would only introduce a normalisation constant for a given foil.

6.2) Selection of the Foils.

6.2.1) Criteria Used in Selecting.

It was decided to use as many threshold reactions as possible with thresholds below 14 Mev. The basic criterion was that activities of significant statistical magnitude could be obtained after irradiating for a reasonable time in the experimental assemblies with the source strength the accelerator could provide. The observed activity should be unambiguous so that it can be attributed to a definite reaction and the interfering activities, if any, could be eliminated and definite conclusions could be obtained. In practice this amounted to studying the following properties:

(i) Cross-section availability;

(ii) Cross-section magnitude and shape;

(iii) Half-life of the product nucleus;

(iv) Decay scheme of the product nucleus - energy and branching ratio of the decay products;

(v) All other possible reactions in the target material with neutrons of possible energies in the system;

(vi) Availability of the material in useable quantity and form; this included cost considerations; and

(vii) Physical and chemical compatibility of the material during use.

Several foils which would otherwise have been ideal had to be eliminated either for one or other reasons listed above. In many cases half-life was the deciding factor. The minimum half-life of the reaction of interest had to be such that time was sufficient to take the foils out and count at least several of them before the activities died away; the minimum half-life is thus about 10 minutes.

6.2) contd.

6.2.1) contd.

The maximum half-life had to be such that enough activity was induced during a continuous irradiation, which could be at the most a working day; other practical considerations reduced the time to about 5 hours. The maximum half-life that has been used was 15 hours. Several reactions which were otherwise very attractive and have been successfully used with reactors could not be used because of their longer half-lives (a few days). In particular, $^{32}S(n,p)\ ^{32}P$ with a low threshold and cross sections well known had to be rejected because of its half-life of 14.3 days.

$^{64}Zn(n,p)\ ^{64}Cu$ with threshold below 1 Mev and a tolerable half-life of 12.8 hours was considered, but ^{64}Cu cannot be easily counted because of interference from the 13.8 hours reaction $^{68}Zn(n,\gamma)\ ^{69}Zn$, which also has similar beta and gamma energy characteristics. Another reaction, $^{115}In(n,n')\ ^{115m}In$ with a threshold at 0.5 Mev had its feeble 0.335 Mev gamma-peak virtually swamped by the gamma ray spectrum from ^{116}In produced by the (n,γ) reaction with ^{115}In.

$^{103}Rh(n,n')\ ^{103m}Rh$, another isomeric reaction with a low threshold at about 0.4 Mev has not been used because of the lack of information about its cross-section. Also the material is expensive and its 20-kev X-ray emitted from internal conversion requires a special detection system to measure [102].

Fission foils were not used because of ambiguity inherent in the measurement of their activities due to their

6.2) contd.

6.2.1) contd.

natural radio-activity and the change in the fission product distribution with incident neutrons [103,104] . Also the easily available ^{238}U has got a threshold energy very similar to that for the $^{31}P(n,p)$ reaction.

6.2.2) Foils Selected:

Five reactions were finally chosen among the threshold foils. These are:

$^{63}Cu(n,2n)\ ^{62}Cu$

$^{27}A\ell(n,\alpha)\ ^{24}Na$

$^{56}Fe(n,p)\ ^{56}Mn$

$^{27}A\ell(n,p)\ ^{27}Mg$

$^{31}P\ (n,p)\ ^{31}Si$

Thus from an independent search a selection was made, which with one or two more reactions of longer half-lives has been used in other laboratories and by now seem to have become a standard set, for non-fission threshold detectors. This is not surprising since the same criteria for selection are used and the performance of the foils in and around reactor environment is similar.

The $^{63}Cu(n,2n)$ was ideal for measuring the primary neutron distribution in the assembly. The cross-section beginning from 11 Mev rises rapidly and at 14 Mev has a high value. Since very few neutrons are produced due to inelastic scattering or fission at these energies they are practically avoided by this reaction. $A\ell(n,\alpha)$ and $^{56}Fe(n,p)$ have similar cross-section profile, but $^{56}Fe(n,p)$ has somewhat lower threshold at about 5 Mev, while the $A\ell(n,\alpha)$ threshold is at 6 Mev. $P(n,p)$ has the lowest threshold in the combination

6.2) contd.

6.2.2) contd.

at about 1.5 Mev; Aℓ(n,p) is in between P and Fe at 3.5 Mev.

They all have sufficient cross-section at 14 Mev, so that they could be calibrated with the source neutrons. Cross-sections at other energies are sufficiently known.

6.3) Nuclear and Material Constants of the Threshold Foils.

Data shown in this section has been mostly taken from refs. 105-110.

6.3.1) Material Constants of the Foils.

Element.	Atomic Number.	Atomic Weight.	Density gm/cc	Isotrope abundance (%)
Copper	29	63.57	8.89	^{63}Cu 69.1%
				^{65}Cu 30.9
Aluminium	13	26.97	2.70	^{27}Aℓ 100
Iron	26	55.85	7.85	^{54}Fe 5.84
				^{56}Fe 91.68
				^{57}Fe 2.17
				^{58}Fe 0.31
Phosphorus	15	3.98	2.20 (red)	^{31}P 100

6.3) contd.

6.3.2) Nuclear Constants for $^{63}Cu(n,2n)\ ^{62}Cu$ Reaction:

Threshold at, E_{th} = 11.0 Mev

Cross-section at 14-Mev:

microscopic = 554 mb.

per gm of ^{62}Cu, $\Sigma_m = 3.629 \times 10^{-3}\ gm^{-1}cm^2$

With fission neutrons:

effective threshold energy E_{eff} = 13.7 Mev

average cross-section in Watt-spectrum, $\bar{\sigma}_f$ = 0.0867 mb.

Disintegration data of ^{62}Cu

Half-life = 10.0 min

β^+, E_{max} = 2.91 Mev, 97% of the decay

E γ_1 = 0.88 Mev, 0.3% " "

γ_2 = 1.13 Mev, 0.1% " "

γ_3 = 1.17 Mev, 0.5% " "

The activity can be measured from the 0.51 Mev annihilation peak of β^+. The foil can be put inside a thick aluminium disc to stop the positions; this increases the efficiency. It is called a foil converter.

Competing Reactions:

reaction	energy, E	σ at E	σ at 14 Mev.	Half life
$^{62}Cu(n,\gamma)^{64}Cu$	Thermal	3.5b	×	12.9 hrs.
"	Res.Int.	4.0b	×	"
$^{65}Cu(n,2n)^{64}Cu$	E_{th}=9.8 Mev		1.0b	"
$^{65}Cu(n,p)\ ^{65}Ni$	E_{th}=1.32 Mev		25 mb	2.6 hrs.
$^{65}Cu(n,\gamma)\ ^{66}Cu$	Thermal	1.8b	×	5.1 mins.

Disintegration data for above:

6.3) contd.

6.3.2) contd.

^{64}Cu	β^+ ,	0.66 Mev,	19%	of the decay
	β^- ,	0.57 Mev,	43%	" "
	γ's	less than 1%		" "
^{65}Ni	β_1	2.12 Mev,	57%	" "
	β_2	1.0 Mev,	14%	" "
	β_3	0.60 Mev,	29%	" "
	γ_1	0.37 Mev,	4.5%	" "
	γ_2	1.11 Mev,	16%	" "
	γ_3	1.48 Mev,	25%	" "
	other γ's each less than 1%			
^{65}Cu	β_1	2.63 Mev,	91%	of the decay
	β_2	1.50 Mev,	9%	" "
	γ	1.04 Mev,	9%	" "

In the absence of thermal and significant epithermal neutrons the (n,γ) reactions should not seriously interfere. The ^{65}Ni production cross-section is small at 14 Mev, its γ-energies are different from the annihilation γ-energy, the β^--particles can be absorbed in the foil converter. However some interference can be expected from the annihilation gammas produced by the $^{65}Cu(n,2n)^{64}Cu$ reaction. Its cross-section is high at 14 Mev but the half life is very long; its contribution can be kept small with short irradiation time.

6.3.3) Nuclear Constants for $^{27}Al(n,\alpha)^{24}Na$ and $^{27}Al(n,p)^{27}Mg$ Reactions:

(n,α): cross section at 14 Mev

microscopic = 126 mb

6.3) contd.

6.3.3) contd.

per gm of Aℓ, $\Sigma_m = 2.815 \times 10^{-3}$ gm^{-1} cm^2

With fission neutrons

effective threshold energy, E_{eff} = 8.5 Mev

measured average $\bar{\sigma}_f$ = 0.60 mb.

Disintegration date for ^{24}Na

Half-life = 15 hrs.

E_{max} of β_1 , 1.39 Mev, 99% of the decay

E γ_1 , 2.75 Mev, 100% " "

γ_2 , 1.37 Mev, 100% " "

(n,p): Cross section at 14 Mev

microscopic = 85 mb

per gm of Aℓ, $\Sigma_m = 1.899 \times 10^{-3}$ gm^{-1} cm^2

With fission neutrons

effective threshold energy, E_{eff} = 5.8 Mev

measured average $\bar{\sigma}_f$ = 4.43 mb

Disintegration data for ^{27}Mg

Half-life = 9.5 mins.

E_{max} of β_1 = 1.75 Mev, 70% of the decay

β_2 = 1.57 Mev, 30% " "

E of γ_1 = 0.84 Mev, 30% " "

γ_2 = 1.01 Mev, 30% " "

Competing Reactions:

	energy	σ	half-life
^{27}Aℓ(n,γ)^{28}Aℓ:	Thermal	210 mb	2.3 mins.
	Res.Int.	160 mb	"

Disintegration data for ^{28}Aℓ

E_{max} of β = 2.86 Mev 100%

E of γ = 1.78 Mev 100%

6.3) contd.

6.3.3) contd.

The (n,γ) cross-section for Aℓ is small. If the activity due to it is significant, it can be reduced by waiting after irradiation; by 20 mins the (n,γ) activity is reduced to less than $\frac{1}{2}\%$ at the stop of irradiation.

The peaks of (n,α) and (n,p) are separated in pairs; both the gamma peaks of (n,α) are of higher energies than the (n,p) peaks. In gamma-counting there will be interference from the Compton continuum of the (n,α) gammas; this can be reduced by shorter irradiation.

6.3.4) Nuclear Constants for $^{56}Fe(n,p)^{56}Mn$ Reaction:

Cross-section at 14 Mev:

microscopic = 106 mb

per gm of ^{56}Fe, $\Sigma_m = 1.048 \times 10^{-3}$ $gm^{-1}cm^2$

With fission neutrons

effective threshold energy = 7.4 Mev

measured average $\bar{\sigma}_f$ = 0.84 mb,

Disintegration data for ^{56}Mn

Half-life = 2.58 hrs.

E_{max} of β_1 = 2.86 Mev, 60% of the decay

β_2 = 1.05 Mev, 24% " "

β_3 = 0.75 Mev, 15% " "

E of γ_1 = 0.84 Mev, 99% " "

γ_2 = 1.81 Mev, 23% " "

γ_3 = 2.11 Mev, 14% " "

6.3) contd.

6.3.4) contd.

Competing Reactions.

	Energy, E	σ at E	σ at 14 Mev	Half-life
$^{54}Fe(n,\gamma)^{55}Fe$	Thermal	2.2b	×	2.6 yrs.
$^{58}Fe(n,\gamma)^{59}Fe$	Thermal	0.9b	×	45.1 days
$^{54}Fe(n,2n)^{53}Fe$	E_{th} = 13.9 Mev.		~ 2 mb.	8.9 min
$^{56}Fe(n,2n)^{55}Fe$	E_{th} = 10 Mev		0.5 b	2.6 yrs.

Interference from the competing reactions can be expected to be small, because of long half-lives or small cross-sections. Also the gamma peaks of ^{54}Mn, particularly the predominant 0.84 Mev ones is well separated from the gammas of other competing reaction products.

6.3.5) Nuclear Constants for $^{31}P(n,p)^{31}Si$ Reaction:

Cross-section at 14 Mev

microscopic = 85 mb

per gm of ^{31}P, $\Sigma_m = 1.653 \times 10^{-3}$ gm^{-1} cm^2

With fission neutron spectrum

effective threshold energy = 3.7 Mev

average $\bar{\sigma}_f$ = 40.4 mb.

Disintegration data of ^{31}Si

Half-life = 2.60 hrs

E_{max} of β = 1.48 Mev, 99.9% of decay

E of γ = 1.26 Mev, ~ 0.07%

Competing Reactions:

	Energy, E	σ at E	σ at 14 Mev	Half-life
$^{31}P(n,\gamma)^{32}P$	Thermal	190 mb	×	14.3 days
	Res. Int.	92 mb	×	"
$^{31}P(n,2n)^{30}P$	E_{th} = 12.3 Mev		14 mb	2.6 m

6.3) contd.

6.3.5) contd.

Disintegration data of ^{30}P

E_{max} of β^+ = 3.24 Mev, 99.5% of decay

E of γ = 2.16 Mev, 0.5% " "

Thermal and epithermal (n,γ) cross-section is again small; in addition the half-life is very large. Interference from (n,2n) can be expected. ^{31}Si and ^{30}P are both effectively pure beta emitters. However, the half-life of ^{30}P is only one-tenth of that for ^{31}Si decay; also the cross-section of (n,2n) reaction is smaller at 14 Mev and below.

6.3.6) Cross-sections of the Reactions in the Energy Range of Interest:

The cross-section curves of the reactions are shown in Figure 6.2. They are given here on a linear scale. Most of the data has been taken from the Euratom compilation [111]. Though all the threshold reactions used here have been considered there, it does not give the best value; instead, several curves for the same reaction from various experimental results are drawn on a long-linear scale. The best value has to be decided by the reader, which is not a pleasant task, the cross-section being on long scale. There are gaps in energy range for some of the reactions. There is a gap in P(n,p) curves from 9.5 to 13.75 Mev and in Aℓ(n,p) curves from 8 to 12 Mev. Since the cross-sections at these energies is slowly varying reasonable interpolation can be made. The values selected from the Euratom compilation are compared with the less comprehensive French compilation [115]

FIG. 6.2. -- Cross Sections of the Threshold Reactions in the Energy Range of Interest.

(Dotted portions of the curves are extrapolated. $^{63}Cu(n,2n)$ cross section used, at 14 Mev, was 554 mb ±7%.)

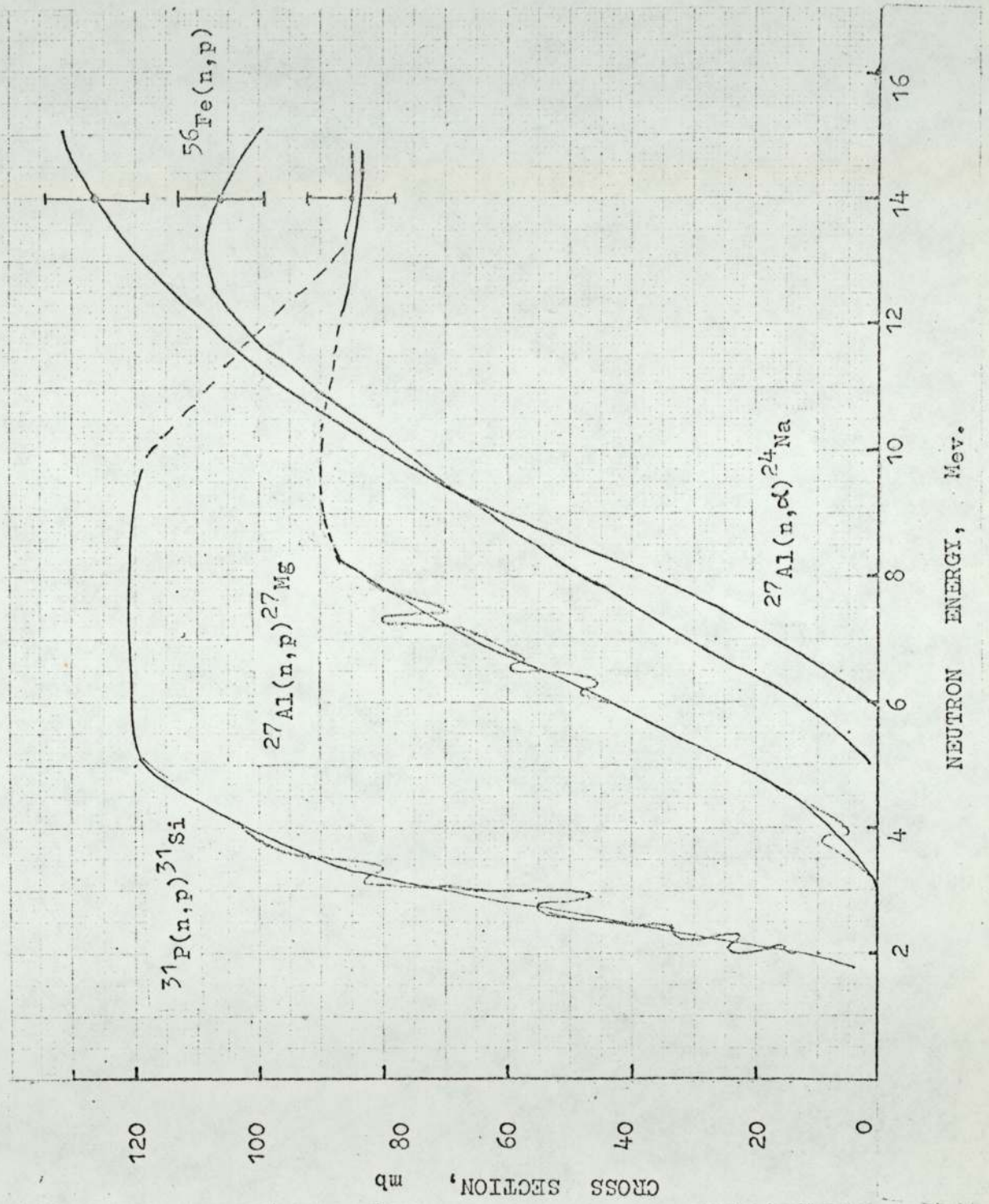

6.3) contd.

6.3.6) contd.

and other values reported [112-114]. The quoted error for the best values of the cross-sections is ± 6% and for the rest ± 10% in ref. 111, which reflects uncertainty in the values used in the present work.

6.3.7) Preparation and Uses of the Threshold Foils:

Foil is a general term used for activation detectors, while in practice they are often in the form of discs or pellets. Because of their smaller cross-sections the threshold foils are usually much larger and thicker than the resonance foils. The activity of these foils is uniformly distributed in thickness but self absorption of the emitted radiation in the foil can be significant. For beta-counting the maximum useful thickness is of the order of the range of beta particles.

Copper foils were made by punching from a metallic sheet 1.6 mm in thickness and of 99.9% purity. Foils of four different surface areas were used three of them discs and one rectangular. To identify, they are termed differently:

Cu-Disc	diameter	av.wt.
type - 2	2.0 cm.	4.65 gms.
type - 3	3.2 cm.	11.45 gms.
type - 5	5.0 cm.	28.35 gms.

Cu-Rect	area	av.wt.
L-type	4.1 cm × 3.2 cm	18.10 gms.

The reason for taking several dimensions of copper was that while the smaller type-2 is adequate to measure the primary neutrons at any pint there can be some variation of it due to foil dimensiins - particularly in the iron-uranium assembly

6.3) contd.

6.3.7) contd.

because of the cylindrical shape of the uranium rods. The bigger foils type-3 and type-5 were used to find the first group flux in phosphorus and iron and aluminium foils respectively. The L-type had a breadth nearly equal to the diameter of the uranium rods and was placed symmetrically just above the central uranium rod to give the average first group flux at the particular radial distance and this distribution was needed for the removal-diffusion calculation.

The iron and aluminium foils were obtained through the Shielding Group of AERE, Harwell, who have used similar foils in their shielding measurements. Diameter of the aluminium foils was 5.08 cm. (2 in) and that of the iron foils 4.92 cm. Original thickness of both types was 0.32 cm; they were machined to a thickness of 0.20 cm each. The diameters were not reduced further as that would decrease sensitivity. Average wieght of the iron foils was about 29.8 gms and that of the alumium foils 11.0 gms.

Phosphorus was used in the form of red phosphorus, reagent grade (BDH Chemicals Ltd). The powder was encased in a melinex tray, made from 0.0127 cm (0.005 in) thick melinex sheet pressed in a heated disc. The trays had about 3 mm edge bent outward. The face of the tray was covered with very thin melinex foil of thickness 0.0013 cm (0.0005 in). The melinex foil was fixed on the bent edge with araldite. Each tray contained 1.7 gm of red phosphorus. Depth of the tray

The Foils Used and other Associated Items.

6.3) contd.

6.3.7) contd.

was 0.26 cm and its facial diameter 3.2 cm. They were counted with a plastic scintillator with the thin melinex side on it.

Foil Carriers. Foil carriers made of thin aluminium were used to place the foils in the irradiation position through the narrow gaps left between the iron plates of the assemblies. They were 70 cm long and 5 cm wide cut into shape from 0.07 cm aluminium sheet. At 66 cm (24 in) from one end holes were punched to locate and position the foils. Two types of holes 3.7 cm and 2.1 cm in diameter were used. The phosphorus and copper type-3 foils fitted into the larger types of holes while the copper type-2 and indium foils (described later) fitted into the carriers with 2.1 cm diameter holes. Foils were then rigidly attached to the carrier with sellotapes. The larger copper foils and aluminium and iron foils were fixed on the carriers with larger holes, sitting just above the holes. The effect of the carrier, particularly for the primary source neutrons was therefore minimised.

6.4) Resonance Foils.

6.4.1) Detection properties:

The (n,γ) reaction of some of the nuclei has a high cross section for thermal neutrons, followed by high resonances in the epithermal energy regions. Foils using these reactions are called resonance foils and have been widely used to measure low energy neutrons, particularly in well-moderated systems. The thermal and non-thermal

6.4) contd.

6.4.1) contd.

activities can be separated by covering the foils with heavy thermal neutron absorbers such as cadmium. It usually happens that the first resonance is the most prominent one and in ' $^1/E$-spectrum' which is characteristic of the region between thermal and fission energies in a moderating medium, the epithermal activities can give magnitude of the flux at precise energy corresponding to the first resonance. Foils used this way can give information up to a few kev.

The characteristics of the resonance foils are considerably different from the threshold foils. Because of their high cross sections they are much thinner and smaller than the usual threshold foils. Even then the self-shielding of the inner layers of these foils by the outer layers is important, so that the activity along the thickness vary. Several corrections become necessary to the observed data to obtain information about the flux. Important theoretical developments have taken place for these corrections. However tests of these theories and the reported use of the foils are limited to thermal reactors and other moderated systems.

In the present work the $In^{115}(n,\gamma)In^{116m}$ reaction has been used to measure the thermal neutron intensities inside the assemblies. Thermal and other low energy neutrons can enter a system due to reflection from the floor and shielding of the set-up, in addition to whatever is produced by slowing down inside the assemblies, which can be expected to be very small. This

6.4) contd.

6.4.1) contd.

reaction of indium persists up to the Mev region, though with very small cross sections.

6.4.2) Thermal and Resonance flux separation:

By covering indium with cadmium, the thermal neutrons are prevented from reaching the indium. The cadmium relative cross section is such that neutrons below 0.4 ev can be assumed to be cut-off while those above reach it. The reaction rate in a $^1/E$ spectrum is then given by

$$\text{reaction rate} = \frac{q}{\xi \Sigma_s} \int_{0.4 \text{ ev.}}^{\infty} \sigma(E) \frac{dE}{E} \qquad 6.5$$

where q is the slowing down density and ξ is the average logarithmic energy decrement of the nuetrons in the moderator. The integral in the above equation is known as the resonance integral. If this integral is known the total resonance flux can be obtained from the observed activities. The resonance cross section is composed of two parts - the $^1/v$ part on which the resonances are superimposed. In a $^1/E$ spectrum the integral due to $^1/v$ part is $I(^1/v) = 0.5\ \sigma_0$ where σ_0 is the cross section at 0.025 ev. The total integral

$$I_r = I(^1/v) + I' \qquad 6.6$$

where I' is called the reduced integral, which is mostly due to the predominant resonance.

The activity observed in a cadmium covered foil due to the total resonance is

6.4) contd.

6.4.2) contd.

$$A_r = N \phi_r I_r \qquad 6.7$$

where N = number of atoms of the isotope of interest in the foil, I_r is the resonance integral and ϕ_r is the corresponding flux. In a bare foil activity is added due to thermal neutrons

$$A_{th} = N \phi_{th} \sigma_{th} \qquad 6.8$$

where σ_{th} is the thermal neutron activation cross-section and ϕ_{th} is the thermal flux, so that the activity in the bare foil is

$$A = A_r + A_{th} = N \phi_{th} \sigma_{th} + N \phi_r I_r \qquad 6.9$$

A_r and A are the experimentally determined quantities. The ratio A/A_r is called cadmium ratio Rcd; with the above equations

$$(Rcd-1) = \phi_{th} \sigma_{th} / \phi_r I_r \qquad 6.10$$

The left side of eqn. 6.10 is a measure of how well the neutrons are thermalised. Also we have

$$\phi_{th} = \frac{A}{N \sigma_{th}} \left(1 - \frac{1}{Rcd}\right) \qquad 6.11$$

From 6.11 the thermal flux can be calculated and from 6.7 the resonance flux.

6.4.3) Correction Factors for Resonance Foils:

The following perturbing effects can occur and corrections are necessary to obtain the unperturbed flux distribution from the measured activities:

6.4) contd.

6.4.3) contd.

(i) Flux depression in the vicinity of the foil;

(ii) Shadowing of the inner layers of the foil by the outer layers;

(iii) Mutual shadowing of the neighbouring foils;

(iv) Shadowing of the foil due to the cadmium cover.

The third-effect, shadowing due to neighbouring foils can be eliminated during irradiation by proper separation of them from each other. The fourth one, the cadmium correction factor is solved on an empirical basis while for the first two factors, theories have been developed by several authors.

The self-shielding factor is termed G and the flux depression factor H, so that the combined correction factor called perturbation factor is

$$F = G \times H. \qquad 6.12$$

In general G and H have different values for both the thermal and resonance neutrons. However for a single resonance peak the depression effect is negligible (H = 1), because after one crossing of the detector, a neutron of the resonance energy will have to be scattered in the medium before returning to the detector, and in a moderating medium its energy will then be lower than the resonance energy. For measurement of thermal flux alone, the corrections due to resonance neutrons need not be applied, as the bare and cadmium covered activities due to resonance energy neutrons are the same.

6.4) contd.

6.4.4) Calculation of the Correction Factors:

There are two widely used theoretical calculations of the perturbation, one due to Bothe [116] and the other to Skyrme [117], both arriving from different considerations. Bothe considered the case of a spherical shell detector and used one speed diffusion theory. From the formulae for the shell he arrived at the formula for a disc by intuitive means. His theory has later been modified by Tittle [118] and as it stands, it gives sufficient agreement with experimental results, particularly for foils of smaller radius [119]. Skyrme used transport-perturbation theory in his analysis, also considering only the one speed case. Skyrme's theory has also been modified, among others by Ritchie and Eldridge [120]; the modified theory has been compared with experimental results by Walker et al. [124], who find good agreement for indium foils of thickness up to 0.025 inch in water for thermal neutrons and also by others [122, 123].

However it is easier to compute numerical values from Bothe-Tittle relations than the Skyrme's one; for the latter uses a semi-empirical parameter 'g' which is more involved.

The equation for G, first derived by Bothe is given below. A dimensionless quantity T, foil thickness in absorption lengths ($T = t/\lambda_a = t\Sigma_a$) is first defined. For a monoenergetic isotropic flux

$$G(T) = \frac{1-e^{-T}(1-T)-T^2E_1(T)}{2T} \qquad 6.13$$

6.4) contd.

6.4.4) contd.

where $$E_1(T) = \int_T^\infty \frac{e^{-Tx}}{x}\, dx \qquad 6.14$$

and x is the physical thickness variable. Defining

$$\alpha = 1-e^{-T}(1-T)- T^2E_1(T) \qquad 6.15$$

$$G(T) = \frac{\alpha}{2T} \qquad 6.16$$

α as a function of $t\Sigma_a$ has been calculated by Tittle.

The flux depression factor H, for the thermal neutron, as modified by Tittle is given by

$$H = \frac{1}{1+ \frac{\alpha}{2}\left(\frac{3}{2}\,\frac{R}{\lambda_{tr}}\,\frac{L}{R+L} - 1\right)} \qquad 6.17a$$

if $R > 2\lambda_{tr}$

or

$$H = \frac{1}{1+0.34\alpha\,\frac{R}{\lambda_{tr}}} \qquad \text{if } R << \lambda_{tr} \qquad 6.17b$$

where R = foil radius, cm

λ_{tr} = transport mean free path of the moderating medium, cm.

$$= \frac{\lambda_s}{1-\bar{\mu}}$$

L = diffusion length in the medium.

For a weakly absorbing media

$$L^2 = \frac{\lambda_{tr}\,\lambda_a}{3} \qquad 6.18a$$

For a moderately strong absorbing medium

$$L^2 = \frac{\lambda_{tr}\,\lambda_a}{3\left(1 - \frac{2}{5}\,\frac{\lambda_r}{\lambda_a}\right)^2} \qquad 6.18b$$

6.4 contd.

6.4.4) contd.

An interesting case of eqn. 6.17b is when the transport mean free path is very large; for this case $H \simeq 1$. This is the case for a medium like aluminium for which $\lambda_{tr} \simeq 12$ cm but not for say water where $\lambda_{tr} \simeq 0.5$ cm. For thermal neutrons in iron $\lambda_{tr} \simeq 1.2$ cm, which is a case in between, but still eqn. 6.17b should be valid and a small flux depression can be expected ($H = .967$). These equations for H are strictly for thermal neutrons, but can be expected to give approximate results for higher energy neutrons with equivalent parameters for the groups.

The expression for G is rather more general and gives approximate values for the indium resonance. A better approximation for resonance self shielding is given in ANL-5800, [124]:

$$G(T) = \frac{T_o}{2} \int_{1/2 T_o}^{\infty} y^{-2}\, e^{-y}\left[I_o(y)+I_1(y)\right] dy \qquad 6.19$$

where T_o is the foil thickness in absorption mean free path at the peak of the resonance, and $I_o(y)$ and $I_1(y)$ are modified Bessel functions of the first kind and of zero and first orders respectively. Eqn.6.19 has been computed, and G(T) as a function of indium thickness is given graphically in ref. 124 and is compared with experimental values which are found to agree. Zijp [125] also gives resonance neutron self-shielding factors for indium, which are also computed values. They agree reasonably well with the ANL-5800 data except for the thinnest foil (below 1 mil).

6.4) contd.

6.4.5) Cadmium Shadow Effect Correction.

The cadmium cover, though its cross-section is low compared to the indium resonances, removes some of the resonance neutrons. The factor by which the cadmium covered indium foil activities must be multiplied in order to obtain activities without the effect of cadmium is the correction factor needed, F_{cd}. Experimentally, it can be determined for a given thickness of indium foils by using cadmium covers of different thickness and extrapolating the activities to zero cadmium thickness. This factor also depends upon the thickness of the indium foils used. The true absorption by cadmium will not depend on the medium except insofar as the medium might affect the anisotropy of the neutron flux.

The factor F_{cd} can also be approximately calculated from the relation [118]:

$$F_{cd} = \frac{1}{1-\alpha} \qquad 6.20$$

where α is the value for cadmium corresponding to the indium resonance energy, as has been defined by eqn.6.15. For a typical value of cadmium thickness of 1 mm. (0.040 in.), F_{cd} for the indium resonance at 1.44 ev and with foil thickness 100 mg/cm^2 is about 1.15.

In addition cadmium also removes neutrons at other energies. With 1 mm thick cadmium only 40% of the $^1/v$ component of the resonance integral contributes to the activation [124b]. Another minor correction that needs be considered is the contribution of thermal neutrons to the activation of the foil covered with cadmium. For a 1 mm. cadmium cover this is less than 1% [124b].

6.5) Use of $^{115}In(n,\gamma)^{116m}In$-Reaction.

6.5.1) Indium foils and Cadmium Covers:

Indium in its pure form is very soft. To give rigidity an alloy of indium-bismuth was prepared with 25% indium by weight. Bismuth has very low thermal and fast neutron cross-sections. Both of these metals were supplied by Halewood Chemicals Ltd., with quoted purity of 99.999%. Foils of two thicknesses, 0.53 mm and 0.91 mm but of the same diameter 1.43 cm and the same material composition were used for flux distribution measurements; they are denoted X-type and O-type respectively. Two other types of indium foils with 10% and 5% indium weight and the same thickness and radius as the X-type has also been used for the purpose of estimating self-shielding and other perturbation effects. Otherwise most of the flux distribution measurements were done with the X-type foils.

Cadmium covers were 1 mm thick with slight depressions inside to accommodate the foils; amount of cadmium at the edges of the foils was 1.6 mm. The physical constants of the indium foils are summarised below:-

Type	Radius	Thickness	% of In by weight	Thickness for In.
O-type	0.71 cm	0.091 cm	25%	146 mg/cm^2
X-type	0.71 cm	0.053 cm	25%	116 mg/cm^2
T-type	0.71 cm	0.053 cm	10%	46 mg/cm^2
F-type	0.71 cm	0.053 cm	5%	23 mg/cm^2

The optimum thickness for β-counting is about 100 mg/cm^2 with indium alone in the foil. With more indium the beta-count rate falls off slowly. But in an alloy the relationship is different. There is a loss in beta counting sensitivity with bismuth as used here. However the foils were

6.5) contd.

6.5.1) contd.

both beta and gamma counted.

For the X-type foils the factors G = 0.845 and H = 0.967 for thermal neutrons in iron, i.e. the perturbation factor F = G × H = 0.817.

6.5.2) Material and Nuclear Constants of In:

Material Constants:

Atomic mass	= 114.82
Mass density	= 7.28 gm per c.c.
Melting point	= 156.4°C
Number of Atoms	= 0.005247×10^{24}/gm
	= 0.0382×10^{24}/c.c.
Isotopic Composition:	In 115 = 95.77%
	In 113 = 4.23%

Fast Neutron Cross-sections.

Reaction.		Half life	Cross Section at 14 Mev.
$In^{115}(n,2n)In^{114m}$	I.	42 msec.	800 mb
	II.	50 d	1550 mb
$In^{115}(n,p)Cd^{115}$		2.3 d	15 mb
$In^{115}(n,\alpha)Ag^{112}$		3.2 h	2.5 mb
$In^{115}(n,n')In^{115m}$		4.5 h	$\bar{\sigma}_f$ = 180 mb.

(n,γ) Cross-Sections:

	Half life	σ_0(2200m/s)
$In^{113}(n,\gamma)In^{114}$	42 sec	2.0 b
$(n,\gamma)Im^{114m}$	49 d	56 b
$In^{115}(n,\gamma)In^{116}$	13 s	52 b
$(n,\gamma)In^{116m}$	54 m	161 b

6.5) contd.

6.5.2) contd.

Resonance parameters of In^{115}:

The first resonance at 1.44 ev is the most prominent one with a peak value of 27,500 b; the next ones at 3.9 ev and 9.1 ev have only 460 b and 125b peak values. In BNL-325 [112] the resonances are shown resolved up to 130 ev only. Later works show resolved resonances up to 1 kev. [126]. Throughout literature several values are given for the resonance integral. Recent measured values by Ryves [127] are:

σ_0(2200 m/s) = 161 $\pm$ 3b

Reduced integral = 2710 $\pm$ 200 b.

$^1/v$ contribution = $.5\sigma_0 \simeq$ 80b, so that the total resonance activation integral $\simeq$ 2800b.

Disintegration Data of In^{116}:

E_β(max) = 1 Mev, 51% of the decay

0.87 Mev 28%

0.60 Mev 21%

γ_1	= 0.137 Mev	3%
γ_2	= 0.385	1%
γ_3	= 0.415	36%
γ_4	= 0.435	0.6%
γ_5	= 0.820	17%
γ_6	= 1.09	53%
γ_7	= 1.29	80%
γ_8	= 1.49	11%
γ_9	= 1.72	< 0.4%
γ_{10}	= 1.77	1.5%
γ_{11}	= 2.12	20%

(Total of γ's more than 100% as there are multiple cascades).

6.5) contd.

6.5.3) Use of $^{115}In(n,\gamma)^{116m}In$ reaction for Fast Neutron Detection.

In a fast system, in the absence of materials of light atomic weight hardly any neutrons can be expected below the kev region. $^{115}In(n,\gamma)$ resonances are only below 1 kev; after that the (n,γ) cross section is smoothly falling but it persists in the Mev region. Between 0.2 Mev and 2 Mev, the cross section is nearly constant at amount 200 mb; after 2 Mev it drops rapidly. In the absence of significant reflection from the biological shield and the floor there should not be any contribution from the resonances and the high energy part is an excellent cross-section distribution to supplement the P(n,p) reaction. The decay products - both gamma and beta rays have satisfactory properties for detection. The other reaction that might interfere, $^{115}I(n,n')$ with threshold at 0.5 Mev has a feeble activity with a 0.335 Mev gamma (no beta), and can be eliminated by biasing the gamma counter.

The cross-section for (n,γ) in the high energy region of interest is not covered by any single author. However values by different authors in the overlapping regions agree sufficiently.

6.6) Counting Systems.

6.6.1) Scintillation Counting.

The foils were counted by scintillation detectors for either beta or gamma activities. The gamma-counting was done with a 7.6 cm × 7.6 cm (3 in × 3 in) cylindrical NaI(Tℓ) crystal, the pulses being analysed and recorded in a 400 channel analyser. Though sodium iodide has excellent

6.6) contd.

6.6.1) contd.

response to beta particles, due to its hygroscopic nature, the crystal is encapsuled in an air tight metallic container and the majority of the beta particles cannot get through. Silicon-31 from P(n,p) reaction, which is a pure beta emitter was counted with a separate beta counter with an NE-102A plastic scintillator.

While activities can be measured with other instruments such as Geiger-Müller tubes, semiconductor radiation detectors, pulse ionization chambers and proportional counters, their performance is limited by long resolving time and poor energy resolution property and low efficiency, particularly for the gamma rays. Scintillation counters have very short resolving times and NaI(Tℓ) scintillators have high efficiency and good energy resolution for gamma rays. In measurements of activities in foil detectors where several competing reactions may be present, the ability to discriminate against the gammas from other reactions is an advantage. For this good energy resolution is desirable.

6.6.2) <u>The Multichannel Analyser</u>:

The 400-Channel RIDL (Radiation Instrument Development Laboratory) analyser, model 34-27 (Fig.6.3) can be used for several purposes and its system components are arranged accordingly. In the present work it was mostly used at first to study the differential γ-spectrum from the scintillation detector and later to count inte-

FIG. 6.3

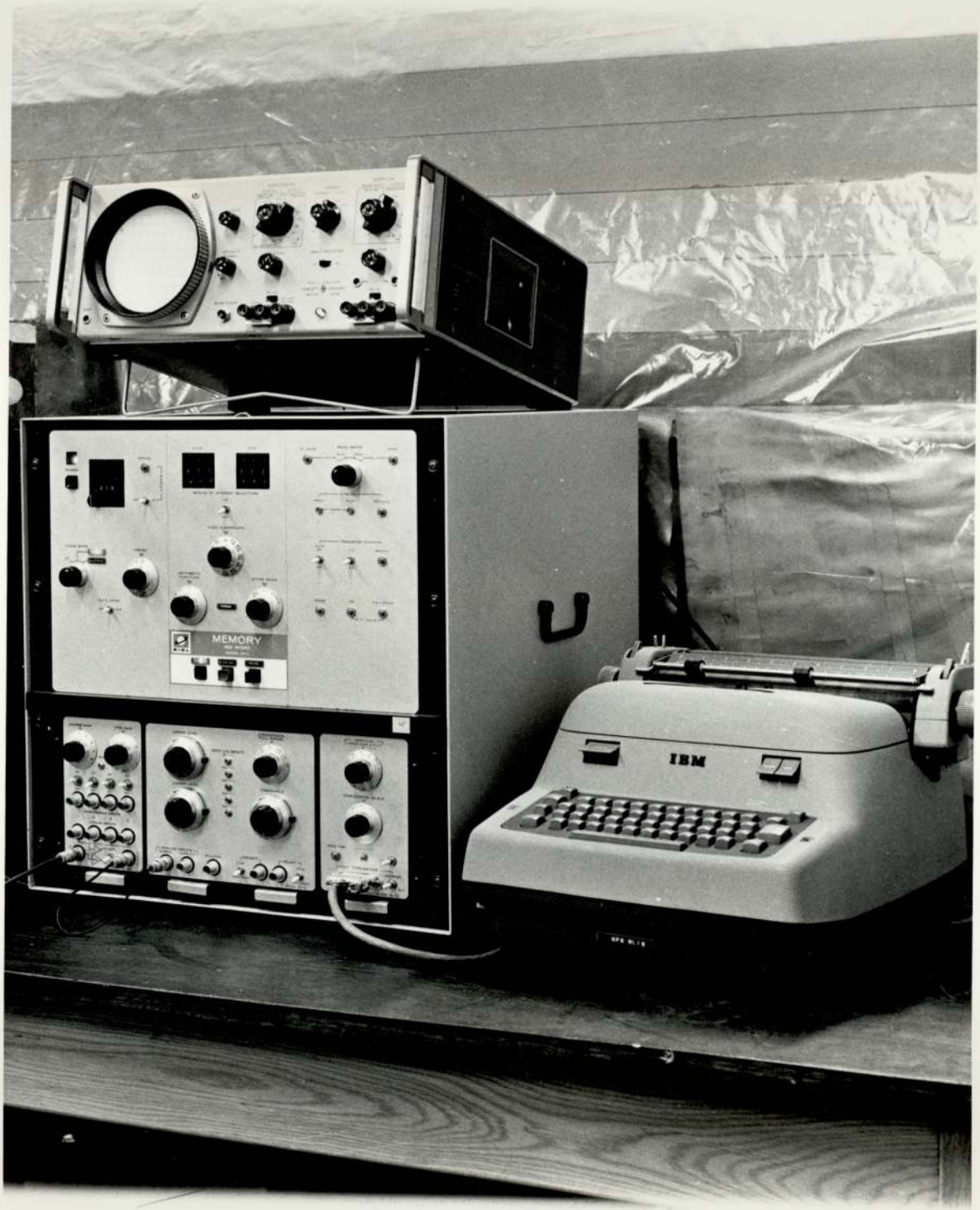

6.6) contd.

6.6.2) contd.

grated pulses of a selected portion of the spectrum. For pulse height analysis (PHA) operation and storage, the block diagram of the components was as shown in Fig.6.4; during this each input pulse into the system is evaluated in the analogue to digital converter (ADC) and a channel number is assigned. A dead time is introduced in the ADC during this processing, which for this equipment was (20.5 + N/4) micro-seconds, where N is the channel number. The dead-time is automatically compensated if the device called 'live-timer' is used.

However, for integrated counting of the output from the discriminator, when the arrangement is called Time Sequence Scaling, the ADC is bypassed (Fig.6.4), and no significant dead time is involved in the equipment. In this operation all the pulses during a pre-set time are recorded in one channel of the memory. This time could be preset between 0.01 and 99.99 minutes in 0.01 minute increments. After this time, the incoming pulses would be recorded in the next channel and the recycling is automatic. Time for moving to the new address is approximately 11 microsecond. During this interval the scaler could record one pulse if any, and add it to the new channel.

6.6.3) <u>The Beta Counter</u>:

The beta counter is shown in Figure 6.5. It has facility for two counting channels which could be used coupled to or independent of one another. Only one of two channels was used; a block diagram of it is given in Figure 6.6.

FIG. 6.4 -- Block Diagram of Components of the Multi-channel Analyser for PHA Operation.

(During TSS mode the ADC is bypassed; cf. figure 5.12)

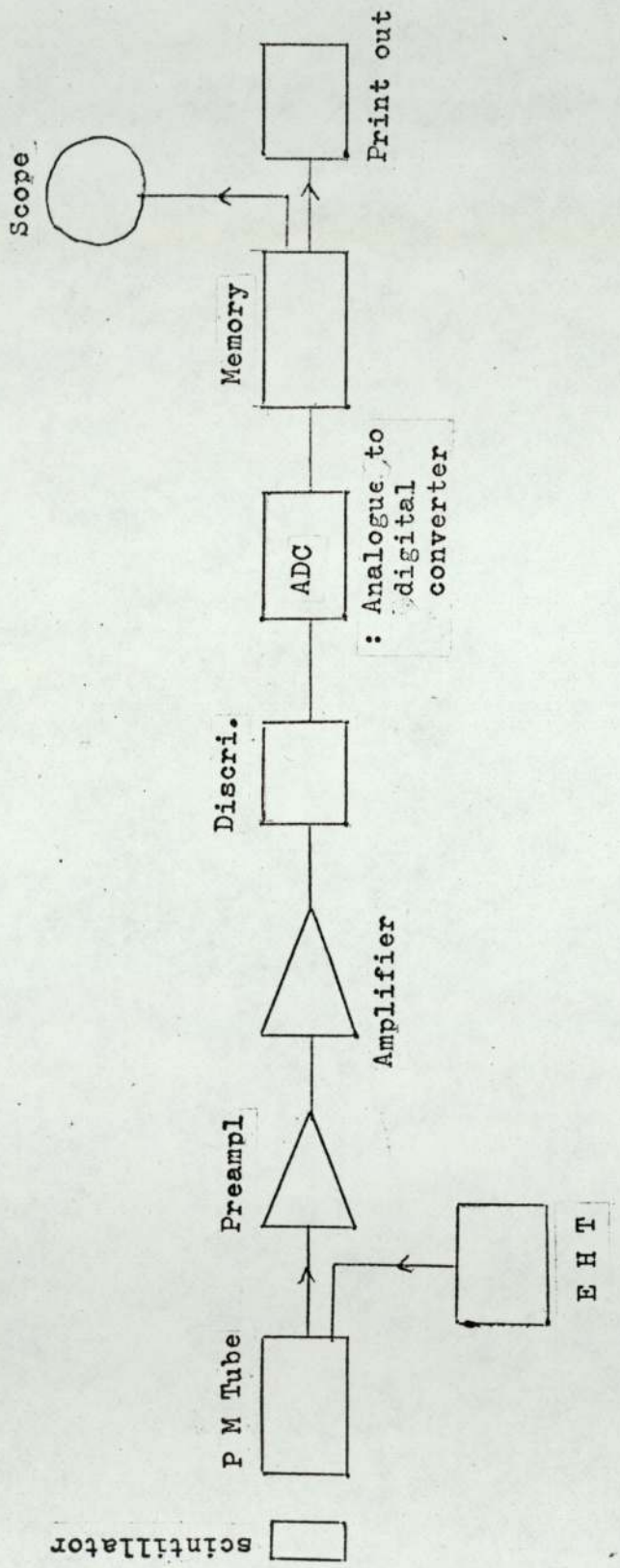

FIG. 6.5

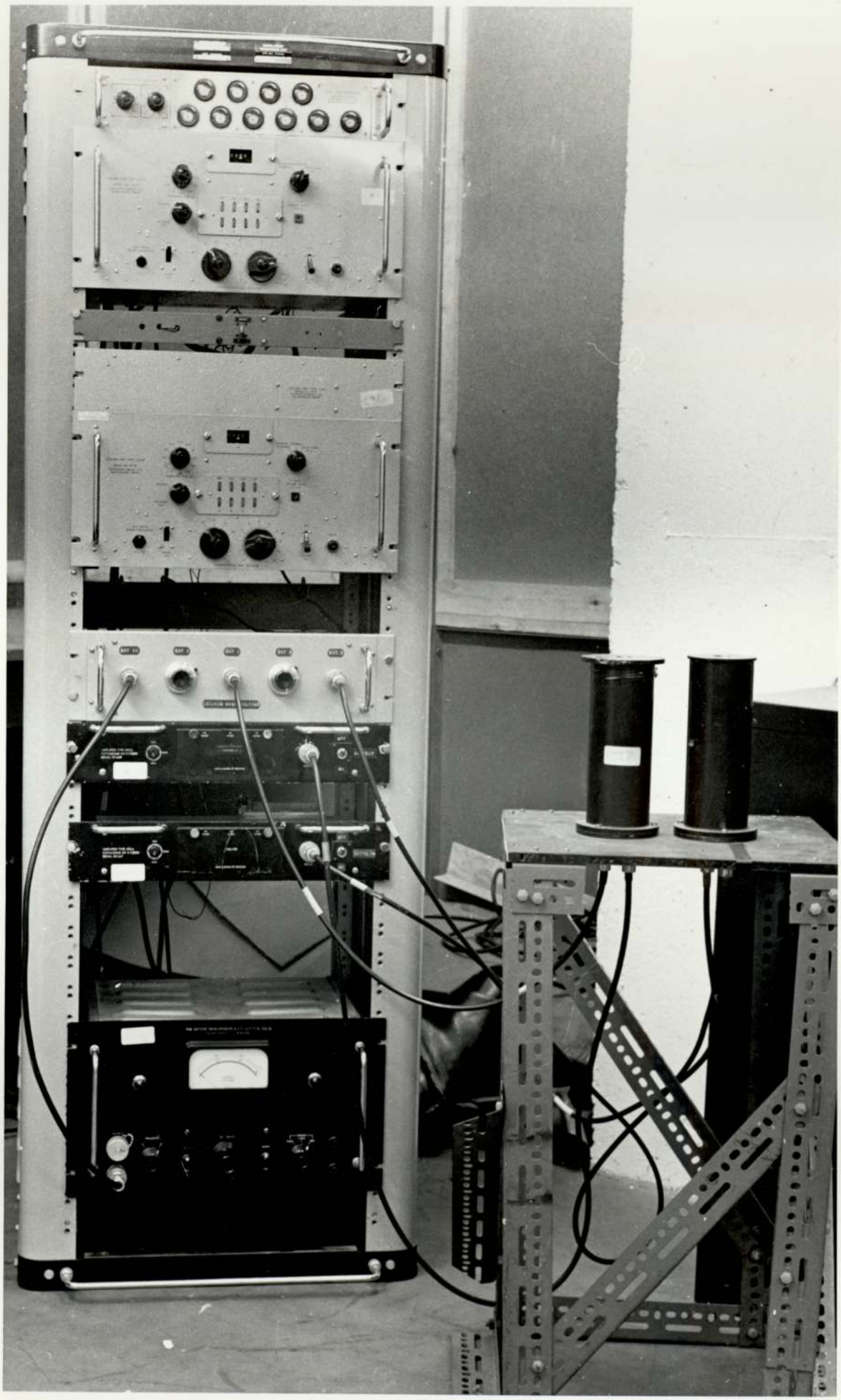

FIG. 6.6 -- Block Diagram of the Components of the Beta Counter.

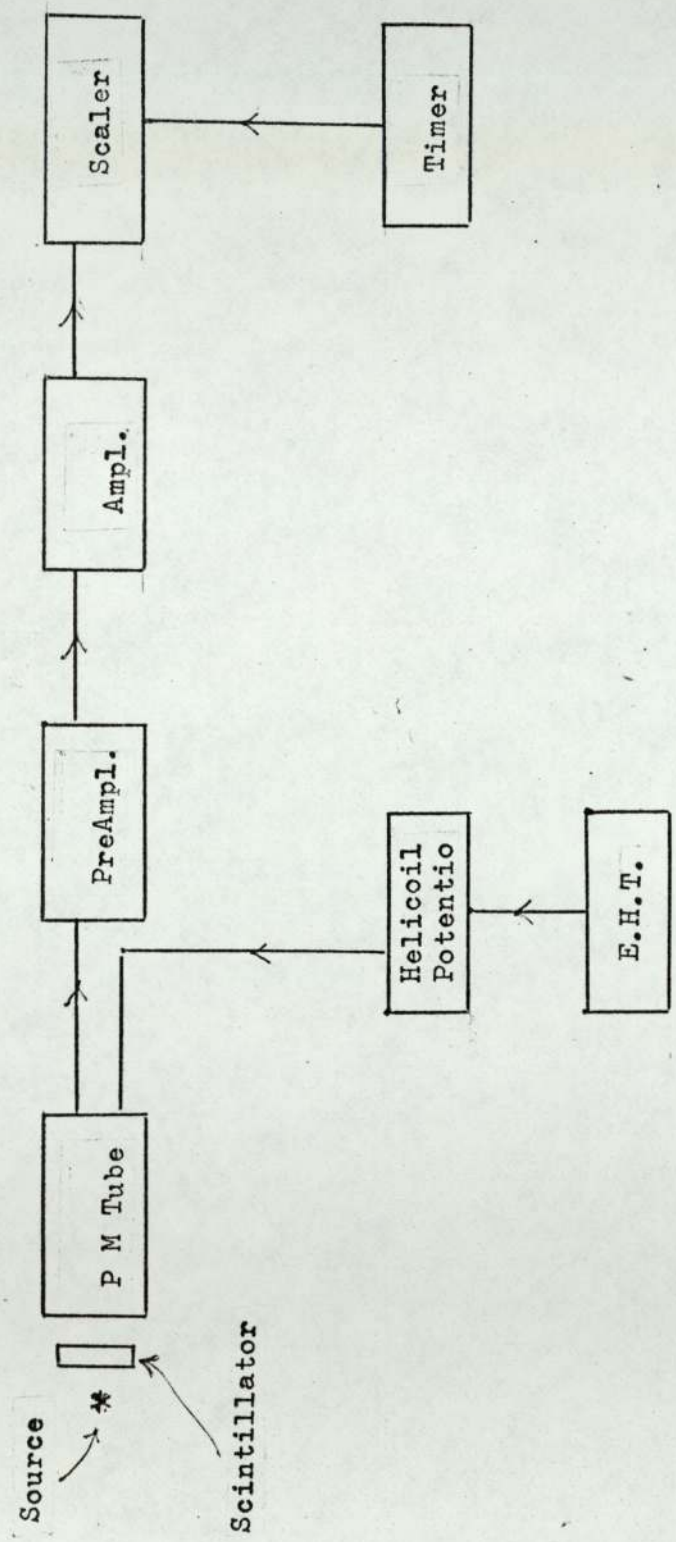

6.6) contd.

6.6.3) contd.

The NE-102A plastic scintillator 38 mm in diameter and 5 mm thick was covered with 0.02 mm aluminium foil to exclude light. A 32 mm aperture in the case containing the scintillator served to locate the foils to be counted. An EMI 6097B photomultiplier with an applied potential of about 1300V converted the scintillations into electrical pulses.

6.7) Derivation of Flux from Activities:

6.7.1) The Activity Equations:

It is found that the rate of disintegration from a radioactive sample is proportional to the number of sample atoms present at the time. Thus

$$\frac{dN}{dt} \propto - N(t) \qquad 6.21$$

the negative sign indicating a decrease in the number N of atoms with time. If the proportionality constant is denoted by λ, then

$$\frac{dN}{dt} = - \lambda N(t) \qquad 6.22$$

λ is called the decay constant, and is constant for the given substance. It is numerically equal to the fraction of atoms decaying per unit time and its dimension is time^{-1}.

Integration of equation 6.22 gives

$$\ell nN = - \lambda t + C \qquad 6.23$$

where C is a constant. Applying the initial condition, at $t = 0$, $N = N_o$, C is obtained. Taking then antilog for the expression one gets

$$N = N_o e^{-\lambda t} \qquad 6.24$$

6.7) contd.

6.7.1) contd.

This is the exponential decay law of radioactivity, which tells that the number present at any time of the parent atoms decays exponentially with time. Other expressions can be derived from eqn.6.24. Thus multiplying both sides by λ, and with the help of eqn. 6.22 one gets the equation for activity

$$I(t) = I_o\, e^{-\lambda t} \qquad 6.25$$

where $I(t)$ is the activity, the decay rate at the instant t, and I_o is that at $t = 0$.

A parameter, half life is defined as the time taken by a radioactive sample to decrease to half its original number and hence the activity. Using either eqn. 6.24 or 6.25 one gets for half life

$$T_{\frac{1}{2}} = 0.693/\lambda \qquad 6.26$$

Half-life like λ is a parameter peculiar to a radioactive nuclei. However half-life is a more practical quantity and many radio-active sample can be identified simply by determining its half-life. The original-time referred to in the previous equations can be any convenient time and time measured from thereon.

6.7.2) Production of Radio-active Nuclides:

When a specimen is placed in a uniform flux of neutrons ϕ, radioactive nuclides are produced; at the same time they also decay. The net production rate is then given by

Net Production Rate = Formation Rate + Decay Rate

$$\frac{dN}{dt} = V\, \Sigma_a \phi - \lambda N \qquad 6.27$$

6.7) contd.

6.7.2) contd.

where N refers to the number of radioactive atoms existing at time t in the sample of volume V, which has the activation cross-section Σ_a per c.c. It is assumed that at zero time the number of active atoms is zero. After a sufficiently large time an equilibrium is reached when the decay rate is equal to the formation rate; this is the saturation condition when N_∞ numbers are present. Then from 6.27

$$V\Sigma_a \phi = \lambda N_\infty$$

or
$$N_\infty = \frac{V\Sigma_a \phi}{\lambda} \qquad 6.28a$$

or
$$I_\infty = V\Sigma_a \phi \qquad 6.28b$$

Substituting back in eqn. 6.27 and integrating

$$-\ell n(N_\infty - N) = \lambda t + \text{Constant.}$$

the constant, being given by the initial condition, is $-\ell n\, N_\infty$.

Hence

$$N = N_\infty \left(1 - e^{-\lambda t}\right) \qquad 6.29$$

Here t is the irradiation time. Multiplying both sides of 6.29, activity is obtained

$$I = I_\infty \left(1 - e^{-\lambda t}\right) \qquad 6.30$$

with the saturation activity I_∞ defined by eqn.6.28b. Eqn.6.30 tells that the saturation value is reached only exponentially, starting from zero, and that in a constant flux after one half-life of irradiation 50% of the maximum value is attained; after two half-lives 75% and after three half-lives 87½% and so on. In general, fraction of the maximum value, I_∞ after n half-lives, is given by the geometric series:

6.7) contd.

6.7.2) contd.

$$I_n/I_\infty = \tfrac{1}{2} + (\tfrac{1}{2})^2 + (\tfrac{1}{2})^3 + \ldots + (\tfrac{1}{2})^{n-1} + (\tfrac{1}{2})^n$$

$$= \tfrac{1}{2} + \tfrac{1}{4} + \tfrac{1}{8} + \tfrac{1}{16} + \ldots + \frac{1}{2^n} \qquad 6.31$$

These considerations show that practical limit for irradiation time is about 3 to 4 half-lives.

6.7.3) Derivation of Saturated Normalised Activity:

From the observed activities the saturated activity I_∞ is calculated. If this is normalised to one gram of the activated isotope in the sample

$$\frac{I_\infty}{m} = \frac{N_o}{A}\,\sigma_a\phi \qquad 6.32$$

where N_o = Avogadro's number, A is the atomic weight of the sample material, m its mass and σ_a is the microscopic activation cross-section. From eqn.6.32, knowing all other quantities, the flux ϕ can be obtained. However, with a threshold reaction the foil is activated by all neutrons with energies above the threshold energy of reaction. Here both σ_a and ϕ are in general functions of energy E. Eqn.6.32 is then extended to

$$\frac{I_\infty}{m} = \frac{N_o}{A}\int_{E_{th}}^{\infty} \sigma_a(E)\,\phi(E)\,dE \qquad 6.33$$

The integral can be called response integral per atom. The $\sigma_a(E)$ is known but the product over the integration limit is unknown - the only unknown in equation 6.33. Measurement of activity from a threshold foil is capable

6.7) contd.

6.7.3) contd.

of yielding this integral value at the point of irradiation. Denoting this as an average value over the limit the form expressed as in eqn.6.32 is again obtained.

Now, if a foil is counted at a time t' after the end of the irradiation with a counter of fractional efficiency k and a count rate C is observed then

$$I_{\infty} = \frac{C\, e^{\lambda t'}}{k\left(1 - e^{-\lambda t}\right)} \qquad 6.34$$

The wait time t' is taken at the mid-point of the interval during which count is recorded. Strictly the exponential should be integrated over the interval and average value used but if the interval is small compared to half-life eqn.6.34 is accurate enough; for one minute counting interval of an activity of half-life 10 minutes and using the mid-point the error is less than 0.01 per cent.

The saturated normalised activity per minute per gram of the isotope for a normalised source strength is then

$$\frac{N_o}{A}\left[\sigma_a \phi\right] = \frac{Q_N\, C_i\, e^{\lambda t_i'}}{Q_{AVG}\, k\, m_i\, Z\left(1 - e^{-\lambda t}\right)} \qquad 6.35$$

where m_i = wt of the ith foil
A = atomic weight of the foil material
Z = isotopic fraction of nuclides of choice
λ = disintegration constant per min
t = irradiation time in min
t_i' = wait time for ith foil count
C = counts observed per min
k = counts per disintegration in foil
N_o = A_{VO} number
Q_{AVG} = source strength during irradiation
Q_N = normalisation source strength

6.7) contd.

6.7.3) contd.

The square brackets in the left side indicates the integral value as defined by 6.33. To express activity per gm instead of the integral is to represent values as the same order of magnitude as observed counts rate.

Right hand side quantity of eqn.6.35 is computed by the program 'FOILSNACT' for each foil together with counting standard error, from the activation data. This is termed SNACT in the program output.

6.7.4) Irradiation History: Q_{AVG}

As indicated in the chapter on production of neutrons, the output of neutrons vary during the irradiation. This affects the foils differently due to their different half-lives. The effective source strength of neutrons can be found if the variation of source strength during the irradiation is known as a function of time. The total time of irradiation t is divided into N equal intervals each of duration δt, so that $N \times \delta t = t$. For the m th time interval call flux at a foil ϕ_m. Activity induced during the interval is given by eqn. 6.30; for the rest of the time it decays which is given by eqn.6.24. Combining these two, the activity due to the m th interval at the end of irradiation, δA is proportional to the following:-

$$\delta A \propto \phi_m \left(1 - e^{-\lambda . \delta t}\right) e^{-\lambda (N-m) . \delta t}$$

This relation is exact; the only approximation is that flux was constant during δt. Accuracy of this assumption is improved by keeping δt small compared to foil half-life.

6.7) contd.

6.7.4) contd.

Typically δt was 1 min. For all the intervals the above expression is summed up:

$$A \propto \sum_{m=1}^{m=N} \phi_m \left(1 - e^{-\lambda . \delta t}\right) e^{-\lambda (N-m) . \delta t} \qquad 6.36$$

The effective average flux ϕ_{avg} is obtained from here as that flux which at a constant level for the same irradiation time would give the same activity A at the end of irradiation; this is obtained by equating the right hand side of eqn.6.36 to

$$\phi_{avg} \left(1 - e^{-\lambda t}\right).$$

The corresponding constant source strength is Q_{avg}. Since the relationship between flux and source and source and the alpha-particle counts are linear, variation in flux or source strength can be obtained from variation in alpha-counts. The known geometry and the anisotropy factors relate alpha counts to neutron source strength. Program EFFNEUTSCE was written to compute Q_{avg} from the alpha counts history.

6.7.5) Methods for Treatment of Threshold Foil Data:

There are several ways in which threshold foil data is treated and compared with calculated values. These can be termed integral methods and differential methods.

In the integral methods the activity distribution in the system is compared with the corresponding theoretically calculated activity distribution conducted from spectral analysis and foil cross-section data. This way, the experimental results are preserved as the reference points and the

6.7) contd.

6.7.5) contd.

effect of calculation techniques and the cross-section data is tested to give agreement. The results can be presented and compared either graphically or in tabulated form.

Integral methods are however indirect. The ideal method would be to construct the differential flux from foil activation data and compare the computed flux at energy points or at least for energy groups. Several techniques have been put forward and demonstrated for what is termed unfolding of activation data and obtain differential flux [128-134]. None of these methods have proved very satisfactory though some seem promising. The main disadvantage is that the differential cross-section data for activation reaction is known only to about 10% accuracy. The nature of mathematics in several of the unfolding techniques is such that this uncertainty is magnified several times while constructing the flux. The other drawback is that very often results obtained oscillate and sometimes even show negative flux. This can happen from 'mis -match' of foils among themselves or from nature of mathematics itself so that the values obtained are not unique.

Some of the unfolding techniques are described briefly. The effective threshold technique of Hurst [128] is based on an idealised step-function of cross-section defined with fission neutrons; the unknown spectrum is assumed to be similar to the fission spectrum in profile. The polygonal and polynomial methods were developed by Uthe [129]. In polygonal method the spectrum is a polygon

6.7) contd.

6.7.5) contd.

whose parameters are determined from activation data. For the polynomial method the spectrum is represented as a polynomial in ascending powers of energy. The number of activation reactions determine the order of truncation of the power series and the coefficients are obtained from activation data. The orthonormal expansion method developed by Hartmann [130] and modified by Lanning and Brown [131] assumes that the spectrum can be represented by an expansion of orthonormal function, each function being a linear combination of the activation cross-section. The method is equivalent to a least squares approximation but it usually requires many detectors with threshold energy evenly distributed through the energy region of interest.

There is also the "perturbation" method of Grundl and Usner [132], the series expansion method of Di Cola and Rota [133] and iterative method of McElroy [134]. Computer codes, SPECTRA [135] and SAND-II [136] have been developed, but their use has not yet been sufficiently well reported to estimate their reliability and versatility.

In the present work the traditional method of comparing the experimental values of the response integral with computed values obtained from multi-group analysis of the flux spectrum has been adopted.

6.8) Performance of the foils in the Assemblies and Recovery of Proper Activities.

The gamma spectrum from foil was studied to identify the reactions and relative contribution from competing

6.8) contd.

reactions. From this the necessity to eliminate the secondary activities, either by bias setting or controlling irradiation time and waiting time - or both was investigated. Within this limit settings were determined to obtain a satisfactory workable background to count ratio and acceptable counting statistics. The half-lives of the decays were studied to estimate any remaining contribution from other competing reactions.

6.8.1) Background Spectrum of the Gamma Analyser:

The background pulses observed in scintillation counting can be internal and external. The internal background may result from thermionic emission from the cathode or from the dynodes, spurious light flashes due to fluorescence of the glass envelope of the photomultiplier and from contamination and impurities in the phosphor itself. The background due to external effects may result from cosmic rays, radioactivity in the walls and floors of the room in which the equipment is situated, and from both neutron and gamma ray fields in the laboratory. The background due to external effects can obviously be reduced by shielding the crystal and placing it as far away as possible from the walls and floors.

The NaI crystal of the gamma-analyser was shielded by about 5 cm. thick lead around the sides of the crystal. However following the operation of the accelerators considerable activity due to the 25 min ^{128}I resulting from the (n,γ) reaction with the ^{127}I in the NaI scintillator was observed. This would make the subsequent use of the gamma analyser for foil counting for about an hour after the end of irradiation unsatisfactory. Not much improvement

6.8) contd.

6.8.1) contd.

was observed by covering it with cadmium. However by using a cap-like shield around and over the crystal, made of paraffin wax of about 4 cm. thickness and inner surface lined with cadmium, the 25 min activity could be reduced to an undetectable level. An activity was observed only due to the (n,n') reactions of iodine and sodium with the penetrating neutrons of higher energies but this would vanish as soon as the irradiation stopped. The paraffin cap could be easily removed following an irradiation.

However there was a permanent background spectrum with the gamma counter which could not be removed by shielding. A background spectrum counted for 20 mins is shown in Figure 6.7, which can be identified as the ^{40}K spectrum, with its 1.46 Mev peak. Owing to its ^{40}K content, one gram of natural potassium emits 28 beta particles and 3.6 gamma rays per second with energies of respectively 1.32 Mev and 1.46 Mev. From the counts under the peak it is estimated that about 1.7 gm of natural potassium in the crystal could have given the spectrum, which gives about 0.9% by weight or about 0.6% by atom of contaminant potassium in the sodium content of the crystal. This is quite possible. Glass envelopes of photomultipliers are also known to have potassium contamination. Some contribution to the spectrum might have come from there as well.

6.8.2) Energy Calbiration of the Gamma Analyser:

Positions in channel of the peaks from gamma sources of known energies are shown in Figure 6.8. Excellent

FIG. 6.7 -- Back-ground Spectrum of the Gamma-counter

(Counted for 20 minutes.)

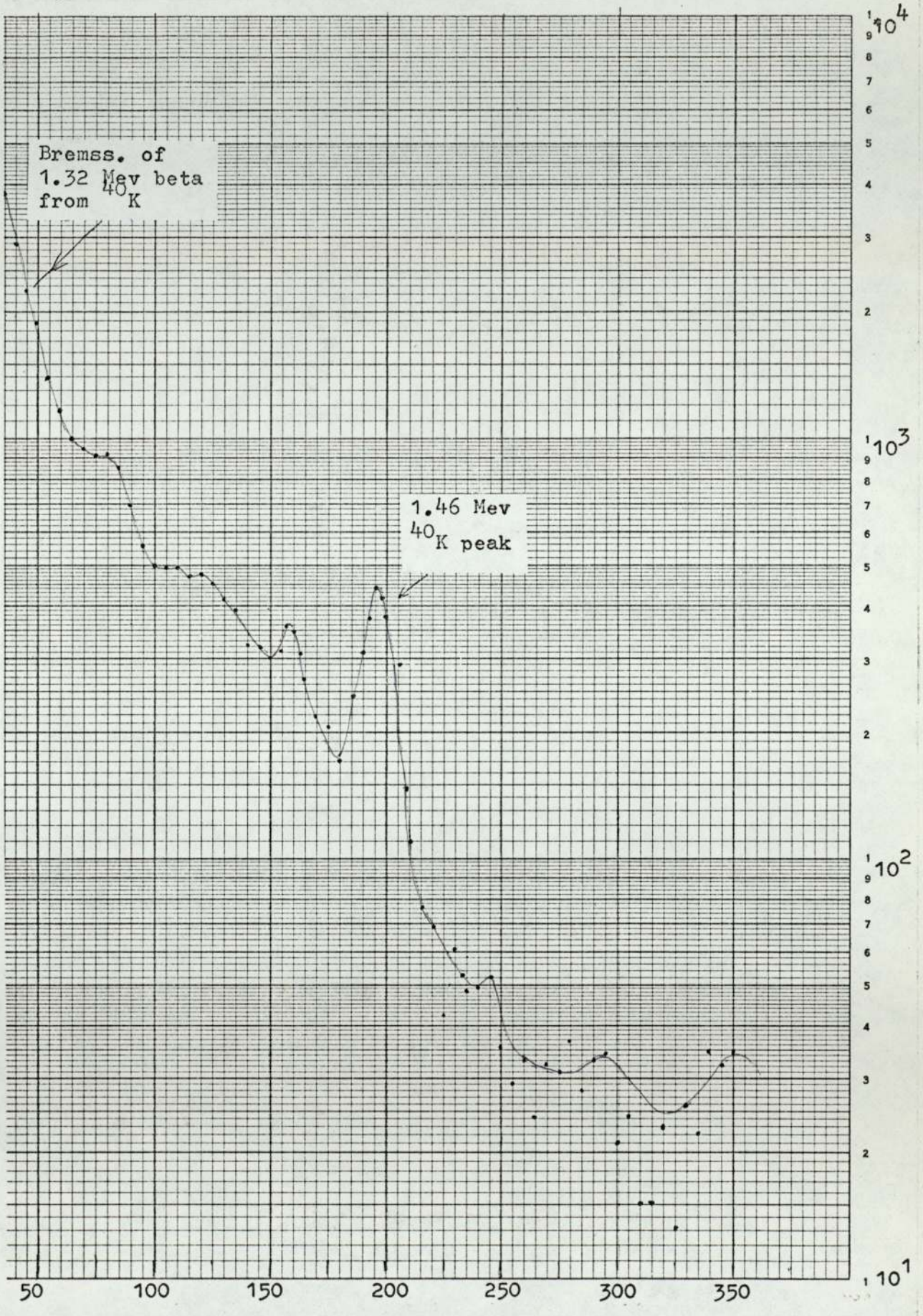

6.8) contd.

6.8.2) contd.

linearity with the four reference peaks due to ^{137}Cs, ^{54}Mn and ^{60}Co indicates the reliability of the system. This calibration also served later to locate the chosen parts of the spectrum for different foils. Over the period of use the gain of the amplifier changed slightly after servicing or maintenance; it might have also altered due to seasonal temperature change in the laboratory. The calibration was therefore checked every time irradiations were made. When the positions of the peaks had altered they were brought to original positions by manupulating the fine gain of the amplifier; a slight change was sufficient.

Later, peaks from foils were noted and their plot on the energy calibration curve showed that the linearity was not maintained at higher energies. It was still linear for the 1.81 Mev and 2.21 Mev peaks from ^{56}Mn of the Fe(n,p) reaction. But the 2.75 Mev peak from ^{24}Na of $A\ell(n,\alpha)$ reaction was found under-amplified and falls short by about 15 channels (Fig.6.8).

6.8.3) Positioning the Foils for Counting.

The foils were positioned on the top of the aluminium container covering the crystal for counting; the position was fixed with the help of cardboard frames cut in the form of rings, the inner diameter being the same as that of the foil or the foil converter in the case of the copper foils - there being one ring for each type of foil. The outer diameter of the rings was the same as that of the aluminium container and the ring was attached to the latter with pieces of sellotape. This way, foils could be centrally

FIG. 6.8-- Energy Calibration of the gamma-counter.

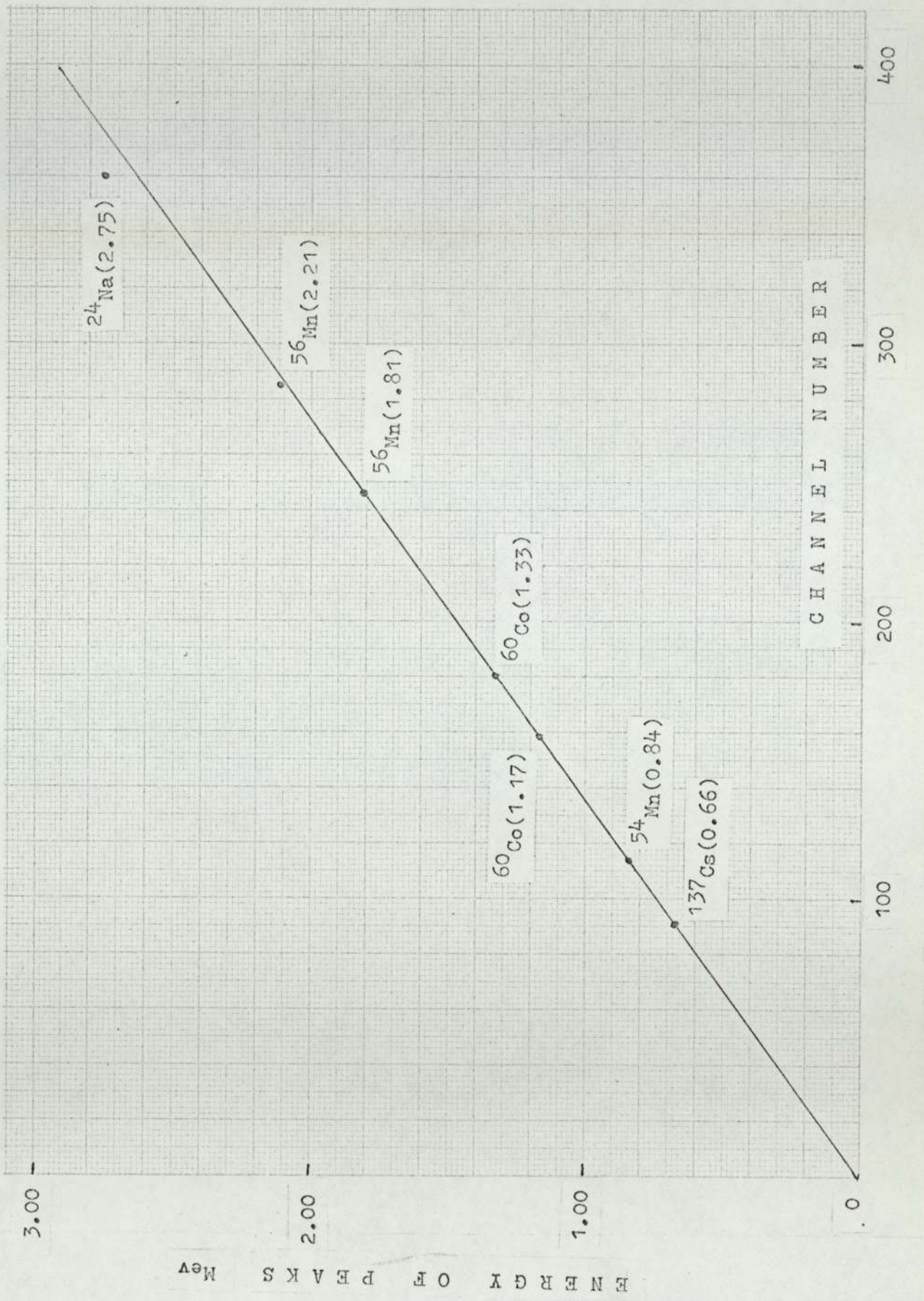

6.8) contd.

6.8.3) contd.

positioned for counting to within ± 1 mm.

6.8.4) Elimination of Competing Reactions:

$^{63}Cu(n,2n)$. The annihilation 0.51 Mev peak from the positrons was counted for this reaction. As most of the annihilation takes place after the positron has slowed down the copper foils were placed inside a foil converter made from aluminium for counting. The range of 2.9 Mev positrons in aluminium is 5.5 mm. The thickness of aluminium around foil was 6 mm. Each type of copper foil had one converter with the same thickness of aluminium but of different diameters. The L-type foil was counted inside the converter for foil type-5. The converters served to confine the activity within a given volume, so that the annihilation quanta did not originate from the lead shield and the structural frame for the photomultiplier tube container.

Possible interference to the main reaction of Cu could be the $Cu^{63}(n,\gamma)$ and the $Cu^{65}(n,2n)$ reactions. Both have Cu^{64} as the reaction product which decays by 0.66 Mev positron in 19% of the decays. Since Cu^{64} has a half-life of 12.9 hours its build-up evidently can be minimised by short irradiation period and its contribution reduced by counting as soon as possible after the end of the irradiation. The $Cu^{63}(n,\gamma)$ cross-section is low compared with many other (n,γ) cross-sections. Also thermal and epi-cadmium neutron fluxes were assumed to be small. Contribution from $Cu^{65}(n,2n)$ on the other hand could not be

6.8) contd.

6.8.4) contd.

neglected as its cross-section at 14 Mev is 1.0 barn, about twice as much for the main reaction $Cu^{63}(n,2n)$. Preliminary calculations indicated contribution from $Cu^{65}(n,2n)$ for a typical irradiation time of 30 mins and counting period up to waiting time of 20 mins, could be 2%. In some cases waiting period was still longer. Also a plot of the uncorrected data for half-life indicated the contribution from longer lived ^{64}Cu. The program SUBSECACT was written to subtract the contribution from $Cu^{65}(n,2n)$. All copper foil counts were treated this way. The output from SUBSECACT is produced in a way to be input of the code FOILSNACT. Observed count for a copper foil and the corrected values are shown in Figure 6.9 for up to about $1\frac{1}{2}$ hrs of waiting. The subtracted counts fall in a straight line on the log-linear plot which gives a half-life of about 10 mins. This indirectly confirms that contribution from the possible (n,γ) reaction with ^{63}Cu is negligible. This particular foil was irradiated for 20 mins and was located in the second gap of the iron cylinder. Similar graphs were obtained from copper foils in the other assembly and also from calibration irradiations.

<u>Aℓ(n,α) and Aℓ(n,p)</u>. The same foils were used to measure the (n,α) and (n,p) reactions induced in the aluminium foils. Two full spectra from an aluminium foil 20 mins and 2 hours after the end of irradiation are shown in Figure 6.10. The foil was irradiated for about $2\frac{1}{2}$ hours. The interesting feature is that after a waiting

FIGURE 6.9- $^{63}Cu(n,2n)$ Activities Corrected by Program 'SUBSECACT'; Activities due to $^{65}Cu(n,2n)$ of Half-life 12.9 Hours and Threshold at 9.8 Mev. have been Subtracted.

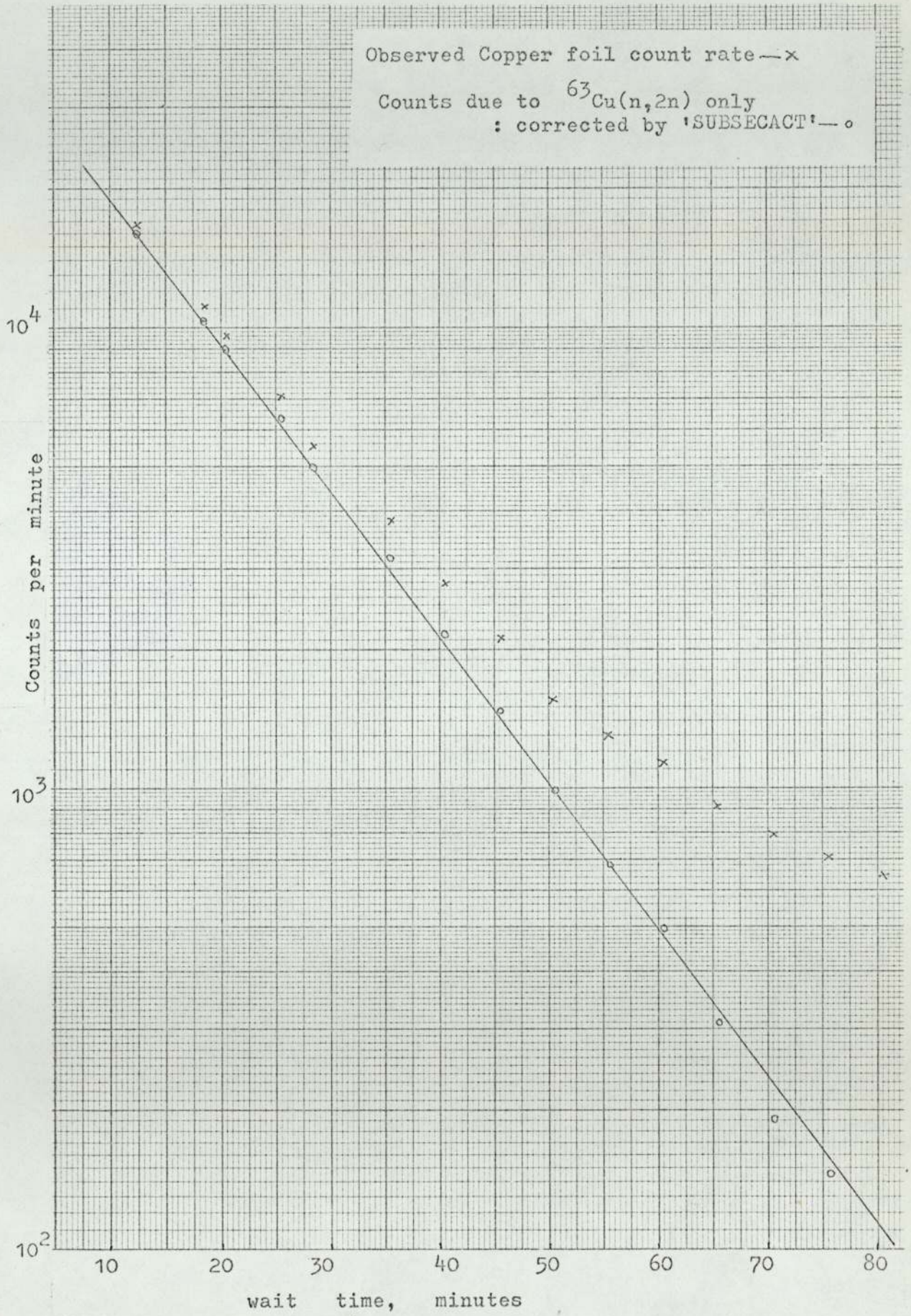

FIG. 6.10 -- Spectra from an Irradiated Aluminium Foil after two different waiting times.

(Counted for the same period of time.)

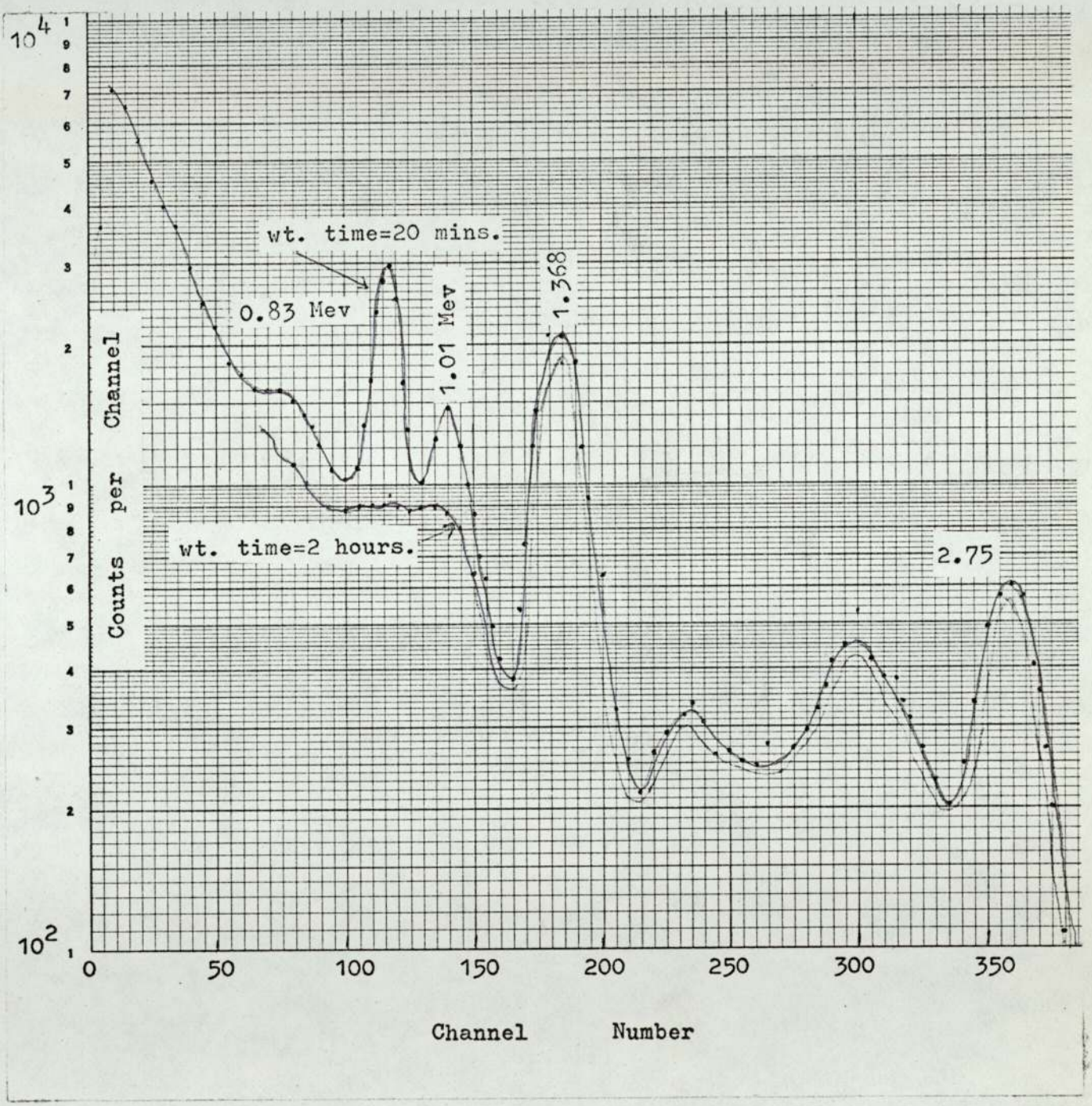

6.8) contd.

6.8.4) contd.

period of 2 hours 1.01 and 0.83 Mev peaks have vanished while the rest of the spectrum has hardly changed. From this, contributions due to (n,p) and (n,α) can be identified. Al(n,p) reaction could be eliminated by setting a lower bias to cut-off everything below channel number 160; and it was not necessary then to wait a long period to let the (n,p) peaks decay. However the (n,p) peaks were sitting on the Compton continuum of the (n,α) peaks. True counts due to the (n,p) reaction could only be recovered by analysing the composite curve graphically. The foil was counted beginning from soon after irradiation until the (n,p) activity virtually vanished and the remaining activity was then extrapolated up to zero waiting time. Hence the (n,α) contribution in the earlier counts was deduced and subtracted from the total to get the (n,p) activity. The (n,p) activity almost vanished at waiting of about 90 mins. The foil had to be counted for another 30 or 40 mins to obtain reliable points for the (n,α) alone so that it could be easily extrapolated. A check for reliability of the (n,p) data alone could be obtained by noting whether they give a line for a half-life of 9.5 min. The composite activity curve and the recovered (n,p) activity curve are given in Figure 6.11 for one foil. As can be seen, the 2.3 min half-life of aluminium thermal neutron activation did not show up in the (n,p) curve.

The (n,α) contribution could be kept to a minimum by choosing a short irradiation time (typically 30 mins for Al-n,p activation) and by setting bias to observe the narrow region for the 1.01 and 0.83 Mev peaks.

FIG. 6.11 -- Recovery of the Al(n,p) Activity from the Observed Activities.

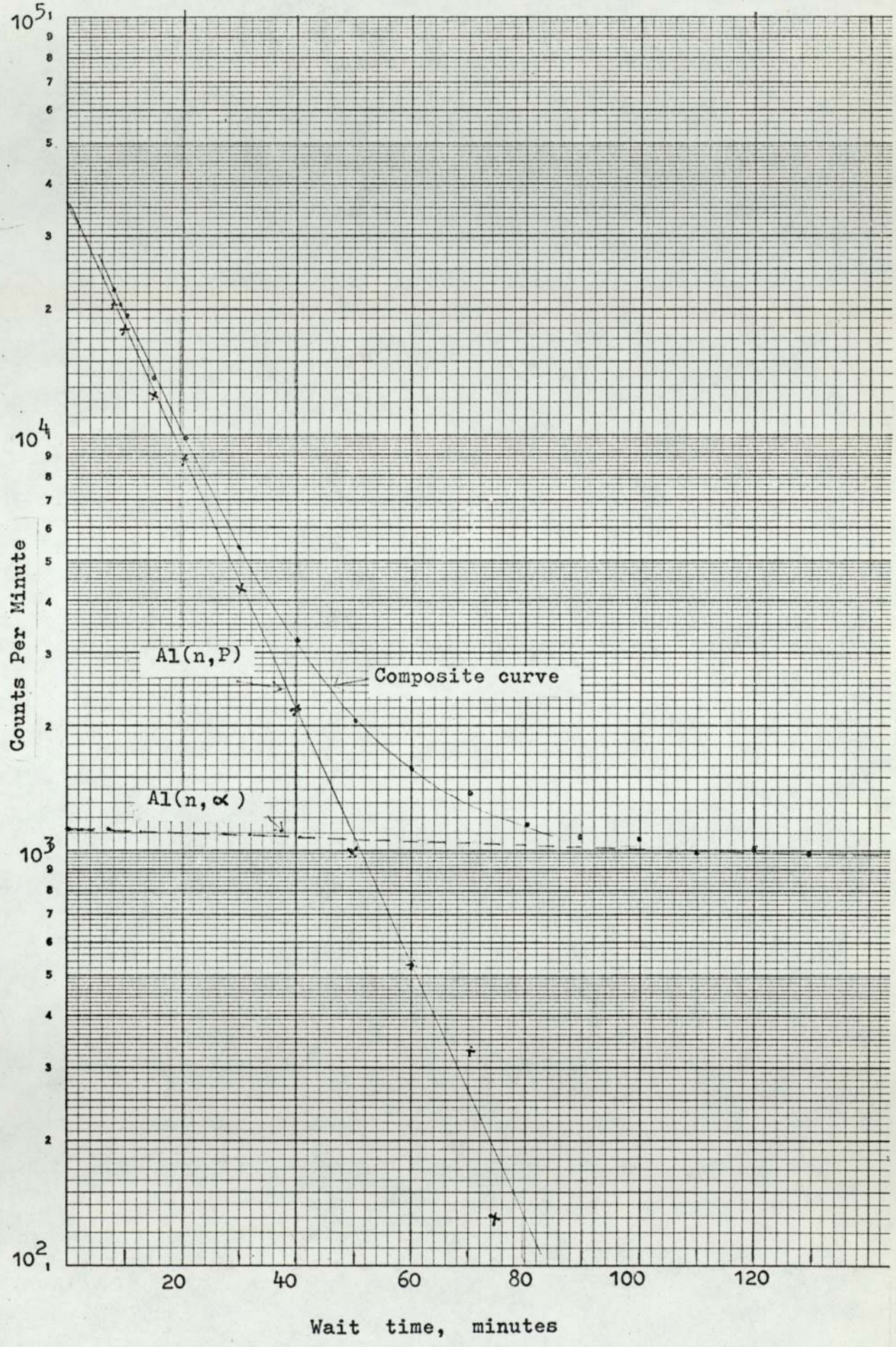

6.8) contd.

6.8.4) contd.

$^{31}P(n,p)^{31}Si$. Counting irradiated phosphorus in the beta counter from 5 mins to 3 hours showed two components in the half-life curve - one of 2.5 min and the other of about 2.6 hours. Up to 15 mins waiting time the 2.5 min component made significant contribution to the activity but by 25 min it became negligible. After that the 2.6 hour activity predominated. For phosphorus foil counting at least half an hour of decay time was allowed.

The beta counter was otherwise trouble free. Its background was around 70 per min, which is much smaller than the background count from the gamma counter, mainly due to small volume of scintillator and non-contamination of its materials.

$^{56}Fe(n,p)^{56}Mn$. This gave a clean spectrum from manganese-56 and there was no interference from other activities. The 0.84 Mev peak gamma-ray was the prominent one and this peak was selected for counting. Plot of activity against time gave a half-life of about 2,5 hours.

$^{115}In(n,\gamma)$. The spectrum obtained with the gamma analyser showed that ^{116m}In was the reaction product and no competing reaction could be detected from the observation of spectra with foils irradiated for one to two hours. The half-life obtained from selected peak counts in the gamma counter and from beta counts both gave a value of 54 mins. As the physical thickness of the foils was large - larger than the range of some of the beta particles, information from inner layers was not indicated in beta counting, while in gamma counting the total activity

6.8) contd.

6.8.4) contd.

in the whole volume of the foils could be directly obtained and the flux perturbation by the neighbouring foils, if any, could be easily ascertained. Some perturbation was observed when the foils were close to each other; the proper separation distance of the foils was obtained from the gamma counts. However, the background count rate for the gamma-peak counting was about five times larger than in the beta counter and better statistics could be obtained easily with the latter.

6.8.5) Bias Setting in the Gamma Counter:

The parts of the spectra chosen for different foils for gamma counting is given below:-

Reaction	Part of the Spectrum Selected
^{63}Cu (n,2n)	0.51 Mev annihilation peak
^{27}Al (n,α)	1.37 Mev peak and above
^{56}Fe(n,p)	0.84 Mev peak
^{27}Al(n,p)	0.83 and 1.0 Mev peaks
^{115}In(n,γ)	1.0 and 1.3 Mev peaks

Discriminator settings were chosen to correspond to the valleys in either sides, so that any error in re-setting the bias later was minimised. The discriminator dial setting error was better than $\pm$ 4 kev and the error in counting due to it is negligible.

6.9) Absolute Calibration of Counting:

Calibration of counting is needed in order to obtain the counter efficiency for the reaction and to obtain the

6.9) contd.

absolute activity.

6.9.1) Methods for Counting Efficiency Determination:

In principle, it is possible to compute the efficiency of both beta and gamma scintillation counters for a particular foil, if the solid angle the foil makes at the counter, the energy of the radiations and the thickness of the foils and other materials covering the scintillators are known. But several corrections have to be made, which can introduce large uncertainties.

When the absolute counting efficiency is needed usually the activation foils are counted by the following methods: $4\pi\beta$-γ coincidence, $4\pi\beta$ counts in the flow chambers and the gamma-photo peak counting. Because of the large thickness of the threshold foils, a large factor for self-absorption is involved if the beta-particles are counted. To avoid this the reaction products are extracted by various means and thin samples for $4\pi\beta$ counting are prepared from the irradiated foils. The beta-gamma coincidence counting technique is strictly applicable only to nuclides with a simple β-γ decay scheme - a single decay branch, to which all beta rays and all gamma rays belong. Bell and Mill [137] reports of a systematic discrepancy between the coincidence mthods and 4π methods. The discrepancy though small for hard betas, is about 7% for soft betas.

For counting the gamma peaks with scintillators the counter may be calibrated with standard sources of known strength [139,140]. In some cases the standard source can be the same nuclide as the decay product, and the calibration is direct except that corrections may be

6.9) contd.

6.9.1) contd.

necessary for the geometry factor due to different size of the foil. But in general the standard sources have different energies and the efficiency for the foil has to be interpolated. In such cases one is limited to counting the photo-peak only and corrections become necessary for contribution from the Compton continuum of the higher energy peaks, which themselves are not suitable for counting because of smaller heights.

6.9.2) Calibration with D-T Neutrons:

Since the absolute source strength of the neutrons from the D-T reaction can be measured, calibration with them is direct. However hardly any work on calibration of threshold foils with mono-energetic neutrons has been reported, though fission source neutrons have been used [149]. Neutrons from D-T reaction with low energy accelerators are strictly mono-energetic particularly in the direction of 90° to the beam and have sufficient strength so that good statistics can be obtained with most of the threshold foils. The advantages are several. Thus any part of the gamma spectra can be arbitrarily chosen for counting to give higher count rate and count to background ratio than with a peak alone. In addition, the correction factors, such as self-absorption, back scattering and contributions due to gamma rays in beta counting and contribution from the Compton continuum, photo peak area determination, self-absorption and contribution from the betas and uncertainty in the branching ratios of decay schemes in gamma counting - need not be separately

6.9) contd.

6.9.2) contd.

considered.

The main disadvantage with calibration using accelerator produced neutrons is that foils of longer half-lives (i.e. days) cannot be used, as the irradiation time is limited. Another disadvantage is that cross-sections at 14 Mev have been measured, over the years, by several workers and there is a wide spread in the reported values. However, since the compilation by Paulsen and Liskien [111], it is now possible from judicious consideration of the reported values to find reliable cross section values at 14 Mev.

6.9.3) Improvement in Accuracy by Rotation.

The accuracy in calibration with a D-T point source depends upon three factors: the counting accuracy following irradiation, the accuracy in determining nuetron source strength from alpha particle detection, the determination of distance between the irradiated foil and the neutron source. Error due to the last factor is discussed here.

There was an uncertainty in the position of the beam spot on the target whichwas 25 mm in diameter. Normally the beam would fall on the target in a diffuse circle of about 12 mm dia. The combined effect of these two factors gives an uncertainty of about 12 mm in the target to foil distance. The uncertainty in the flux falling on the foil can be reduced by increasing the

6.9) contd.

6.9.3) contd.

source to foil distance, R, but a large distance gives poor counting statistics and an increase in the relative number of reflected neutrons. Accuracy of calibration should be better than that of foil counts in assemblies. For a value of R = 127 mm (5 in), an uncertainty of 12 mm can give a maximum possible error of $\pm$ 20% in the estimated flux. But it is found that by rotating the foil around the target the negative and positive errors cancel out to a large extent and the error in flux can be reduced by a factor of 20.

In the diagram below the centre of the circle is 0 and let the position of the source b 0'. A is the position of the foil at any instant as it rotates along the circle. The average flux received by the foil is the same as the average flux receivd by the circumference of the circle from the source at 0'. If a is the radius of the circle then the assumed flux for the source position at the centre 0 is given by

$$\phi_o = \frac{Q}{4\pi a^2} \qquad 6.37$$

where Q is the source strength. The corresponding activity Act_o is proportional to ϕ_o.

If θ is the angle A makes with the diameter through 00' then the flux due to source at 0' is

$$\phi = Q \frac{d\Omega}{4\pi} \frac{1}{a d\theta}$$

where $d\Omega$ is the elemental solid angle made by the elemental arc length $ad\theta$ at A with 0'. But since the activity induced is proportional to the volume of the foil the effect of

6.9) contd.

6.9.3) contd.

variation of solid angle cancels out and the activity is simply given by the inverse square relationship. If D'A = r

$$\text{Act} \propto \frac{Q}{4\pi r^2} \qquad 6.38$$

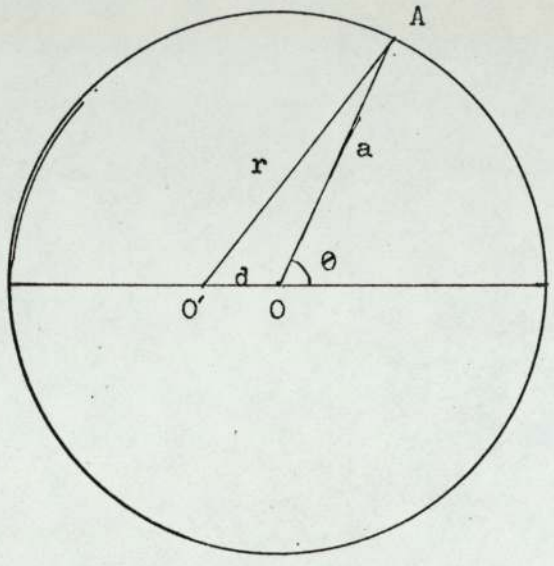

The average activity is obtained by integrating over θ; the integration limit from 0 to π is adequate as the effects are symmetrical in the upper and lower half of the circle:

$$\overline{\text{Act}} \propto \frac{\int_0^{\pi} \text{Act}(\theta)\,d\theta}{\int_0^{\pi} d\theta} = \frac{1}{\pi}\int_0^{\pi} \text{Act}(\theta)\,d\theta \qquad 6.39$$

From 6.37, 6.38 and 6.39 we have

$$\frac{\bar{\phi}}{\phi_o} = \frac{\overline{\text{Act}}}{\text{Act}_o} = \frac{a^2}{\pi}\int_0^{\pi} \frac{d\theta}{r^2} \qquad 6.40$$

where Act_o is the activity for flux ϕo and $\bar{\phi}$ is average flux. r can be expressed as $r^2 = a^2+d^2+2ad\cos\theta$ where d = OO', the

6.9) contd.

6.9.3) contd.

displacement of the source. Substituting in eqn.6.40 we have

$$\frac{\overline{Act}}{Act_o} = \frac{a^2}{\pi}\int_0^{\pi} \frac{d\theta}{a^2 + d^2 + 2adcos\theta}$$

A general expression is obtained by putting $d/a = D$, a dimensionless quantity:

$$\frac{\overline{Act}}{Act_o} = \frac{1}{\pi}\int_0^{\pi} \frac{d\theta}{1+D^2+ 2Dcos\theta} \qquad 6.41$$

Equation 6.41 can be numerically computed. Program CALROTCEFF was written and the ratio for step values of D has been computed. From the ratio error is directly estimated. Results are shown graphically in Figure 6.12. It is noted that for a displacement of the source position from the centre, by 12.7 mm, of a circle of radius 127 mm when D = 0.1, the error is only 1%. It can be seen that the error increases approximately as D^2; thus for D = 0.2 the error is about 4%.

It will be seen that due to any displacement of the source position from the centre of the circle the foil receives excess flux compared with that for no displacement. The activity is thus underestimated and the counter efficiency is over-estimated by the same factor.

Second Method. The true distance of the foil from the effective point source during an irradiation can also be determined by positioning two foils B_1 and B_2 in line with the centre of the target. Assuming that the effective point source lies in the line we have

FIGURE 6.12--Correction Factor for off-Centre Target in Foil Calibration with Rotating Wheel.

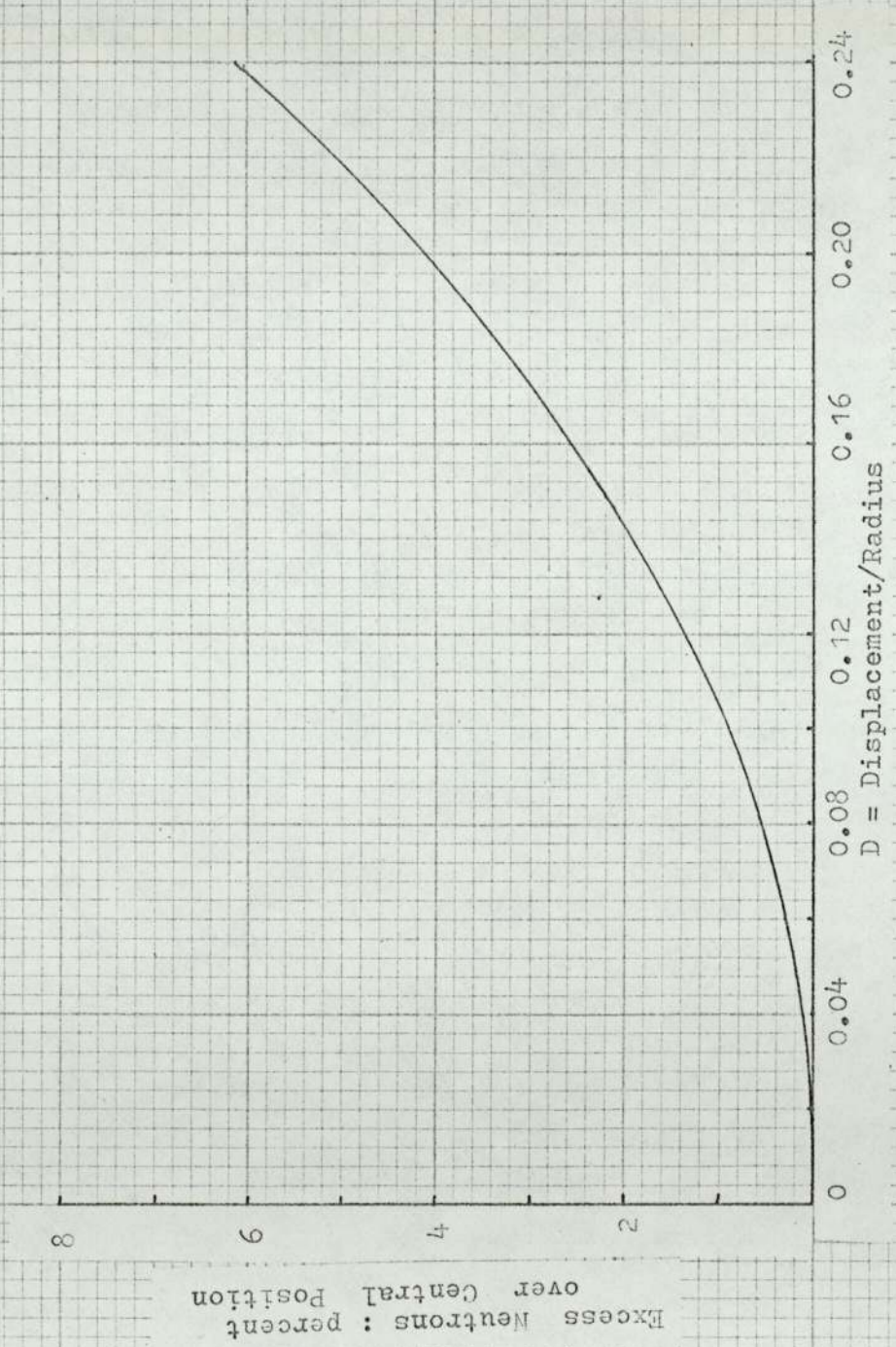

6.9) contd.

6.9.3) contd.

$$A_1 R_1^2 = A_2 R_2^2 \qquad 6.42a$$

where A_1 and A_2 are normalised activities of the foils

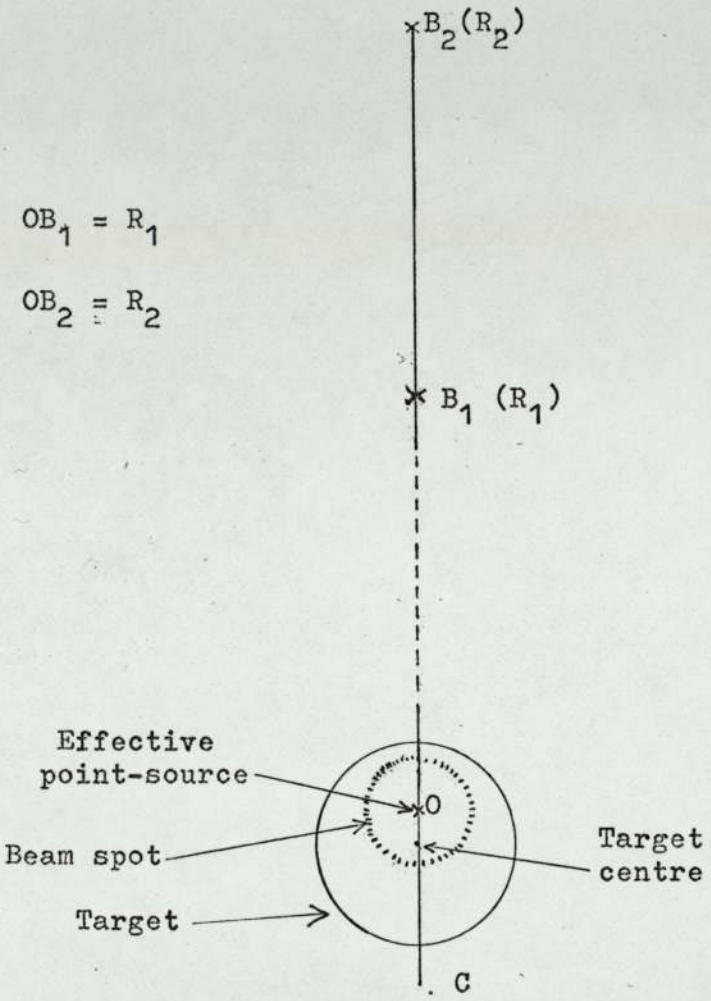

at B_1 and B_2 respectively and R_1 and R_2 are their respective distance from the source. If $(R_2-R_1) = \ell$, then

$$R_1 = \frac{\ell}{\left(\sqrt{\frac{A_1}{A_2}} - 1\right)} \qquad 6.42b$$

The distance ℓ can be accurately measured. If R_1 and R_2 are large compared to the target size then for a small displacement of the beam spot (and hence source point) on either side of the line B_2B_1C the relation 6.42a is still valid within desired accuracy, and the flux for A_1 is essentially given by inverse square law with R_1 as the distance given by eqn.6.42b

6.9) contd.

6.9.3) contd.

when the source strength is known.

Some of the results were obtained by this method for comparison with results by rotation. The drawback of this method is that the sensitivity is decreased due to square-rooting of the activities. Main calibration readings were taken by rotation.

6.9.4) Arrangement for Rotation:

The rotation was obtained with a ring 25.4 cm (10 in) in diameter with 6.3 cm in width, made of 3 mm aluminium. The ring was supported on the spindle of an electric motor and two small plastic wheels. The arrangement can be seen in Figure 6.13. To give enough gripping friction two O-rings were put on the motor spindle. The motor and the plastic wheels were mounted on an angle framework, so that the ring could be easily placed and its position adjusted around the target cap, at 90° to the beam so that the foils received the same angular flux as in the experimental assemblies. The foils were attached to the inner side of the aluminium ring with sellotape and could be rotated at about 2 revolutions per minute around the target. Foils with long half-lives - Fe, P and $A\ell(n,\alpha)$ - were irradiated together while Cu and $A\ell$ for (n,p) were irradiated separately for shorter duration. Also one or two indium foils were attached to the ring to measure thermal and resonance energy neutron flux.

For calibration irradiations the iron plates were removed from the experimental cell. To reduce thermal neutron contamination the concrete walls of the cell and

FIG. 6.13

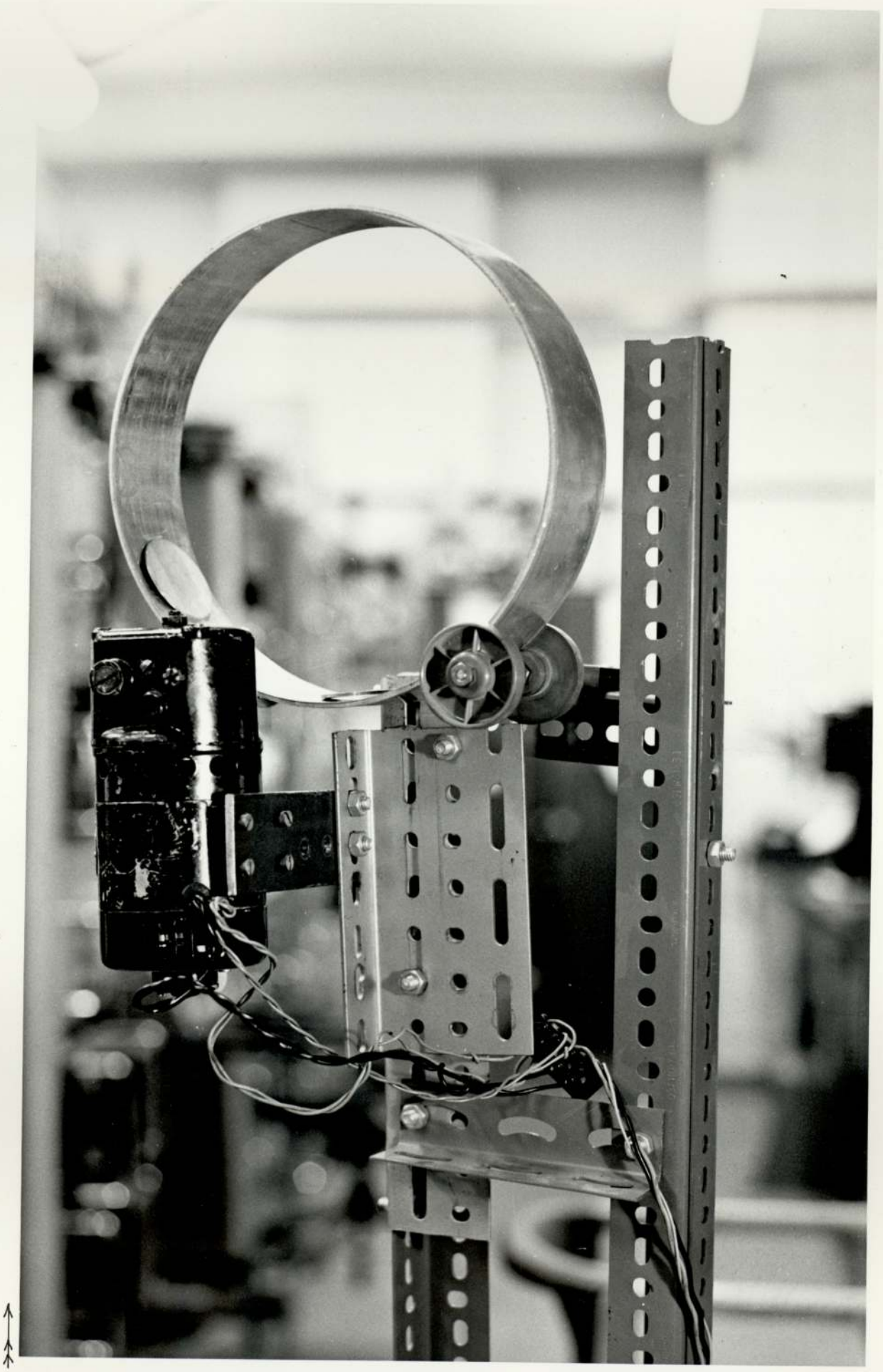

6.9) contd.

6.9.4) contd.

the floor were lined with cadmium sheets. The water thank shield at the top also had cadmium sheets at its bottom. The cadmium lining was partial - leaving exposed parts in the corners and the bends -, the indium activities were low and estimated thermal flux level was of the same order of magnitude as in the experimental assemblies. No activities were observed in the threshold foils due to thermal neutrons.

6.9.5) Calibration Values.

The fractional counting efficiency k - the number of counts observed per decay of the activated atoms in the foil - were experimentally obtained under conditions mentioned above. This is directly obtained if the induced activities are known. The activities induced were estimated from the reaction cross-sections at 14 Mev. The values for k are given below:-

	Reaction	k
1.	$^{63}Cu(n,2n)$	
	(i) foil type - 2	0.1050
	(ii) foil type - 3	0.0994
	(iii) foil type - 5	0.0890
	(iv) L-type foils	0.0933
2.	$^{27}A\ell(n,\alpha)$	0.1370
3.	$^{56}Fe(n,p)$	0.0578
4.	$^{27}A\ell(n,p)$	0.0474
5.	$^{31}P(n,p)$	0.1310

6.9) contd.

6.9.5) contd.

The standard error associated with k was estimated to be about ± 2%. This composed of uncertainty due to foil distance (1.2%), determination of source strength (1.4%) and systematic error in foil counting (0.6%). For Al(n,p) an additional uncertainty of 1% was allowed for recovery of the proper activity from the composite curve; this gives a total error of ± 2.25% for it.

Error in the cross-sections at 14 Mev, used to estimate the activities is not included in it. This error to a large extent cancels out so far as k is concerned while translating the observed counts in the assemblies to the activities. This is discussed more, later in Chapter 9, on the results.

6.9.6) Efficiency for In-foil counting:

In principle, resonance foils can be calibrated with a standard known thermal neutron source. In the absence of any such facility indium foils could not be calibrated. Indium foils were counted for gross beta activities with the beta counter and gamma counted for the peaks at 1.09 Mev and 1.29 Mev. In order to draw conclusions the beta and gamma counting efficiencies were calculated from standard relations.

Gamma-Counting efficiency.

This has been calculated after Heath [141] and Grosgean and Bossaert [142]. For a disc-type source which is centrally situated around the extended axis of a cylindrical crystal, and parallel to its face, the absolute detection efficiency is given by

6.9) contd.

6.9.6) contd.

$$T(E) \simeq T_o(E) + L \frac{R^2}{2r^2} + M \frac{R^4}{3r^4} \qquad 6.43$$

where $T(E)$ = absolute total detection efficiency for the source emitting γ's of energy E

$T_o(E)$ = absolute detection efficiency for a source situated on the axis of the scintillator at the same height as the disc source

$\tau(E)$ = absorption coefficient per unit length of the scintillator

r = radium of the crystal

t = its height

R = radius of the disc source $[R < r]$

h = distance of the source to the surface of the scintillator

and L and M are two finite size correction factors and are functions of h, τ and r. $T_o(E)$, is given in refs.142 and 141, for several standard size NaI(Tℓ) scintillators and as a function of the gamma ray energy E. The correction factors L and M are also tabulated. T(E) can be computed from there. $T_o(E)$ is the detection efficiency if the entire source were concentrated at its centre; the correction factors make very small contributions for the geometrics used.

The peak-to total ratio of count rate has been experimentally determined by Heath [141] and is given graphically as a function of gamma-energy. From there with knowledge of branching ratio in gamma emission the peak counts can be related to the absolute disintegration rate. A small correction has been made for Compton contribution in the 1.09 Mev peak from 1.29 Mev; contribution in both due to the higher peaks have been neglected as they are of lower

6.9) contd.

6.9.6) contd.

intensities - by a factor of about 10. The efficiency is 13.3%.

Beta counting Efficiency:

Beta counts need two corrections - due to self-absorption and due to back scattering. The correction due to self-absorption has been calculated after Cohen [143]. For an absorbing thin sheet of thickness t mg/cm^2 between the foil and the detector the fraction reaching the detector surviving absorption is found to be given by

$$f = e^{-t/\alpha} \qquad 6.44$$

where α is a constant which is independent of absorbing material but depends on the energy of the beta-particles. The self-absorption can be obtained by integrating this equation through the thickness of the foil, giving the fraction transmitted

$$T = \frac{\alpha}{t_o}\left(1 - e^{-t_o/\alpha}\right) \qquad 6.45$$

where t_o is the thickness of the foil; it is assumed activity is uniformly distributed along the thickness. The exponential in eqn. 6.45 approaches zero as to increases, and practically this is zero when the thickness is equal to the range of the betas; when the thickness is larger than range no contribution can reach from beyond the range. Fraction transmitted by the thickness equal to range R(mg/cm^2) is

$$T_\infty = \frac{\alpha}{R} \qquad 6.46$$

For beta particles whose E_{max} is below 2.5 Mev, the range is given by Katz and Penfold [144] as

6.9) contd.

6.9.6) contd.

$$R = 412\ E_{max}^{n} \qquad 6.47$$

$$\text{with } n = 1.265 - 0.094 \ln E_{max}$$

where E_{max} is in Mev and R in mg/cm^2. The ranges of the three energy groups of beta particles from ^{116m}In 1 Mev (51%), 0.87 Mev (28%) and 0.60 Mev (21%) is computed from this equation; they are 412, 344 and 211 mg/cm^2 respectively. The thickness of the X-type foils were t_o = 464 mg/cm^2, which is larger than the range for all cases. Of the total activity induced in a foil the fraction in the range = R/t_o.

Cohen [143] experimentally determined the values of α for various energy groups and the results are given graphically by him. Values for the three groups are taken from there and T_∞ is calculated according to eqn.6.46.

The absorption by the aluminium foil of 0.02 mm (t = 5.4 mg/cm^2) can be calculated with the same values of α, but for this eqn. 6.44 is valid. The transmission fraction is called T(Al).

A 2π-reception geometry can be approximated for a thin foil just on the scintillator, giving a geometry factor 0.5.

All these values for the three groups are shown in the table below.

6.9) contd.

6.9.6) contd.

TABLE - 6.1

Values for calculation of transmitted fraction of the betas from X-type Infoils.

Energy Mev	Decay fraction, d	Range R mg/cm²	R/t_o	α mg/cm²	$\alpha/R = T_\infty$	T(Al)
1.0	0.51	412	0.888	70	0.170	0.926
0.87	0.28	344	0.741	60	0.174	0.914
0.60	0.21	211	0.455	40	0.189	0.873

If A_o is the activity in the whole foil then number of transmitted beta particles for each group is given by

$$\overline{T} = 0.5 \times A_o \times d \times \frac{R}{t_o} \times \frac{\alpha}{R} \times T(A\ell) \qquad 6.48$$

However the transmitted numbers are enhanced by a back-scattering factor f_β. The back-scattering is due to multiple Rutherford scattering. A saturation in f_β is reached for a thickness of the material of about $^1/_5$ the range of the betas in the material. The saturation back scattering factor $f_{\beta sat}$ as a function of Z, the atomic number is graphically given by Price [145] for several beta energies. This is reproduced in Figure 6.14. These energies are different from those for indium. The values for indium-betas are obtained by interpolation of those given in Price's curves for a fixed value of Z = 83, the atomic number of bismuth. Since 75% of the material is bismuth, $f_{\beta sat}$ is taken assuming whole material is bismuth. The error due to it is small as the value of the factor for Z = 49 of indium is not much different from that for Z = 83. The interpolation graph is shown in Figure 6.15,

FIGURE 6.14 Saturation Back-Scattering Factor as a Function of Atomic Number of Back-Scattering Material for Various Energies of the Beta-Particles. (From Price, ref. 145.)

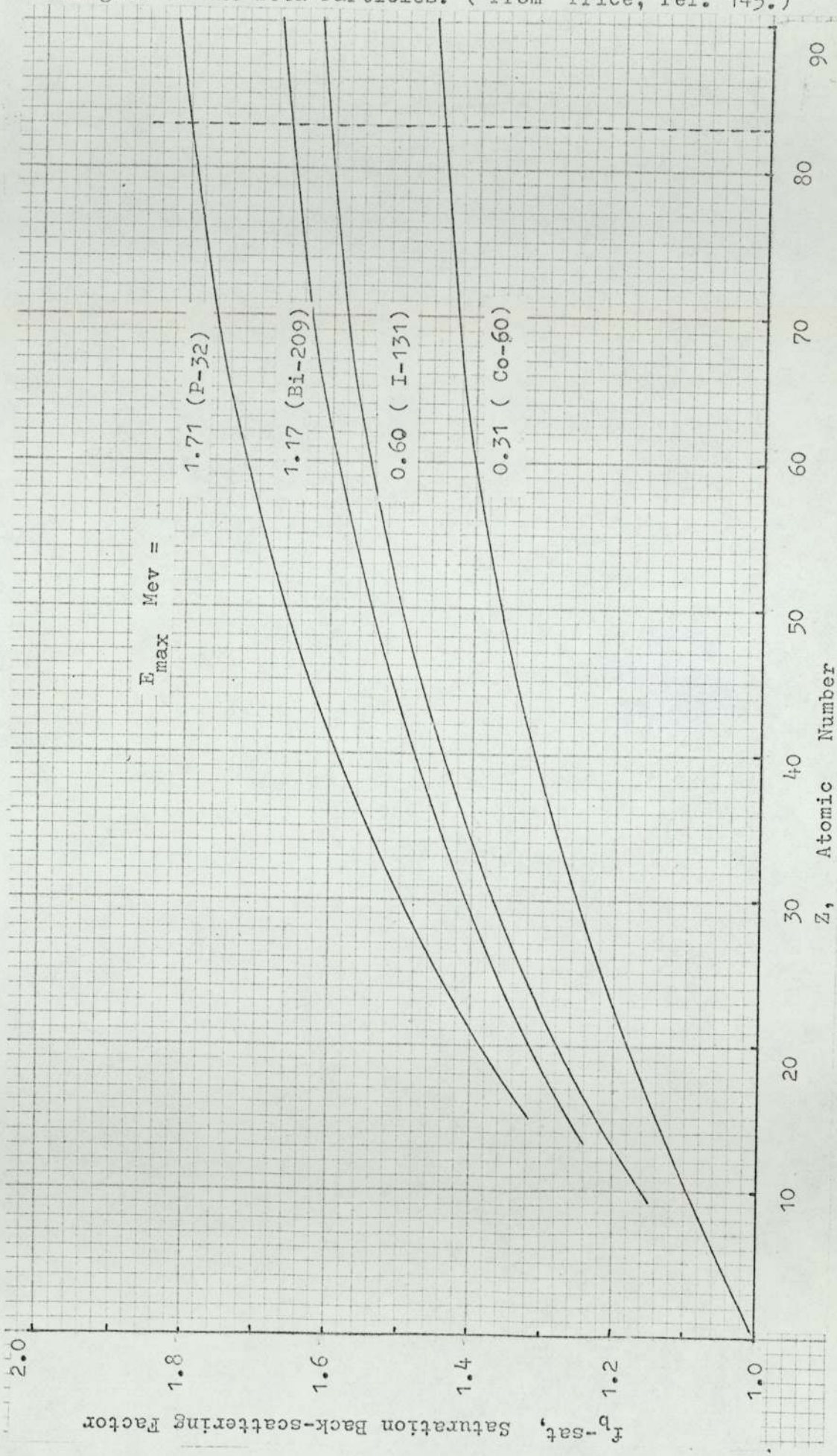

Figure 6.15--Plot of f_b-sat as a Function of E_{max} at Z = 83, Interpolated from the Previous Figure.

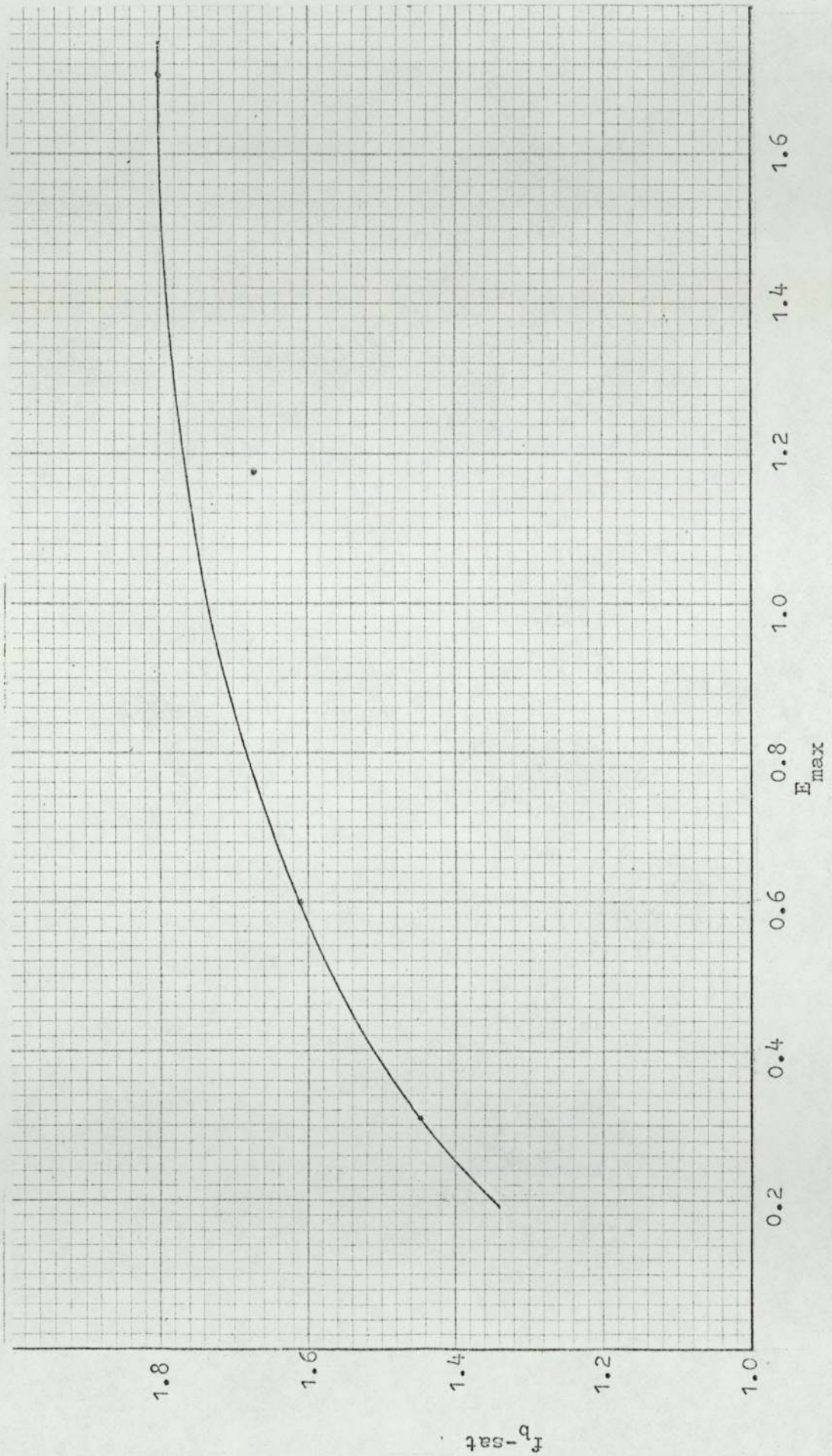

6.9) contd.

6.9.6) contd.

from where $f_{\beta sat}$ at the three indium energies is taken. The final values are given below.

Energy	$\overline{T}$	$f_{\beta sat}$	$\overline{T} \times f_{\beta sat}$
1 Mev	$0.0356A_o$	1.72	$0.0612A_o$
0.87	$0.0165A_o$	1.70	$0.0280A_o$
0.60	$0.0079A_o$	1.60	$0.0126A_o$
		Total =	$0.1018A_o$

Hence counting efficiency $\simeq$ 10.2%.

6.10) Estimates of Accuracy of Results: Error Analysis.

Estimates of errors and propagation of error in the combined results was calculated using standard methods [146-148].

6.10.1) Propagation of Errors.

If a quantity Q is a function of several measured quantities x,y,z ... the error in Q due to errors δx, δy, δz ... in x,y,z ... respectively is given by

$$\delta Q = \frac{\partial Q}{\partial x}\,\delta x + \frac{\partial Q}{\partial y}\,\delta y + \frac{\partial Q}{\partial z}\,\delta z + \ldots \qquad 6.49$$

Further, if δx, δy, δz ... can have any value between $-e_1$ and $+e_1$, $-e_2$ and $+e_2$, $-e_3$ and $+e_3$ ... respectively, then the most probable value of δQ is given by

$$(\delta Q)^2 = \left(\frac{\partial Q}{\partial x} \times e_1\right)^2 + \left(\frac{\partial Q}{\partial y} \times e_2\right)^2 + \left(\frac{\partial Q}{\partial z} \times e_3\right)^2 + \ldots \qquad 6.50$$

In equation 6.50, it is assumed that x,y,z etc.,

6.10) contd.

6.10.1) contd.

can be measured independently of each other. Such errors are called independent errors for which there is some possibility of compensation due to errors in each. In physical situations this is commonly encountered. If that is not the case then it becomes necessary to couple the errors with a correlation coefficient, which must be separately obtained [147].

Equation 6.50 is generally used for usual cases. The limits of individual errors e_1, e_2 etc., are the assumed inaccuracies in direct measurements such as length. For measurements of statistical nature e.g. counts from an equipment the standard deviation σ is obtained. The statistical measurements are given by the bell-shaped Gaussian distribution for measurements of the event and the frequency of the measured values of the same quantity. If N is the observed count then the standard deviation which is normally used is

$$\sigma = \pm \sqrt{N} \qquad 6.51$$

The probability that the estimated counts range $N \pm \sqrt{N}$, includes the "true-value" is 68.3%.

6.10.2) Standard Errors of Composite Functions.

If a number of measured quantities m_1, m_2 ... have standard errors σ_1, σ_2 ... respectively then the standard error of composite functions are given by the following relations, which can be proved from the basic principles:

6.10) contd.

6.10.2) contd.

(1) the sum $m_1 + m_2$ is $\sqrt{(\sigma_1^2 + \sigma_2^2)}$

(2) the difference $m_1 - m_2$ is $\sqrt{(\sigma_1^2 + \sigma_2^2)}$

(3) the prodct $m_1 m_2$ is $\sqrt{(m_2^2 \sigma_1^2 + m_1^2 \sigma_2^2)}$

(4) the power m_1^p is $p m_1^{p-1} \sigma_1$

(5) division, $\sqrt{(\sigma_1^2/m_2^2 + \sigma_2^2 m_1^2/m_2^4)}$

It also follows, if M is the arithmetic mean of $m_1, m_2 \ldots m_n$ then standard deviation σ_M of M is given by

$$\sigma_M^2 = (\sigma_1^2 + \sigma_2^2 + \ldots + \sigma_n^2)/n^2$$

6.10.3) Standard Error of Weighted Mean.

If the data $x_1, x_2 \ldots x_n$ have frequencies $f_1, f_2 \ldots f_n$ respectively then the weighted mean is

$$\bar{x} = \frac{\Sigma f_s x_s}{\Sigma f_s}$$

The standard deviation of the mean is

$$\sigma_R = \left[\frac{\Sigma f_s (x_s - \bar{x})^2}{(n-1)\Sigma f_s} \right]^{\frac{1}{2}} \qquad 6.52$$

and the standard error of the mean is

$$\sigma_m = \frac{\sigma_R}{\sqrt{n}} \qquad 6.53$$

When the frequencies are all equal each observation x_s can still be given a weight proportional to the reciprocal of the square of its standard error.

6.10.4) Standard Error of True Counts.

The true counts per minute from foil counts

6.10) contd.

6.10.4) contd.

are obtained by subtracting the background count rate from the observed count rate with the foil on the counter.

Let the total counts be TC obtained in ΔTC minutes and the background counts TBG in ΔBG minutes, then the true count per minute is

$$CPM = \frac{TC}{\Delta TC} - \frac{TBG}{\Delta BG} \qquad 6.54$$

The standard deviation of CPM is given by

$$\sigma^2 = \frac{TC}{(\Delta TC)^2} + \frac{TBG}{(\Delta BG)^2} \qquad 6.55$$

Thus the statistics is improved by increasing the time for which the foil is counted and that for background. The foil count rate is often limited as several foils have to be counted but the deviation due to background can be improved by increasing the time independently.

CHAPTER 7

SURVEY OF POSSIBLE CALCULATION METHODS.

7.1) Introduction.

The general behaviour of the neutrons in a medium can be described by the same mathematical methods as those describing the thermodynamical behaviour of the molecules in a gas, formulated by Maxwell and Boltzmann in the last century. The first attempt to use the Boltzmann transport equation for the solution of neutron slowing down problems was perhaps that by Ornstein and Uhlenbeck [164] in 1937, though Fermi had made simple calculations from different considerations [165]. Since then, the first concentrated intense work was done during the short period of Manhattan project and by the end of the decade following the second world war, the main characteristics of neutron slowing down and transport was known. Later developments were mostly dictated by the availability of the high-speed computers. However, the increase in the intensity of the efforts have also made the computational aspect compartmentalised and a great many techniques now available as codes are presented to the users as mere "black-boxes", with possible prospect of a 'push-button' atuomation in the reactor physics calculations, but available only to large organizations having the proper computers.

Among the reactor physics problems perhaps, computational technique is the one least discussed in the published papers; often just the name of the code is mentioned. Thus the problems of adaptation of a method and much of the valueable experience is not immediately available to others. Only a few conferences [166] devoted to calculation methods and techniques have taken place. Standard textbooks give the fundamental analytical definitions of many methods possible for calculations, but between analytical description and application to physically significant problems

7.1) contd.

(e.g. application of the boundary conditions and adaptation for computers) there is a wide gap.

Some of the trouble may be due to the nature of the mathematics, but some seems to be due to a lack of tradition as well. Thus though it is known that slowing down by inelastic scattering is of great practical importance in view of the tremendous prospects for the fast reactors in future, in the standard textbooks [171, 172] inelastic processes are completely neglected. It has been known for years that, among the many solutions of the transport equation that are published [169,170], there is a great lack of problems of practical interest or physical usefulness. Even compilation works such as those prepared by the Russian Academy of the Sciences [167] or by Greenspan et al. [168], are either dedicated to mathematical abstraction or merely general introduction.

These facts are kept in view while the computational methods are considered.

7.2) Specification of the Problem.

The choice of calculation method depends upon the nature of the problem. It is customary to recognize the traditional reactor physics calculations as of two types - of core and of shielding. Adaptation and usefulness of the methods vary accordingly.

In core problems the study of reactivity and criticality and also variation in time is of main importance. Due to fission, 'up-scattering' has to be included and multigroup calculations are coupled. Often parameters such as buckling and reactivity need to be obtained and flux distributions can be

7.2) contd.

obtained from there. In core problems the average neutrons of energies of a few Mev and below are of main interest, but in shielding the problems are characterised by the deep penetrating fast nuetrons.

The present problem has the characteristic of mono-directional fast neutrons encountered in shielding problems; but it does not have the large dimensions of a shield so that the advantages of asymptotic solutions are not available for its solution. It has a size similar to that for some fast reactor cores, but it does not have the complexity of a continuous fission spectrum as primary neutrons. On the other hand, due to the higher energy of the primary neutrons the first order diffusion approximations often adequate for most of the core calculations cannot be expected to be sufficient here. Apart from the extreme anisotropy in their elastic scattering behaviour, the other important feature is that inelastic scattering is the most important interaction and slowing down mechanism. For the assembly containing uranium feedback of fission neutrons to higher energy groups has to be considered but fission is not important enough to simplify calculations with introduction of buckling.

7.3) The Boltzmann Transport Equation.

For generality, the Boltzmann transport equation is given below in terms of the seven dimensional phase-space $(\overline{r}, E, \overline{\Omega}, t)$. This phase-space consists of three spatial co-ordinates, two direction defining angles, the particle energy, and time. The variable which is convenient for analysis is the flux, which is particle density multiplied by particle speed. The flux quantity used, is the angular flux, denoted by $\phi(\overline{r}, E, \overline{\Omega}, t)$ and defined as the number of particles that cross a unit area normal to

7.3) contd.

the direction $\bar{\Omega}$ per unit time with energies in dE about E and in a direction that lies in $d\bar{\Omega}$ about $\bar{\Omega}$. This function is more properly called the differential energy - and angle - spectrum of the number flux density, but the simple expression angular flux has become standard terminology. Integrating the angular flux over all directions yields the scalar flux, given by

$$\phi(\bar{r},E,t) = \int_{\Omega} \phi(\bar{r},E,\bar{\Omega},t)\, d\bar{\Omega} \qquad 7.1$$

and having the units: neutrons cm^{-2} sec^{-1} Mev^{-1}. This scalar flux is sometimes referred to as a total flux, although it is differential with respect to energy.

The Boltzmann transport equation can be derived simply from the consideration of neutron balance - that neutron losses are equal to neutron gains with a differential element of phase space $d\bar{r}\, dE\, d\bar{\Omega}$. For steady state ($d\phi/dt = 0$), the equation can be written as

$$\nabla.\Omega\phi(\bar{r},E,\bar{\Omega}) + \Sigma_t(\bar{r},E)\,\phi(\bar{r},E,\bar{\Omega})$$

$$= S(\bar{r},E,\bar{\Omega}) + \iint \Sigma_S(\bar{r},E' \rightarrow E,$$

$$\bar{\Omega}' \rightarrow \bar{\Omega})\,\phi(\bar{r},E',\bar{\Omega}')dE'\, d\Omega' \qquad 7.2$$

where,

$\nabla.\Omega\phi(\bar{r},E,\bar{\Omega})dE\, d\bar{\Omega}$ = net convective loss at $\bar{r}$ of particles with energies in dE about E and with directions which lie in $d\bar{\Omega}$ about $\bar{\Omega}$ per unit volume per unit time,

$\Sigma_t(\bar{r},E)\phi(\bar{r},E,\bar{\Omega})dE\, d\bar{\Omega}$ = collision loss at $\bar{r}$ of particles with energies in dE about E and directions which lie in $d\bar{\Omega}$ about $\bar{\Omega}$ per unit volume per unit time,

7.3) contd.

$S(\bar{r},E,\bar{\Omega})dE\ d\bar{\Omega}$ = source particles emitted at $\bar{r}$ with energies in dE about E and directions which lie in $d\bar{\Omega}$ about $\bar{\Omega}$ per unit volume per unit time,

$\left[\iint \Sigma_s(\bar{r},E' \to E,\ \bar{\Omega}' \to \bar{\Omega})\phi(\bar{r},E',\bar{\Omega}')\ dE'\ d\bar{\Omega}'\right]$ = inscattering gain at $\bar{r}$ of particles with energies in dE about E and directions which lie in $d\bar{\Omega}$ about $\bar{\Omega}$ per unit volume per unit time,

$\Sigma_t(\bar{r},E)$ = total macroscopic cross-section at $\bar{r}$ evaluated at the energy of the incident particle,

$\Sigma_s(\bar{r},E' \to E,\bar{\Omega}' \to \bar{\Omega})dE\ d\bar{\Omega}$ = differential scattering cross-section which described the probability that a particle with an initial energy E' and an initial direction $\bar{\Omega}$ undergoes a scattering collision at r which places it into a direction that lies in $d\bar{\Omega}$ about $\bar{\Omega}$ with a new energy in dE about E.

It is assumed that the euqation is linear, so that Σ_s, Σ_t etc. are not function of ϕ. The factor that dominates the transport equation in the anisotropy in scattering and source. The solution of the transport equation represents the average value of the particle flux or particle density. The solutions are inherently complex due to the integro-differential form of the equation, and exact solutions are limited to a few highly specialized problems. The most pratical techniques are approximate and essentially numerical in nature; the more general ones are the spherical harmonics method, the discrete ordinates technique and the moments method. A family of methods stems from the spherical harmonics expansion: the Legendre expansion, the

7.3) contd.

P_n approximation, the P_1 approximation or diffusion theory with and without energy dependence, etc. There are also the combination methods such as the removal diffusion method. The Monte Carlo method, which is altogether different in approach, and works on the statistical simulation of the physical process, in principle can be made to approach the exact solution of the Boltzmann equation.

7.4) Methods for Solution of the Transport Equation.

7.4.1) Spherical Harmonics Method.

Basically the spherical harmonics technique consists in expanding the angle dependent terms in the transport equation as an infinite power series in the variable μ, the direction cosine, with coefficients that depend upon the position only. The distributions are considered to be rotationally invariant with respect to the coordinate direction which defines μ. The series used is the spherical harmonics of the first kind, the Legendre polynomials $P_\ell(\mu)$. Expanding the angular neutron flux and source term in terms of these polynomials give

$$\phi(\bar{r},\mu) = \sum_{\ell=0}^{\infty} \frac{2\ell+1}{2} \phi_\ell(\bar{r})\, P_\ell(\mu) \qquad 7.3$$

$$S(\bar{r},\mu) = \sum_{\ell=0}^{\infty} \frac{2\ell+1}{2} S_\ell(\bar{r})\, P_\ell(\mu) \qquad 7.4$$

where $\phi_\ell(\bar{r})$ = position dependent Legendre coefficients corresponding to the neutron flux = $\int_{-1}^{1} \phi(\bar{r},\mu) P_\ell(\mu) d\mu$ 7.5

7.4) contd.

7.4.1) contd.

$S_\ell(\bar{r})$ = position dependent Legendre coefficients corresponding to the source term

$$= \int_{-1}^{1} S(r,\mu)\, P_\ell(\mu)\, d\mu \qquad 7.6$$

Since for most practical situations the differential scattering cross-section depends only on the change in direction as denoted by $\mu_o = \bar{\Omega}_o \Omega'$, the series expansion for $\Sigma_S(\bar{\Omega},\bar{\Omega}')$ is made in terms of the Legendre polynomials $P_\ell(\mu_o)$, i.e.

$$\Sigma_S(\mu_o) = \sum_{\ell=0}^{\infty} \frac{2\ell+1}{2}\, \Sigma_{s\ell}\, P_\ell(\mu_o) \qquad 7.7$$

where $\Sigma_{s\ell}$ = Legendre coefficients corresponding to differential scattering cross-sections,

$$= \int_{-1}^{1} \Sigma_s(\mu_o)\, P_\ell(\mu_o)\, d\mu_o \qquad 7.8$$

The spherical harmonics form of the Boltzmann equation is obtained by introducing the above series representations for $\phi(\bar{r},\mu)$, $S(\bar{r},\mu)$ and $\Sigma_s(\bar{\Omega},\bar{\Omega}')$ into it and then multiplying each term by the Legendre polynomial $P_\ell(\mu)$ and integrating over all μ (from -1 to +1). Practical methods of solution require that the series of representation of $\phi(\bar{r},\mu)$ be limited to a finite number of terms, for example to (n+1) terms; n is called the truncation number and the corresponding calculation is referred to as the P_n approximation. Substituting equations 7.3, 7.4 and 7.7 into the Boltzmann equation and by use of the orthogonality

7.4) contd.

7.4.1) contd.

property,

$$\int_{-1}^{+1} P_\ell(\mu)\, P_n(\mu) d\mu = 0, \text{ if } \ell \neq n$$

$$= \frac{2}{2\ell+1}, \text{ if } \ell = n \qquad 7.9$$

a set of coupled differential equations is obtained. This set of equations no longer involves the directional variables and therefore is more amenable to solution. For numerical computation they may be transformed into finite difference equations.

The application of the spherical harmonic techniques to the transport equation is inherently complex. The problem becomes formidable if they are tried for multigroup-energy cases. For simpler cases, such as one-dimensional geometry it becomes possible to use the method. For one dimensional plane geometry the equations are discussed by Roos and Sangren [150], Murray [151] and Clark [152]; for spherically symmetric case they have been considered by Bareiss [153] and by Pendlebury and Underhill [154].

The P_1-approximation is equivalent to diffusion theory and involves only a linear representation, which restricts its utility to situations wherein the neutron flux is nearly isotropic. It has been found and reported that the P_3 approximation of the spherical harmonic method is a definite improvement over the P_1 approximation, but the complexity also increases. Multigroup calculations of higher approximations have hardly been reported.

7.4) contd.

7.4.2) Discrete Ordinates S_n-Method.

The discrete ordinates S_n-method is a means of effecting a numerical solution of the energy dependent linear Boltzmann transport equation. The original method of discrete ordinates is attributed to Wick [157] and to Chandrasekhar [158], who used it for radiative transfer problem of astrophysics. It has been first applied to neutron transport problems by Carlson [159,160].

In the S_n method, the integro-differential Boltzmann equation is integrated over angle by assuming the angular dependence of flux to be linear in each of n-intervals. It is usually applied to the one-velocity equations which are used in multigroup theory. However, it requires the diffusion approximation. The angular flux for any group, assuming linearity between segments, is given by

$$\phi(\bar{r},\mu) = \frac{\mu-\mu_{j-1}}{\mu_j-\mu_{j-1}} \phi(\bar{r}, \mu_j) + \frac{\mu_j-\mu}{\mu_j-\mu_{j-1}} \phi(\bar{r},\mu_{j-1}) \qquad 7.10$$

where $\mu_{j-1} \leq \mu \leq \mu_j$

$j = 0,1,2, \ldots n.$

The order of approximation is characterised by the number of segments n which is used. This approximation is then used to reduce the one-velocity Boltzmann equation to a set of n equations in the n+1 variables, $\phi(\bar{r},\mu_j)$. An additional equation is obtained by setting $\mu = -1$, directly in the one-velocity Boltzmann equation. The resulting set of equations is then solved numerically for the fluxes.

7.4) contd.

7.4.2) contd.

The equations for the various energy groups are solved in order of decreasing energy. If the source term contains fission iteration is performed.

The S_n-method has been applied to a variety of criticality and shielding problems. For the time-independent case, the anistropic scattering has been solved for spherically symmetric cases. Since the transport equation in general, is not separable, two dimensional cases become very complicated.

However, for numerical computations the S_n-method is much simpler than the spherical harmonics method.

7.4.3) Application of Diffusion Theory.

An approach to the particle transport problems that neglects the detailed directional aspects of the particle motion is that of diffusion theory. The basic assumption of elementary diffusion theory is the validity of Fick's law, which states that the net current of neutrons in the direction away from the region of greater neutron density is proportional to the negative gradient of the flux:

$$J(\bar{r}) = - D.\nabla\phi(\bar{r}) \qquad 7.11$$

where D is the position independent diffusion coeffi cient and $\nabla\phi(\bar{r})$ is the gradient of the total neutron flux.

For steady state, the phase space of original transport equation is reduced to three position variables as denoted in general vector notation $\bar{r}$, and the corresponding equation called diffusion equation is

7.4) contd.

7.4.3) contd.

$$D\nabla^2\phi(\bar{r}) - \Sigma_a\phi(\bar{r}) + S(\bar{r}) = 0 \qquad 7.12$$

where the second term represents loss due to absorption, the third term the general source term and the first term is the leakage term incorporating Fick's law. The diffusion equation has the same form as the P-1 approximation to the spherical harmonics treatment of the Boltzmann equation.

Certain limitations are inherent in diffusion theory; these are: (i) the scattering process is assumed to be isotropic in the laboratory frame of reference, (ii) the directional distribution of the particle flux is nearly isotropic, (iii) the diffusing medium must be a poor absorber, and (iv) the results are invalid for regions within 2 or 3 mean free paths of boundaries, strong sources and strong absorbers. The existence of these limitations is a clear indication of the approximate nature of the diffusion theory, insofar as the physical situation is concerned. However, with certain modifications of the system parameters, the diffusion theory solutions of many problems compare favourably with solutions obtained with more exact theories. Thus the diffusion coefficient D which from elementary theory is given by $1/(3\Sigma_s)$, is replaced for weak absorption and moderate anisotropic scattering by

$$D = \frac{1}{3\,\Sigma_{tr}} \qquad 7.13$$

where $$\Sigma_{tr} = \Sigma_s(1-\mu) \qquad 7.14$$

and μ is the average cosine of the scattering angle per

7.4) contd.

7.4.3) contd.

collision in the laboratory system. For larger deviations, D is represented by further modified forms, for use in the diffusion equations.

The other 'transport-correction' that is often used for boundary conditions at free-surfaces is that the solution of the diffusion equation vanishes at a distance,

$$d = 0.71\ \lambda_{tr} \qquad 7.15$$

For treatment of continuous spectrum the energy range is divided into discrete groups and the diffusion equation is used for each group with the appropriate parameters. The ease with which diffusion equations can be treatment has made them most widely used of all the methods for reactor analysis.

7.4.4) Fermi-Age Theory.

Uncer certain circumstances, approximate solutions to the Boltzmann equation can be obtained by the Fermi-age technique, which can give the space and energy variations in the neutron flux.

The age equation is based upon the continuous slowing down model, and it is assumed that the behaviour of all the neutrons can be expressed by an average value. One important result of the continuous slowing-down model is the identification of the neutron slowing down density as

$$q(\bar{r},E) = \xi\ \Sigma_s\ \phi(\bar{r},E) \qquad 7.16$$

which is the number of neutrons slowing down below a given

7.4) contd.

7.4.4) contd.

energy E, per unit time per unit volume, and ξ is the mean logarithmic energy decrement, which is a function of the mass number of the nuclei of the medium only. The diffusion equation is written with the slowing down source as above and then a new variable, called Fermi-age is introduced.

Ideally, Fermi-age is suitable for elastic scattering slowing down by heavy moderators, though it has been used for neutron slowing down in water as well. Avery [161] has tried to use Fermi-age model for neutron slowing down in water and iron laminations, by defining a separate and modified ξ for the inelastic collisions with iron atoms, but did not meet good success.

7.4.5) Moments Method.

The moments method has been used to solve the transport equation, particularly for deep penetration of gamma-rays and neutrons [162] in the shields. The moments method has the advantage that fore-knowledge about the behaviour of the solution can be incorporated analytically, thereby obtaining solution of stated accuracy with reduced labour. However, for practical reasons, the application of the moments method to the solution of the transport equation is limited with respect to the source and shield configurations; it is usually applied only in finite homogeneous media with plane, line or point sources.

Moments are taken of the angular flux, merely to solve the equation and no particular meanings are given to the moments. They are regarded simply as a transform, much

7.4) contd.

7.4.5) contd.

the same as the Laplace or the Fourier transforms. The desired flux is constructed by some matrix inversion.

7.5) Other Methods.

7.5.1) Monte Carlo Method.

In Monte Carlo calculations, the random statistical behaviour of the neutrons in a medium is simulated in accordance with the known probability laws. Each neutron is taken from some parent population through sampling procedures and is followed as it undergoes random walks and from the record of individual histories, the distribution of the neutrons in space according to their energies is determined. For statistical reliability a large number of neutrons has to be followed. With the availability of large high speed computers Monte Carlo calculations have become powerful tools for detailed study of reactivity as well as shielding performances. They are also used to check the results obtained with different approximate methods.

The probability laws which determine the behaviour of the neutrons can be abstract analogues of processes in the real world, when they are called "direct analogue" process. However, the calculations can be shortened by using artificial probability laws when a set of biases are used; they are "non-analogue" processes. The data obtained has to be reprocessed so that the results corresponding to the real probability laws can be recovered. The use of completely artificial probability laws is the most devious of all Monte Carlo strategies.

7.5) contd.

7.5.2) Kernel Technique.

The kernel technique, also called the method of Green's functions has been used for shielding calculations of both gamma rays and neutrons. The parameters for neutron problems has however been developed mostly for hydrogeneous shields.

The point kernel $K(|\bar{r} - \bar{r}'|)$ is formally the solution of the unit point source problem and is defined as the desired response of a detector (particle flux, energy flux or dose) at the space point $\bar{r}$, due to a unit point source of radiation at the space point $\bar{r}'$. This kernel provides the means for solving a variety of problems which involve distributed sources. The total response at a point is obtained by integrating over the surface or the volume for a surface or a volume source respectively, each element of surface or volume being considered as a point source. The utility of the method is considerably enhanced if the integral can be evaluated analytically.

7.5.3) Removal Diffusion Method.

A method which is relatively easy to handle but has been successful in predicting the multigroup flux in shields is the removal diffusion method. In treatment it is very similar to the multigroup diffusion calculations except that the high energy penetrating neutrons are exactly represented on a semi-empirical basis and the slowing down of these to lower energies is treated according to the diffusion theory. The unremoved neutrons can be obtained from an experimentally determined parameter, called the removal cross-section; in

7.5) contd.

7.5.3) contd.

cases where this is not directly available, it is equated to the transport cross-section. When the latter is used, the calculation is called the Spinney method. The empirical parameters can be used in materials of large thickness if hydrogen is present in it; they have been obtained as such in the measurements with the Oak Ridge National Laboratory, Lid Tank Shielding Facility [163], data from which are used for the reactor shielding calculations. Hydrogen subsequently slows down and removes the unremoved flux. But they can be used in any media provided the removal cross-section for it is known. This is described further in the next chapter.

7.6) Intercomparison of the Different Methods.

As the aim of any computational work is to find the solution as accurately as possible, in the absence of any exact analytical solutions one is led to consider a Monte Carlo calculation, as it can incorporate, in principle, any arbitrary geometry, source anisotropy and scattering properties and still give the "exact" solution. But, apart from cost and labour involved in Monte Carlo calculations it has also other limitations. Given that the microscopic cross-section data used in the calculation is accurate enough, it can confirm whether or not the experimental results obtained are reliable. But the computations are hardly of any use in other systems. Multi-energy group calculations, on the other hand, can test a set of group parameters and whether proved right or wrong at least set a precedent and the conclusions become useful for future reference and use. The time and labour investment needed in any Monte Carlo calculation render them unsuitable for common use. For one

7.6) contd.

dimensional cases, in general, Monte Carlo methods are not used since S_n-calculations are faster and equally reliable. Even for two dimensional problems Monte Carlo and discrete ordinate methods are comparable, but for three dimensional problems, Monte Carlo can claim superiority.

In recent times, the Monte Carlo code developed at the Oak Ridge National Laboratory, O5R has been widely used. The code is designed to suit a variety of problems with complex geometries. The user has however to provide several subroutines. Studies were made of the O5R code to assess its suitability for the present problem; but the necessity for a large computer core size and other considerations made it impractical to use.

Among the other methods for calculation, the S_n-method is the best approximation to the transport equation solution, and after the multigroup diffusion calculations, multigroup S_n calculations have been more widely used for the fast reactor analysis. The code DSN has been used by many. Recently a two dimensional discrete ordinate code DOT, has been developed at the RSIC, Oak Ridge, but its immediate applicability to the geometry of the present problem was not evident from a preliminary study of the program. Also, specific need of particular IBM computers do not place these American programs within reach of general users.

Among other methods, the spherical harmonics i.e. P_n-approximations are the only suitable ones that can treat anisotropic scattering and applicable to finite systems. Due to their increasing complexities, the higher order approximations for multigroup calculations are limited to one-dimensional cases only. Thus Leipunski et al. [156] reported of multigroup P_3

7.6) contd.

calculations in the iron blanket of a fast reactor, but was limited to one dimension only. They could not find good agreements with the experimental results which they concluded was because the leakage could not be adequately represented in a one dimensional treatment. Another disadvantage of the P_n method is that it cannot be said 'a priori' how many harmonics are needed for the convergence of a problem.

The other possible methods that were considered, were the conventional multigroup diffusion and the removal-diffusion methods. For a conventional diffusion calculation two disadvantages were noted: first, that only mild anisotropy can be incorporated in them by introducing transport corrections in the diffusion coefficient and the extrapolated distance, and second, the group cross-section sets commonly available, which are aimed at analysing reactor problems only, include all the neutrons above about 3 Mev in one group which could not possibly represent the predominant 14 Mev neutrons. Satisfactory solution to both these problems were obtained.

The transcendental equation giving the diffusion coefficient for stronger anisotropy that is represented by the first order transport correction and that is commonly used, could be solved. The diffusion coefficient so obtained, substituted in the diffusion equations, gave a better representation. Also, a group cross-section set, that considers 14 Mev neutrons and divides the energy range from 14 Mev to 3 Mev into five groups was available. An examination showed that sufficient energy resolution for the threshold foils could be obtained with this set.

The removal-diffusion calculations was found especially attractive for the problem. The mono-directional 14-Mev

7.6) contd.

neutrons could be exactly represented by an exponential and treatment of this extreme case by diffusion equation could be avoided. The secondary neutrons born from inelastic scattering or fast fission can be expected to be adequately isotropic - within the range that diffusion calculations are known to be satisfactory.

The approximation that could not be improved was the geometry approximation - the cylindrical shell was idealised as a spherical shell. This was imposed by the point source. This approximation would have been the same also in other computational methods, except perhaps the Monte Carlo method. However, in the removal-diffusion computation the distribution of the primary neutrons (14 Mev) would be the same in both cases - the cylindrical shell and spherical shell; this is concluded from the microscopic removal cross-section yielded from the experimental observations in the cylindrical shell. For the lower energy groups, the leakage along the faces and the sides will be somewhat misrepresented. Such spherical approximations are known to have been made in less advantageous cases.

The removal diffusion code RASH, developed by the Shielding Group at AERE, Harwell, was studied for use; but it was observed that transfer of neutrons is allowed in it only to the adjacent groups. This could not represent inelastic scattering neutrons, which can traverse almost any number of groups in one collision. However, RASH served as an example for removal-diffusion calculation and several aspects of it was learned from this program which was found useful in writing a code for the present problem.

CHAPTER 8.

FLUX CALCULATIONS BY MULTIGROUP DIFFUSION AND REMOVAL DIFFUSION METHODS.

8.1) Introduction.

Multigroup diffusion equations were numerically solved, idealizing the experimental assemblies as spherical shells. Modifications were introduced by using diffusion coefficients with higher order corrections for anisotropic scattering, than obtained with commonly used transport cross-section for defining the diffusion coefficient. For the iron-uranium assembly fission was introduced, the steady state flux being found by iterations.

In the removal diffusion calculations the spatial distribution of the top group was accurately represented by an exponential form experimentally obtained from activation data. The lower groups were then treated by diffusion equations.

Main source of data was the 20-group Yiftah-Sieger cross-section set [173], that includes inelastic slowing down from an upper limit of 14 Mev. Also used was the Russian multigroup set [179] due to Abagyan et al. Its highest energy limit is however 10.5 Mev.

Two more groups at the top with boundaries at 12 Mev and 14 Mev were added to it from the Yiftah-Sieger set. The results obtained agree reasonably with the experimental values and show some interesting features.

8.2) Multigroup Diffusion Calculations.

In multigroup calculations the continuous neutron energy in a medium is divided into a finite number of energy (or lethargy) groups, and the spatial distribution of neutron flux is obtained for each group. Within the gth group, which extends from E_{g-1} to E_g, neutrons are assumed to diffuse according to one-velocity diffusion equation as they suffer collisions and move to other groups or leak out of the system.

8.2) contd.

The gth group can be defined in terms of the energy limits or identically lethargy limits - by the integral

$$\phi_g(\bar{r}) = \int_{u_{g-1}}^{u_g} \phi(\bar{r},u)du \qquad 8.1$$

where u_g and u_{g-1} are the upper and lower lethargies of the group respectively and $\phi(\bar{r},u)$ is the lethargy dependent flux at the point $\bar{r}$. The diffusion scattering, absorption and other interactions are described in terms of suitably averaged diffusion coefficients and cross-sections which are collectively known as group constants.

8.2.1) Definition of the Group Constants.

When the basic data for nuclear cross-sections of the various events as a function of energy in the energy range of interest are known, they are averaged within groups with respect to flux. Thus

$$\sigma_{x,g} = \frac{\int_{u_{g-1}}^{u_g} \sigma_x(u)\phi(\bar{r},u)du}{\int_{u_{g-1}}^{u_g} \phi(\bar{r},u)du} \qquad 8.2$$

where σ_x may be $\sigma(n,\gamma)$, σ_f, σ_s etc.

It is assumed that the flux can be written as separable function: $\phi(\bar{r},u) = f(\bar{r})\phi(u)$. This is never strictly true, but it must be assumed to carry out multigroup calculations. This enables the constants to be defined as function of group-width and independent of the geometry

8.2) contd.

8.2.1) contd.

under study. As a result, group constants consistent in different systems but function only of the medium and energy emerge. With this assumption, equation 8.2 becomes

$$\sigma_{x,g} = \frac{1}{\phi_g} \int_{u_{g-1}}^{u_g} \sigma_x(u)\ \phi(u)du \qquad 8.3$$

where ϕ_g is the constant $\int_{u_{g-1}}^{u_g} \phi(u)du$. To evaluate the integral in equation 8.3 it is necessary to assume a form for $\phi(u)$. In thermal reactors this is very easy as the slowing down spectrum is $^1/E$, so that $\phi(u)$ can be taken as constant in this range and the thermal group is given by a Maxwellian. But in fast systems there is no such well defined spectrum. One consequence of this is that for fast systems several groups are needed for correct representation, 2 or 3 groups are often adequate for thermal reactors. For fast systems the spectrum of a 'typical' reactor is chosen, so that it can represent similar systems. In principle, for another system the flux may vary; for such case the parameters obtained with flux for the typical reactor can first be used to calculate for the new system, and the group constants could then be calculated with the flux just obtained and calculations repeated with this revised set; this iteration can be repeated several times. However this would be an extremely laborious and costly procedure

8.2) contd.

8.2.1) contd.

and is hardly warranted in view of the uncertainty in the basic cross-section data. Equation 8.3 has to be numerically integrated, since the flux does not have a simple numerical form.

The macroscopic values can be obtained from the microscopic constants, as given by equation 8.3, by multiplying with the number density of the constituent materials in the system.

Diffusion Coefficient. The diffusion coefficient for any group g is by definition given by

$$D_g = \frac{\int_{u_{g-1}}^{u_g} D(u)\ \nabla^2\phi(\bar{r},u)du}{\int_{u_{g-1}}^{u_g} \nabla^2\phi(\bar{r},u)du} \qquad 8.4$$

With the separability of $\phi(\bar{r},u)$ $[= f(\bar{r}).\phi(u)]$, it becomes

$$D_g = \frac{1}{\phi_g}\int_{u_{g-1}}^{u_g} D(u)\ \phi(u)du \qquad 8.5$$

In practice, this can be calculated from the averaged transport cross-section, if that approximation is sufficient. For higher order of accuracy D is given by the transcendental equation [174]:

8.2) contd.

8.2.1) contd.

$$\frac{\Sigma_s}{2}\sqrt{\frac{D}{\Sigma_a}}\,\ell n\left[\frac{\Sigma_T+\sqrt{\Sigma_a/D}}{\Sigma_T-\sqrt{\Sigma_a/D}}\right]=\frac{1+3D\,\Sigma_s\bar{\mu}}{1+D\,\Sigma_T\bar{\mu}} \qquad 8.6$$

where Σ_T, Σ_s and Σ_a are the macroscopic total, scattering and absorption cross-sections respectively, and $\bar{\mu}$ is the average value of the cosine of the scattering angle in the laboratory coordinate system. To compute D for any group-g the corresponding group values of the macroscopic cross-sections are substituted in equation 8.6.

Group-transfer Cross Sections. The transfer of neutrons by scattering from one group to another is given by the group transfer cross sections $\Sigma(g \to h)$. These are so defined that $\Sigma(g \to h)\ \phi_g(\bar{r})$ is equal to the number of neutrons which are transferred from the gth to the hth group per c.c. per second at the point $\bar{r}$. Transfer cross-sections may be written as sum of two parts: the elastic transfer cross section $\Sigma_s(g \to h)$ and the inelastic transfer cross section $\Sigma_i(g \to h)$.

Consider first the evaluation of $\Sigma_s(g \to h)$. The value of these constants depends upon both the nuclear properties of the materials in the medium and the number of groups used in the calculation. In particular, if the maximum increase in lethargy of a neutron undergoing an elastic collision is less than the width of every group, neutrons from one group can be elastically scattered only into the next adjacent group. In this case only h = g+1 need be considered; for the other groups it is zero. The groups are said to be directly

8.2) contd.

8.2.1) contd.

coupled, so far as elastic scattering is concerned. The minimum energy of a neutron after an elastic collision is α-times its initial energy, where

$$\alpha = \left(\frac{A-1}{A+1}\right)^2 \qquad 8.7$$

and A is the mass number of the moderating medium. The condition for direct coupling is that for all g's

$$E_{g-1} - E_g \geq (1-\alpha)E_{g-1} \qquad 8.8a$$

or $$u_g - u_{g-1} \geq \ell n \left(\frac{1}{\alpha}\right) \qquad 8.8b$$

For iron, this gives

$$E_{g-1} - E_g \geq 0.07\, E_{g-1}$$

The constants for $\Sigma_s(g \to g+1) \equiv \Sigma_{er,g}$ can be computed for directly coupled situation in the following way. The total number of scattering collisions per c.c. in the gth group is $\Sigma_{sg}\, \phi_g$. If ξ is the average lethargy increase in an elastic collision, it follows that neutrons require $(u_g - u_{g-1})/\xi$ collisions on the average in order to traverse the group. Hence the number of neutrons scattered out of the gth group per c.c. per second must be $\xi\, \Sigma_{sg}\, \phi_g (u_g - u_{g-1})$, which enter the (g+1)th group. The cross-section is thus

$$\Sigma_{er,g} = \frac{\xi\, \Sigma_{sg}}{u_g - u_{g-1}} \qquad 8.9a$$

If the scattering is anistropic in the centre of mass

8.2) contd.

8.2.1) contd.

system, the transport correction may be introduced to it, when the cross section becomes

$$\Sigma_{er,g} = \frac{\xi \Sigma_{sg}(1-\bar{\mu})}{u_g - u_{g-1}} \qquad 8.9b$$

The group transfer cross sections for inelastic scattering can be computed if the inelastic probability distribution function $p(u \rightarrow u')du'$ is known; this is then flux averaged. In literature, the data is given as elements of ineastic matrix $P_{g \rightarrow g+k}$, defined as the relative probability that a neutron in group g experiencing an inelastic scattering event will afterward be found in group g+k. For low energy incident neutrons where the energy levels can be resolved the excitation functions for the individual levels are used; the values are experimental results supplemented by optical-model calculations. Above the energy where the levels overlap - above 2 Mev for fissionable nuclei and 5 Mev for iron - the evaporation model of Weisskopf is used. The expression in this model is characterised by nuclear temperature T which is slowly varied from group to group as it varies with incident neutron energy.

Fission. The treatment for fission neutron distribution is similar to that for inelastic scattering with the evaporation model, except that the final energy group h can be above the incident energy group g_r. Otherwise, the treatment is made simplier in that one expression for $\chi(u)$ can be used for different incident neutron energies, so that for fission occurring in any

8.2) contd.

8.2.1) contd.

the quantity χ_g, the fraction of fission neutrons appearing in the gth group is given by

$$\chi_g = \int_{u_{g-1}}^{u_g} \chi(u)du \qquad 8.10$$

with $\chi(u)$, the full fission spectrum normalised to one emitted neutron.

However, it is necessary to take into account the fact that the average number of neutrons emitted per fission depends upon the energy of the incident neutron. For fission induced by neutrons of the gth group, the average value of ν is given by

$$\nu_g = \frac{1}{\phi_g} \int_{u_{g-1}}^{u_g} \nu(u)\ \phi(u)du \qquad 8.11$$

8.2.2) Multigroup Equations.

The equations are given below for general case - when fission is present. In case there is no fission in the system, the fission cross sections are put zero and the terms vanish. If fission takes place above certain group (threshold), the cross-sections for the lower energy groups is put zero. However all groups receive neutrons due to fission in any one group.

For the iron-uranium assembly, the medium is considered to be a homogeneous mixture of these two elements; this is valid as the thicknesses of the layers of iron or uranium are small compared to the mean free

8.2) contd.

8.2.2) contd.

paths of the neutrons. The group cross sections are obtained by averaging the number of densities of the nuclei per c.c. Let there be N groups of energies.

The equation for the first group, corresponding to the most energetic neutrons is, where ϕ is a function of only $\bar{r}$ within the group:

$$D_1\nabla^2\phi_1 - \Sigma_{a,1}\,\phi_1 - \Sigma_{er,1}\,\phi_1 - \sum_{h=2}^{N} \Sigma_{in}(1\to h)\,\phi_1 + \chi_1 \sum_{k=1}^{N} \nu_k\,\Sigma_{f,k}\,\phi_k = 0 \qquad 8.12$$

The first term is the leakage loss, the second term gives loss due to absorptions (n,γ; n,p; etc.), the third term elastic removal and the fourth term loss due to inelastic transfer of neutrons to all lower groups; the last term is equal to the total number of fission neutrons appearing in the first group as the result of fissions occurring in all groups.

For a lower energy, gth group the equation is:

$$D_g\,\nabla^2\phi_g - \Sigma_{a,g}\phi_g - \Sigma_{er,g}\phi_g - \sum_{h=g+1}^{N} \Sigma_{in}(g\to h)\,\phi_g + \Sigma_{er,g-1}\phi_{g-1} + \sum_{j=1}^{g} \Sigma_{in}(j\to g)\,\phi_j + \chi_g \sum_{k=1}^{N} \nu_k\Sigma_{f,k}\phi_k = 0 \qquad 8.13$$

Here again, the other terms except the 5th and the 6th terms, are similar to those in equation 8.12. The fifth term is the number of neutrons elastically scattered into the gth group from the (g-1)th - assuming direct coupling. The 6th

8.2) contd.

8.2.2) contd.

term is equal to the number of neutrons inelastically scattered into the gth group from all higher energy groups (and also itself).

8.2.3) Solution of the Equations.

The equations 8.12 and 8.13 were solved for spherical geometry. The one dimensional Laplacian given by

$$\nabla^2 = \frac{d^2}{dr^2} + \frac{c}{r}\frac{d}{dr} \qquad 8.14$$

(where c = 0 for slab, 1 for cylinder and 2 for sphere), was written in finite difference. Two boundary conditions used were:

(i) the net current is zero at the inner boundary i.e. at the inner radius of the spherical shell - except for the neutrons due to any source located in the sphere;

(ii) flux is zero at the extrapolated distance i.e. at a further distance of 0.71 λ_{tr} from the outer radius.

The numerical scheme is shown in Appendix 1; the recurrence relation used is also derived there. The program FASTNFLUX was written to solve the multigroup equations.

In principle, flux at any group can be computed if fluxes at all the other groups are known; also as can be seen from equations 8.12 and 8.13 the flux of the same group needs to be known to take into account self-scattering of the inelastic matrix and also fission. When fission is

8.2) contd.

8.2.3) contd.

absent the lower energy groups need not be known. When inelastic scattering within the group is small - as is often the case - only information about the higher energy fluxes is needed; in this case, once the top group is known all the succeeding groups can be calculated in turn. The top group can be calculated when the point source at the centre is specified.

When fission is present, the program initially neglects fission to provide a guess at the flux distributions. After calculating through to the Nth group this way, it repeats the cycle, this time including fission in each group calculated from the previously found flux distributions. This cycle can be repeated any desired number of times. Because fission is not very predominant the flux values converge rapidly with only a few iterations (typically 5).

The code can also give the estimated foil activation for the different foils as output, when the group averaged activation cross sections are supplied. It can be shown that for a uniform flux within the group, the average activation cross section is the arithmetic mean within the group limit.

8.3) Removal-Diffusion Calculation.

It is found that the distribution of the first group neutrons as given by copper activity can be represented by an expression

8.3) contd.

$$\phi_n = \frac{Q}{4\pi R_n^2} \; e^{-\Sigma_r (R_n - R_1)} \qquad 8.15$$

where R_n is the radial distance of the nth space-point in the assembly from the point source of strength Q, R_1 is the inner radius of the assembly, and ϕ_n is the flux at the nth space point. The constant Σ_r is called the macroscopic removal cross-section.

In the removal-diffusion calculations equation 8.15 with the numerical values for Σ_r is used to describe the first group flux instead of equation 8.12. The lower groups are treated by equation 8.13 as before. There is option in the program FASTNFLUX to calculate the first energy group either from the the diffusion equation or from the removal equation.

Phenomenologically, the removal process can be considered equivalent to the total reaction rate minus the forward component of the scattering process. This suggests that the removal cross-section is effectively the same as the transport cross-section, i.e.

$$\Sigma_r = \Sigma_{tr} = \Sigma_T - \mu\Sigma_s \qquad 8.16$$

In large shields, removal cross-section may not remain constant over the sample thickness. This is due to the build up of the neutrons scattered from the adjacent parts of the shield. In the practical shield computations, in which removal cross section has been basically used, experimentally obtained values are given preference. In shields however the slowed down flux is often estimated from the fermi-age estimation rather than multi-group scattering matrix. In systems, such as the experimental assemblies in the present study the removal cross-section

8.3) contd.

does not vary significantly with thickness. This is because, the sample thickness is comparable with the mean free path of the 14-Mev neutrons. Also, the 14 Mev nutron scattering with iron and uranium is highly forward peaked; as very few neutrons are scattered backwards or sideways not many are available to come back in the original direction after multiple scattering, so that the build up is negligible.

The microscopic removal cross-section, σ_r is the constant per atom. This has been calculated by Avery et al. [175], as a function of energy for several materials of interest for reactors, as the removal cross-section is the same as the transport cross-section. In general σ_r decreases with increasing energy for a given element and it increases with increasing atomic-weight at a given energy. At 14-Mev σ_r for iron has been calculated by Avery et al. to be about 1.42 barns; the same value is obtained from experimental distribution of the flux in the iron-cylinder. For Uranium σ_r at 14 Mev is about 3.0 barns. The increase in σ_r with the atomic weight is due to the following reasons. σ_r can be expressed as

$$\sigma_r = \sigma_T - \mu\,\sigma_s$$
$$= \sigma_{ne} + (1-\mu)\sigma_s \qquad 8.17$$

At high energies the non-elastic cross-section (σ_{ne}) is nearly equal to the geometrical cross-section of the nucleus, and this increases smoothly with the mass number as the radius increases. The second term makes only a small contribution because of the large value of μ at high energies. According to this consideration, removal cross section per unit mass should vary roughly as $A^{\frac{1}{3}}$,

$$\text{i.e. } \frac{\Sigma_r}{\rho} \propto A^{0.33}$$

8.3) contd.

The macroscopic removal cross-section for a mixture can be obtained by simple volume average,

$$\overline{\Sigma}_r = \frac{\text{Sum}(\Sigma_{ri}\ V_i)}{\text{Sum}\ V_i}$$

where V_i is the volume occupied by the ith constituent.

8.4) Cross-section Data for Calculation.

As mentioned earlier, the source of data for the multigroup calculation was the 20-group cross-section set due to Yiftah and Sieger [173]. This set has been devised by the authors for application to fast reactor experiments with 14 Mev neutrons, particularly pulsed sources. This is an extension of the previous 16-group YOM set, which has been widely used by various fast reactor centres. The 16-group set with some modifications was used by Borgwaldt et al. [176], to analyse the SUAK fast reactor assembly at Karlsruhe with 14-Mev pulsed sources. The 20-group set developed was based on the similar experiences of the 16-group set, as well as intercomparisons with the cross-section sets given in the following: the second edition of ANL-5800 [177], Karlsruhe cross-section compilation [178], the Russian 25-group cross-section constants [179]. None of these previous groups include 14 Mev neutrons, and are mainly for fast reactors as such. The group structure of the 20-group set is as follows:

Group	Energy
1	14-12 Mev
2	12-10
3	10- 6
4	6- 3.668
5	3.668-3.0
6	3.0 - 2.225

8.4) contd.

Group	Energy
7	2.225 - 1.35
8	1.35 - 0.825
9	825 - 500 kev
10	500 - 300
11	300 - 180
12	180 - 110
13	110 - 67
14	67 - 40.7
15	40.7 - 25
16	25 - 15
17	15 - 9.1
18	9.1 - 5.5
19	5.5 - 2.1
20	2.1 - 0.5 kev

Thus, above the phosphorous (n,p) - threshold there are 7 groups up to 14 Mev.

The Russian ABBN set [179], which considers the self shielding corrections for the lower energy groups, has 10.5 Mev as its highest energy limit. Calculations have also been performed with this set - the top two groups up to 14 Mev have been supplemented from the Yiftah-Seiger set. Inelastically scattered neutrons and fission induced neutrons from the 14-12 Mev and 12-10.5 Mev groups can move to any of the lower groups of ABBN; these source terms have been assigned by analogy with the Yiftah-Sieger data. The other groups of ABBN - set are as follows

10.5 - 6.5 Mev
6.5 - 4.0
4.0 - 2.5
2.5 - 1.4
1.4 - 0.8 Mev etc.

CHAPTER 9.

EXPERIMENTAL AND CALCULATED ACTIVITY DISTRIBUTIONS AND OTHER RESULTS.

9.1) Introduction.

The absolute activity distributions of the foils in the two assemblies are finally produced in this chapter. The experimentally obtained values are shown and compared with the activity distributions predicted from multigroup diffusion and removal-diffusion calculations.

Multigroup data sets were described in the last chapter. We were led to introduce small but important and logical modifications to the Yiftah-Sieger data. These are briefly described.

All results are absolute saturated activities per minute per gram of the isotope concerned and normalised to a source strength of 1.5×10^9 neutrons per second.- unless otherwise mentioned. Most experimental results presented are output from the program FOILSNACT which computes the above quantities for each reading.

Determination of removal cross-sections for the source neutrons in the two assemblies with the observation of copper activities are discussed first. This is then followed by presentation of threshold foil activities first in the iron assembly and then in the iron-uranium assembly. Each reaction is shown in one graph. The values predicted by calculations are explained next. The extent to which the experimental and calculated activities agree or disagree as a function of position in the assemolies are indicated; in these more stress is given to the phosphorus results as this foil had the lowest threshold.

The results with $^{115}In(n,\gamma)$ reaction are then compared and discussed. Division of the results in this way were prompted by the fact that the results in the two assemblies had many features in common and considering them together avoided much duplication and repetition. Some of the other results of

9.1) contd.

interest are shown after that.

General conclusions that emerge from these studies are summarised in the following chapter.

9.2) Determination of the Removal Cross Sections.

The removal cross sections for the source neutrons were needed to present their distributions in the assemblies and to compute the lower energy neutron distributions from there. This is obtained from the normalised Cu activity distribution along the vertical line through the source. The plot of $4\pi R_n^2 A_n$ against R_n, where A_n is the saturated copper activity at the radial position R_n, on semi-log scales gives straight-lines for each assembly. Figures 9.1 and 9.2 are two of such plots for the iron and the iron-uranium assemblies respectively. It can be shown from equation 8.15 that equation for such a straight line in each assembly is given by

$$\log_e (4\pi R_n^2 A_n) = K - \Sigma_{rem} R_n \qquad 9.1$$

where K is a constant. Thus the negative slope gives the removal cross-section Σ_{rem} for each assembly.

To determine Σ_{rem}, the absolute source strength of the neutrons need not be known. Thus, the uncertainty in absolute efficiency of the counter and that in the source strength determination during the irradiation do not enter Σ_{rem}. However, an additional uncertainty is introduced due to R, which is squared and multiplied with A, the activity. These experimental errors are shown on each point in the graphs.

9.2.1) Σ_{rem} for the Iron Assembly.

The graph shown in Fig.9.1 is a typical one for

FIGURE 9.1--Plot of $4\pi R^2 A$ vs. R' for the Copper foils in Iron-Assembly.

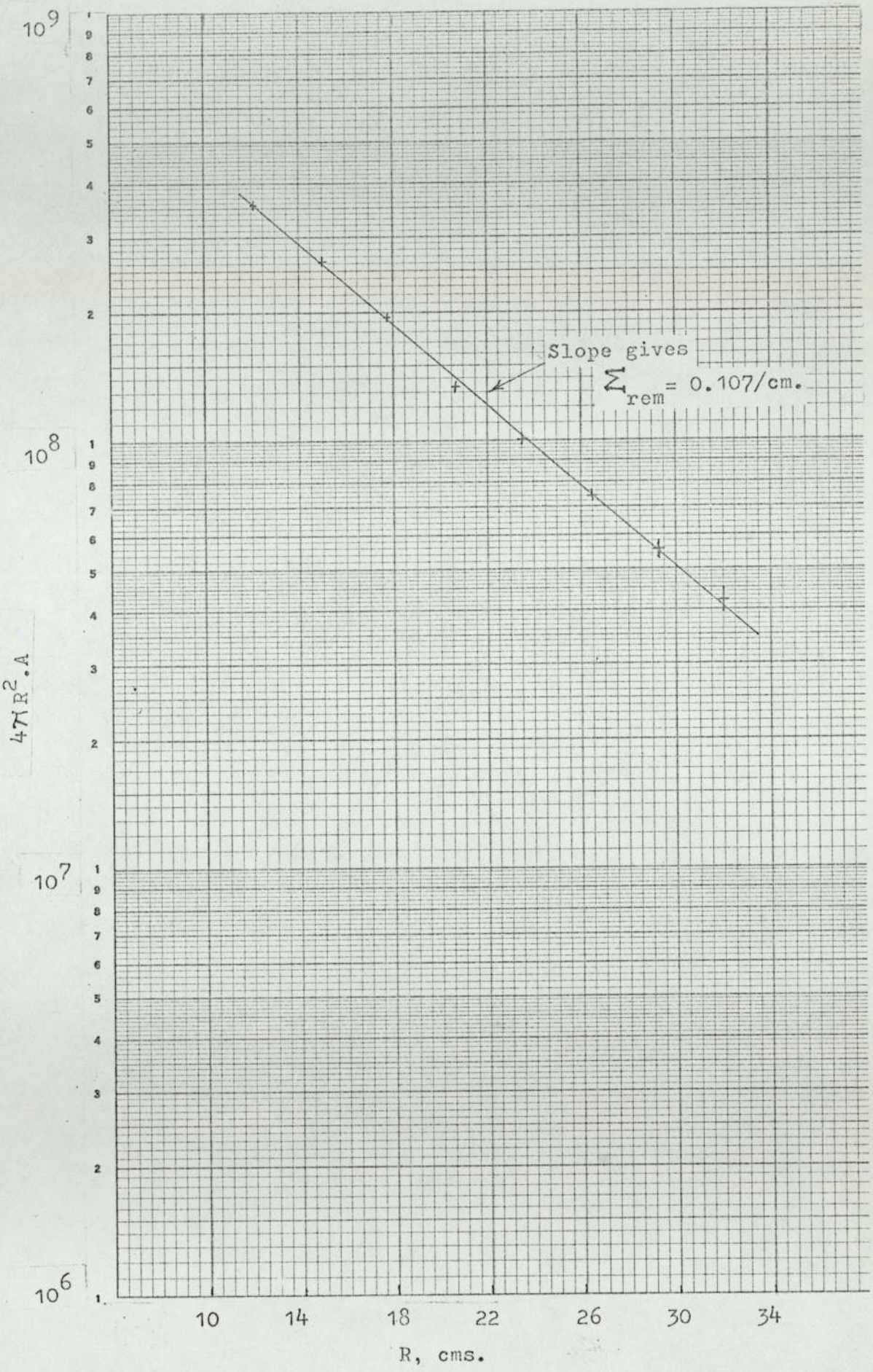

9.2) contd.

9.2.1) contd.

the iron assembly; the average value of the removal cross section was obtained from several such curves which gave for the iron assembly:

$$\Sigma_{rem} = 0.106 \pm 0.0015 \text{ cm}^{-1} \qquad 9.2$$

This value of the removal cross section for the iron assembly gives a microscopic removal cross section for the 14-Mev neutrons as 1.406 barns per atom of iron, when the number density of the iron atoms in the assembly is considered. This compares favourably with the calculated values of removal cross-section, for iron, predicted by Avery et al. [175] and which have been used in the absence of direct experimental measurements, on a provisional basis for the removal diffusion shielding calculations with the RASH-program [175] . In the tabulated values there it can be compared that at 13.5 Mev they predict 1.48 barns and at 14.5 Mev 1.39 barns as the removal cross sections per iron atom.

9.2.2) Σ_{rem} for the Iron-Uranium Assembly.

The situation is somewhat different in this assembly, particularly because of the cylindrical shape of the uranium rods. The empirical basis of the removal cross-section is more apparent in this case. It would not be very easy to compute the average removal cross-sections from the dimensions and conversely, the microscopic removal cross section for uranium could not be directly obtained from the observed macroscopic removal cross section. The observations were particularly checked with the four different

FIGURE 9.2-- Plot of '$4\pi R^2 A$ vs. R' for the Copper Foils in Iron-Uranium Assembly.

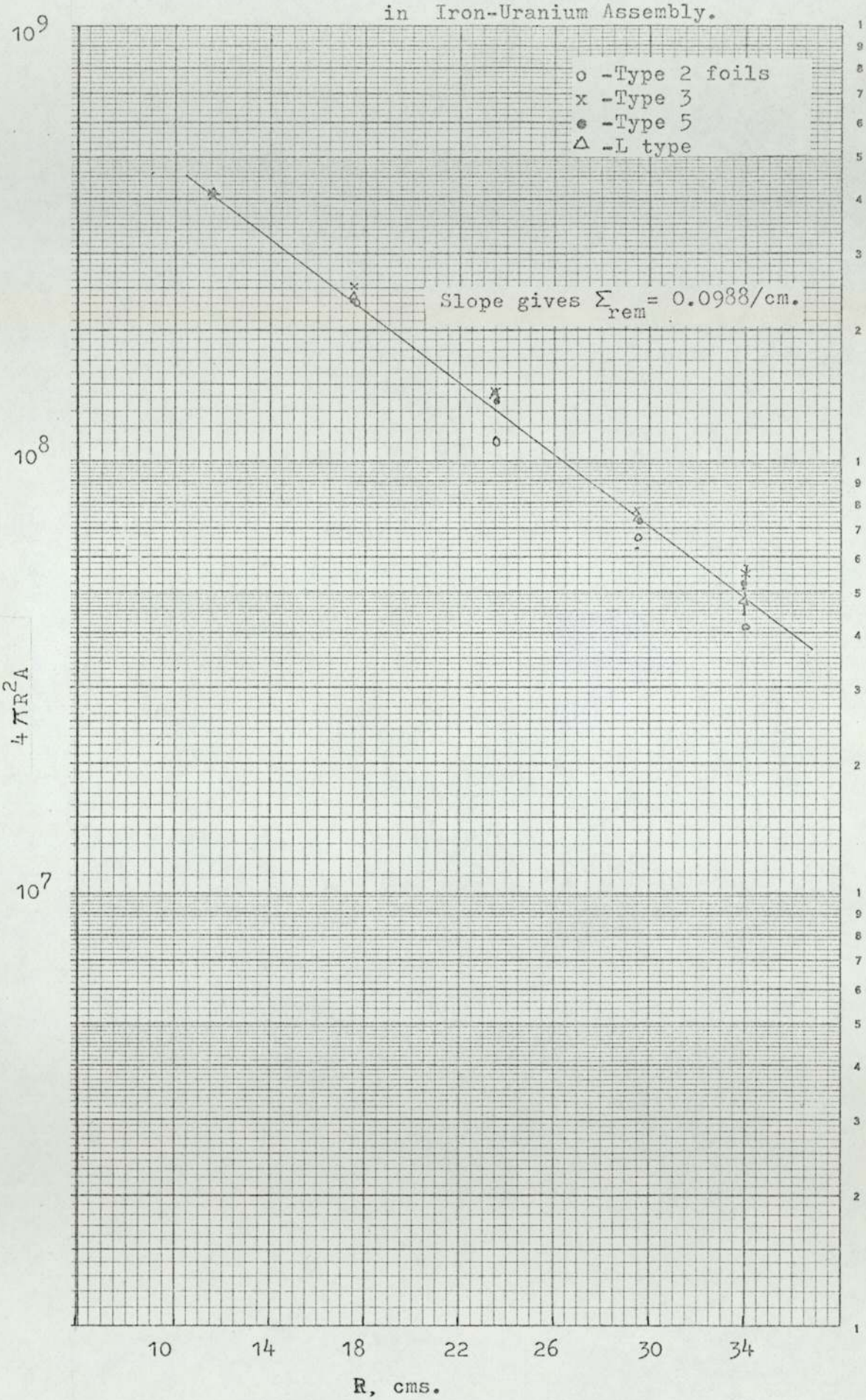

9.2) contd.

9.2.2) contd.

types of copper foils, which were specially made for this assembly.

Typical experimental points from four different runs with the four types are shown in Fig.9.2. The smallest type-2 foils would give no reliable results and except for the first point the other points with this foil would hardly be reproducible. Since no such difficulty was encountered in the other assembly, it can be concluded this was because of the non-uniformity of the uranium as the slight displacement in positioning these foils could result a different effective shield thickness. Compared to these for the L-type foils, say, because their widths were equal to those of the uranium bars, a lateral displacement in positioning would hardly matter. Since the uranium rods were touching each other, the amount of material an L-type foil would miss from the central bar underneath it due to lateral displacement it would gain from the next bar over which it had moved by almost the same amount. To some extent the same was the case for the other two bigger types of copper foils. Though these foils in this assembly did not give as smoothly lying points as in the iron assembly, for all practical purposes the points could be presented by a straight line and the slope gave

$$\Sigma_{rem} = 0.0988 \pm 0.0020 \text{ per cm.} \qquad 9.3$$

for this assembly

9.3) Experimental Activity Distributions for the Threshold Foils.

The absolute activity distributions of the threshold foils are shown in Figures from 9.3 to 9.11. Figures 9.3a and 9.3b show copper activity distributions in the iron and the iron-uranium assemblies respectively. Figures 9.4 to 9.7b are for the other threshold foils in the iron assembly while 9.8 to 9.11 for them in the iron-uranium assembly.

The experimental uncertainties are shown on the points. These include those of the source strength determination ($\pm$ 1.5%), determination of the calibration of the counting systems ($\pm$ 2%) and systematic error for counting of the foils following irradiation in the assemblies. No error has been included due to uncertainty in the cross sections ($\pm$ 6% to 10%) at 14 Mev, used for calibration of counting in these figures; errors due to this should be cancelled to a large extent when converting the counts into activities following irradiation in the assemblies. The counting statistics following irradiation in the assemblies gave mostly an uncertainty of less than $\pm$ 1% for the nearest foil but this gradually increased with increasing R up to about $\pm$ 6% for the outermost foils of copper, iron and phosphorus. The statistics were poor for the aluminium foils particularly for (n,α) counting. Though Aℓ-foils were of the largest size, being of low density material they had less mass. For the $A\ell(n,p)$ activity some extra uncertainty was introduced to recover the true activities from the analysis of the compositive curves for each foil; these gave a statisticaluncertainty of about $\pm$ 8% for the outermost $A\ell(n,p')$ counts. However, for $A\ell(n,\alpha)$ some of the counts gave $\pm$ 15 to 20%. Long half life was the main reason; in addition $A\ell(n,\alpha)$ has the second highest threshold of the foils used.

The combined uncertainties gave an error limit of about

9.3) contd.

± 3% for the inner foils (small R), while for the outer foils the uncertainity is mostly dominated by the counting statistics and the combined error is not much different from that.

The observed activities were checked for mutual perturbation by the foils - particularly shadowing of the source neutrons by the earlier foils. This was done by keeping the earlier foils in one irradiation and removing some of them in another. No noticeable perturbation with the threshold foils could be detected.

9.4) Multi-group Data Modifications.

The calculations were at first done with the Yiftah-Sieger multigroup data sets as given. However as some of the results were somewhat suspect, examinations revealed that the authors have worked out inelastic group transfer parameters only for (n,n') reactions, throughout the compilation. However many of the reactor materials have significant cross sections for emission of a second and some even a third neutron, at 14-Mev. Since, in the assemblies studied in the present work the great bulk of the group transfer of the neutrons - from the source energy to all the lower groups - were taking place through inelastic scattering, the predicted results could be naturally expected to be wrong if some erroneous inelastic data were used. Some inconvenience was caused as no warning of this was given by the authors in their volume.

Anyway, detailed considerations of the data showed that the results could be significantly improved by small alterations. This is because, according to the theory of inelastic scattering (also mentioned in Chapter 2) at high energies, the first neutron of the (n,2n) reaction comes out from the same nuclear state as

9.4) contd.

for the (n,n') reaction and both can be given a single energy-profile. Apparently the inelastic scattering probabilities P_{ij} in the Yiftah-Sieger set were worked out for this profile, so that the P_{ij} values could be used for the first neutron of the (n,2n) reaction. The second neutron profile is different and could not be so easily incorporated; anyhow energies of the second neutrons are smaller. As the iron (n,2n) threshold is at about 11 Mev, with 14 Mev incident energy the second neutron would probably come out with a maximum energy of about 3 Mev and the majority would with lower energies. It was considered that the majority of these would not seriously affect the threshold foils used in this work. On the other hand the inelastic neutrons come out of heavy nuclei with a Maxwellian distribution and therefore also are associated with the lower energies i.e. both the neutrons associated with (n,2n) will have energies around the lower parts. In any case not much is definitely known about (n,2n), (n,3n) ... reactions and their products. So one has to be satisfied with the half-a-loaf.

The same correction was introduced for the first neutron of (n,2n) reaction of uranium-238 and also for that of (n,3n), since according to theory the (n,n') neutron and the first neutrons of (n,2n) and (n,3n) have a single profile - the same Maxwellian - though they, perhaps, occupy different energy regions. Similarly the second neutron of (n,2n) and (n,3n) will have one profile, but these and the third neutron of the (n,3n) could not be included in the calculations. These put uranium in a somewhat worse situation than iron. Also the threshold for the (n,2n) reaction is much lower for uranium-238: about 6.5 Mev, which means with 14 Mev incident energy the second neutron can come out with

9.4) contd.

a maxumum of 7.5 Mev. The threshold for (n,3n) is 12 Mev. Hence the maximum energy for the third neutron can be 14-12 = 2.0 Mev. Thus the third neutrons would not interact much with the threshold foils but the (n,2n) neutrons would contribute to at least P(n,p), Aℓ(n,p) and Fe(n,p) reactions - more than the iron (n,2n) would. Also, while iron (n,2n) cross section at 14 Mev is only 0.5 barns, uranium (n,2n) cross section is 1.0 barns and (n,3n) 0.4 barns. However, things are not as bad for uranium as it looks here. Because of significant contribution from the fission neutrons in uranium (the number being $\nu \times \sigma_f$) the relative importance of the second neutron in (n,2n) decreases; also uranium is only 30% by atoms in the iron-uranium assembly. The modifications in the Yiftah-Sieger data finally amounted to changing the inelastic scattering cross-sections of iron and uranium as follows:

	Original	Modified
iron	0.88 b	1.38b (= 0.88 + 0.50)
uranium	0.27 b	1.67b (= 0.27 +1.0+0.40)

To identify, they are termed Original Yiftah-Sieger and Modified Yiftah-Sieger data.

To supplement the ABBN set with two high energy groups, the modified values are directly used.

9.5) Threshold Foil Activities Predicted by Calculations and Comparisons.

The calculated activities are shown together with the experimental values in each of the Figures 9.3 to 9 11. The calculated values are for sphere of same inner and outer radii as the experimental assembly. The removal-diffusion calculations with the modified Y-S and the ABBN data sets are shown for all the

9.5) contd.

four threshold reactions in both the assemblies. The removal-diffusion calculations with the original Y-S data are also shown for these foils in the FeU assembly, for comparison. As is to be expected, the calculations with the original Y-S data fall more short of experimental values as the threshold of the foil concerned lowers. Thus with $Al(n,\alpha)$ and $^{56}Fe(n,p)$ the difference for using the modified data is not very much and the predictions come very close to experimental values in any case. This is because not many of the secondary neutrons produced in the assemblies are born with energies above the threshold energies of these reactions. Noticeable difference due to the modifications can be seen for the $Al(n,p)$ reaction (Fig. 9.10). For the $P(n,p)$ reactions the difference is more appreciable; experimental values are higher. With the original Y-S data the agreement for phosphorus is poor indeed in both the assemblies (Figs.9.7a and 9.11). With the modified data the removal-diffusion results in the iron assembly comes to within about 5% of the experimental values from about 15% with the original data. In the Fe-U assembly on the other hand the original data gives about 25% lower values than the experimental, while with the modified data the calculated values at similar points are about 15% lower. Thus the disagreements are more for the Fe-U assembly. From comparisons it seems this is possibly because more of the secondary neutrons have not been included for uranium. The cross section for the emission of second neutron from iron is only 0.5 barn while that from ^{238}U is 1.4 barns. In addition the second neutron from ^{238}U can have maximum energy of 7.5 Mev. The third neutron of ^{238}U compares with the second neutron from iron in energy and cross-section.

The removal-diffusion values obtained with the ABBN data comes close to those with the modified Y-S data but tend to

9.5) contd.

be closer to the experimental results.

The differences between the removal diffusion calculations in the two assemblies and the experimental values are tabulated below for the $^{31}P(n,p)$ reaction. The experimental points are read from the experimental curves at rounded values of R. Comparisons are made in terms of the following parameter:

$$\% \text{ diff} = \frac{\text{Expt} - \text{Cal}}{\text{Expt}} \times 100$$

TABLE 9.1a

Comparisons of the $^{31}P(n,p)$ activity distributions in the Iron Assembly: Expt and Rem Diffn Calculations.

R cms	Expt. Act. from graph	% diff Org.Y-S	% diff Mod.Y-S	% diff ABBN
11.0	1.3×10^5	+ 12%	+ 5.6%	+ 5.8%
12.0	1.05×10^5	+ 14.4	+ 6.8	+ 7.0
16.0	4.7×10^4	18.9	7.8	7.6
21.0	1.85×10^4	19.4	4.5	4.4
16.0	7.8×10^3	19.4	2.6	2.1
32.0	2.8×10^3	+ 19.9%	+ 2.8%	+ 2.3%

TABLE 9.1b

Comparisons of $^{31}P(n,p)$ activity distributions in the Fe-U Assembly: Experimental and Rem-diffn calculations

R cms.	Expt.Act. from graph.	% diff. Org.Y-S.	% diff Mod.Y-S	% diff ABBN
10.0	1.5×10^5	+ 2.7%	- 1.4%	- 2.4%
11.5	1.15×10^5	+10.5	+ 5.5	+ 4.3
15.0	6.2×10^4	18.9	+12.4	+10.8
20.0	2.65×10^4	22.6	14.6	12.4
25.0	1.21×10^4	25.4	16.7	14.4
30.0	5.4×10^3	24.1	14.7	12.2
34.0	2.95×10^3	27.0	18.0	15.6

Fig. 9.3a. $^{63}Cu(n,2n)$ Activity Distribution in the IRON- Assembly.

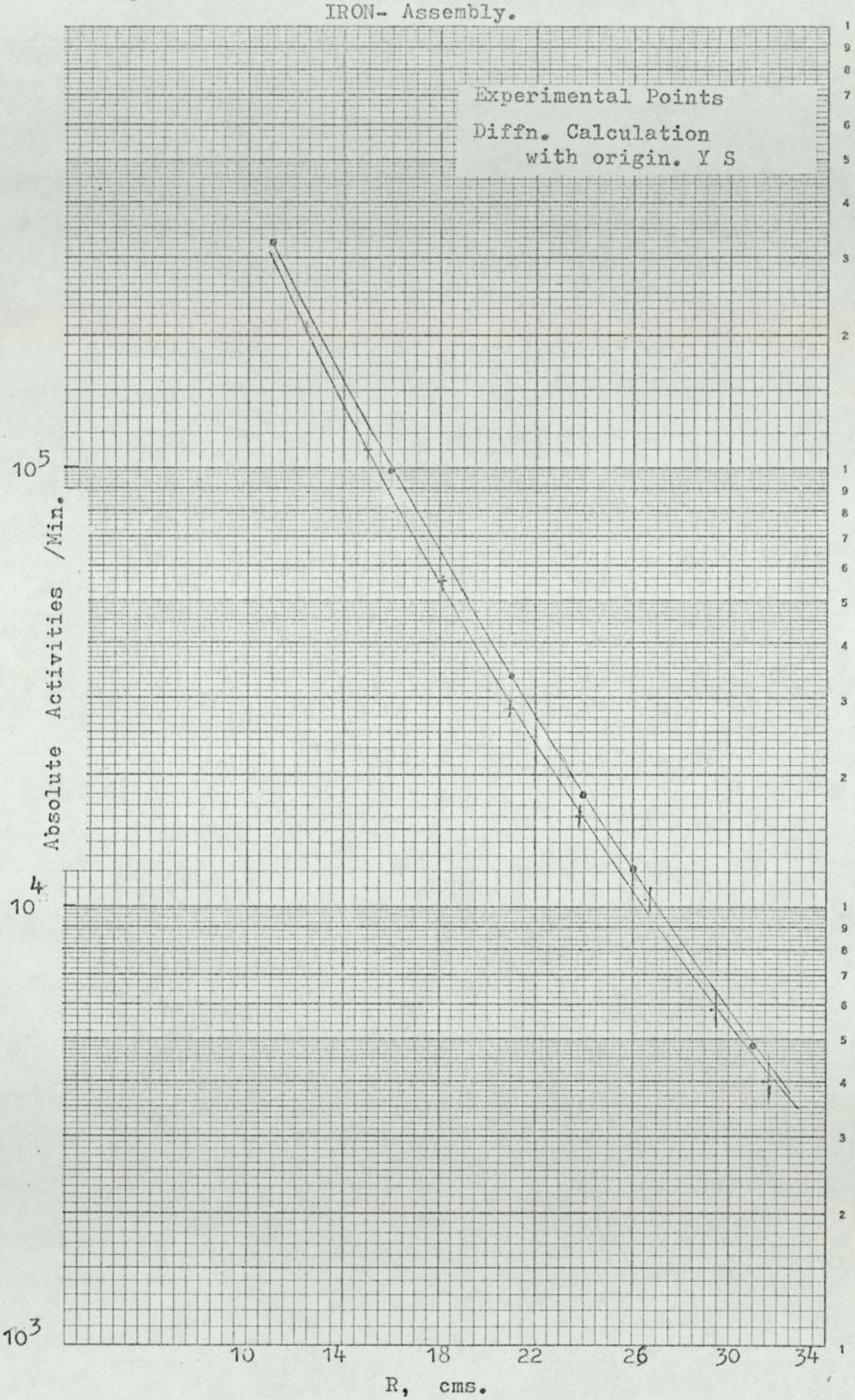

FIG. 9.3b. $^{63}Cu(n,2n)$ Activity Distribution in the IRON-URANIUM Assembly.

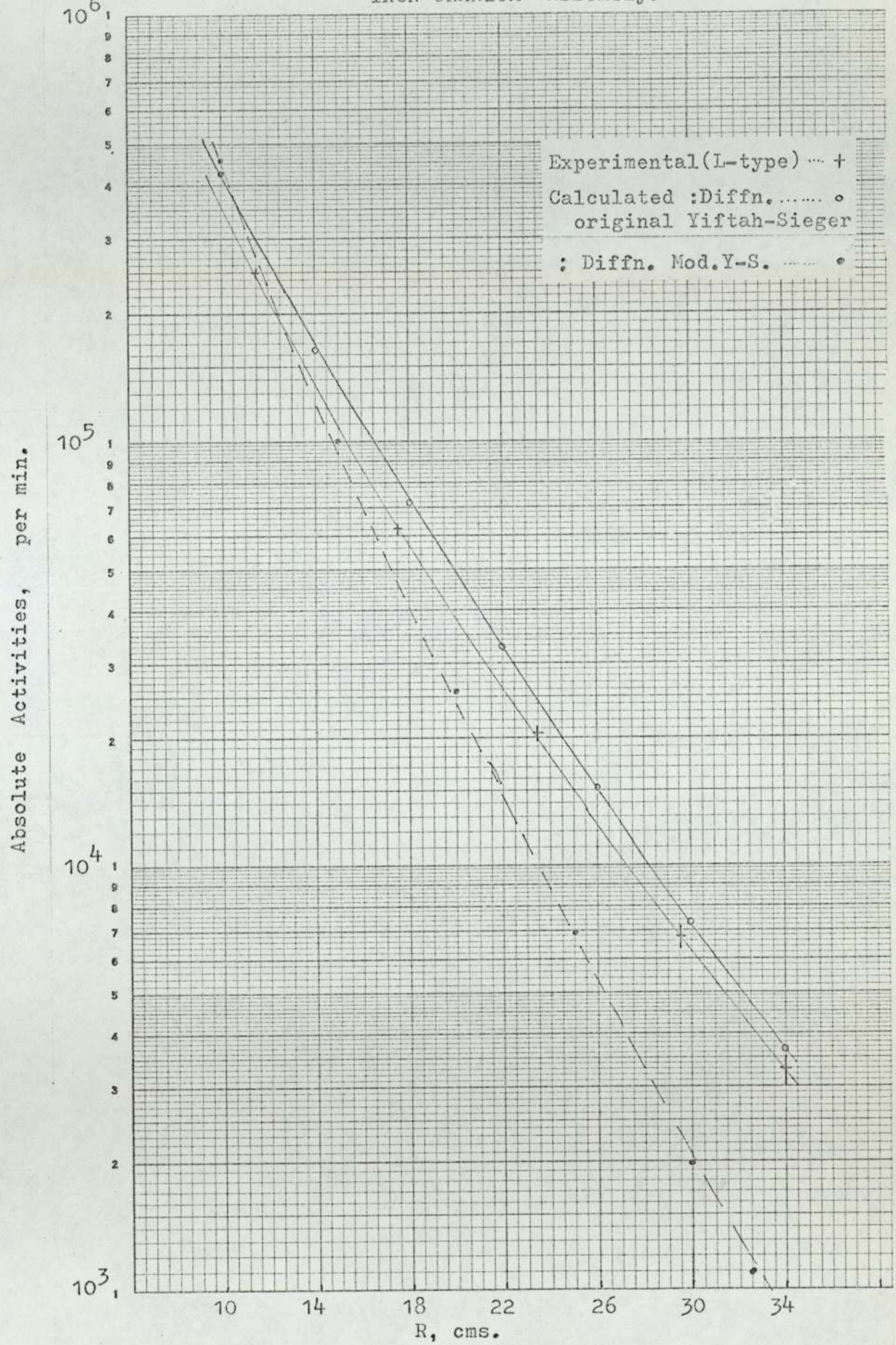

FIG.9.4.-- Al(n,α) Activity Distribution in the IRON Assembly.

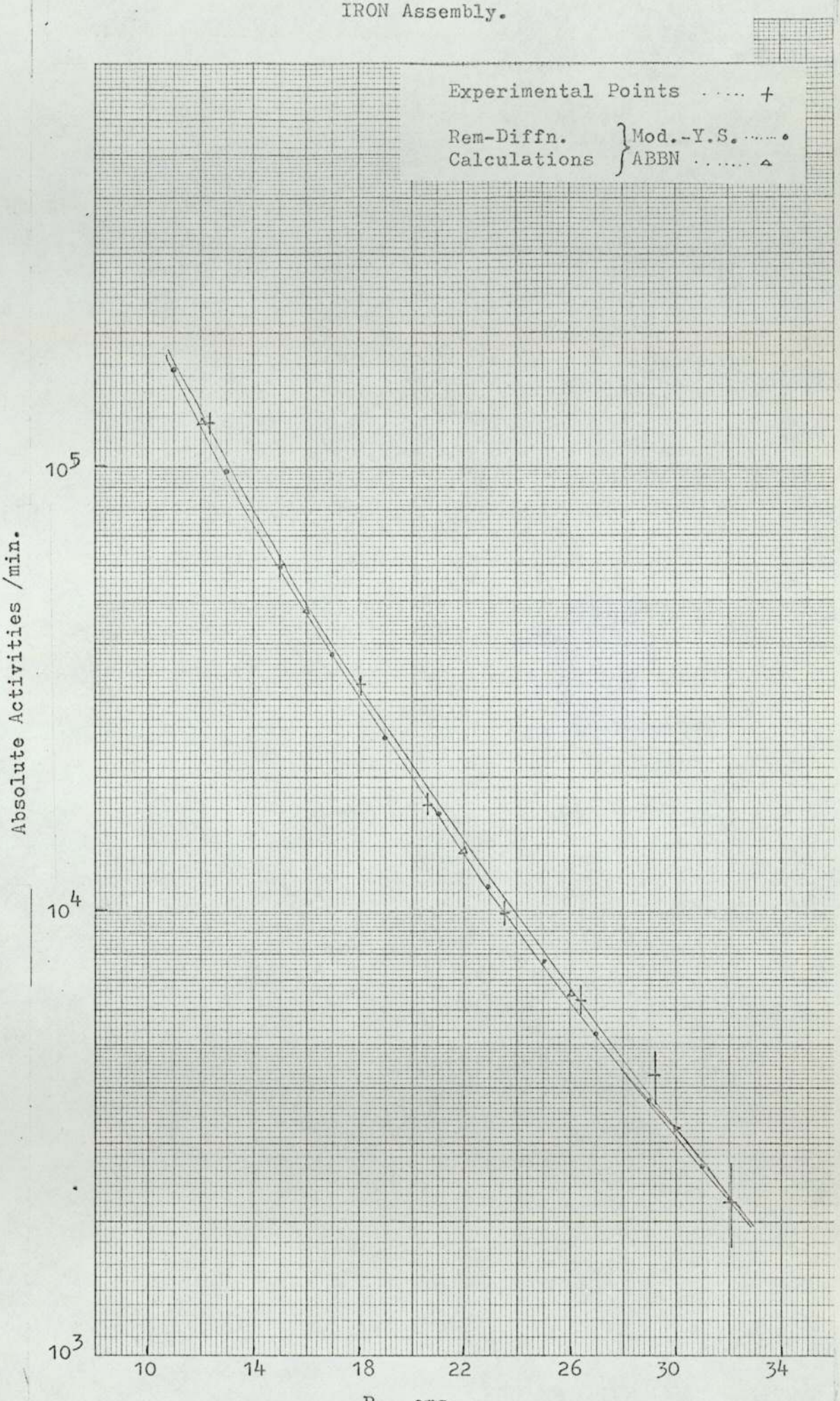

FIG.9.5--^{56}Fe(n,p) Activity Distribution in the IRON Assembly.

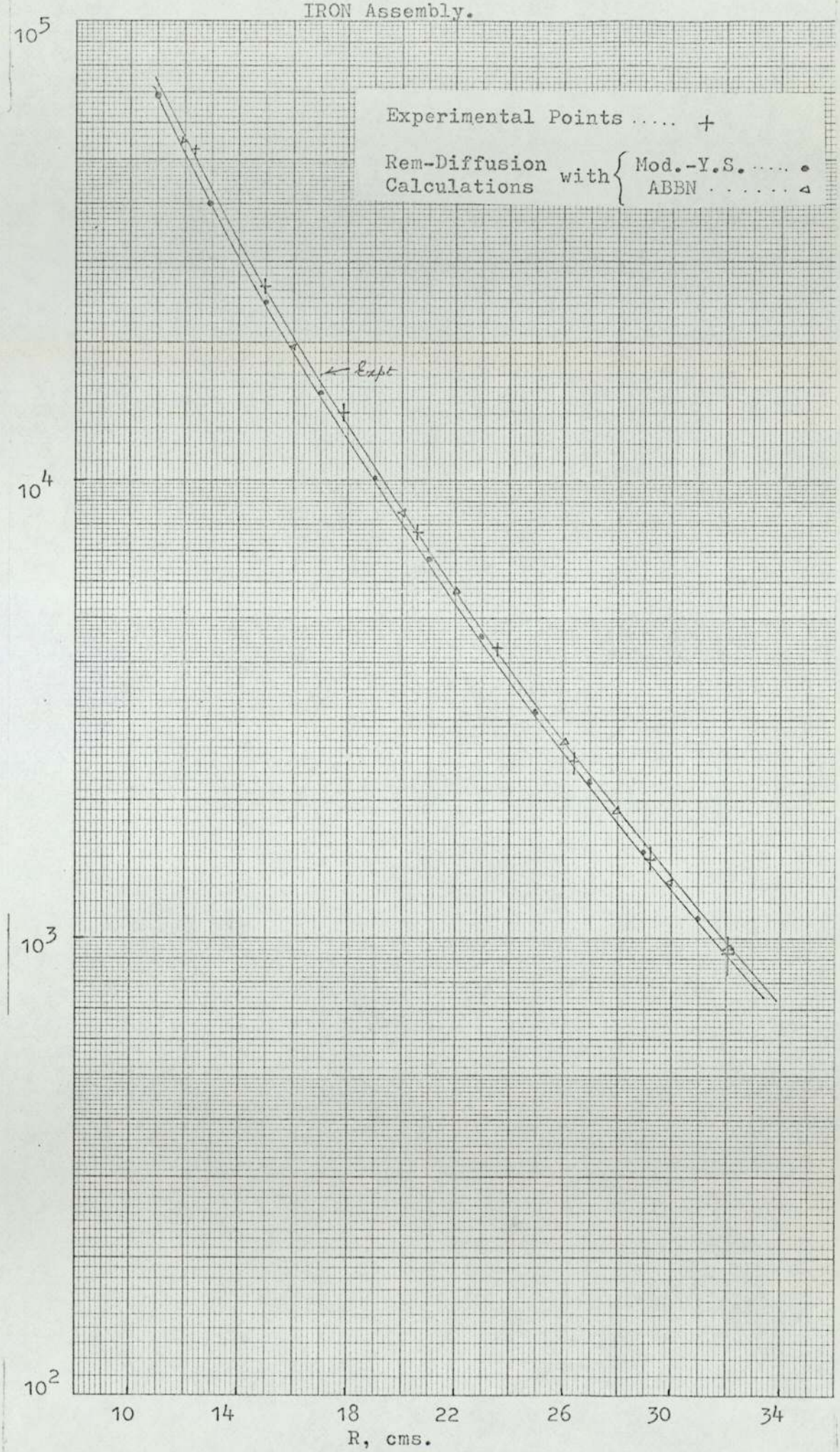

FIG.9.6 -- Al(n,p) Activity Distribution in the IRON Assembly.

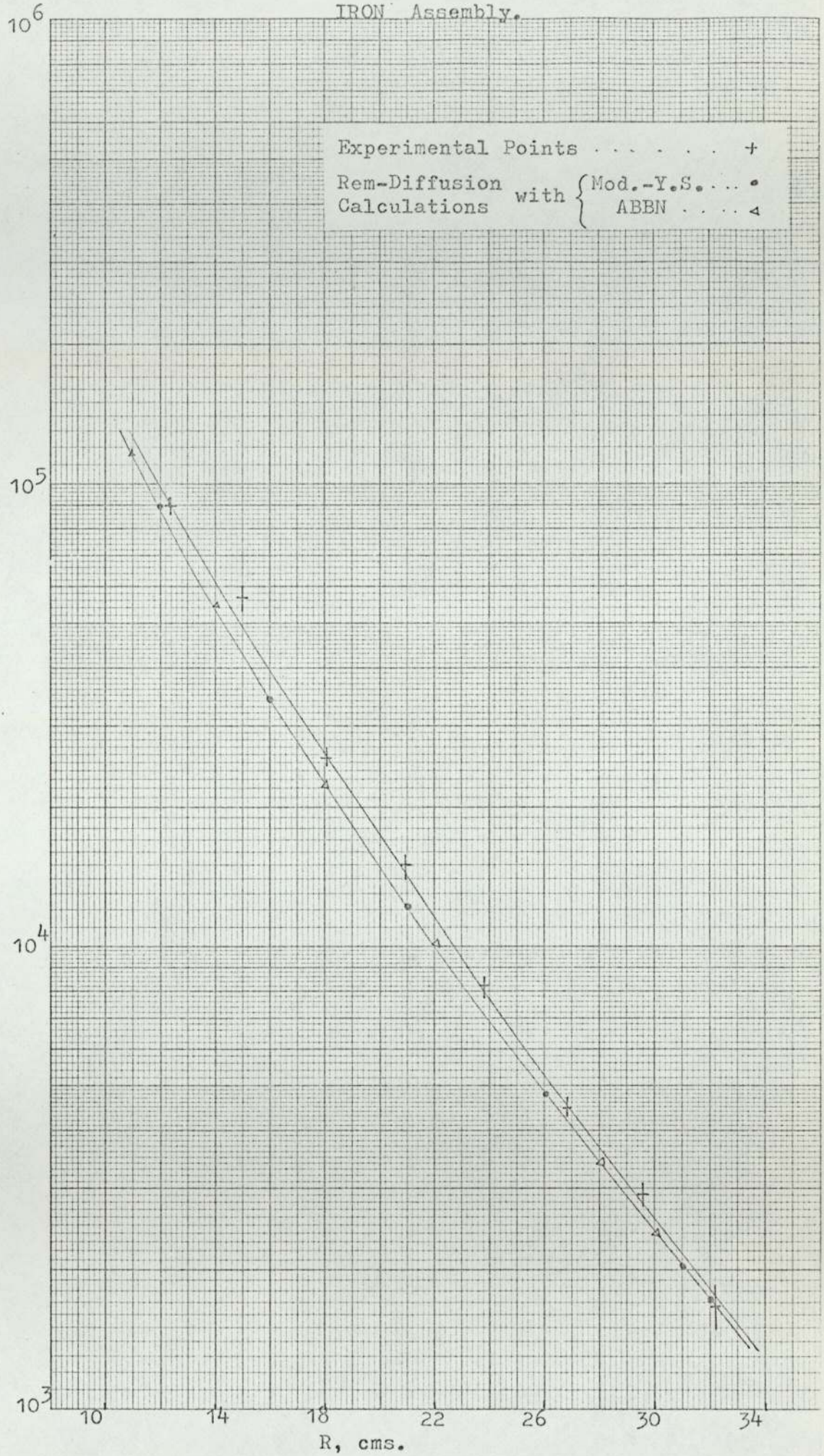

Fig. 9.7a.-- P(n,p) Activity Distribution in the IRON - Assembly.

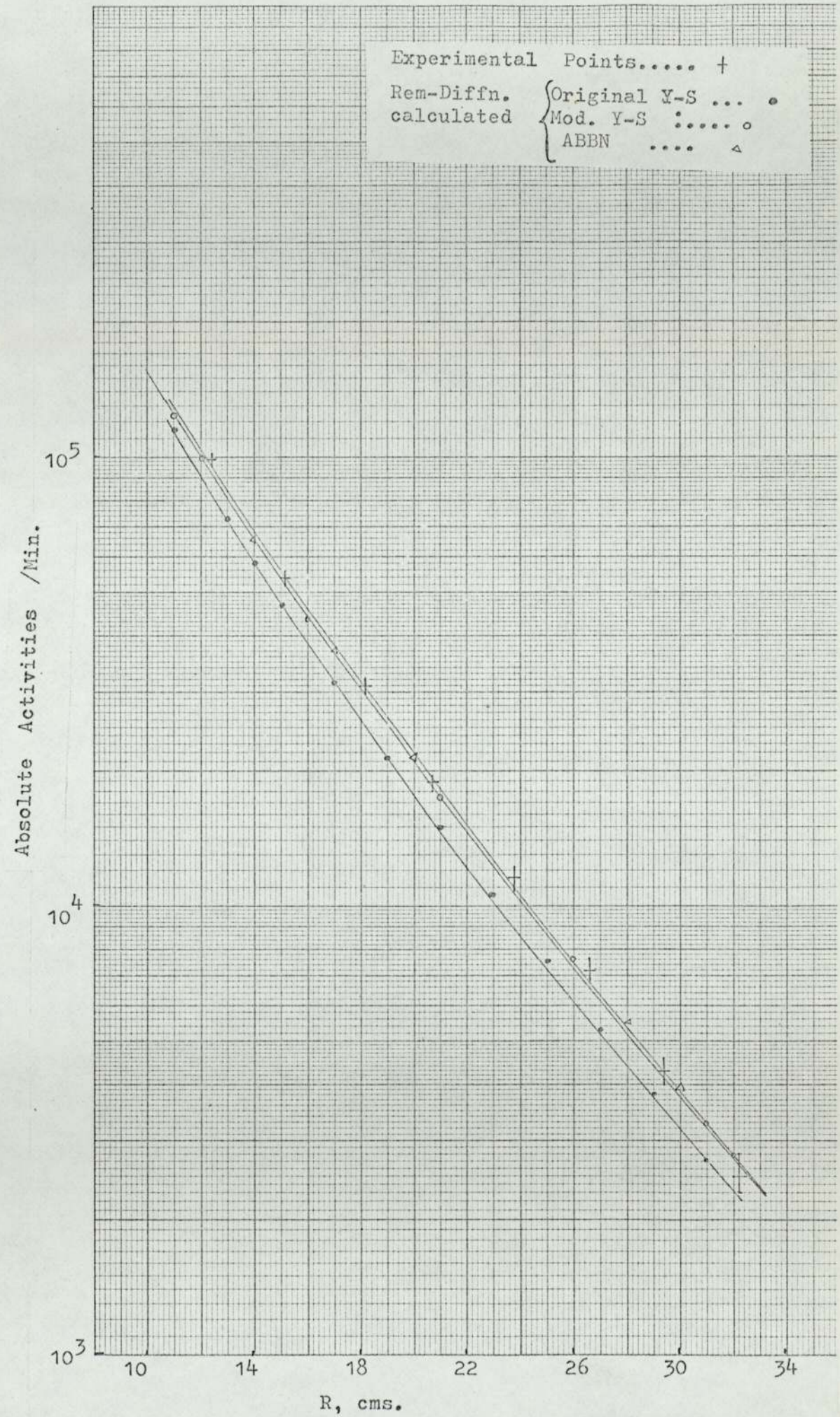

FIG.9.7b.-- P(n,p) Activity Distribution in the IRON-Assembly.

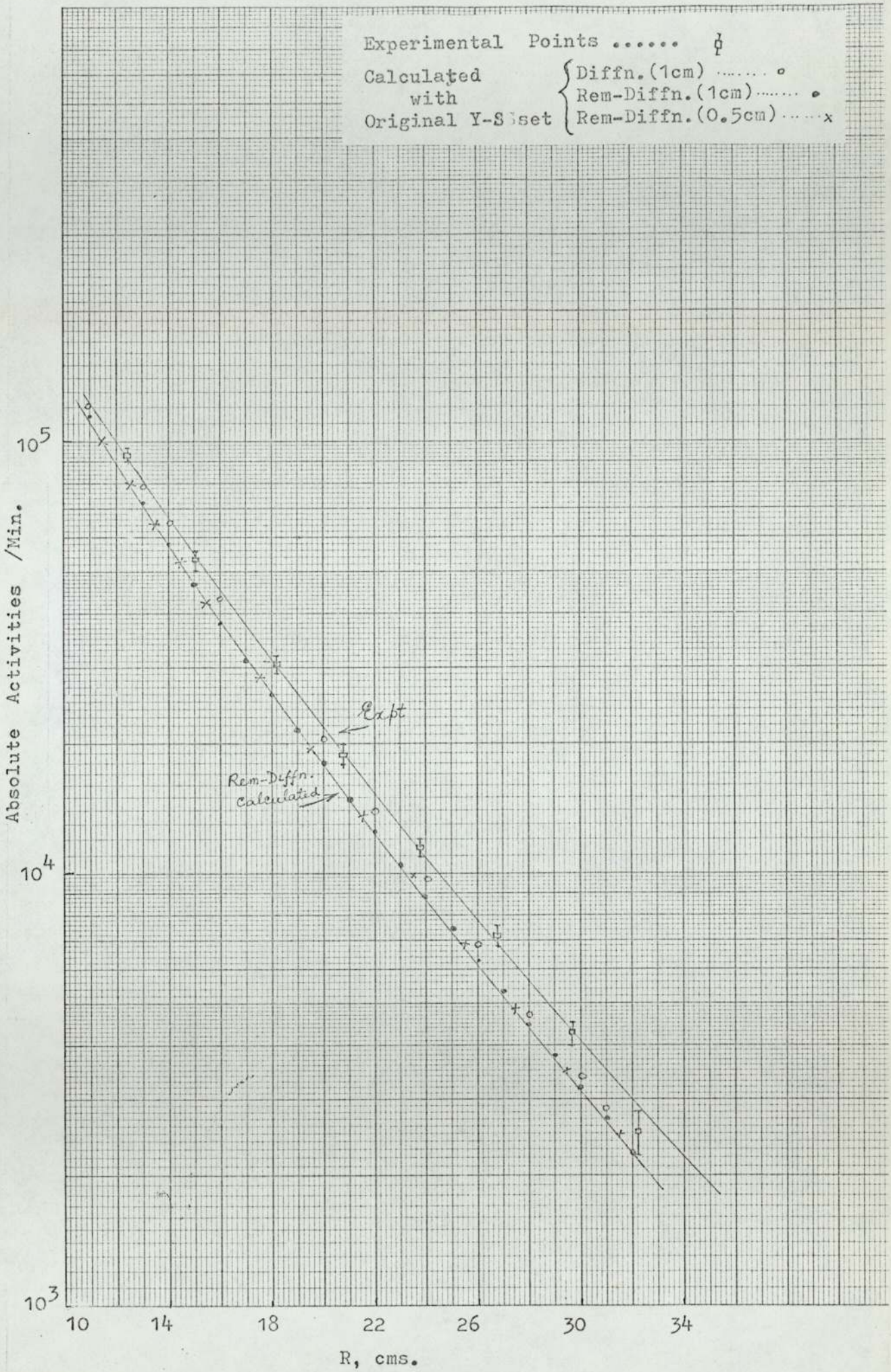

FIG. 9.8.-- Al(n,α) Activity Distribution in the IRON-URANIUM Assembly.

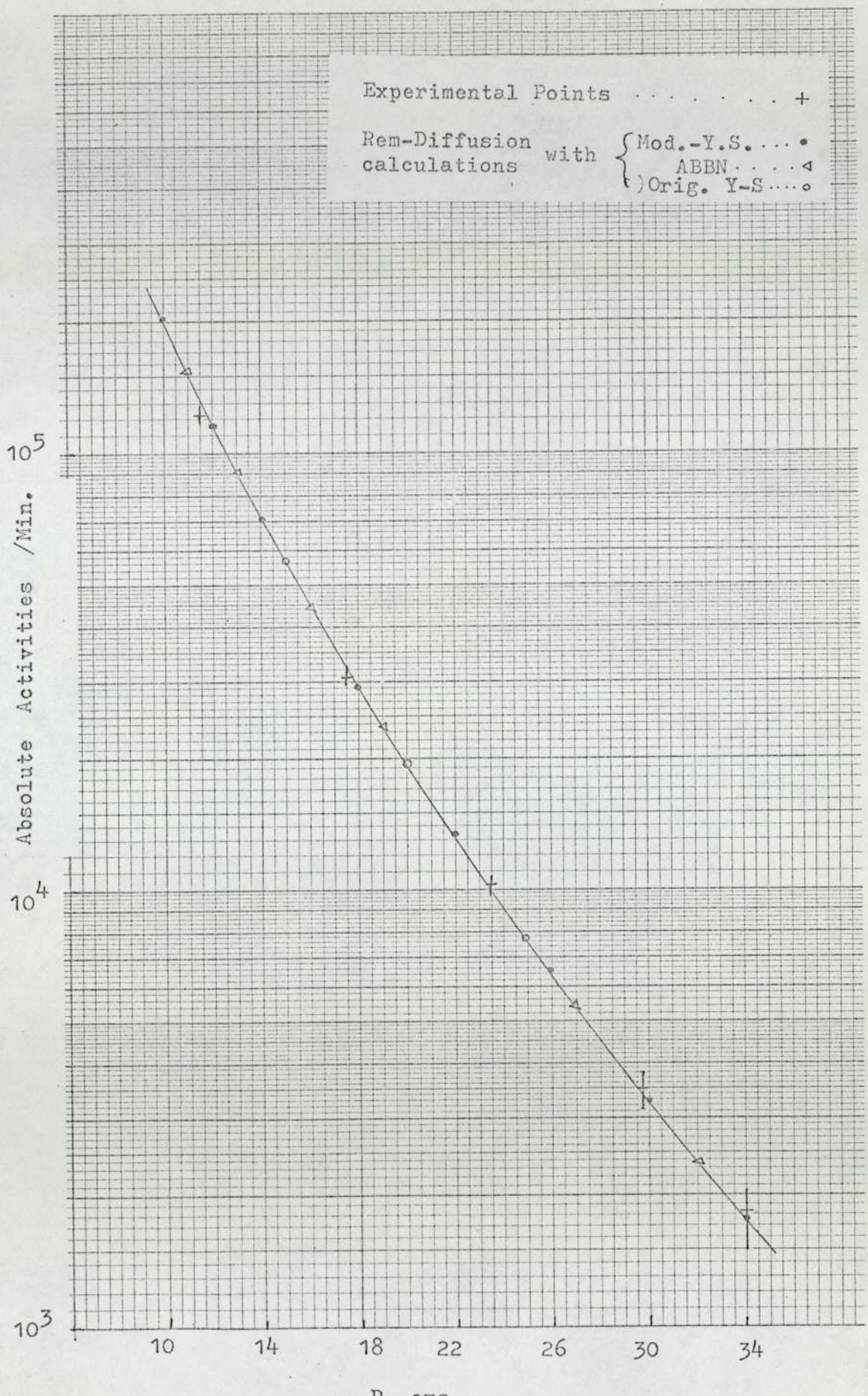

FIG. 9.9 -- ^{56}(Fe(n,p) Activity Distributions in the IRON- URANIUM Assembly.

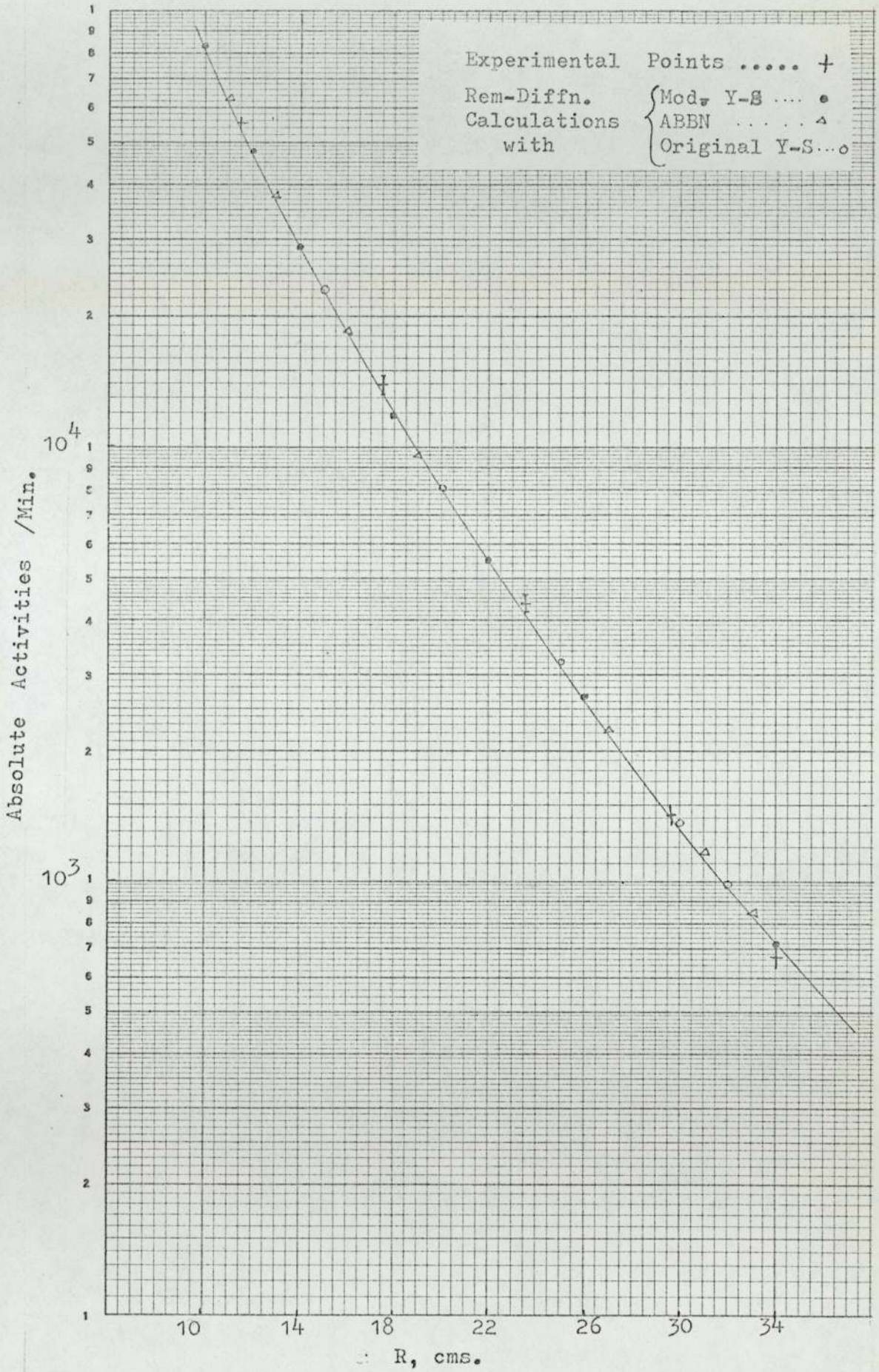

FIG. 9.10.-- Al(n,p) Activity Distribution in the IRON-URANIUM Assembly.

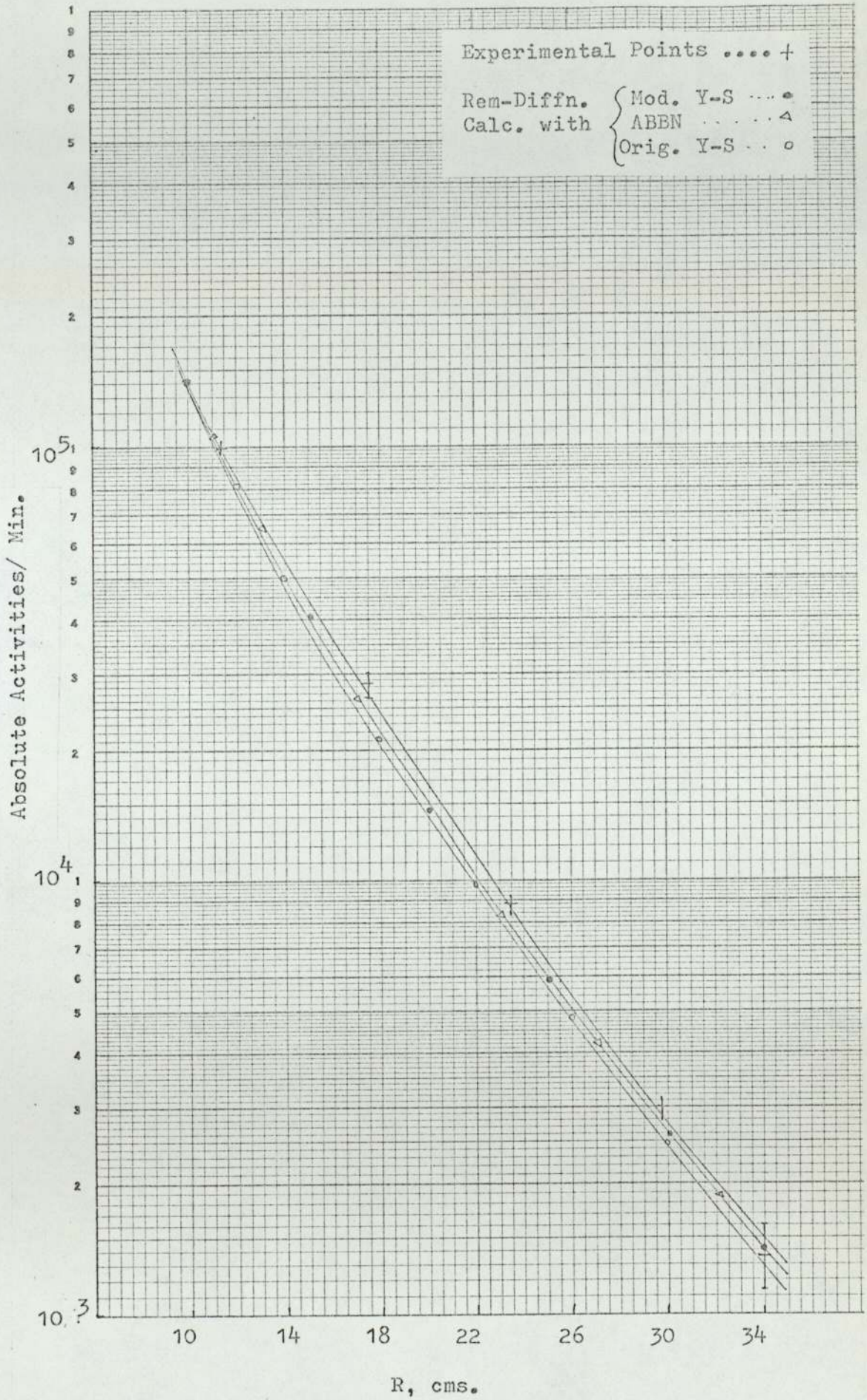

FIG. 9.11.-- P(n,p) Activity Distribution in the IRON-URANIUM Assenbly.

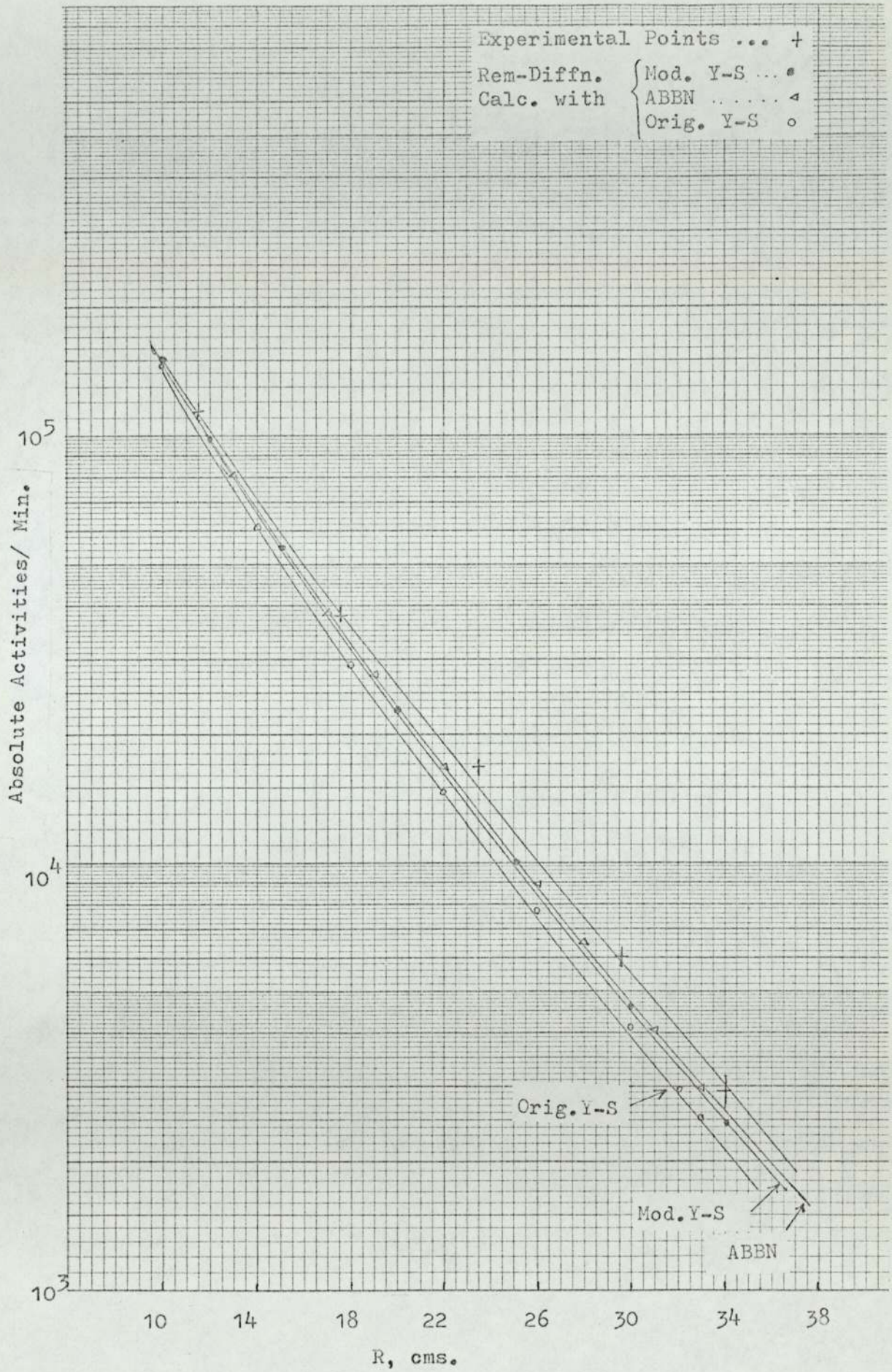

9.5) contd.

The diffusion calculations in which the only difference is that the highest energy group flux distribution was found by diffusion, were also carried out with the data sets. The copper activity in the Fe-U assembly predicted by the diffusion calculations are shown in Fig.9.3b and as can be seen the modified Y-S data predicts a much faster rate of fall than experimentally obtained. The main reason is that Diffusion phenomena as understood and defined cannot be applied for the outward directed source neutrons which are so highly anisotropic in their scattering behaviours ($\bar{\mu} = 0.83$); the diffusion coefficient D obtained from the Lamarsh-equation is therefore fictitious for the 14 Mev source neutrons. The lower energy neutrons though have very similar values of $\bar{\mu}$, are not monodirectional. It is thus concluded that the removal-diffusion is the only suitable method.

Somewhat tolerable agreements for the copper activities shown by the diffusion calculations with the Original Y-S data set must be by-chance and meaningless.

9.6) <u>In(n,γ) Activities.</u>

In(n,γ) activities are shown in Figures 9.12 and 9.13 for the iron and the iron-uranium assemblies respectively.

The rapid rise in the activities towards the outer edge of the assemblies indicates the presence of reflected low energy neutrons from the surround, particularly the water shield above the assemblies. As the cross section of the $^{115}In(n,\gamma)$ reaction rapidly increases with decreasing neutron energy, particularly below 1 kev, it was concluded that the activities induced due to high energy neutrons would not be recoverable because of low cross sections. However from the indium activities

9.6) contd.

the level of the thermal flux could be obtained. Thermal flux level estimated from this shows that it was small throughout the assemblies. This was due to the cadmium around the assemblies and at the bottom of the water shield. But the region above the cadmium cutoff had easily moved into. This is clearly demonstrated if the curves II and III for the iron assembly in Figure 9.12 are compared. In 1970 the iron assembly was reassembled to repeat some of the observations taken earlier in 1969. It just happened that in 1970 the water tank was left at about 20 cm above the outer boundary of the assembly while in 1969 it was only about 6 cm above - other arrangements being the same. The difference in the absolute values and also the shape between the cadmium covered activity distributions in these two occasions (curves II and III) show the effect of the water tank. However, there was no practical difference in the thermal flux levels as obtained. This also perhaps explains the level of the observed activities between about one and two order of magnitude higher than the calculated level. However, the flux level of these low energy neutrons is not so high (discussed below); the especially high cross sections of indium for the epithermal neutrons gave high activity. The average energy of the indium-activating neutrons was obtained as follows.

9.6.1) Average Activation Cross Section of In(n,γ)Neutrons.

With the theory for correction of the self-shielding effect in a resonance foil discussed in Chapter 6, the average flux inside the foil can be calculated if the foil dimensions and cross sections of the detecting neutrons are given. Working backwards, from

FIG.9.12-- In(n,Y) Activity Distribution in the IRON-Assembly.

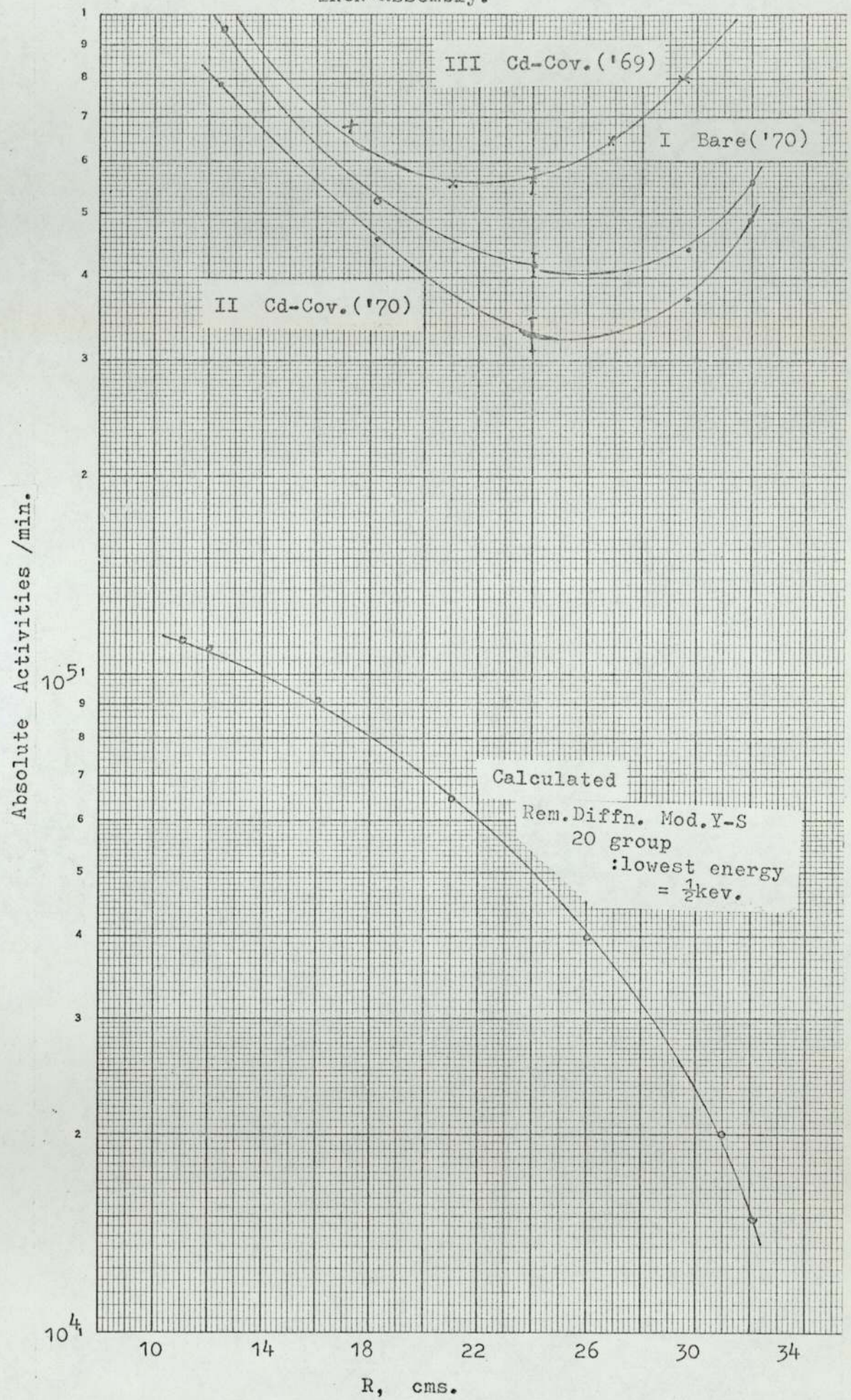

FIG.9.13.-- In(n,γ) Activity Distributions in the IRON-URANIUM Assembly
Calculated curve by Removal Diffn. with modified Y-S data; Lowest Energy = $\frac{1}{2}$ kev.

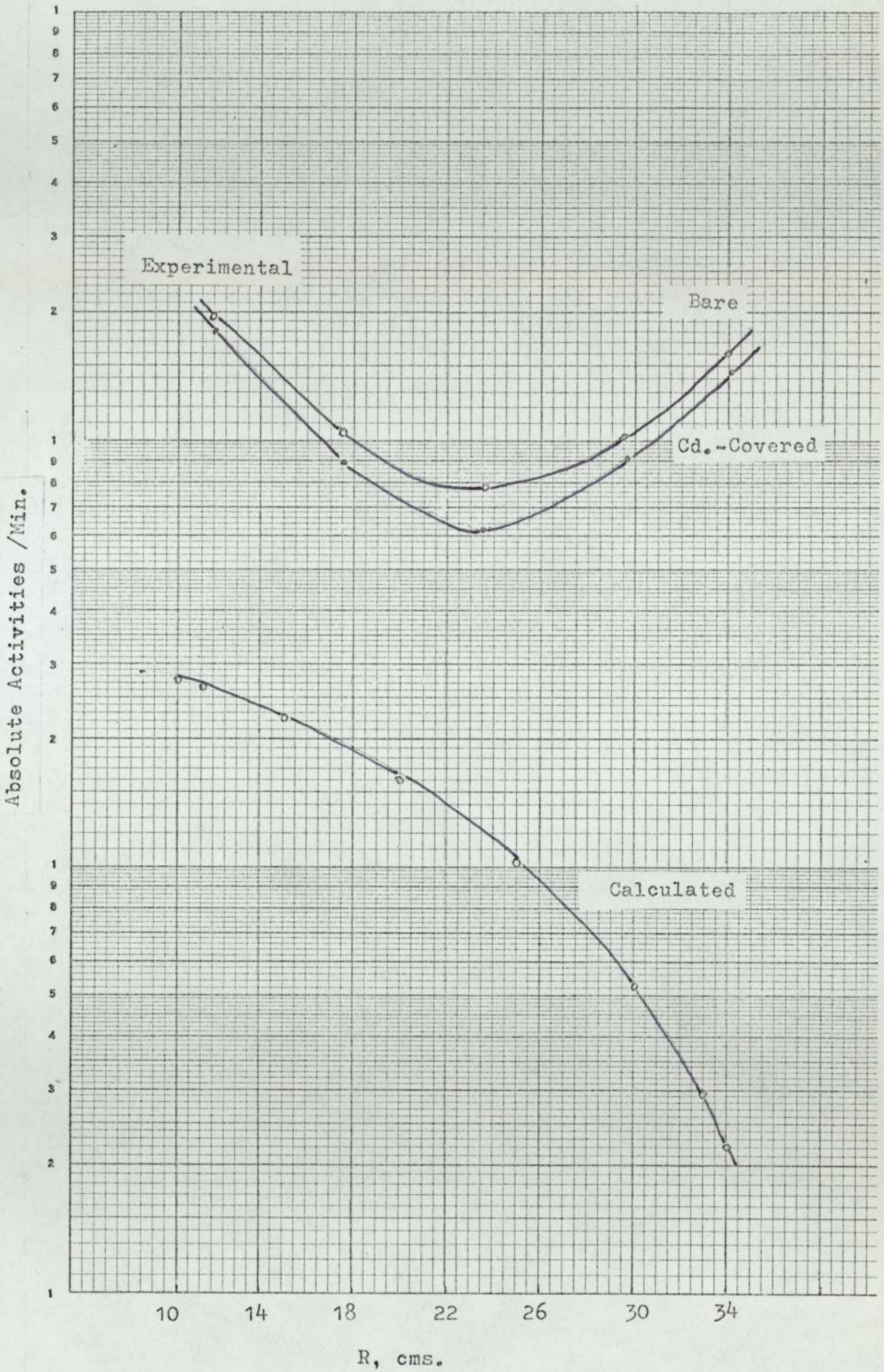

FIG.9.14.-- Activity Distribution in the 5 F-type Indium Foils : Irradiated at the Third Gap in the IRON Assembly.

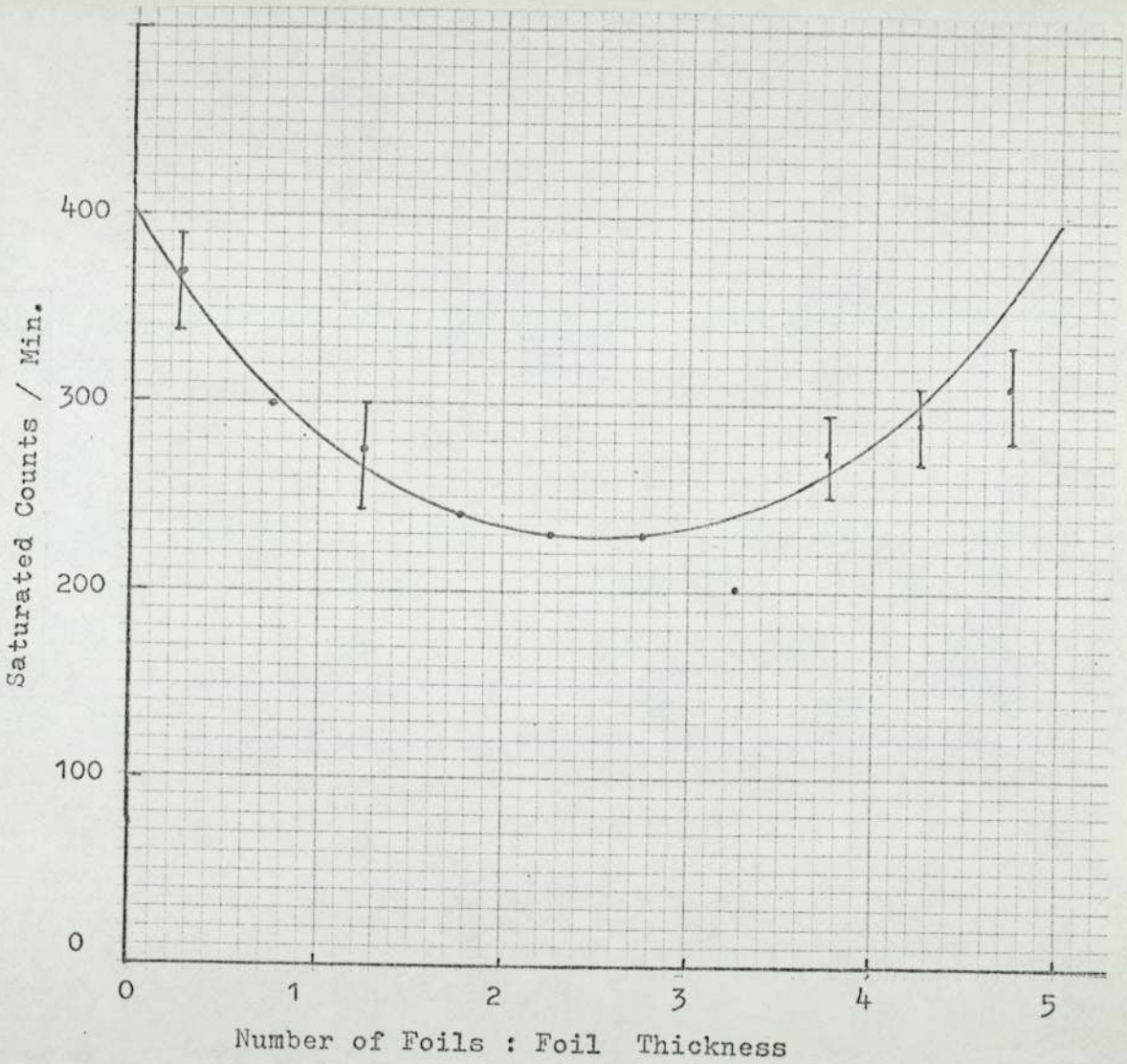

9.6) contd.

9.6.1) contd.

a known average flux, the average cross sections have been obtained from the relations given by the theory. From the average cross-section thus obtained their average energy has been identified to an approximate value.

The average flux has been obtained from the flux distribution observed in 5 F-type foils piled one above the other and placed in a Cd-box and exposed to radiations inside the iron assembly. The F-type indium foils were made of 5% by weight of indium, compared to 25% by weight of the X-type foils which were mainly used to obtain the activity distributions inside the assemblies. Otherwise both types were of the same general thicknesses and radii. Assuming the internal flux depression is the same for the same amount of indium the distribution in the 5 F-type foils is the same as in an X-type foil - only the scale stretched five times for the former. The activity distribution obtained with the 5 foils is shown in Figure 9.14. They were counted for beta-activities. Counted with both faces on the counter, each foil gave two readings. From this the value obtained was

$$\frac{\bar{\phi}_u}{\phi_s} \simeq 0.725$$

where $\bar{\phi}_u$ is the volume average flux and ϕ_s is the flux at the surface. According to theory this gives

The average absorption cross-section as calculated to be ~ 1670 barns. This puts the average energy of the neutrons at near the first resonance of ^{115}In to 1.4 ev. This analysis indicates the activity is mainly due to the neutrons just above the thermal cut-off; the thermals themselves

9.6) contd.

9.6.1) contd.

reflected by the water shield were absorbed by the cadmium below the tank and above the assembly.

Corresponding to an activity level of 3×10^5 (in the middle position of the iron assembly) per minute and the cross-section obtained (1700 b), the average flux is only $\sim 5 \times 10^2$ neutrons sec^{-1} cm^{-2}.

The activity curves for the iron-uranium assembly (Fig.9.13) has the similar shape but considerably lower. This could be explained by noting that the iron-uranium assembly (in the upper measuring section) had more material than the iron-assembly as a result of which fewer of the fast neutrons were leaking out of the former and so fewer returning back. Also uranium is more effective capturer of intermediate and low energy neutrons than iron. It does not seem legitimate to conclude that the earlier half of the curves are mainly due to the neutrons degraded by the assembly, even though the shape of this part is similar to that of the corresponding calculated curve. The gap is too large. The low energy neutrons - some of them - could have come from the concrete surround; particularly the hollow inner section in the assembly will let the source neutrons enter the concrete directly and be returned as epithermal (thermal being shielded by cadmium plates placed across the openings) unattenuated, which can explain the higher activities for the inner foils. The curves reverse their trend as the foils come nearer towards the outer boundary and near the water tank.

9.6) contd.

9.6.2) Thermal Flux Levels in the Assemblies.

The thermal flux can be obtained from the difference in the activities of the bare foils from the cadmium covered foils in the assemblies - curves I and II respectively in Fig.9.12 for the iron assembly. These give thermal flux level of $\sim 2 \times 10^3$n sec^{-1} cm^{-1} at the middle position (R = 20). The cadmium ratio is between 1.15 and 1.3 in the assembly. The thermal flux at three different positions of the iron assembly is given below. They are corrected for the perturbation effects. The thermal flux as percentage of the 14 Mev source neutrons at those positions are shown for comparison.

TABLE 9.3

Measured thermal neutron flux (cm^{-2} sec^{-1}) in the Iron Assembly - absolute value and prcportion to the 14 Mev neutrons.

Position R,cm	Thermal Flux	Therms/14 Mev Flux
12.4 cm	5.36×10^3	$\sim$ 0.8%
18.1 cm	2.0×10^3	$\sim$ 1.0%
29.2 cm	2.18×10^3	$\sim$ 10%

The average resonance flux in the iron assembly it was noted, was $\sim 5.2 \times 10^2$; this is not corrected for perturbation effect. With correction this gives about 3×10^3 neutrons cm^{-2} sec^{-1}.

In the iron-uranium assembly, the thermal flux level was smaller by a factor of about 5. The maximum ratio of the thermal to 14 Mev flux gives about 5% towards the outer boundary.

9.6) contd.

9.6.2) contd.

Even 10% or more thermal flux is not significant for the threshold foils. All the foil materials used, fortunately have low thermal cross sections, and also advantageous half-lives for thermal activation. For example 10% thermal flux would contribute less than 1% of the activity in the copper foil counts. The thermal and resonance activation cross sections and half-lives of the major isotopes of the threshold foils are reviewed below. They can be compared with the ^{115}In cross sections given in the last row.

Reaction	Therml, σ_o (at 2200 m/sec)	Res.Intgr.	Half-life
$^{63}Cu(n,\gamma)$	3.5 b	4.0 b	12.8 hr.
$^{65}Cu(n,\gamma)$	1.8 b	-	5.1 min.
$^{27}Al(n,\gamma)$	210 mb	160 mb	2.3 min.
$^{54}Fe(n,\gamma)$	2.5 b	-	2.7 yr.
$^{58}Fe(n,\gamma)$	1.0 b	-	45 d.
$^{31}P(n,\gamma)$	190 mb	92 mb	14.3 d
$^{115}In(n,\gamma)$	161 b	2790 b	54 m.

9.7) Effects of Mesh Spacing on Calculations.

The calculated results in the previous sections were mostly performed with mesh spacings of 0.5 cms. To find the effect of finite width of mesh spacing some of the calculations were repeated with twice this width i.e. with 1 cm. The values for phosphorus are compared in Fig. 9.7b. No significant difference

9.7) contd.

occurs with changed mesh spacings. 5 mm is in fact quite small compared with the mean free paths of the neutrons - in particular, the neutrons measured with the threshold foils - in the assemblies.

9.8) Other Computed Results of Interest.

Some of the spectrum distributions obtained with the calculations are shown in Figures 9.15 to 9.18. They were obtained by removal diffusion calculations and using the modified Y-S data.

The multi-group spectra down to the 15th group (lower energy 25 kev) are drawn at three spatial points - the inner and the outer radii and after 10 cm of penetration into the assemblies (Figs. 9.15 and 9.17), while few selected group distributions are shown in Figs. 9.16 and 9.18.

The iron window at 29 kev belongs to group-15. But it does not show any unusually high flux level, indicative of streaming. The group-15 flux is comparatively at higher level in the Fe-U assembly than in the Fe assembly (Figs. 9.16 and 9.18). More secondary neutrons at lower energies are born in the Fe-U assembly. The spectra otherwise peak at the 9th group in both and are falling in either energy direction. The 9th group (825 to 500 kev) is just below the iron inelastic threshold.

FIG. 9.15. -- Computed Multigroup Spectra in the IRON Assembly. above 25 kev : Rem.Diffn. Calculated with modified Y-S data, at the inner and outer radii and R = 21cms.

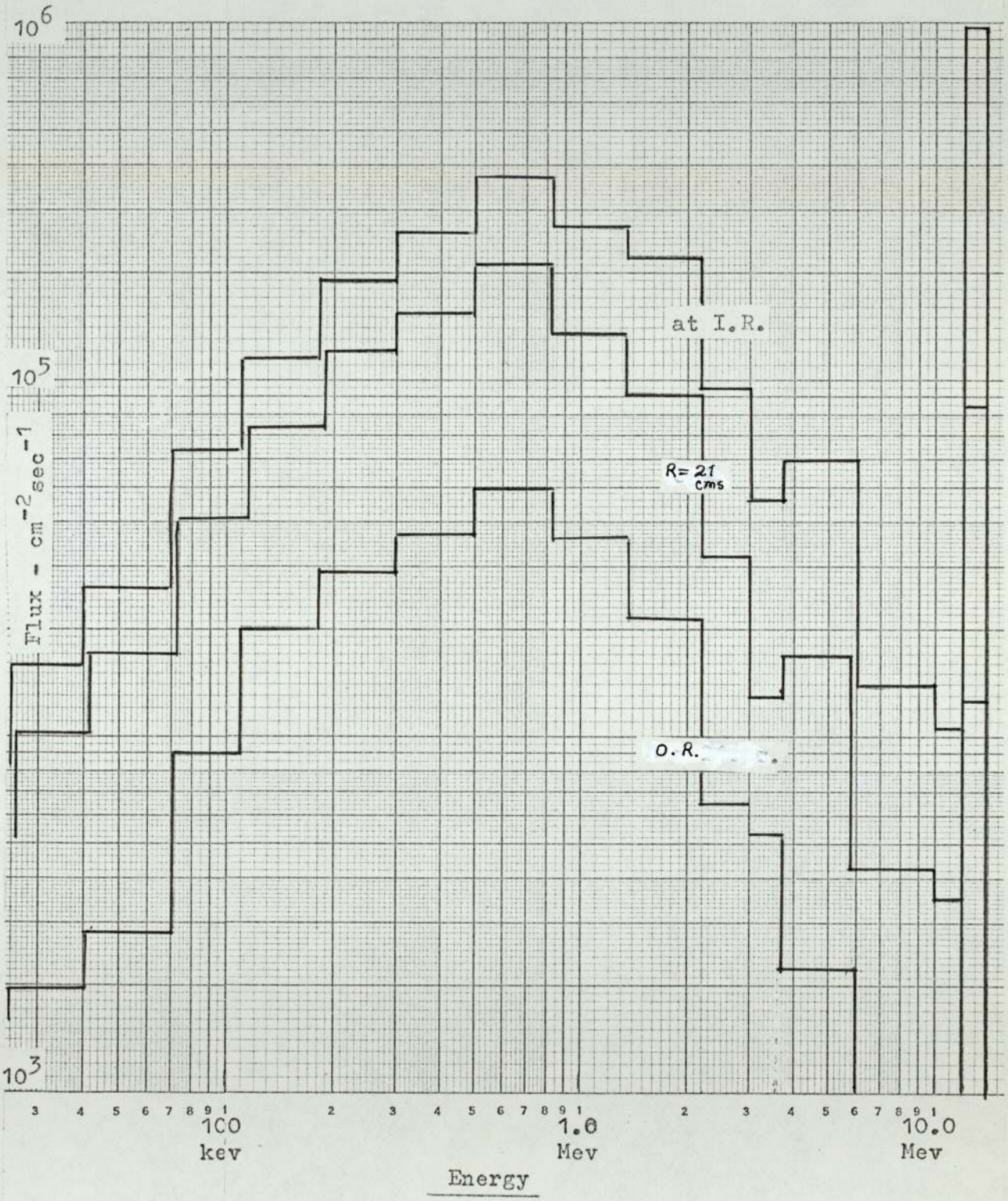

FIG. 9.16.-- Spatial Distribution of some of the Group Fluxes in the IRON Assembly : Rem.Diffn. Calculated with modified Y-S data.

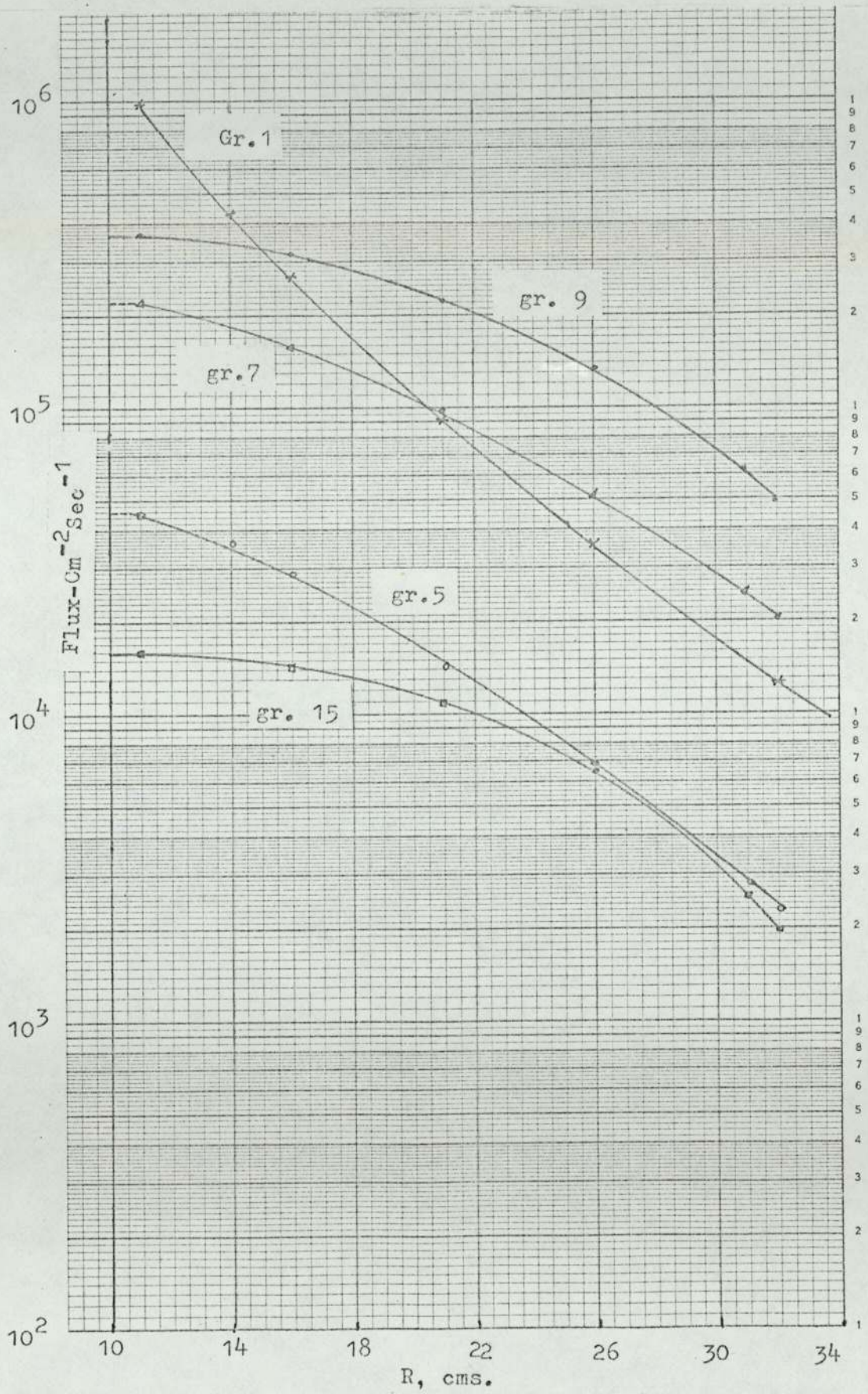

FIG. 9.17. -- Computed Multigroup Spectra in the IRON_URANIUM Assembly above 25 kev at the Inner and Outer Radii and R = 20 cms. : Rem.Diffn. Calculated with Modified Y-S Data.

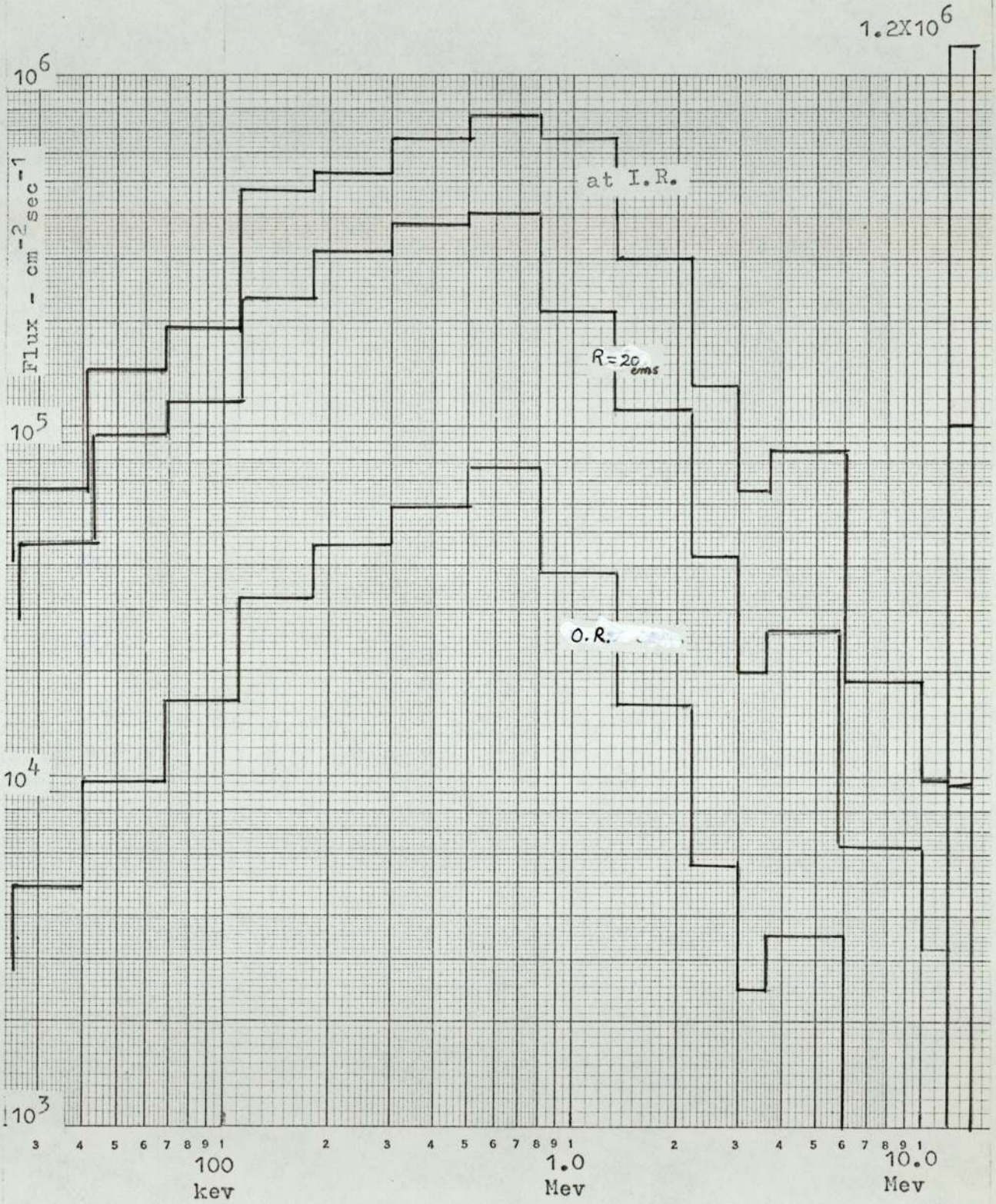

FIG. 9.18.-- Spatial Distribution of some of the Group Fluxes in the IRON-URANIUM Assembly : Rem.Diffn. Calculations with Modified Y-S Data.

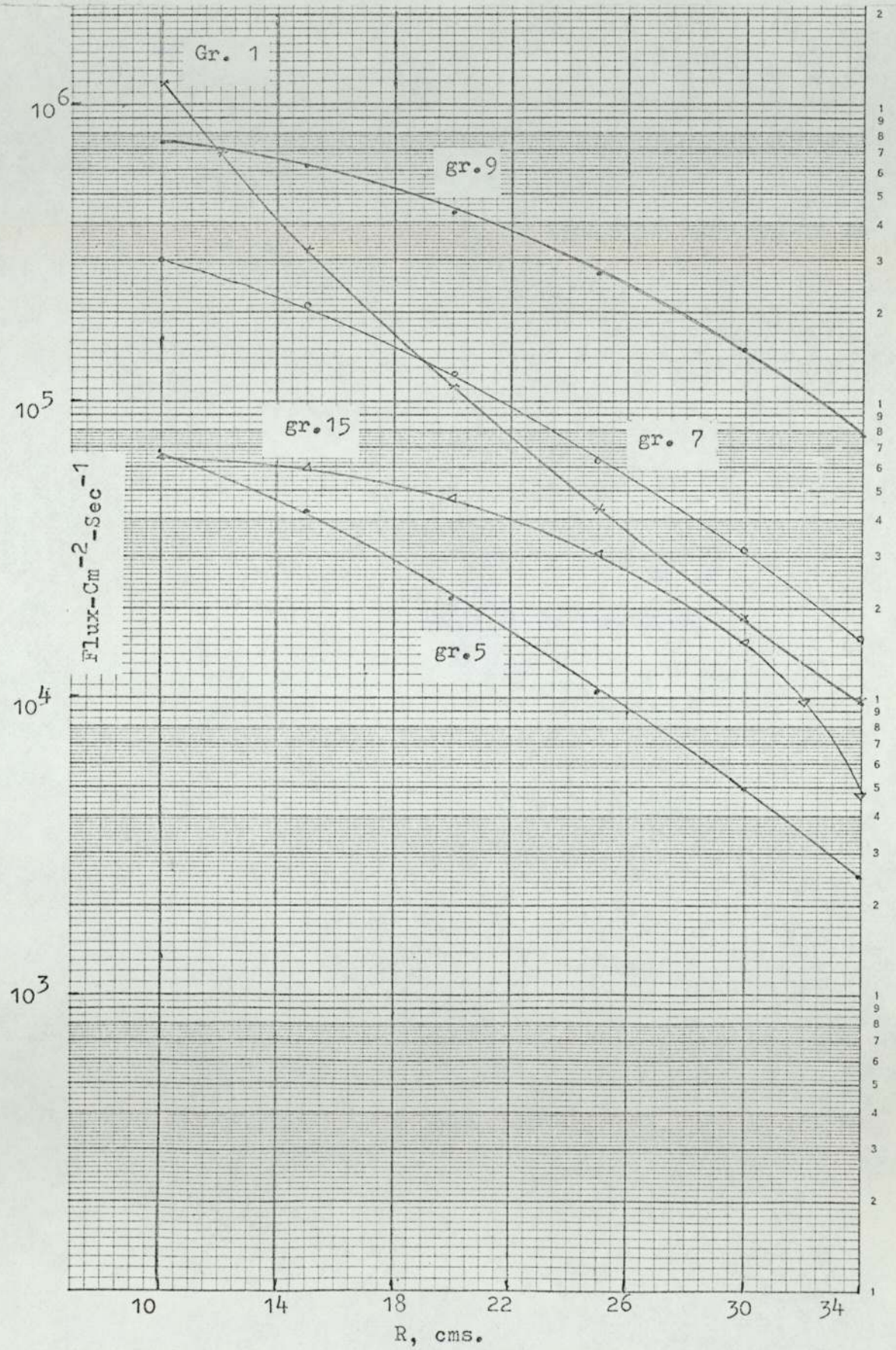

CHAPTER 10

GENERAL CONCLUSIONS

The experimental and the computed results have been discussed and compared in detail in the foreceeding chapters; several important conclusions, particularly about the data sets and methods and techniques of calculations that emerged from the comparisons, have been made there. The following general conclusions can, however, be briefly mentioned.

(i) The 20-group data set of Yiftah and Sieger provides values of sufficient reliability for the iron and uranium experiment with 14 Mev source neutrons. Nevertheless, modifications are needed for the inelastic scattering probabilities and the cross-sections, since the YS set completely ignores the multiple neutron emissions which at 14 Mev can have considerable cross-sections for medium and heavy elements; the situation becoming worse for the heavier elements. However, a large section of the secondary neutrons can be included by replacing the (n, n′) cross-section by the total non-elastic neutron emission cross-sections and still using the original "inelastic" (i.e. n, n′) scattering probability matrix. This modification can be easily done only for the source neutrons; for the lower groups detailed study would be needed for group-averaging. In view of this shortcoming of the data the agreement obtained in the present study is reasonable; this is because of the low abundance of uranium - about 30% by atom. If an assembly containing mostly uranium is studied with a 14 Mev neutron source, the YS data will fail more dramatically.

This confusion that exists about the secondary neutrons is rather general and is partly caused by more than one usage for the word "inelastic". Legitimately only the (n, n′) neutrons should be meant, but all the secondary neutrons emitted as a result of (n, n), (n, 2n), (n, 3n)..... reactions are also collectively referred to as inelastic, particularly in reactor

physics, the reason being that multiple emissions hardly have any importance in proper reactors. Another reason was that until recently not enough was known about the multiple-emission neutrons. The approach has been often rationalised by saying that all the secondary neutrons from various processes cannot be differentiated experimentally. Perhaps it is time to assign a separate term for the combined secondary neutrons, particularly when sufficient is known about them for the common elements.

(ii) By using a 'hybrid' set comprised of the Russian ABBN data below 10.5 Mev and comparing the results, it can be concluded that the other data values of YS, at least between 2 and 10 Mev, have the same order of reliability as those of ABBN which have received a wide testing and confirmation by now.

(iii) The removal cross-section obtained for the 14 Mev neutrons in iron confirms the value, within experimental error, computed and suggested by Avery et al [175] at that energy point. They have put forward removal cross-section values for most of the reactor materials from 0.5 Mev up to 17.5 Mev, but these are to be considered tentative until experimentally verified. Since the same basis of calculation has been used it gives hope that the other values of these authors are also reliable, subject to the condition that the microscopic cross-sectional data for the materials used by Avery et al in the energy range concerned are sufficiently reliable.

(iv) The transport and slowing down of the Mev neutrons in heavy and medium-heavy materials can be described by the diffusion equations when they are born inside the medium - if the Lamarsh equation [174] is used to calculate the diffusion coefficient. D based upon

transport cross-section does not seem to be adequate for them. However, the Lamarsh equation too breaks down for the highly anisotropic mono-directional source neutrons.

(v) The uncertainty of the threshold foils that has been generally existing even for the commonest reactions might be dispelled since the Euratom compilation. However, this is yet an unfinished work; if some values were recommended for the reactions in this work the cross-sections could be consistently tested by the different laboratories and the right values more quickly ascertained. The use of the log-log scale, perhaps imitating the Barn-book introduces an additional source of error and does not seem to have been essential for threshold reactions. The ability to put confidence limits for the cross-sections of a set of at least half-a-dozen convenient threshold foils of different thresholds, to within a few percent will make available a very convenient fast neutron spectrometer with the combination of several advantages, some of which none of the present-day fast neutron spectrometers can offer. Several of the promising mathematical techniques demonstrated successful for unfolding the threshold foil activation data and to construct differential spectrum have not been able to establish themselves, mainly due to the large uncertainty of the foil cross-sections.

The cross-sections selected from the Euratom compilation and used for the present work are shown in Figure 6.2. The agreement with the experimental values has been satisfactory. However, what the comparisons have tested are not the absolute values but rather for the lower energies the values relative to those at 14 Mev - whatever value might have been assigned at that energy point. It must be conceded this is a poor test, particularly for threshold cross-sections.

(vi) It has been shown by the calculations that no streaming of the neutrons is expected in the energy region belonging to the "window" in the iron cross-section at 29 kev. This is because not many of the secondary neutrons are born around this energy region and the iron assembly was not thick. Rather a moderate streaming sets in as the neutrons fall below the iron inelastic threshold. The uranium inelastic threshold at 44 kev is ineffective due to the same reason as the iron "window" at 29 kev. These conclusions, however, could not be verified experimentally because of the interference of the low energy neutrons reflected from the shielding materials around.

APPENDIX 1.

NUMERICAL SCHEME USED FOR MULTIGROUP FLUX CALCULATIONS.

The diffusion equations can be abbreviated as

$$D_g \nabla^2 \phi_g - A_g \phi_g + S_g = 0 \qquad \text{A1.1}$$

where A_g is the sum of neutron sinks and S_g is the sum of neutron sources. This is for any group g, but for simplicity the group subscript is dropped henceforth. The term S is a summation for sources from several other groups and assumed known. In special cases when S includes contribution from the same group the corresponding term is given by flux in the group obtained in the previous iteration or by other approximations as explained in the text; it does not include the flux value ϕ_g to be calculated by eqn.A1.1.

For one dimensional cases the Laplacian is given by

$$\nabla^2 = \frac{d^2}{dr^2} + \frac{c}{r}\frac{d}{dr} \qquad \text{A1.2}$$

where c is the geometry index and is 2 for sphere; for cylinder c is 1 and for slab, 0. The diffusion equation is, then given by

$$D\left(\frac{d^2\phi}{dr^2} + \frac{c}{r}\frac{d\phi}{dr}\right) - A\phi + S = 0 \qquad \text{A1.3}$$

Equation A1.3 is approximated by a finite difference equation. The medium is divided into mesh structure of equidistant mesh spacing a, so that the distance of the nth mesh point from the centre of origin is $r_n = na$. If ϕ_n is the flux at that point then for one dimensional cases the first differential

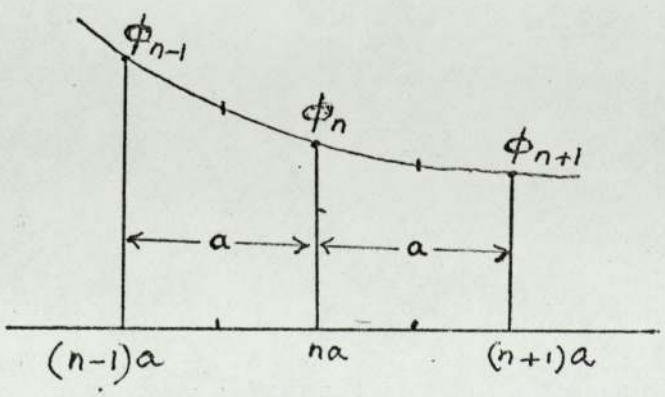

can be written as

$$\left(\frac{d\phi}{dr}\right)_n = \frac{\phi_{n+1} - \phi_{n-1}}{2a} \qquad \text{A1.4}$$

For the same order of truncation error the double differential is obtained from the first differentials at mid-points:

$$\left(\frac{d\phi}{dr}\right)_{n-\frac{1}{2}} = \frac{\phi_n - \phi_{n-1}}{a}$$

$$\left(\frac{d\phi}{dr}\right)_{n+\frac{1}{2}} = \frac{\phi_{n+1} - \phi_n}{a}$$

Hence, $$\left(\frac{d^2\phi}{dr^2}\right)_n = \frac{\phi_{n+1} - 2\phi_n + \phi_{n-1}}{a^2} \qquad \text{A1.5}$$

The diffusion equation for the nth mesh point, assuming homogeneous medium, so that D is constant, is thus:

$$D\left[\frac{\phi_{n+1} - 2\phi_n + \phi_{n-1}}{a^2}\right] + \frac{c}{r_n}\left[\frac{\phi_{n+1} - \phi_{n-1}}{2a}\right] - A\phi_n + S = 0 \qquad \text{A1.6}$$

or $$2r_n\left(\phi_{n+1} - 2\phi_n + \phi_{n-1}\right) + ac\left(\phi_{n+1} - \phi_{n-1}\right)$$

$$- \frac{2a^2 r_n A_n \phi_n}{D} + \frac{2a^2 r_n S_n}{D} = 0$$

Collecting terms for flux at each mesh point and rearranging we get

$$\phi_{n+1} = \left[\frac{2 + a^2\frac{A_n}{D}}{1 + \frac{ac}{2r_n}}\right]\phi_n - \left[\frac{2r_n - ac}{2r_n + ac}\right]\phi_{n-1} - \left[\frac{a^2}{1 + \frac{ac}{2r_n}} \cdot \frac{S_n}{D}\right] \qquad \text{A1.7}$$

or $$\phi_{n+1} = M_n \phi_n - N_n \phi_{n-1} - R_n \qquad \text{A1.8}$$

where the terms in the square brackets in eqn.A1.7 define M_n, N_n and R_n respectively.

Now, suppose equation A1.8 is expressible as

$$\phi_n = \alpha_n \phi_{n+1} + \beta_n \qquad \text{A1.9}$$

where α_n and β_n are to be obtained. The flux at (n-1)th point is, according to above

$$\phi_{n-1} = \alpha_{n-1}\, \phi_n + \beta_{n-1} \qquad \text{A1.10}$$

Substituting equation A1.10 into equation A1.8 we get

$$\phi_{n+1} = M_n\, \phi_n - N_n(\alpha_{n-1}\, \phi_n + \beta_{n-1}) - R_n$$

or
$$\phi_n = \frac{\phi_{n+1}}{M_n - N_n\, \alpha_{n-1}} + \frac{N_n \beta_{n-1} + R_n}{M_n - N_n \alpha_{n-1}} \qquad \text{A1.11}$$

Comparing the coefficients of equations A1.9 and A1.11, α_n and β_n are obtained:

$$\alpha_n = \frac{1}{(M_n - N_n \alpha_{n-1})} \qquad \text{A1.12}$$

$$\beta_n = \alpha_n(N_n \beta_{n-1} + R_n) \qquad \text{A1.13}$$

This shows that α_n and β_n can be calculated if the corresponding values at the previous mesh points are known. The first value can be obtained at the inner boundary from the boundary condition and the succeeding values of α and β can be determined up to the outer boundary. ϕ_n can then be calculated backwards (i.e. for decreasing values of n) according as equation A1.9.

Boundary Conditions.

The inner boundary condition is obtained from known neutron current. For the source neutrons this is obtained from source specification and is used for diffusion calculation of the source group; for neutrons at other energies, from consideration of symmetry the net current is set zero. For outer boundary condition flux is set zero at the extrapolated distance.

For the formulation of finite difference equations, it is customary to assume that, at the physical boundary between two regions the materials extend into one another by one mesh point [197]. Thus if the inner boundary is at the Mth mesh point, the differentials are obtained between the (M-1)th and the Mth mesh points. Hence the current

$$J_M = - \frac{D(\phi_M - \phi_{M-1})}{a}$$

$$\therefore \phi_{M-1} = \phi_M + \frac{J_M \cdot a}{D} \qquad \text{A1.14}$$

Comparing this with the general equation A1.10, we get

$$\alpha_{M-1} = 1 \qquad \text{A1.15}$$

and $$\beta_{M-1} = \frac{J_M a}{D} \qquad \text{A1.16}$$

with J_M given by for source neutrons

plane source: $c = 0$, $J_M = Q$ (Q neutrons cm^{-2} sec^{-1})

line source: $c = 1$, $J_M = \frac{Q}{2\pi Ma}$ (Q neutrons cm^{-1} sec^{-1})

point source: $c = 2$ $J_M = \frac{Q}{4\pi M^2 a^2}$ (Q neutrons sec^{-1})

For neutrons of all other energies $J_M = 0$, hence

$$\beta_{M-1} = 0 \qquad \text{A1.17}$$

For the outer boundary condition consider the diagram below. The flux at the Nth mesh point, the physical outer boundary is ϕ_N. The extended mesh point is (N+1) and the flux

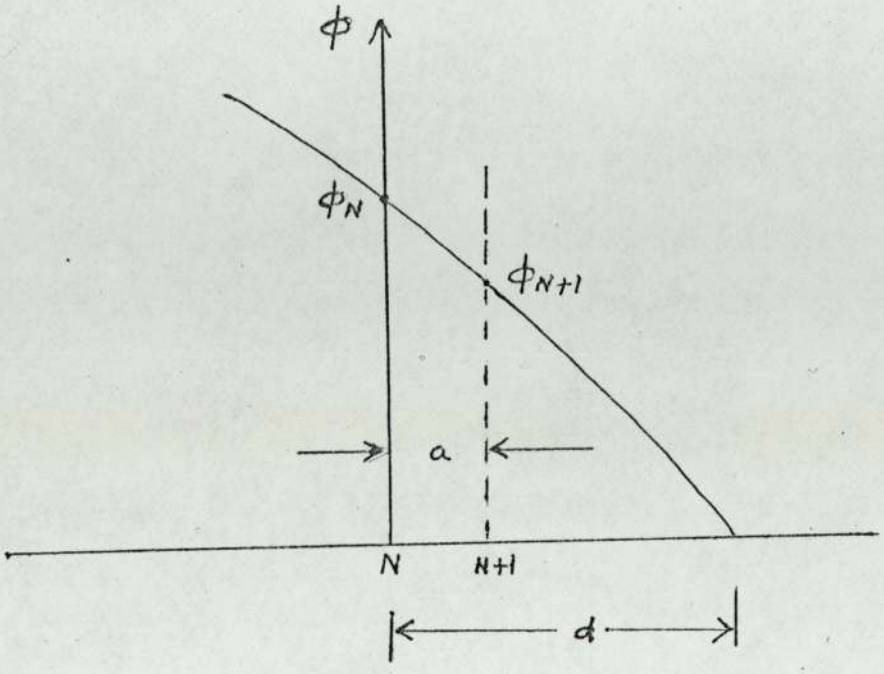

which would follow from the extrapolated curve is ϕ_{N+1}. From the similar triangles we have

$$\frac{\phi_N}{d} = \frac{\phi_{N+1}}{d-a}$$

or $$\phi_{N+1} = \phi_N \left(1 - \frac{a}{d}\right) \qquad \text{Al.18}$$

The general expression Al.9 gives

$$\phi_N = \alpha_N \phi_{N+1} + \beta_N$$

With Al.18 we get, $\phi_N = \alpha_N \phi_N \left(1 - \frac{a}{d}\right) + \beta_N$

$$\therefore \phi_N = \frac{\beta_N}{1 + \frac{a}{d}\alpha_N - \alpha_N} \qquad \text{Al.19}$$

with $d = 0.71 \lambda \text{ tr.} = 2.13D$

This allows the extrapolation distance to be variable with the groups according to different value of D for each group. The

physical boundary is fixed and flux is calculated only at the Nth mesh (equation A1.18).

The program FASTNFLUX was written to calculate flux according to the above scheme and conditions.

COMPUTER PROGRAM DTANGENYLD

(Cf. Art. 5.3.4)

```
'BEGIN' 'COMMENT' DTANGENYLD, DT NEUTRONS LINESHAPE, AVERAGE ENERGY
                  AND RELATIVE YIELD;
'INTEGER' PHN,J;
'REAL' IGN,RDN,AN,SUMN,SUMNEN,AVE;
'REAL''ARRAY' ED,SR,TC,SIG,N,EN,NEN[1:13];
'FOR' J:=1 'STEP'1 'UNTIL'13'DO'
 'BEGIN'
  ED[J]:=READ;
  SR[J]:=READ;
  TC[J]:=READ;
  SIG[J]:=READ;
 'END';
'FOR' PHN:=0 'STEP' 10'UNTIL' 180'DO'
'BEGIN'
     NEWLINE(3);
     WRITETEXT('('       NEUTRON ANGLE=')');
     PRINT(PHN,3,0);
     NEWLINE(2);
     SUMN:=0;
     SUMNEN:=0;
     RDN:= PHN*3.1416/180;
    'FOR' J:=1 'STEP'1 'UNTIL' 13 'DO'
    'BEGIN'
          EN[J]:= 0.08*ED[J]*COS(2*RDN)+0.8*(0.6*ED[J]+17578)+0.8*
                  COS(RDN)*SQRT(0.4*ED[J]*(0.6*ED[J]+17578)*(1-ED[J]
                  *SIN(RDN)*SIN(RDN)/(10*(0.6*ED[J]+17578))));
          IGN:=SQRT(9.9468*(0.5996+17578/ED[J]));
          AN:=((COS(RDN)+SQRT(IGN*IGN-SIN(RDN)*SIN(RDN)))'**'2)/(IGN
                  *SQRT(IGN'**'2-SIN(RDN)*SIN(RDN)));
          N[J]:= 1000*SIG[J]*TC[J]*AN/SR[J];
          PRINT(ED[J],3,1);
          SPACE(3);
          PRINT(EN[J],5,2);
          SPACE(3);
          PRINT(N[J],3,2);
NEWLINE(1);
          NEN[J]:= N[J]*EN[J];
          SUMN:=SUMN+N[J];
          SUMNEN:=SUMNEN+NEN[J];
    'END';
     NEWLINE(2);
     WRITETEXT('('NTRN YIELD=')');
     PRINT(SUMN,0,4);
     AVE:=SUMNEN/SUMN;
     NEWLINE(1);
     WRITETEXT('('AV ENERGY=')');
     PRINT(AVE,0,4);
     'END';
     'END';
```

COMPUTER PROGRAM DTNTAVAIS

(cf. Sec. 5.4.3)

```
'BEGIN' 'COMMENT' DTNTAVANIS, AVERAGE NEUTRON TO ALPHA ANISOTROPY;
'INTEGER' K;
'REAL' PHN,PHAL,RDN,RDAL,SUMY,SUMZ,AVA,USUMY,USUMZ,UAVA;
'REAL' 'ARRAY' ED,NED,IGN,AN,AA,A,AAL,IGAL,Y,Z,N,SIG,SR,UY,UZ[1:13];
PHN:=READ; 'COMMENT' NEUTRON ANGLE;
PHAL:=READ;'COMMENT' ALPHA ANGLE;
RDN:=PHN*3.1416/180;
RDAL:=PHAL*3.1416/180;
WRITETEXT('('NEUTRON ANGLE=')');
PRINT (PHN,3,2);
NEWLINE(1);
WRITETEXT ('('ALPHA ANGLE=')');
PRINT (PHAL,3,2);
'FOR' K:=1 'STEP'1 'UNTIL' 13 'DO'
'BEGIN'
ED[K]:=READ;
SR[K]:=READ;
N[K]:=READ;
SIG[K]:=READ;
NED[K]:= (.5996+17578/ED[K]);
IGN[K]:= SQRT(9.9468*NED[K]);
IGAL[K]:= SQRT(.631R*NED[K]);
AN[K]:= ((COS(RDN)+SQRT(IGN[K]'**'2-SIN(RDN)'**'2))'**'2)/
(IGN[K]*SQRT(IGN[K]'**'2-SIN(RDN)'**'2));
AAL[K]:=((COS(RDAL)+SQRT(IGAL[K]'**'2-SIN(RDAL)'**'2))'**'2)/
(IGAL[K]*SQRT(IGAL[K]'**'2-SIN(RDAL)'**'2));
A[K]:= AN[K]/AAL[K];
Y[K]:= A[K]*N[K]*SIG[K]/SR[K];
Z[K]:=N[K]*SIG[K]/SR[K];
UY[K]:=A[K]*SIG[K]/SR[K];
UZ[K]:=SIG[K]/SR[K];
'END';
SUMY:= ((Y[1]+Y[13])+4*(Y[2]+Y[4]+Y[6]+Y[8]+Y[10]+Y[12])
+2*(Y[3]+Y[5]+Y[7]+Y[9]+Y[11]));
SUMZ:= (Z[1]+Z[13]+4*(Z[2]+Z[4]+Z[6]+Z[8]+Z[10]+Z[12])
+2*(Z[3]+Z[5]+Z[7]+Z[9]+Z[11]));
USUMY:=((UY[1]+UY[13])+4*(UY[2]+UY[4]+UY[6]+UY[8]+UY[10]+UY[12])
+2*(UY[3]+UY[5]+UY[7]+UY[9]+UY[11]));
USUMZ:=((UZ[1]+UZ[13])+4*(UZ[2]+UZ[4]+UZ[6]+UZ[8]+UZ[10]+UZ[12])
+2*(UZ[3]+UZ[5]+UZ[7]+UZ[9]+UZ[11]));
NEWLINE(2);
AVA:=SUMY/SUMZ;
WRITETEXT('('AV ANISOTROPY FOR TRIANGULAR DISTR=')');
PRINT(AVA,2,4);
UAVA:=USUMY/USUMZ;
NEWLINE(2);
WRITETEXT('('AV ANISOTROPY FOR UNIFORM DISTR=')');
PRINT(UAVA,2,4);
'END';
```

COMPUTER PROGRAM FOILSNACT

(cf. Art. 5.7.3)

```
    'BEGIN' 'COMMENT' SATURATED NORMALISED ACTIVITY OF FOILS AND ERRORS;
    'INTEGER' NF,F,TBG,TC,RR;
   'REAL' RADT,DELBG,BG,DELTC,K,L,HLF,LAMDA,QREF,QAVG,S,SL,CPM,M,Z,R,DR,
          SNACT,SIGMA,SIGSQ,FRDV,PCDV,RMFLX,SIGRF,RFMAX,RFMIN,
WTME,SDSQ,SNMAX,SNMIN;
        'COMMENT' TBG IS TOTAL BACKGROUND IN DELBG MINS, F IS FTH FOIL,
          NF IS TOTAL NO OF FOILS, TC IS OBSERVED COUNT IN DELTC MINS,
          RR IS REPEAT INSTRUCTION, RADT IS IRRADIATION TIME IN MINS,
         K IS COUNTING EFFICIENCY AS FRACTION, HLF IS HALFLIFE OF FOIL,
          QNOR AND QAVG ARE NORMALISATION AND EXPT SOURCE STRENGTH,
          CPM IS TRUE COUNT PER MIN, Z IS ISOTOPE FRACTION, M IS MASS
          OF THE FUIL IN GMS, SNACT IS SATURATED NORMALISED ACTIVITY,
          SIGMA IS STANDARD DEV OF SNACT, STDV THAT FOR CPM, PCDV IS
        THAT OF BOTH IN PERCENT, RMFLX IS 4PI*SNACT*R*R, R IS DISTANCE
          OF FOIL FROM TARGET, DR IS ERROR IN R, SNMAX SNMIN ETC ARE
          CORRESPONDING LIMIT VALUE WITH ERRORS;
         'COMMENT' SUPPLY DATA IN ORDER OF HLH,NF,RADT,QNOR,QAVG,Z,K,
           TBG,DELBG,DR, THEN COLUMNS OF F,TC,DELTC,WTME,M,R,THEN RR=99
           IF THERE IS ANOTHER DATA SET;
     REPEAT:
      HLF:=READ;
      NF:=READ;
      RADT:=READ;
      QREF:=READ;
      QAVG:=READ;
Z:=READ;
    K:=READ;
    TBG:=READ;
    DELBG:=READ;
    BG:=TBG/DELBG;
    DR:=READ;
    NEWLINE(4);
    WRITETEXT('('HALFLIFE=')');
    PRINT(HLF,4,2);
    NEWLINE(1);
    WRITETEXT('('IRRADIATION TIME=')');
    PRINT(RADT,4,2);
    NEWLINE(1);
    WRITETEXT('('REF SOURCE=')');
    PRINT(QREF,0,4);
    NEWLINE(1);
    WRITETEXT ('('EXPT SOURCE=')');
    PRINT(QAVG,0,4);
     S:= QREF/QAVG;
NEWLINE(1);
WRITETEXT ('('QREF/QAVG=')');
PRINT(S,3,3);
NEWLINE(1);
WRITETEXT('('K=')');
PRINT(K,1,4);
    LAMDA:=0.693/HLF;
     L:=1/(1-EXP(-LAMDA*RADT));
    SL:=S*L;
     NEWLINE(2);
WRITETEXT ('('''('2S')'F'('4S')'R'('6S')'CPM'('7S')'SNACT'('9S')'
SNMAX'('7S')'
              SNMIN'('5S')'SIGSQ'('7S')'PCDV'('9S')'RMFLX'('7S')'
```

```
      C1:=ACTO1*EXP(-LMD1*WTM);
      C2:=ACTO2*EXP(-LMD2*WTM);
      FRC1:=C1/(C1+C2);
      CPM1:=FRC1*TRC;
      TC1BG:=(CPM1+BG)*DELTC;
      TC1:=CPM1*DELTC;
      CPM2:=TRC-CPM1;
      PC2:=(CPM2/TRC)*100;
      PRINT(F,2,0);
      PRINT(TC1BG,6,0);
      PRINT(TC1,4,2);
      PRINT(DELTC,3,1);
      PRINT(WTM,3,2);
      PRINT(FRC1,1,4);
      PRINT(PC2,2,2);
      SPACE(3);
      PRINT(TC,4,0);
      NEWLINE(2);
    'END';
    RR:=READ;
    'IF'RR=99'THEN''GOTO'REPEAT;
'END';
```

COMPUTER PROGRAM EFFNEUTSCE

(cf. Art. 5.7.4.)

```
'BEGIN' 'COMMENT' PYSTF017,EFFNEUTSCE;
'INTEGER' M,N;
'REAL' DT,G,QREF,TH,L,QINF,QAVG,T,NORM;
N:=READ;    'COMMENT' N IS NUMBER OF TIME STEPS;
DT:=READ;   'COMMENT' DT IS STEP LENGTH IN SECONDS;
G:=READ;    'COMMENT' G RELATES ALPHA COUNT TO SOURCE STRENGTH;
QREF:=READ; 'COMMENT' QREF IS REFERENCE SOURCE STRENGTH;
NEWLINE(1);
WRITETEXT('('QREF=')');
PRINT(QREF,0,4);
'BEGIN'
'REAL' 'ARRAY' ALPHA[1:N]; 'COMMENT' TOTAL ALPHA COUNTS IN TIME DT;
'FOR' M:=1 'STEP' 1 'UNTIL' N 'DO' ALPHA[M]:=READ;
AGAIN:
TH:=READ; 'COMMENT' TH IS HALF LIFE IN SECONDS;
'IF' TH<0 'THEN' 'GOTO' FINISH;
L:=0.693/TH;
QINF:=0;
'FOR' M:=1 'STEP' 1 'UNTIL' N 'DO'
QINF:=QINF+ALPHA[M]*EXP(-L*DT*(N-M));
QINF:=QINF*G*(1-EXP(-L*DT))/DT;
QAVG:=QINF/(1-EXP(-L*DT*N));
T:=DT*N;
NORM:=QREF/QINF;
NEWLINE(3);
WRITETEXT('('HALFLIFE=')');
PRINT(TH,6,1);
NEWLINE(1);
WRITETEXT('('QINF=')');
PRINT(QINF,0,4);
NEWLINE(1);
WRITETEXT('('QAVG=')');
PRINT(QAVG,0,4);
NEWLINE(1);
WRITETEXT('('TIME=')');
PRINT(T,6,1);
NEWLINE(1);
WRITETEXT('('NORM=')');
PRINT(NORM,0,4);
'GOTO' AGAIN;
'END';
FINISH:
'END';
```

COMPUTER PROGRAM SUBSECACT

(cf. Art. 6.8.4)

```
'BEGIN' 'COMMENT' SUBSECACT, SUBTRACTION OF SECONDARY ACTIVITY;
  'INTEGER' NF,F,TBG,TC,RR;
  'REAL' RADT,DELBG,BG,      DELTC,TH1,TH2,LMD1,LMD2,SIG1,SIG2,M1,M2,
   K1,K2,ACTO1,ACTO2,WTM,C,C1,C2,FRC1,TRC,CPM1,CPM2,PC2,TC1,TC1BG;
       'COMMENT'NF IS TOTAL NO OF FOILS F, TBG IS TOTAL BACKGROUND
        COUNTS IN DELBG MINS, TH1 HALFLIFE OF ACTIVITY  USED,
        TH2 THAT OF SECONDARY ACTIVITY, SIGS ARE ACTIVATION CROSS
        SECTIONS, MS MASS RATIOS,RADT IS RADIATION TIME,TC IS
        COMBINED COUNTS   OBSERVED IN DELTC MINS,K5 ARE DECAY FRACS;
'COMMENT' SUPPLY DATA IN ORDER OF TH1,TH2,M1,M2,SIG1,SIG2,K1,K2RADT,TBG,
        DELBG,NF,THEN COLUMNS OF F,TC,DELTC,WTM,THEN RR;
   REPEAT:
    TH1:=READ;
    TH2:=READ;
    M1:=READ;
    M2:=READ;
    SIG1:=READ;
    SIG2:=READ;
    K1:=READ;
    K2:=READ;
    RADT:=READ;
    TBG:=READ;
    DELBG:=READ;
    NF:=READ;
    WRITETEXT('('TOTAL'('1S')'BG=')');
    PRINT(TBG,4,0);
    NEWLINE(1);
    WRITETEXT('('DEL'('1S')'BG=')');
    PRINT(DELBG,4,2);
    NEWLINE(1);
    WRITETEXT('('HALFLIFE=')');
    PRINT(TH1,3,2);
    WRITETEXT('('MINUTES')');
    NEWLINE(1);
    WRITETEXT('('NF=')');
    PRINT(NF,3,0);
    NEWLINE(1);
    WRITETEXT('('RADTME=')');
    PRINT(RADT,4,2);
    NEWLINE(2);
    BG:=TBG/DELBG;
    LMD1:=0.693/TH1;
    LMD2:=0.693/TH2;
    ACTO1:=SIG1*M1*(1-EXP(-LMD1*RADT))*K1;
    ACTO2:=SIG2*M2*(1-EXP(-LMD2*RADT))*K2;
  WRITETEXT('('F'('6S')'TC1BG'('7S')'DELTC'('4S')'WTME'('6S')
'TC1'('4S')'FRC1'
            ('6S')'PC2'('6S')'TC'('2C')'')');
    'FOR' F:=1 'STEP' 1 'UNTIL' NF 'DO'
    'BEGIN'
      F:=READ;
      TC:=READ;
      DELTC:=READ;
      WTM:=READ;
      C:=TC/DELTC;
      TRC:=C-BG;
```

```
            RFMAX'('7S')'RFMIN'('2C')''')';
  'FOR' F:=1 'STEP'1 'UNTIL'NF 'DO' 'BEGIN'
    F:=READ;
    TC:=READ;
    DELTC:=READ;
    WTME:=READ;
    M:=READ;
    R:=READ;
    CPM:=TC/DELTC-BG;
SNACT:=(SL*CPM*EXP(LAMDA*WTME))/(K*M*Z);
    SDSQ:=TC/(DELTC*DELTC)+BG/DELBG;
    FRDV:=SQRT(SDSQ)/CPM;
    SIGMA:=FRDV*SNACT;
    SNMAX:=SNACT+SIGMA;
    SNMIN:=SNACT-SIGMA;
    SIGSQ:=SIGMA*SIGMA;
    PCDV:=FRDV*100;
    RMFLX:=SNACT*R*R*12.5664;
    SIGRF:=RMFLX*FRDV;
    RFMAX:=RMFLX+SIGRF;
    RFMIN:=RMFLX-SIGRF;
    PRINT(F,2,0);
    PRINT(R,2,1);
    PRINT(CPM,4,2);
    PRINT(SNACT,6,2);
    PRINT(SNMAX,6,2);
    PRINT(SNMIN,6,2);
    PRINT(SIGSQ,6,2);
    PRINT(PCDV,3,5);
    SPACE(1);
    PRINT(RMFLX,8,0);
    PRINT(RFMAX,0,3);
    SPACE(1);
    PRINT(RFMIN,0,3);
    NEWLINE(2);
  'END';
    PAPER THROW;
    RR:=READ;
    'IF'RR=99 'THEN''GOTO'REPEAT;
    'END';
```

COMPUTER PROGRAM CALROTCEFF

(cf. Art. 6.9.3)

```
'BEGIN'
'INTEGER' M, MMAX, N, NMAX;
'REAL' DELD, D, Z, CF;
NMAX := READ;
'COMMENT' NMAX IS TOTAL STEPS OF THE HALF CIRCLE FOR NUMERICAL INT;
MMAX := READ;
'COMMENT' MMAX IS TOTAL NUMBER OF STEPS FOR D;
DELD := READ;
'COMMENT' DELD IS  STEPS OF D, DELD*MMAX MUST BE LESS THAN 1;
'BEGIN'
'REAL' 'ARRAY' SUM[0:MMAX];
'FOR' M:=0 'STEP' 1 'UNTIL' MMAX 'DO'
SUM[M]:=0;
'FOR' N:=1 'STEP' 1 'UNTIL' NMAX 'DO'
'BEGIN'
 Z:= COS(1.5708*(2*N-1)/NMAX);
'FOR' M:=0 'STEP' 1 'UNTIL' MMAX 'DO'
'BEGIN'
D:= DELD*M;
SUM[M]:= SUM[M]+1/(1+D*D+2*D*Z);
'END';
'END';
'FOR' M:=0 'STEP'1'UNTIL' MMAX 'DO'
'BEGIN'
D:= DELD*M;
CF:= SUM[M]/SUM[0];
NEWLINE(1);
PRINT(D,1,4);
PRINT(CF,1,6);
'END';
'END';
'END';
```

COMPUTER PROGRAM FASTNFLUX

(cf. Art. 8.2.3)

```
'BEGIN' 'COMMENT' PYSTF017,ZFASTNFLUX,MULT1GROUP FINITE DIFFERENCE
      CALCULATIONS FOR FAST NEUTRON FLUXES;
'INTEGER' C,G,I,J,K,M,N,NN,NMAT,FN,NSTOP,SCN,ITN,NFOIL;
'REAL' ND,DR,O,AA,BB,Z,Y,W;
SELECT OUTPUT (0);
G:=READ; 'COMMENT' NUMBER OF ENERGY GROUPS;
NMAT:=READ; 'COMMENT' NUMBER OF MATERIALS;
DR:=READ; 'COMMENT' MESH INTERVAL;
M:=READ; 'COMMENT' INNER BOUNDARY AT MDR;
N:=READ; 'COMMENT' OUTER BOUNDARY AT NDR;
NN:=((N-M+1)'/'10)*10+M-1;
NFOIL:=READ; 'COMMENT' NUMBER OF DETECTOR FOILS;
'BEGIN'
'REAL' 'ARRAY' SFIS,SCAP,STR,SEL,SINT,MU,NU,FIS,NUF,CAP,TR,EL,REM,X,SC,
            MSC,D[1:G],P[1:G,1:G],
            IN[1:G-1,2:G],F[1:G,M:N],A,B[M-1:N],SCE[M:N],
            ACT[M:N],ATWT[1:NFOIL],SIGACT[1:NFOIL,1:G];
'FOR' I:=1 'STEP' 1 'UNTIL' G 'DO'
'BEGIN'
            SC[I]:=0;
            MSC[I]:=0;
            FIS[I]:=0;
            NUF[I]:=0;
            X[I]:=READ;
      CAP[I]:=0;
      TR[I]:=0;
      EL[I]:=0;
      REM[I]:=0;
'END';
'FOR' I:=1 'STEP' 1 'UNTIL' G-1 'DO'
'FOR' J:=I+1 'STEP' 1 'UNTIL' G 'DO'
IN[I,J]:=0;
            FN:=READ; 'COMMENT' 1=FISSION,0=NO FISSION;
            NSTOP:=READ; 'COMMENT' NO OF ITERATIONS,IF FN=0,NSTOP=1;
'FOR' K:=1 'STEP' 1 'UNTIL' NMAT 'DO'
'BEGIN'
      ND:=READ; 'COMMENT' NUMBER DENSITY;
      'FOR' I:=1 'STEP' 1 'UNTIL' G 'DO'
      'BEGIN'
            MU[I]:=READ; 'COMMENT' MEAN SCATTERING COSINE;
            NU[I]:=READ; 'COMMENT' NEUTRONS PER FISSION;
            SFIS[I]:=READ; 'COMMENT' MICROSCOPIC FISSION;
            STR[I]:=READ; 'COMMENT' MICROSCOPIC TRANSPORT;
            SEL[I]:=READ; 'COMMENT' MICROSCOPIC ELASTIC;
            SCAP[I]:=READ; 'COMMENT' MICROSCOPIC CAPTURE;
            SINT[I]:=READ; 'COMMENT' MICROSCOPIC INELASTIC TOTAL;
            'FOR' J:=I 'STEP' 1 'UNTIL' G 'DO'
            P[I,J]:=READ; 'COMMENT' INELASTIC PROBABILITIES;
      'END';
      'FOR' I:=1 'STEP' 1 'UNTIL' G 'DO'
      'BEGIN'
            CAP[I]:=CAP[I]+SCAP[I]*ND;
AA:=(STR[I]-SINT[I]-SCAP[I]-SFIS[I])*ND;
            BB:=AA/(1-MU[I]);
            TR[I]:=TR[I]+AA;
            SC[I]:=SC[I]+BB;
```

```
            MSC[I]:=MSC[I]+BB*MU[I];
            AA:=SFIS[I]*ND;
            FIS[I]:=FIS[I]+AA;
            NUF[I]:=NUF[I]+AA*NU[I];
            EL[I]:=EL[I]+SFL[I]*ND;
            REM[I]:=REM[I]+SINT[I]*ND*(1-P[I,I]);
    'END';
    'FOR' J:=1 'STEP' 1 'UNTIL' G-1 'DO'
    'FOR' J:=I+1 'STEP' 1 'UNTIL' G 'DO'
    IN[I,J]:=IN[I,J]+SINT[I]*ND*P[I,J];
'END';
'FOR' I:=1 'STEP' 1 'UNTIL' G 'DO'
'BEGIN'
    REM[I]:=REM[I]+EL[I]+CAP[I]*FIS[I];
    MU[I]:=MSC[I]/SC[I];
Y:=REM[I]/SC[I];
W:=0.21;
AA:=0.0;
'FOR' W:=W+0.05 'WHILE' AA 'LE' 1 'DO'
'BEGIN'
Z:=SQRT(Y/W);
AA:=EXP(2*Z*(1+3*W*MU[I])/(1+3*W*MU[I]*(1+Y)))*(1+Y-Z)/(1+Y+Z);
BB:=W-0.06;
'END';
W:=BB;
AA:=0.9;
'FOR' W:=W+0.01 'WHILE' AA 'LE' 1 'DO'
'BEGIN'
Z:=SQRT(Y/W);
AA:=EXP(2*Z*(1+3*W*MU[I])/(1+3*W*MU[I]*(1+Y)))*(1+Y-Z)/(1+Y+Z);
BB:=W-0.011;
'END';
W:=BB;
AA:=0.9;
'FOR' W:=W+0.001 'WHILE' AA 'LE' 1 'DO'
'BEGIN'
Z:=SQRT(Y/W);
AA:=EXP(2*Z*(1+3*W*MU[I])/(1+3*W*MU[I]*(1+Y)))*(1+Y-Z)/(1+Y+Z);
BB:=W-0.001;
'END';
D[I]:=BB/SC[I];
'END';
'FOR' I:=1 'STEP' 1 'UNTIL' G 'DO'
'BEGIN'
NEWLINE(1);
PRINT(I,2,0);
PRINT(NUF[I],1,6);
PRINT(FIS[I],1,6);
PRINT(TR[I],1,6);
PRINT(EL[I],1,6);
PRINT(REM[I],1,6);
PRINT(SC[I],1,6);
PRINT(MU[I],2,3);
PRINT(D[I],1,6);
PRINT((2.13*D[I]),1,6);
'END';
NEWLINE(1);
'FOR' I:=1 'STEP' 1 'UNTIL' G-1 'DO'
'FOR' J:=I+1 'STEP' 1 'UNTIL' G 'DO'
'BEGIN'
```

```
PRINT(IN[I,J],1,6);
NEWLINE(1);
'END';
'FOR' I:=1 'STEP' 1 'UNTIL' NEOIL 'DO'
'BEGIN'
      ATWT[I]:=READ;
      'FOR' J:=1 'STEP' 1 'UNTIL' G 'DO' SIGACT[I,J]:=READ;
'END';
NEXT:
SELECT OUTPUT (0);
C:=READ; 'COMMENT' SLAB 0, CYLINDER 1, SPHERE 2;
'IF' C<0 'THEN' 'GOTO' FINAL;
NEWLINE(3);
WRITETEXT('('C=')');
PRINT(C,2,0);
A[M-1]:=1;
SCN:=READ; 'COMMENT' GR1 FLUX 0=CALC 1=READ 2=EXP REM CALC;
WRITETEXT('('SOURCE=')');
PRINT(SCN,2,0);
'IF' SCN=0 'THEN'
'BEGIN'
      Q:=READ;
      I:=1;
'END';
'IF' SCN=1 'THEN'
'BEGIN'
      'FOR' J:=M 'STEP' 1 'UNTIL' N 'DO' F[1,J]:=READ;
      I:=2;
'END';
'IF' SCN=2 'THEN'
'BEGIN'
Q:=READ;
AA:=READ;  'COMMENT' GR1 EXPONENTIAL REMOVAL CROSS SECTION;
'FOR' J:=M 'STEP' 1 'UNTIL' N 'DO'
'BEGIN'
'IF' C=0 'THEN' F[1,J]:=Q*EXP(-AA*DR*(J-M));
'IF' C=1 'THEN' F[1,J]:=Q*EXP(-AA*DR*(J-M))/(6.284*DR*J);
'IF' C=2 'THEN' F[1,J]:=Q*EXP(-AA*DR*(J-M))/(12.568*DR*DR*J*J);
'END';
I:=2;
'END';
ITN:=1;
ITERATE:
'IF' I=1 'THEN'
'BEGIN'
      'IF' C=0 'THEN' B[M-1]:=Q*DR/D[1];
      'IF' C=1 'THEN' B[M-1]:=Q/(6.284*M*D[1]);
      'IF' C=2 'THEN' B[M-1]:=Q/(12.568*DR*M*M*D[1]);
      'FOR' J:=M 'STEP' 1 'UNTIL' N 'DO' SCE[J]:=0;
'END';
AGAIN:
'IF' I>1 'THEN'
'BEGIN'
      B[M-1]:=0;
      'FOR' J:=M 'STEP' 1 'UNTIL' N 'DO'
      'BEGIN'
            SCE[J]:=EL[I-1]*F[I-1,J];
            'FOR' K:=1 'STEP' 1 'UNTIL' I-1 'DO'
            SCE[J]:=SCE[J]+IN[K,I]*F[K,J];
            'IF' FN=1 'AND' ITN >1 'THEN'
```

```
            'FOR' K:=1 'STEP' 1 'UNTIL' G 'DO'
            SCE[J]:=SCE[J]+X[I]*NUF[K]*F[K,J];
        'END';
'END';
'FOR' J:=M 'STEP' 1 'UNTIL' N 'DO'
'BEGIN'
A[J]:=(2*J+C)/(2*J*(2+REM[I]*DR*DR/D[I])-(2*J-C)*A[J-1]);
B[J]:=A[J]*((2*J-C)*B[J-1]+2*J*SCE[J]*DR*DR/D[I])/(2*J+C);
'END';
F[I,N]:=B[N]/(1+A[N]*(DR/(2.13*D[I])-1));
'FOR' K:=N-1 'STEP' -1 'UNTIL' M 'DO'
        F[I,K]:=A[K]*F[I,K+1]+B[K];
I:=I+1;
'IF' I 'LE' G 'THEN' 'GOTO' AGAIN;
ITN:=ITN+1;
'IF' ITN 'LE' NSTOP 'THEN'
'BEGIN'
        'IF' SCN=0 'THEN' I:=1;
        'IF' SCN>0 'THEN' I:=2;
        'GOTO' ITERATE;
'END';
'FOR' I:=1 'STEP' 1 'UNTIL' G 'DO'
'BEGIN'
NEWLINE(2);
WRITETEXT('('GROUP=')');
PRINT(I,2,0);
NEWLINE(1);
NN:=((N-M+1)'/'10)*10+M-1;
'FOR' J:=M 'STEP' 10 'UNTIL' NN 'DO'
'BEGIN'
        'FOR' K:=J 'STEP' 1 'UNTIL' J+9 'DO'
        PRINT(F[I,K],0,3);
        NEWLINE(1);
'END';
J:=NN;
'FOR' J:=J+1 'WHILE' J 'LE' N 'DO'
PRINT(F[I,J],0,3);
'END';
'FOR' K:=1 'STEP' 1 'UNTIL' NFOIL 'DO'
'BEGIN'
'FOR' J:=M 'STEP' 1 'UNTIL' N 'DO'
'BEGIN'
ACT[J]:=0;
'FOR' I:=1 'STEP' 1 'UNTIL' G 'DO' ACT[J]:=ACT[J]+F[I,J]*SIGACT[K,I];
ACT[J]:=36.15*ACT[J]/ATWT[K];
'END';
NEWLINE(2);
WRITETEXT('('FOIL=')');
PRINT(ATWT[K],3,4);
NEWLINE(1);
'FOR' I:=M 'STEP' 10 'UNTIL' NN 'DO'
'BEGIN'
'FOR' J:=I 'STEP' 1 'UNTIL' I+9 'DO' PRINT(ACT[J],0,3);
NEWLINE(1);
'END';
J:=NN;
'FOR' J:=J+1 'WHILE' J 'LE' N 'DO' PRINT(ACT[J],0,3);
'END';
'GOTO' NEXT;
FINAL:
'END';
'END';
```

LIST OF REFERENCES

1. J. M. Blatt and V. F. Weisskopf;
   "Theoretical Nuclear Physics", John Wiley,
   New York, (1952)

2. D. J. Hughes
   "Neutron Cross Sections", Pergamon Press, (1957)

3. M. A. El-Guebely and M. El-Nadi;
   Proc.2nd Geneva Conf. Vol.14, United Nations, (1958)

4. M. Borman
   Nuclear Physics, 65, 257 (1965)

5. S. T. Butler.
   Phys.Rev., 106, 272 (1957)

6. S. T. Butler et al.
   Phys.Rev., 112, 1227 (1958)

7. W. Hauser and H. Feshbach
   Phys. Rev., 87, 366 (1952)

8. L. Wolfstein
   Phys. Rev., 82, 690 (1951)

9. P. A. Moldauer
   Phys. Rev., 123, 968 (1961);
   Phys. Rev., 129, 754 (1963)

10. Björklund and H. Feshbach
    Phys. Rev., 109, 1295 (1958)

11. J. C. Hopkins and M. G. Silbert
    Nuclear Science and Engineering, 19, 431 (1964)

12. A. M. Weinberg and E. P. Wigner
    "The Physical Theory of Neutron Chain Reactors"
    The University of Chicago Press,(1958)

13. Barschall et al.
    Phys. Rev., 72, 881 (1947);
    Phys. Rev., 72, 875 (1947)

14. H. F. Dunlop and R. N. Little
Phys. Rev., 60, 693 (1941)

15. B. T. Feld
Phys. Rev., 75, 1115, (1949)

16. E. R. Graves and L. Rosen
Phys. Rev., 89, 343 (1953)

17. P. H. Stelson and C. Goodman
Phys. Rev., 82, 69 (1951)

18. B. G. Whitmore
Phys. Rev., 92, 654 (1953)

19. E. S. Troubetzkoy
NDA Report 2111-3, Vol.C, (1959)

20. K. Parker
"Neutron Cross Section of ^{238}U in the energy range 1 Kev - 15 Mev".
AERE Report No. O-79/63, Part 1, (1962)

21. L. Cranberg and S. Levin
Phys. Rev., 103, 343, (1956)

22. H. H. London, et al.
Phys. Rev., 112, 1192, (1958)

23. J. H. Coon, et al.
Phys. Rev., 111, 251, (1958)

24. L. Rosen and L. Stewart
Phys. Rev., 107, 824, (1957)

25. J. T. Prud'homme et al.
Phys. Rev., 118, 1059, (1960)

26. G. C. Bonazolla, et al.
Nuclear Physics, 51, 353, (1964)

27. W. G. Davey,
Nuclear Science and Energy, 39, 337, (1970)

28. J. Y. Barre, et al.
Proc.of the Symp.Physics of Fast Reactors,
BNES, London (1969), Paper 1.15

29. H. Paulsen and A. Liskien
Proc. of Radiation Measurements in Nuclear Power,
Institute of Physics and Physical Society, (1966),
page 357.

30. W. E. Kinney and F. G. Percy
Nuclear Science and Engg., 40, 396, (1970)

31. J. R. Lamarsh
"Introduction to Nuclear Reactor Theory"
Addison-Wesley, (1966)

32. R. H. Stokes et al.
Proc.2nd Geneva Conf. 15, 179, (1958)

33. N. Bohr and J. A. Wheeler
"Mechanism of Nuclear Fission",
Phys. Rev., 56, 426, (1939)

34. W. J. Swiatecki
Proc. Symp. on Physics and Chemistry of Fission, 1, 3,
IAEA, Vienna, (1965)

J. R. Nix and W. J. Swiatecki
"Studies in the Liquid Drop Theory of Nuclear Physics"
Nuclear Physics, 71, 1, (1965)

35. Porter and Thomas
Phys. Rev., 104, 483, (1956)

36. E. Vogt
Phys. Rev., 112, 203, (1958)

37. Aage Bohr
Proc. 1st Geneva Conf., 2, 220, (1956)

38. M. F. James
J.of Nuclear Energy, 23, 517, (1969)

39. W. W. Havens and E. Melkonian
Proc.2nd Geneva Conf., 15, 99, (1958)

40. J. A. Farrell
Phys. Rev., 165, 1371, (1968)

41. D. W. Bergen and M. G. Silbert
Phys. Rev., 166, 1174, (1968)

42. M. S. Moore et al.
Phys. Rev., 135, B945, (1964)

43. R. L. Henkel
"Fission by Fast Neutrons"
in Fast Neutron Physics, Part II, Marrion and Fowler (Ed.)
Interscience Publishers, (1963)

44. S. P. Kalinin and V. M. Pankratov
Proc.2nd Geneva Conf., 16, 136 (1958)

45. A. Hemmendinger
Proc.2nd Geneva Conf., 15, 663

46. W. D. Allen and R. L. Henkel
Progress in Nuclear Energy, Ser.I, 2, (1957)

47. P. H. White
J.of Nuclear Energy, 19, 325, (1965)

48. P. H. White and G. P. Warner
J.of Nuclear Energy, 2, 671, (1967)

49. V. M. Pankratov
J.of Nuclear Energy, 18, 215, (1964)

50. W. B. Lowenstein and D. Okrent
"The Physics of Fast Power Reactors"
Proc.2nd Geneva Conf. I.A.E.A., 637, (1958)

51. B. E. Watt
Phys. Rev., 87, 1037, (1952)

52. L. Ganberg et al.
Phys. Rev., 103, 662, (1956)

53. T. W. Bonner et al.
Phys. Rev., 87, 1032, (1952)

54. National Bureau of Standards (U.S.)
Handbook 63, pp.78, (1967)

55. R. B. Leachman
Phys. Rev., 101, 1005, (1956)

56. Usachev and Trubitsyn
As quoted by Bondarenko et al., Reference 57

57. I. I. Bondarenko et al.
Proc.2nd Geneva Conf., 15, 353, (1958)

58. M. Soleilhac et al.
J.of Nuclear Energy, 23, 257, (1969)

59. J. S. Fraser and J. C. D. Milton
Annual Review of Nuclear Science, 16, (1966)

60. J. Terrell
Phys. Rev., 113, 527, (1959)

61. R. B. Leachman
Proc.2nd Geneva Conf. 15, 331 (1958)

62. R. J. Doyas and R. J. Howerton
"Incidence Energy Dependence of Fission Spectra"
Rept. UCRL-50755, (1969)

63. L. G. Alexander
Annual Review of Nuclear Science, 14, (1964)

64. P. H. White
J.of Nuclear Energy, 16, 261, (1962)

65. K. W. Allen et al.
J.of Nuclear Energy, 14, 100, (1961)

66. J. W. Weale et al.
J.of Nuclear Energy, 14, 91, (1961)

67. J. Thomas
Proc.of the Symp.on Neutron Detection, Dosimetry and Standardization,
Harwell, 1962
IAEA, Vienna, 1, 215, (1963)

68. R. A. Karam and T. F. Parkinson
Trans.of Ann.Nucl.Soc., 6, 239, (1963)

69. P. W. Benjamin et al
"The Analysis of Recoil Proton Spectra"
AERE Report No. O-9/68.

70. A. Sayres
Rev.Sci.Instr., 35, 431, (1964)

71. J. C. Hopkins and B. C. Diven
Proc.of Seminar on the Physics of Fast and Int. Reactors,
IAEA, Vienna, 1, 112, (1961)

72. Y. Furuta et al.
Nucl.Intr. and Meth., 84, 269, (1970)

73. W. R. Barrus and V. V. Verbinski
Proc.of the Special Session on Fast Neutron Spectroscopy
Ann.Nucl.Soc.Shielding Group, California, (1964)

74. V. V. Verbinski et al.
Proc.of the Conf.on Radiation Measurements in Nuclear Power
Institute of Physics and Physical Society, London, pp.220 (1966)

75. D. Storminger
Proc.of Symposium on Neutron Detection, Dosimetry and Standardization, Harwell, 1962,
IAEA, Vienna, 1, 385, (1963)

76. L. Rosen
Proc.of the 1st Geneva Conf., 4, 97, (1955)

77. W. C. Redman and J. H. Roberts
Proc.2nd Geneva Conf., 12, 72, (1958)

78. H. H. Barschall et al.
Rev.of Mod.Phys., 24, 1, (1952)

79. L. K. Burton and A. E. Sonch
Proc.of the Symposium on Neutron Detection, Dosimetry and Standardization, Harwell 1962
IAEA Vienna, 1, 521, (1963)

80. Roger Wallace
Proc.of the Symposium on Neutron Detection, Dosimetry and Standardization, Harwell, 1962
IAEA, Vienna, 1, 584, (1963)

81. R. L. Heath
"Scintillation Spectrometry: Gamma-ray Spectrum Catalogue"
IDO-1688-1, TID-4500, USAEC, (1964)

82. R. D. Smith et al.
Proc.3rd Geneva Conf. 1964, Paper A/Conf/28/P/166

83. H. Borgwaldt et al.
Proc.Symposium on Neutron Detection, Dosimetry and Standardization, Harwell, 1, 399, (1962)

84. "Protection against Neutron Radiation up to 30 Million Electron Volts"
National Bureau of Standards Handbook 63,
US Govt.Printing Press, Washington, April, 1967

85. J. Hacke
Kerntechnik 11, 193, (April, 1969)

86. Technical Bulletin, Societe Anonyme de Machines Electrostatiques
Grenoble, France (June, 1961)

87. J. L. Fowler and J. E. Brolley
Revs.of Mod.Physics, 28, 2(1956), 103

88. J. B. Marion and J. L. Fowler
"Fast Neutron Physics"
Part I, Ch.I.C., Interscience Publishers Inc. N.Y. (1966)

89. J. Benveniste and J. Zenger
"Information on the Neutrons Produced in the $H^3(d,n)He^4$ Reaction"
UCRL-4266, University of California, (1954)

90. I. Kaplan
"Nuclear Physics"
Addison-Wesley Publishing Company, (1964)

91. W. R. Arnold et al.
Phys.Rev., 93, 3(1954), 483

92. J. P. Conner et al.
Phys. Rev., 88, 3(1952), 468

93. "Catalogue of Radioactive Products"
The Radiochemical Centre, Amersham, England, pp.160
Oct.1965

94. J. Chadwick
Radiochemical Centre, Amersham
Private Communication, Oct.1968

95. E. M. Gunnerson and G. James
Nuclear Instruments and Methods, 8, 173, (1960)

96. J. Benveniste et al.
"The Problem of Measuring the Absolute Yield of 14-Mev Neutrons by Means of an Alpha Counter"
UCRL 5619, (1959)

97. E. W. Saker and J. D. L. H. Wood
"Calculated Neutron Yield from Titanium - Tritium Targets under Deuteron Bombardment"
S.E.R.L. Technical Report 17, 61, (1958)

98. S. D. Warshaw
Phys. Rev., 76, 1759, (1949)

99. Reynolds et al.
Phys. Rev., 92, 742, (1953)

100. G. Dearnaley
"Progress in Nuclear Physics"
9, Ch.2., (1964)

101. Fieldhouse
Proc.Symp.on Radiation Measurement in Nuclear Power
Barkeley Nuclear Laboratories (1966), pp.327.

102. R. J. Trebilcock
"Proc.of the Symp.on Neutron Detection, Dosimetry and Standardization"
Harwell 1962
IAEA, 1, 565, (1963)

103. J. R. Bell and J. K. Mills
Document No.NARF-61-18T, MR-N-279, of Nuclear Aerospace Research Facility, US Airforce, (1961)

104. G. S. Hurst et al.
Review of Sci.Instrum., 27, 3,(1956), 153

105. "Nuclear Energy Handbook"
Edited by H. Etherington, McGraw Hill,(1958), Section 2.

106. J. F. Stehn
"Table of Radioactive Nuclides"
Nucleonics, 186, (Nov.1960)

107. R. C. Barrall and W. N. McElroy
Proc.of Symp.on Radiation Accidents,
IAEA Vienna, 251, (1965)

108. C. M. Lederer et al.
"Table of Isotops"
John Wiley, (1967)

109. A. M. Bressesti et al.
Nucl.Sc.Eng. 29, 7-14 (1967)

110. W. L. Zijp
"Review of Activation Methods for the Determination of Fast Neutron Spectra"
RCN-37, Reactor Centrum, Nederland (1965)

111. A. Paulsen and H. Liskien
Rep.EURATOM, EUR 119.e Vol.1 & 2, (1962)

112. BNL-325; Second Edition (1958)
2nd Supplement to the Second Edition, (1966)

113. H. Liskien and A. Paulsen
J. Nuclear Energy, 19, 73 (1965)

114. A. Paulsen and H. Liskien
J.Nuclear Energy, 19, 907, (1965)

115. R. Beauge'
"Effective Cross Section for Detectors of Neutrons by Activation"
CEA (1963)

116. W. Z. Bothe
Physik, 120, 437, (1943)

117. T. H. R. Skyrme
AERE MS-91 and MS-91A (1944);
Second Edition 1961

118. C. W. Tittle
Nucleonics, 8, 6, (1951) 5;
9, 1, (1951) 60.

119. Alain Sola
Nucleonics, 78, (March 1960)

120. R. H. Ritchie and H. B. Edlridge
Nuclear Science and Engineering, 8, 4, (1960), 300

121. W. M. Walker et al.
Canad.J.Phys., 38, 57, (1960)

122. G. C. Hanna
Nucl.Science and Engineering, 15, 3, (1963), 325.

123. F. H. Helm
Nucl.Science and Engineering, 16, 235, (1963)

124. "Reactor Physics Constants"
ANL-5800, Sec.9
Chicago University, Second Edition (1963)
First Edition, Sec.8, (1958)

125. W. L. Zijp
"Review of Activation Methods for Intermediate Nuetron Spectra"
RCN-2405, (Oct.1965)

126. J. H. Neiler
Proc.of Seminar on the Physics of Fast and Intermediate Reactors, Vienna, (1961)
Paper SM-18/73, 1, 95

127. T. B. Ryves
J.of Nuclear Energy, 24, 35, (1970

128. G. S. Hurst et al.
Review of Sci.Instrum., 27, 153, (1956)

129. P. M. Uthe
"Attainment of Neutron Flux Spectra from Foil Avtivation"
WADC-TR - 57 - 3, (1957)

130. S. R. Hartman
WADC Technical Report 57-375
ASTIA Document No. AD 142029, (1957)

131. W. D. Lanning and K. W. Brown
WAPD-T-1380, (Sept.1961)
Proc. ANS Meeting, (Nov.1961)

132. J. Grundl and A. Usner
Nuclear Science and Engineering, 8, 598, (1960)

133. G. Di Cola and A. Rota
Nuclear Science and Engineering, 23, 344, (1965);
also EUR 588. (1964)

134. W. N. McElroy et al.
Nuclear Science and Engineering, 27, 533, (1967)

135. C. L. Green and J. V. Walker
Proc.of Conf.on Radiation Measurements in Nuclear Power
Paper 4.2
Barkeley Nuclear Laboratories, (Sept.1966):
and Rpt. CCC-108, RISC, Oakridge, (1967)

136. W. N. McElroy et al.
Nuclear Science and Engineering, 36, 15, (1969)

137. J. R. Bell and J. K. Mitts
Document No. NARF-61-18T, MR-N-279, (1961)
Nuclear Aerospace Research Facility, US Air Force

138. A. H. W. Aten et al.
Proc.Symp.on Neutron Detection and Dosimetry,
Harwell, 1, 399, (1962)

139. A. M. Bresesti et al.
Nuclear Science and Engineering, 29, 7, (1967)

140. M. Bresesti et al.
Proc.Symp.on Neutron Detection and Dosimetry,
Harwell, 1, 27, (1962)

141. R. L. Heath
"Scintillation Spectrometry: Gamma-Ray Spectrum Catalogue";
IDO-1688-1, TID-4500;
USAEC, (1964)

142. C. C. Grosjean and W. Bassart
"Table of Absolute Detection Efficiences of Cylindrical
Scintillation Gamma-Ray Detectors",
University of Ghent Computing Laboratory,
Ghent, Belgium, (1965)

143. B. L. Cohen
Phys. Rev., 81, 2 (1951), 184.

144. L. Katz and A. S. Penfold
Revs. of Mod. Phys. 24, 1 (1952), 28

145. W. J. Price
"Nuclear Radiation Detection"
McGraw Hill Book Company, Second Ed. (1964)

146. J. Topping
"Errors of Observation and their Treatment"
Chapman and Hall Ltd., London, (1965)

147. Yardley Beers
"Introduction to the Theory of Errors"
Addison-Wesley Publishing Company Inc. (1957)

148. Pugh-Winslow
"The Analysis of Physical Measurements"
Addison-Wesley, (1966)

149. C. Fiche et al.
Proc.of Symp.on Radiation Measurements in Nuclear Power
Berkeley Nuclear Lab., (1966)
Institute of Physics and the Physical Society (1966), pp.322.

150. B. W. Roos and W. C. Sangren
"Advances in Nuclear Science and Technology"
2, Academic Press, (1964)

151. R. L. Murray
"Nuclear Reactor Physics"
Ch.9, Macmillan and Co.Ltd., London, (1959)

152. F. H. Clark
"Advances in Nuclear Science and Technology"
5, Academic Press, (1969)

153. E. H. Bareiss
Proc.2nd Geneva Conf. 16, 505, (1958)

154. E. D. Pendelbury and L. H. Underhill
IAEA Seminar on the Physics of Fast and Intermediate
Reactors, Vienna (1961),
IAEA, II, 75, (1962)

156. A. I. Leipunskii et al.
Proc.3rd Geneva Conf., Paper A/Conf.28/P/368, (1964)

157. G. C. Wick
Physik 121, 702, (1943)

158. S. Chandrasekhar
"Radioactive Transfer"
Clarendon Press, Oxford, (1950)

159. B. G. Carlson
"Solution of Transport Equation by the S_n Method"
Los Alamos Scientific Laboratory Report, LA-1801, (1955)

160. B. G. Carlson and G. I. Bell
Proc.2nd Geneva Conf., 16, 535, (1958)

161. F. Avery
"The Prediction of Neutron Alternation in Iron-Water Shields"
AEEW-R 125, (1962)

162. H. Goldstein
"Fundamental Aspects of Reactor Shielding"
Addison-Wesley Publsihing Co., Ch. 5 & 6, (1959)

163. G. T. Chapman and C. L. Starrs
ORNL-Report 1843, (Sept.1955)

164. Ornstein and Uhlenbeck
Physica, 4, 478, (1937)

165. E. Fermi
Ricerca Scientifica, 7, (2), (1936), 13

166. Proc.of Conf.on the Application of Computing Methods to Reactor Problems, (May, 1965),
Argonne National Laboratories, USAEC Report, ANL-7050, (1965)

167. Numerical Methods for Reactor Calculation
G.I. Marchux (Ed.). Translated by Consultants Bureau, New York (1959)

168. Computing Methods in Reactor Physics
H. Greenspan et al. (Ed.)
Gordon and Breach Science Publishers Inc., New York (1968)

169. J. J. MacInerney
Nucl.Science and Engineering, 22, 215, (1965)

170. N. Papamehl
Nucl.Science and Engineering, 22, 451, (1965)

171. R. V. Meghreblian and D. K. Holmes
"Reactor Analysis"
McGraw-Hill, New York, Ch.4, (1960)

172. A. M. Weinberg and E. P. Wigner
"The Physical Theory of Neutron Chain Reactors"
University of Chicago Press, Chicago, Ch.10, (1958)

173. S. Yiftah and M. Sieger
"Nuclear Cross Sections for Fast Reactors"
IA-980, (1964)

174. J. R. Lamarsh
"Introduction to Nuclear Reactor Theory"
Addison Wesley, 130, (1966)

175. A. F. Avery et al
Report, AWRE-R 3216, (1960)

176. H. Borgwaldt et al.
IAEA Symp.on Pulsed Neutrons
Karlsruhe, 399, (1965)

177. "Reactor Physics Constants"
USAEC Report, ANL-5800, (1963)

178. J. J. Schmidt
Report KFK-120, Karlsruhe, (1962)

179. L. P. Abagyan et al.
"Group Constants for Nuclear Reactor Calculations"
Phys.Energy Inst., USSR, (1962)
Translated by Consultant Bureau, USA, (1964)

180. R. J. Howerton
"Semi-Empirical Neutron Cross Sections: 0.5 to 15 Mev"
Part II, UCRL-5331, (1958)

181. M. D. Goldberg et al.
"Angular Distribution in Neutron Induced Reactions"
BNL-400, (1962)

182. W. G. Cross
Proc.of the Symposium on Neutron Detection, Dosimetry and Standardization,
Harwell (1962), IAEA, Vienna, (1963), I, 389

183. S. Yiftah et al.
"Fast Reactor Cross Sections"
Pergamon Press, New York, (1960)

184. L. K. Burton and A. E. Sonch
Proc.of the Symposium on Neutron Detection, Dosimetry and Standardization
Harwell (1962), IAEA Vienna (1963), 1, 521

185. K. Shure
Nucl.Science and Engineering, 19, 310, (1964)

186. Phillips
Phys.Rev., 90, 532, (1953)

187. B. W. Roos and W. C. Sangren
Advances in Nuclear Science and Technology
2, 320, Academic Press, (1964)